INAUGURAL-DISSERTATION

zur

Erlangung der Doktorwürde

der

Naturwissenschaftlich-Mathematischen

Gesamtfakultät

der

Ruprecht-Karls-Universität

Heidelberg

Vorgelegt von

Marc Biver B.A. (Hons.), M.A. (Oxon.)

aus Winseler, Luxemburg

Tag der mündlichen Prüfung : 11.05.2011

Some Kinetic Aspects of the Mobilization of Antimony from Natural Sources

Gutachter :

Prof. Dr. William Shotyk

Prof. Dr. Heinz Friedrich Schöler

SHORT SUMMARY

The aim of the present thesis is to close some gaps in our understanding of the factors that govern the rates of mobilization of antimony from its natural sources, viz. from its most abundant minerals, namely stibnite, the most abundant antimony mineral, and its principal weathering products in the supergene zone, namely senarmontite, valentinite and stibiconite. Antimony may also become enriched in soils and sediments, as a result of anthropogenic or natural contamination, and be mobilized thence; therefore, the specific mobilization of antimony in the form of Sb(V) from sediment was also considered.

The first (introductory) Chapter is meant to give a comprehensive summary of the known geochemistry of antimony along with an outline of the theoretical basis of most of the material presented in the main chapters.

In the second Chapter, we study the rate of oxidative dissolution of stibnite in acidic solution and derive a rate law in terms of hydrogen ion concentration and dissolved oxygen, and the activation energy of the process is measured. The effect of Fe^{3+} and other trivalent cations on the rate, and the formation of elemental sulfur at the dissolving mineral surface are also examined. In Chapter III, essentially the same study is repeated in basic solution and the observed dissolution rate in a natural system, specifically, the antimony mineralization near Goesdorf (L), is explained on the basis of our findings. Activation energies indicate that the dissolution processes are diffusion controlled in acidic, and surface controlled in basic solution. Another important (new) finding is the promotive effect exerted by metal cations, both in acidic and in basic solution. These are, to our knowledge, the first reported instances of metal-promoted dissolution in the case of a sulfide mineral.

In Chapter IV, we investigate and rationalize the effects of organic ligands which commonly occur in the soil solution on the rate of dissolution of stibnite. Both the *type of ligand* and the *contact time* of the solution with the mineral determine whether an enhancement of the Sb mobilization is to be expected.

In Chapter V, we turn to the oxide minerals of antimony; we derive rate laws for their proton-promoted dissolution over the environmentally relevant pH range (2 to 11) and measure the activation energies of these processes. These energies are in the range of surface controlled mechanisms, except for valentinite in basic solution, which appears to be transport-controlled, and stibiconite, which dissolves with a *negative* activation energy in acidic solution. Negative activation energies for mineral dissolution are exceedingly rare though their existence was predicted on theoretical grounds. Stibiconite represents the first reported oxide mineral with a negative dissolution activation energy. The results from this Chapter permit to derive the following sequence of dissolution rates, valid over most of the pH range 2-11: valentinite>senarmontite>stibiconite>stibnite. Geochemical implications of this order of reactivities are discussed.

In Chapter VI, the mobilizing effect of common inorganic anionic aquatic species on antimony bearing sediment, and on pure phases representative of those present in sediments, is examined. The main objective consists in verifying whether carbonate and phosphate, known to mobilize As from sediments and soils, mobilize Sb as well. Phosphate at environmental concentrations has little impact, while that of carbonate, at environmentally relevant concentrations, is very slight, although significant.

The Appendices contain, among others, detailed experimental results that are merely mentioned in the main text, or that are only presented there in graphical form, as well as the development of a UV-photometric method for the determination of elemental sulfur on mineral surfaces. The method is applied to weathered stibnite in Chapters II and III; it is more sensitive, more economic, more environmentally friendly, and easier to carry out than the literature method.

KURZE ZUSAMMENFASSUNG

Das Ziel der vorliegenden Arbeit besteht darin, einige Lücken in unserem gegenwärtigen Verständnis der Mobilisierung des Elementes Antimon zu schließen. Behandelt wird die Mobilisierung aus Stibnit (Grauspießglanz) und aus den hauptsächlichsten Oxidmineralen Senarmontit, Valentinit und Stibiconit, die in der Natur als Verwitterungsprodukte des Grauspießglanzes auftreten. Untersucht wird außerdem die Mobilisierung des fünfwertigen Antimons aus natürlich kontaminiertem Flußsediment.

Im ersten, einführenden Kapitel, wird die bekannte Geochemie des Antimons möglichst vollständig zusammengefasst und es werden die theoretischen Grundlagen der Kinetik der Mineralauflösungsvorgänge vorgestellt.

Im zweiten Kapitel wird das Reaktionsgeschwindigkeitsgesetz der oxidativen Auflösung von Grauspießglanz in Abhängigkeit der Acidität und der Konzentration an gelöstem Sauerstoff in saurer Lösung experimentell erarbeitet; die Aktivierungsenergie des Vorgangs wird gemessen, der Einfluss des Fe^{3+} und anderer dreiwertiger Kationen wird untersucht, ebenso wie die Bildung elementaren Schwefels an der in Auflösung begriffenen Mineraloberfläche. Im dritten Kapitel wird im Wesentlichen die gleiche Untersuchung in basischer Lösung wiederholt, und die so gewonnenen Erkenntnisse zur Erklärung der Verwitterungsgeschwindigkeiten in einem natürlichen System, dem Antimonvorkommen bei Goesdorf (L), herangezogen. Die Aktivierungsenergien lassen darauf schließen, daß in saurer Lösung die Diffusion geschwindigkeitsbestimmend ist, während es in alkalischer Lösung die Vorgänge an der Mineraloberfläche (d.h. das Herauslösen der Antimonionen aus dem Kristallverband) sind. Eine wichtige neue Erkenntnis besteht in dem geschwindigkeitsfördernden Effekt, den Metallkationen auf den Lösungsvorgang in saurer wie in basischer Lösung ausüben. Solche Effekte sind bereits beobachtet, aber noch nie für ein Sulfidmineral beschrieben worden.

In Kapitel IV wird der Einfluss organischer Liganden, wie sie in der natürlichen Bodenlösung vorkommen, auf die Auflösungsgeschwindigkeit des Stibnits untersucht. Sowohl die *Art des Liganden* wie die *Einwirkungsdauer* der Lösung auf das Mineral bestimmen letztendlich, ob es mit einem gegebenen Liganden zu einer vertärkten Mobilisierung kommt oder nicht.

In Kapitel V werden die Geschwindigkeitsgesetze für die Auflösung der Oxidminerale unter umweltrelevanten Bedingungen (pH Wert von 2 bis 11), sowie Aktivierungsenergien bestimmt. Diese Energien deuten wieder auf oberflächenkontrollierte Auflösungsmechanismen hin. Ausnahmen bilden Valentinit, in alkalischem Milieu, mit einer für Diffusion charakteristischen Aktivierungsenergie, und Stibiconit, in saurer Lösung, mit einer *negativen* Aktivierungsenergie. Negative Aktivierungsenergien sind überaus selten, gleichwohl ihre Existenz für Mineralauflösungsvorgänge aufgrund theoretischer Überlegungen vorhergesagt worden ist. Stibiconit stellt, nach unserem Wissen, das erste beschriebene Beispiel eines Oxidminerals mit negativer Aktivierungsenergie für dessen Auflösevorgang dar. Die Ergebnisse dieses Kapitels erlauben uns, nun die einzelnen Antimonminerale ihrer absteigenden Reaktionsgeschwindigkeit nach wie folgt zu ordnen: Valentinit>Senarmontit>Stibiconit>Stibnit. Diese Reihenfolge gilt praktisch für den ganzen pH Bereich von 2 bis 11. Die geochemische Bedeutung dieser Reihe wird diskutiert.

In Kapitel VI wird der Einfluss der geläufigsten anorganischen, anionischen aquatischen Species auf die Mobiliserung des fünfwertigen Antimons aus oxischem Sediment untersucht. Es wurden auch Versuche an anorganischen Reinphasen (Oxidhydrate des Eisens, Aluminiums und Mangans, sowie Tonminerale) vorgenommen, die repräsentativ für die Zusammensetzung eines Sedimentes sind. Das Hauptziel besteht darin, festzustellen, ob Phosphat und Carbonat –welche bekannterweise Arsen aus Böden und Sediment mobilisieren- auch zu einer verstärkten Mobilisierung von Antimon führen. Phosphat mobilisiert Antimon kaum unter umweltrelevanten

Bedingungen, während Carbonat in diesen Konzentrationen die Mobilisierung zwar signifikant, aber dennoch auch eher unmaßgeblich verstärkt.

In den Anhängen befinden sich einige experimentelle Daten, die in den Hauptkapiteln nur erwähnt oder in graphischer Form dargestellt sind. Dazu kommt noch ein UV-photometrisches Verfahren zur quantitativen Bestimmung elementaren Schwefels an Mineraloberflächen. Diese Methode wird in den Kapiteln II und III auf Stibnit angewandt; sie ist empfindlicher, sparsamer, umweltfreundlicher und einfacher durchführbar als die Literaturmethode.

Erklärung über selbständige Forschungsleistungen

Diese Erklärung bezieht sich auf folgende Arbeiten, die zur Veröffentlichung eingereicht worden sind :

Chapter II : Experimental Studies of Stibnite (Sb_2S_3) Dissolution Kinetics: Effects of pH, Dissolved Oxygen, Ferric Iron and Temperature. Part I : Acidic Solutions.

Chapter III : Experimental Study of Stibnite Dissolution Kinetics : Effect of pH, Dissolved Oxygen, Temperature, and Alkaline-Earth Metal Cations. Part II. Alkaline Solutions and Field Implications.

Chapter IV : Experimental Study of the Kinetics of Ligand-Promoted Dissolution of Stibnite (Sb_2S_3).

Chapter V : Experimental Study of the Kinetics of Proton-Promoted Dissolution of the Secondary Antimony Minerals Stibiconite, Senarmontite and Valentinite under Environmentally Relevant Conditions.

Chapter VI : The Desorption of Sb(V) from Sediments, Hydrous Oxides and Clay Minerals by Carbonate, Phosphate, Sulfate, Nitrate and Chloride.

Appendix AIV : Determination of Elemental Sulfur on Mineral Surfaces, and Application to Weathering of thirteen Sulfides in Acidic Solutions.

Diese Arbeiten sind von mir, Marc Biver, selbständig geplant, durchgeführt, und ausgewertet worden, mit Ausnahme einiger unten aufgeführter Punkte. Die eingereichten Aufsätze habe ich selbst verfasst ; sie sind von Herrn Professor Shotyk vor dem Einreichen gelesen worden und seine Verbesserungsvorschläge sind berücksichtigt worden. In Kapitel IV hat Professor Shotyk die zu verwendende pH-Wert Spanne, ebenso wie die Verwendung eines natürlichen Blätterextraktes („Leaf litter extract") angeregt. Die Einleitung zu Kapitel VI ist zum allergrößten Teil von Herrn Professor Shotyk verfasst worden.

Heidelberg, im Februar 2011

Prof. Dr. W. Shotyk Marc Biver

The results presented in this thesis were submitted for publication in the following journals :

Chapter II : Experimental Studies of Stibnite (Sb_2S_3) Dissolution Kinetics: Effects of pH, Dissolved Oxygen, Ferric Iron and Temperature. Part I : Acidic Solutions.

Geochimica et Cosmochimica Acta

Chapter III : Experimental Study of Stibnite Dissolution Kinetics : Effect of pH, Dissolved Oxygen, Temperature, and Alkaline-Earth Metal Cations. Part II. Alkaline Solutions and Field Implications.

Geochimica et Cosmochimica Acta

Chapter IV : Experimental Study of the Kinetics of Ligand-Promoted Dissolution of Stibnite (Sb_2S_3).

Biogeochemistry

Chapter V : Experimental Study of the Kinetics of Proton-Promoted Dissolution of the Secondary Antimony Minerals Stibiconite, Senarmontite and Valentinite under Environmentally Relevant Conditions.

Chemical Geology

Chapter VI : The Desorption of Sb(V) from Sediments, Hydrous Oxides and Clay Minerals by Carbonate, Phosphate, Sulfate, Nitrate and Chloride.

Journal of Environmental Quality

Appendix AIV : Determination of Elemental Sulfur on Mineral Surfaces, and Application to Weathering of thirteen Sulfides in Acidic Solutions.

Environmental Science and Technology

Acknowledgements

I am indebted to my supervisor, Prof. Dr. William Shotyk, for being the best supervisor one could imagine. I would like to thank him for his expert guidance throughout, as well as his constant encouragement and unfailing support, and the many highly motivating discussions we have had. I want to thank Prof. Dr. Heinz Friedrich Schöler, Prof. Dr. Ulrich Anton Glasmacher and Prof. Dr. Juraj Majzlan for kindly agreeing to act as 'Gutachter' and 'Prüfer', respectively.

I would also like to thank my family, Monique, Lou and Anouk, and my parents Marianne and André for their never ending patience and support, financial and in many other respects.

To my family

TABLE OF CONTENTS

ABBREVIATIONS

BET	Brunauer-Emmett-Teller determination of specific surface area
DOC	Dissolved organic carbon
DP	Differential pulse
DPASV	Differential pulse anodic stripping voltammetry
EXAFS	Extended X-Ray Absorption Fine Structure
HG	Hydride generation
HPLC	High Performance Liquid Chromatography
IC	Ion-chromatography
IARC	International Agency for Research on Cancer
ICP-MS	Inductively coupled plasma-mass spectrometry
ICP-OES	Inductively coupled plasma-optical emission spectrometry
ICP-SMS	Inductively coupled plasma-sector field mass spectrometry
IMA	International Mineralogical Association
INAA	Instrumental Neutron Activation Analysis
LEED	Low-energy Electron Diffraction
NOM	Natural organic matter
PET	Polyeth(yl)eneterephtalate
ppb	parts per billion
ppm	parts per million
PVC	Polyvinylchloride

SIMS	Secondary Ion Mass Spectrometry
XAFS	X-ray Absorption Fine Structure
XANES	X-ray Absorption Near Edge Structure
XPS	X-ray Photoelectron Spectroscopy
XRD	X-Ray Diffraction

SUMMARY

Chapter I is an introductory chapter, in which we review the atomic, physical and chemical properties, the occurrence, production, history, uses, toxicological properties and environmental speciation of antimony, as well as the available analytical techniques for the quantification of this element. Some theoretical aspects of mineral dissolution kinetics, viz. the origin of dissolution rate laws and activation energies and their interpretation are presented. Finally, crystallographic information pertaining to all the mineral phases used in the present thesis is included.

1. Main objectives

The main objective of the present thesis is to contribute to our understanding of the rates of mobilization of antimony from several natural sources of the element.

We begin by studying the mobilization of antimony from its most important (ore) mineral, i.e. stibnite, Sb_2S_3. The parameters in the rate law of oxidative dissolution of stibnite by aqueous solutions are determined experimentally in Chapters II and III. These parameters comprise the orders of the rate law with respect to hydrogen ion concentration and dissolved oxygen, both in acidic and in basic media.

The activation energies of the dissolution are also determined at chosen pH values, over the temperature range from 25 to ca. 50°C, in order to gain an understanding of the rate-determining steps in the dissolution. The determination of activation energies permits the

distinction to be made between surface controlled, and transport (i.e. diffusion) controlled mechanisms (Lasaga, 1984).

In addition to this, ferric iron is known to accelerate the rates of oxidative dissolution of sulfide minerals (Alpers and Blowes, 1994). Environments of acid mine or acid rock drainage are often characterized by elevated iron concentrations (Nordstrom et al., 2000; Nordstrom, 2000); we therefore examine the effect of ferric ion in acidic solution at different concentrations. To further clarify the role of iron ions in the dissolution process, experiments are repeated in the presence of other trivalent ions, i.e. aluminium, Al^{3+}, whose ionic radius is very close to that of iron, and cerium Ce^{3+}, which is about twice as large as the Fe^{3+} cation.

Further, it is known that elemental sulfur forms at the surfaces of dissolving sulfide minerals (McGuire et al., 2000). Past kinetic studies of oxidative weathering mostly neglect this elemental sulfur layer. Hence, kinetic rates based solely on the concentrations of sulfur species released to solution may be inaccurate in this respect. At the end of our weathering experiments, we therefore determine the amounts of elemental sulfur formed at the surface and study their correlation with the overall dissolution rate. The literature method (McGuire et al., 2000) for the quantification of this sulfur layer being unsatisfactory for our purpose, we develop an experimental technique for the determination of this sulfur layer, based on UV-photometry (contained in appendix AIV). Disadvantages of McGuire's method include: large samples that must be

processed, the use of environmentally problematic solvents, costly instrumentation not readily available, and a rather high detection limit.

Ultimately, the rate equations derived in Chapter III, taking into account pH and oxygen status, should have enabled us to predict the weathering rate of stibnite in the context of a natural system, the abandoned antimony mine near Goesdorf, in Luxembourg. This environment is characterized by slightly basic mine drainage waters, owing to the dissolution of dolomitic gangue material (Filella et al., 2009). However, in a laboratory simulation with synthetic mine water, stibnite turned out to weather much faster than predicted on the basis of pH and oxygen saturation alone. Since the mine water carries elevated concentrations of alkaline-earth cations, we were compelled to extend our study to the possible effects of magnesium and calcium on the rates of dissolution.

Complexation by organic ligands may also influence rates of mineral dissolution, an effect termed 'ligand-promoted dissolution' (Sposito, 2004 and references therein). We therefore measured the rates of stibnite dissolution at three different pH values (4, 6, and 8) in the presence of millimolar concentrations of some chosen ligands, which either occur naturally, as such, in the soil solution, or which, by virtue of structural and functional similarities, may serve as proxy compounds for those occurring naturally. The chosen ligands include : acetate, catechol, citrate, cysteine, desferrioxamine-B (DFOB, a natural siderophore), EDTA,

glucose, glycine, oxalate, and salicylate. An experiment is also conducted in the presence of a natural leaf litter extract, prepared from chestnut leaves (Blaser et al, 1984). Since synergistic effects between a siderophore, desferrioxamine-B, and chelating ligands in the dissolution of iron oxide phases are documented in the literature (Cheah et al., 2003), we also conducted experiments with the *mixture* of this siderophore with citrate.

Following the experiments on stibnite, we study the dissolution rates of its main weathering products in the supergene zone, viz. the oxide minerals senarmontite, valentinite and stibiconite (Filella et al., 2009). Again, the whole environmentally relevant pH range is covered by our experiments, in order to measure the reaction order with respect to hydrogen ion concentration. At selected pH values, activation energies are measured. Further, the experiments carried out on stibiconite permit the determination of the solubility of this mineral as a function of acidity, and thus complement the solubility data of antimony oxides available in the literature.

In the final chapter of the thesis, the effect of common anionic aquatic species (chloride, sulfate, nitrate, carbonate and phosphate) on the mobilization of pentavalent antimony from contaminated sediment is studied. The sediment is taken from the drainage adit of the Goesdorf mine. Pure phases, viz. the amorphous hydrated oxides of Fe(III), Al(III) and Mn(IV), as well as the clay minerals kaolinite and montmorillonite, are

also included. The main objective of this part of the study is to find out whether carbonate and phosphate, known to mobilise arsenic from sediments and soils, equally promote the mobilization of its heavier congener, antimony. In addition to this, adsorption envelopes for Sb(V), i.e. the extent of adsorption vs. pH, are constructed for the amorphous hydrous oxides and the clay minerals.

2. Methodology

2.1 Kinetic experiments on stibnite

The rates of dissolution of stibnite under environmental conditions are so slow that they may only be measured in a continuously stirred flow-through reactor. This experimental design has certain advantages over the (simpler) batch design, which are discussed at length by Rimstidt and Dove (1986). The obvious advantage lies in the fact that the system is permanently kept in a state far from thermodynamic equilibrium. In the present case, the flow-through reactor remains the only feasible option, because of the slow dissolution of stibnite. If the experiments were conducted in a batch reactor, very small *changes* in analyte concentration over time would have to be reliably measured against a background of a comparatively high total concentration (which is due to the high *initial* rate of dissolution), and these small changes might easily become entirely absorbed by the experimental error. Below, we shall see that we may opt for the simpler batch design in the case of the dissolution of the oxide minerals. Our flow-through reactor consists of a stirred ultrafiltration cell

(Millipore Amicon Model 8200), of nominal volume equal to 200 ml, ideally suited for our purpose. The body consists of a polysulfone cylinder and is equipped with a suspended acetal/polysulfone stirrer assembly. Materials such as glass or plastics which might release traces of antimony are thus avoided, while maintaining a good resistance to chemicals; the suspended design of the magnetic stirrer ensures that the mineral inside the cylinder is not subject to grinding. All tubing connections are made of semi-rigid FEP tubing, which offers excellent resistance to chemicals and contains no antimony.

The mineral sample (ca 1.5 g, accurately weighed) is loaded into the ultrafiltration cell, the cell is capped, wrapped in aluminium foil to avoid photochemical reactions, and immersed in a constant temperature bath. The solution of the desired ionic strength, pH and oxygen saturation is pumped into the cell by means of a variable speed peristaltic pump, at a typical rate of 8 $mlmin^{-1}$. The feed solution (typically 22 l for a 36 h experiment) is prepared in a PP tank and it is equilibrated in this tank with the desired gases (oxygen/nitrogen mixtures in various proportions) by simple sparging. In acid solutions, the ionic strength of the feed solutions is kept constant at I=0.01 M (except in the solution at pH=1) by the addition of the calculated amount of sodium perchlorate; perchloric acid is used to adjust the pH. Perchlorate and perchloric acid were chosen because of the negligible complexation of metal ions by perchlorate (to avoid ligand-promoted dissolution) (Johanson, 1974). The alkaline feed

solutions are carbonate-bicarbonate buffers whose composition is calculated to give a total ionic strength of I=0.01 M. The effluent from the cell passes through a large Erlenmeyer flask which can be fitted with probes for dissolved oxygen and pH. The effluent from this flask is sampled at regular intervals and its antimony concentration (order of magnitude 100 $\mu g l^{-1}$) measured by differential pulse voltammetry (Quentel and Filella, 2002). After about 22 h, these concentrations reached a constant value, constancy being defined as a series of measurements with standard deviations less than 10%. In practice, the standard deviations are frequently much better. From several hourly measurements at steady state, the rate of dissolution of stibnite is calculated and normalized with respect to the surface area of the mineral, which is determined by a multiple-point BET nitrogen isotherm.

Experiments as described above are carried out at different pH values, different dissolved oxygen concentrations, and different concentrations of ferric, aluminium, and cerium ion (in acid solution), or magnesium and calcium ion (in basic solution). Reaction orders with respect to hydrogen ion concentration and dissolved oxygen concentrations, and the rate constant, are obtained by linear regressions in log-log plots. The dependence on dissolved oxygen and foreign metal cations are also well modeled by Langmuir isotherms (Langmuir, 1916). Activation energies are measured by repeating the experiments at a series

of temperatures between 25 and 50°C and fitting the rate constants to a linearized Arrhenius equation (Laidlar, 1987).

2.2 Experiments on stibnite in the presence of organic ligands and on oxide minerals

The dissolution rates in the experiments involving organic ligands (chapter IV), and the rates of dissolution of senarmontite, valentinite and stibiconite (chapter V), are fast enough to be measured in a batch reactor. This consists of a standard 1 l round-bottom glass flask with two ground necks, immersed in a constant temperature bath. Into this flask the mineral sample (order of magnitude 100 mg), accurately weighed, and the solution (1 l) are loaded. For the study of the effects of organic ligands, these are contained at a concentration of 1 mM in a buffer solution of pH=4, 6 or 8. Good's buffers (Good et al., 1966) are used for pH=6 and 8, and a sulfanilate-sulfanilic acid buffer is used at pH=4. The total concentrations of buffer substances are 0.05 M and the ionic strength of all solutions is adjusted to 0.1 M using sodium perchlorate. The experiments with oxide minerals are carried out with solutions of perchloric acid (in the acidic pH domain), adjusted to ionic strength 0.01 M with sodium perchlorate and carbonate-bicarbonate buffers, calculated to have a total ionic strength of 0.01 M, are used in the basic domain. The suspension is stirred by means of a suspended magnetic stirrer bar, in order to avoid grinding of the mineral. 10 ml samples are withdrawn at regular intervals using a PP-PE syringe fitted with a Millipore CME filter of

0.45 µm porosity. The concentrations in these samples are high enough to be analysed by ICP-OES.

Reaction rates at steady state (at the surface) are determined graphically, by fitting a least-squares line to the linear portion of the graph representing the mobilized mass as a function of time.

From these reaction rates, rate orders and rate constants are obtained as described in section 2.1 above.

2.3 Experiments on sediments

Desorption experiments are conducted on sediment samples, on amorphous hydrous oxides (of Fe(III), Mn(IV) and Al(III)) and on clay minerals (kaolinite and montmorillonite). A highly contaminated sediment sample (312 ppm total Sb) from the Goesdorf antimony mine and the reference material PACS-2 of the Canadian Research Council are chosen for this study. Hydrous oxide phases are prepared by precipitation of the corresponding metal perchlorates with ammonia and hydrogen peroxide, in the case of manganese. The clay minerals are commercial materials.

Hydrous oxides and clays are first loaded with antimony by preparing suspensions of the material in a dilute solution of Sb(V) (4×10^{-7} $moll^{-1}$) in PP centrifuge tubes) and waiting until equilibrium is achieved. The solid is then separated by centrifugation. The supernatant is analysed by differential pulse voltammetry (Quentel and Filella, 2002) in order to be able to calculate the amount of Sb(V) initially adsorbed on the solid. The sediments (obviously without prior loading), loaded hydrous

oxides and clay minerals are then treated with an electrolyte solution containing the anion of interest (chloride, sulfate, nitrate, phosphate or carbonate) to a concentration of 0.083 M in a buffer solution of pH=8 and mixed on an end-over-end tumbler. The solid to liquid ratio varies between 100 and 500 mg in 10 ml of solution. Sample solutions are again separated by centrifugation and analysed by differential pulse voltammetry after 1 h and after 24 h to determine the amount of mobilized Sb(V).

The adsorption envelopes are constructed by equilibrating portions of hydrous oxides or clay minerals with more concentrated solutions of Sb(V) (2×10^{-5} M) in buffer solutions ranging from pH 6 to 11 and measuring the amount of Sb(V) left in the solution after the adsorption step, again by differential pulse voltammetry.

Finally, the extent of desorption of Sb(V) from the sediments is measured as a function of carbonate and phosphate concentrations, ranging from 5×10^{-3} M to 10^{-4} M, in buffer solutions of pH=8. The pH=8 and total carbonate concentration of 5×10^{-3} M are chosen because they are representative of the conditions prevailing in the drainage waters of a natural system of interest, the Goesdorf antimony mine.

2.4 Determination of elemental sulfur

Sulfur is well soluble in cyclohexane and exhibits a strong absorption peak in the ultraviolet, at 206.3 nm. The absorption at this wavelength obeys Beer's law, so that a calibration plot in the range 0-4

mgl^{-1} (as S) may be obtained, with a detection limit well below 1 mgl^{-1}.To measure the amount of elemental sulfur on a mineral, the sample is simply extracted with cyclohexane and the absorbance of the solution is measured at 206.3 nm, from which the sulfur concentration may then be calculated using Beer's law. To illustrate the utility of the method, it is applied to the simulated weathering of some 13 sulfide minerals in perchloric acid solution.

3. Results and Conclusions

3.1 Rate laws of stibnite dissolution

The stibnite dissolution rate was found to be proportional to a fractional power of hydrogen ion concentration, while the rate dependence on dissolved oxygen is best described in terms of Langmuir adsorption (Langmuir, 1916), with saturation occurring at oxygen partial pressures in excess of 0.2 atm:

$$r = k\left[H^{+}\right]^{\alpha} \frac{K\left[O_2\right]}{1+K\left[O_2\right]}$$

where $k=1.14\times10^{-10} \pm 0.09\times10^{-10}$; $\alpha=0.125 \pm 0.006$; $K=2.13\times10^{4} \pm 0.26\times10^{4}$ mol^{-1} l. Alternatively, the rate may be expressed with a fractional order with respect to dissolved oxygen:

$$r = k[H^{+}]^{\alpha}[O_2]^{\beta}$$

Where $k=1.17\times10^{-9}\pm0.01\times10^{-9}$, $\alpha=0.125\pm0.006$, $\beta=0.26\pm0.04$. This equation is only valid up to a partial pressure of oxygen of 0.2 atm, owing to the saturation effect observed at higher partial pressures.

The activation energy at pH=3 in the temperature range 25-40°C is 5.2 ± 0.4 kJ mol^{-1}, suggesting a mixed adsorption and diffusion controlled mechanism (Lasaga, 1984). Ferric iron strongly catalyses the dissolution, with an acceleration of the rate by approximately an order of magnitude for $[Fe^{3+}] = 10^{-3}$ M at pH = 2. The kinetics is again best described in terms of Langmuir adsorption of Fe^{3+} on the stibnite surface, with saturation occurring above ca. 4×10^{-3} M :

$$r = r_{max} \frac{K[Fe^{3+}]}{1 + K[Fe^{3+}]}$$

where r_{max}= $4.6\times10^{-10} \pm 0.3\times10^{-10}$ mol s^{-1} m^{-2} and K=$1.4\times10^{4} \pm 0.5\times10^{4}$ mol^{-1} l.

Aluminium ion, which has an ionic radius (54 pm) almost identical to that of ferric iron (55 pm), produces a similar rate enhancement. The effect of cationic radius on the dissolution rate of stibnite was evaluated using Ce^{3+} (114 pm) which increased the rate even more (radii are from Shannon, 1976).

Stibnite dissolution is incongruent to varying degrees, with elemental sulfur forming a residual surface layer. In the presence of high concentrations of ferric iron, the dissolution becomes highly incongruent, with a substantial accumulation (estimated to be equivalent to 7 to 13 atomic layers) of elemental sulfur. In contrast to Fe^{3+}, neither Ce^{3+} nor Al^{3+} has an effect on the formation of elemental sulfur, clearly demonstrating the important role played by Fe^{3+} in the oxidation of sulfide to elemental sulfur.

In basic solution, the empirical rate law may be written as :

$$r = k\left[H^+\right]^{\alpha} \frac{K\left[O_2\right]}{1+K\left[O_2\right]}$$

with $k=6.3\times10^{-13} \pm 0.7\times10^{-13}$, $\alpha=-0.13\pm0.01$ and $K=7.8\times10^{4} \pm 2.0\times10^{4}$ mol^{-1} l at 25°C with 8 < pH < 11, and dissolved oxygen saturation between 0 and 4 atm. Alternatively, this rate law can also be formulated with a fractional order with respect to dissolved oxygen :

$$r = k[H^+]^{\alpha}[O_2]^{\beta}$$

where $k=1.12\times10^{-11}\pm0.14\times10^{-11}$, $\alpha=-0.13\pm0.01$ and $\beta=0.296\pm0.054$. In contrast to acidic solutions, the dissolution rate in alkaline solution does not reach a maximum when the atmospheric partial pressure of oxygen is achieved. The temperature dependence of the rate between 25°C and 48°C leads to an apparent activation energy of the reaction of 51.8 ± 0.5 $kJmol^{-1}$ at pH=9.9, indicative of a surface-controlled mechanism; this E_A value is much greater than in acidic solutions, where a diffusion-controlled mechanism has been suggested (Lasaga, 1984). A similar transition from low to high activation energy on going from acidic to alkaline conditions was observed in the dissolution of galena (De Guidici et al., 2005). A laboratory simulation of the weathering conditions found in the abandoned antimony mine in Goesdorf (Luxembourg) is carried out, which reveals that the rate is also critically dependent on the concentrations of alkaline-earth cations. Magnesium and calcium are found to increase the dissolution rates substantially (calcium had a stronger effect than magnesium), which is, to our knowledge, the first description of metal-

promoted dissolution of a sulphide mineral (Note that a similar metal-promoting effect of trivalent cations (Fe^{3+}, Al^{3+} and Ce^{3+}) is observed in acidic solution). The amounts of elemental sulfur formed at the weathered stibnite surface in basic solution are also measured and found to correlate very well with reaction rate.

The rate constants, reaction orders and activation energies determined in these chapters are comparable in magnitude to those obtained for other sulfide minerals in the literature, e.g. arsenic sulfides (Lengke and Tempel, 2001, 2002, 2003).

3.2 Effects of organic ligands on stibnite dissolution rate

There is no single, unifying principle to predict whether a given ligand will promote the dissolution, or inhibit it, at a given pH. Very often, ligands show a very complex behaviour in that their effect is pH dependent as well as time dependent, i.e. the initial rates of dissolution, estimated by the mobilised amount of antimony during the first 10 min. of the experiment, may be higher than the blank value, while the rate at steady state may be smaller than the blank value, or vice-versa. Whenever this is the case, then it will depend on the contact time between the mineral and the solution whether more antimony will be mobilised in the presence of the ligand than in its absence, or less. The reader should refer to table IV.2, as an aid to predict what the effect of a given ligand at a certain pH will be. As a general rule, monodentate ligands have little effect or an inhibiting one on the steady state rate.

Polydentate chelating ligands (e.g. EDTA, citrate) promote the rate, at least above a certain threshold pH such that enough functional groups are deprotonated to permit polydentate chelation. This is well exemplified by EDTA, which acts promotively at any pH, and by citrate, which acts promotively only above pH=4 : the 1^{st} two pK_a values of EDTA are 2.0 and 2.6, so that two carboxylate groups are fully deprotonated at the lowest pH in our experiments (pH=4). The 1^{st} pK_a of citric acid is 3.16 and the 2nd is 4.76, so that at pH=4, citric acid behaves as a monodentate ligand. It is only above pH=4.76 that a second acidic group is substantially deprotonated, hence the promotive effect of citrate at pH=8. Ligands capable of forming polynuclear surface chelates, such as DFOB, which has three hydroxamic acid moieties that are far enough apart to span several metal centres on the surface, are found to inhibit the dissolution at all pH values, because the simultaneous, concerted dislocation of more than one metal ion from the surface requires a very high activation energy and is thus kinetically disfavoured. General principles of ligand-promoted dissolution are discussed by Furrer and Stumm (1986).

However, an interesting synergistic effect (Cheah et al., 2003) between DFOB and citrate is observed at pH=4 and 6. Both ligands taken on their own at these pH values have no effect or even an inhibiting one. In combination, they act promotively. The reader should refer to chapter IV for the interpretation of this synergistic effect.

Model calculations show that the dissolution rates do not correlate with the extent of complexation of antimony ions in solutions, as suggested by Ludwig et al. (1995). It is obvious that in the case of polyfunctional ligands capable of forming polynuclear surface complexes, such a correlation need not exist, for the surface complexes in question may well form and be thermodynamically very stable, but their detachment from the surface is kinetically hindered (as explained above in the case of DFOB). There is, however, a good correlation between the rate of dissolution and the pK_a of the last protolysis step believed to be necessary for efficient surface complexation.

3.3 Dissolution rates of the oxide minerals

Batch reactor experiments are carried out in order to derive rate laws for the proton promoted dissolution of the main natural antimony oxide phases, namely stibiconite (idealized composition $SbSb_2O_6OH$), senarmontite (cubic Sb_2O_3) and (metastable) valentinite (orthorhombic Sb_2O_3) over the range $2 \leq pH \leq 11$, under standard conditions and ionic strength $I=0.01$ mol l^{-1}.

The rates of antimony release by stibiconite are $r=(1.5\pm0.2)\times10^{-9}$ $[H^+]^{0.12\pm0.02}$ mol m^{-2} s^{-1} for $2.00 \leq pH \leq 4.74$ and $r=(2.31\pm0.02)\times10^{-10}$ $[H^+]^{-0.049\pm0.004}$ mol m^{-2} s^{-1} for $4.74 \leq pH \leq 10.54$. The rates of dissolution of senarmontite are $r=(4.6\pm2.6)\times10^{-7}$ $[H^+]^{0.54\pm0.05}$ mol m^{-2} s^{-1} for $2.00 \leq pH \leq 6.93$ and $r=(1.7\pm0.3)\times10^{-14}$ $[H^+]^{-0.52\pm0.07}$ mol m^{-2} s^{-1} for $6.93 \leq pH \leq 10.83$.

The rates of dissolution of valentinite are $r=(3.7\pm0.9)\times10^{-7}$ $[H^+]^{0.32\pm0.04}$ mol m^{-2} s^{-1} for $1.97\leq pH\leq4.05$. Above pH=4.58, valentinite is found to dissolve at a constant rate of $r=(3.47\pm0.15)\times10^{-8}$ mol m^{-2} s^{-1}. Activation energies are determined at selected pH values in the acidic and basic domain, over the temperature range 25-50°C. The values for stibiconite are -36.4±1.6 kJ mol^{-1} (pH=2.00) and 58±18 kJ mol^{-1} (pH=8.7). For senarmontite, we find 36±5 kJ mol^{-1} (pH=3.0) and 68±6 kJ mol^{-1} (pH=9.9) and for valentinite 53.5±3.6 kJ mol^{-1} (pH=3.0) and 9.1±2.7 kJ mol^{-1} (pH=9.9). These activation energies are interpreted in the text. Briefly, the dissolution of senarmontite (at both pH values) and valentinite (at pH=3.0) and stibiconite (at pH=8.7) appear to be surface controlled. The activation energy for valentinite at pH=3.0 is anomalously low, indicative of diffusion control (Lasaga, 1984). The activation energy of stibiconite dissolution at pH=2.0 is negative. Negative activation energies of dissolution are very rare, although they have been predicted on theoretical grounds (Casey and Sposito, 1992).

The solubility of stibiconite at 25°C in the pH domain from 2 to 10 is determined; solubilities decrease from 452.0 µg l^{-1} (as Sb) at pH=2.00 to 153.2 µg l^{-1} at pH=7.55 and increase again in the basic region, up to 176.6 µg l^{-1} at pH=9.92.

A graphical synopsis of all the kinetic results, including those of stibnite (Sb_2S_3) from chapters II and III, is presented (fig. V.12). In

general, over most of the pH range from 2 to 11, the following sequence of reactivities is observed :

valentinite>senarmontite>stibiconite>stibnite

The geochemical implications for the weathering of antimony oxide minerals and stibnite, with particular reference to the mobilization of antimony in the context of an abandoned antimony mine (Goesdorf, Luxembourg), are discussed in the text. Briefly, valentinite is found to be a dominant oxide phase at the Goesdorf site (Filella et al., 2009) and the rate of dissolution of valentinite is about two orders of magnitude larger than the rate of dissolution of stibnite. Whether valentinite or stibnite make the dominant contribution to the antimony mobilization at the site therefore depends on the relative magnitudes of the exposed surface areas of the minerals.

3.4 Mobilisation of Sb(V) from sediments

On sediment, phosphate is found to have a strong mobilising ability, while that of carbonate is in general weaker. In the cases of hydrous metal oxides, Sb(V) is most effectively desorbed by phosphate, followed by carbonate. Phosphate also desorbs Sb(V) from the clay minerals, while carbonate has no effect. Envelopes showing the extent of adsorption of Sb(V) as a function of pH in the absence and presence of carbonate reveal that adsorption densities are higher (except in the case of montmorillonite) in the absence of carbonate, suggesting a competition between carbonate and $[Sb(OH)_6]^-$ for surface sites generally, and a lowering of surface

charge in the case of hydrous aluminium oxide. Desorption experiments on sediments with varying concentrations of phosphate and carbonate demonstrate that at environmentally relevant concentrations, desorption by phosphate is negligible while the effect of carbonate is not. Sulfate, chloride and nitrate generally had little effect. The proportion of antimony desorbed in blank experiments coincides with that mobilized in the first fraction of the BCR sequential extraction (Ure and Davidson, 2002) easily exchangeable and carbonate-bound fraction).

3.5 Determination of elemental sulfur on mineral surfaces

The simulated weathering of some 13 sulfide minerals shows that dissolution is always incongruent, with variable but substantial amounts of elemental sulfur formed at the mineral surface. The amounts of sulfur formed at the surface as percent of the total analytically recovered sulfur vary from 21% (pyrrhotite) to 74% (chalcopyrite and zinc blende). Elemental sulfur in the solution phase is also measured by a very sensitive voltammetric technique, and it is found that the solutions to which the weathering mineral has been exposed are highly supersaturated with respect to elemental sulfur. Up to 1.21% of the total analytically recovered sulfur are found as elemental sulfur in the solution phase in the case of arsenopyrite. Full analytical details can be found in tabular form in appendix AIV. This clearly shows that the amounts of elemental sulfur on the mineral surface and even those in solution cannot be neglected and that the concentration of soluble sulfoxy-species may not be the

appropriate reaction progress variable to record when studying dissolution kinetics of sulfides.

The relative resistance to weathering of the studied minerals decreases in the following sequence : stibnite < orpiment < cinnabar < pyrite < bornite < enargite < zinc blende < arsenopyrite < chalcopyrite < galena. For most of the considered minerals, the resistance to weathering is found to be correlated with lattice energy.

4. References

Alpers C.N. and Blowes D.W. (Eds.) (1994) Environmental Geochemistry of Sulfide Oxidation, ACS Symposium Series 550; American Chemical Society, Washington.

Blaser P., Sposito G. and Holtzclaw K.M. (1984) Composition and Acidic Functional Group Chemistry of an Aqeous Chestnut Leaf Litter Extract. *Soil Sci. Soc. Am. J.* **48**, 278-283

Casey W.H. and Sposito G. (1992) On the temperature dependence of mineral dissolution rates. *Geochim. Cosmochim. Acta* **56**, 3825-3830

Cheah S.F., Kraemer S.M., Cervini-Silva J., Sposito G. (2003) Steady-state dissolution kinetics of goethite in the presence of desferrioxamine B and oxalate ligands: implications for the microbial acquisition of iron. *Chem. Geol.* **198**, 63-75

De Giudici G., Rossi A., Fanfani L. and Lattanzi P. (2005) Mechanisms of galena dissolution in oxygen-saturated solutions : Evaluation of pH effect on apparent activation energies and mineral-water interface. *Geochim. Cosmochim. Acta* **69**, 2321-2331

Filella M., Philippo S., Belzile N., Chen Y., and Quentel F. (2009) Natural attenuation processes applying to antimony: A study in the abandoned antimony mine in Goesdorf, Luxembourg. *Science of the Total Environment* **407**, 6205-6216

Furrer G. and Stumm W. (1986) The coordination chemistry of weathering: I. Dissolution kinetics of δ-Al_2O_3 and BeO. *Geochim. Cosmochim. Acta* **50**, 1847-1860

Good N.E., Winget G.D., Winter W., Connolly T.N., Izawa S. and Singh R.M.M. (1966) Hydrogen Ion Buffers for Biological Research. *Biochemistry* **5**, 467-477

Johansson L. (1974) The role of the perchlorate ion as ligand in solution. *Coordination Chemistry Reviews* **12**, 241-261

Laidlar K.J. (1987) Chemical Kinetics. Harper Collins, New York

Langmuir I. (1916) The Constitution and Fundamental Properties of Solids and Liquids. *J. Am. Chem. Soc.* **38**, 2221-2295

Lasaga A.C. (1984) Chemical Kinetics of Water-Rock Interactions. *J. Geophys. Res.* **89**, 4009-4025

Lengke M.F. and Tempel R.N. (2001) Kinetic rates of amorphous As_2S_3 oxidation at 25 to 40°C and initial pH of 7.3 to 9.4. *Geochim. Cosmochim. Acta* **65**, 2241-2255

Lengke M.F. and Tempel R.N. (2002) Reaction rates of natural orpiment oxidation at 25 to 40°C and pH 6.8 to 8.2 and comparison with amorphous As_2S_3 oxidation. *Geochim. Cosmochim. Acta* **66**, 3281-3291

Lengke M.F. and Tempel R.N. (2003) Natural realgar and amorphous AsS oxidation kinetics. *Geochim. Cosmochim. Acta* **67**, 859-871

Ludwig C., Casey W.H. and Rock P.A. (1995) Prediction of ligand-promoted dissolution rates from the reactivities of aqueous complexes. *Nature* **375**, 44-47

McGuire M.M. and Hamers R.J. (2000) Extraction and Quantitative Analysis of Elemental Sulfur from Sulfide Mineral Surfaces by High-Performance Liquid Chromatography. *Environ. Sci. Technol.* ***34*****,** 4651-4655

Nordstrom D.K, Alpers C.N., Ptacek C.J. and Blowes D.W. (2000) Negative pH and Extremely Acidic Mine Waters from Iron Mountain, California*. Environ. Sci. Technol.* **34**, 254-258

Nordstrom D.K. (2000) Advances in the Hydrogeochemistry and Microbiology of Acid Mine Waters. *Int. Geol. Rev.* **42**, 499-515

Quentel F. and Filella M. (2002) Determination of inorganic antimony species in seawater by differential pulse anodic stripping voltammetry: stability of the trivalent state. *Anal. Chim. Acta* **452**, 237-244.

Rimstidt J.D. and Dove P.M. (1986) Mineral/solution reaction rates in a mixed flow reactor: Wollastonite hydrolysis. *Geochim. Cosmochim. Acta* **50**, 2509-2516

Shannon, R.D. (1976) Revised Effective Ionic Radii and Systematic Studies of Interatomic Distances in Halides and Chalcogenides. *Acta Cryst.* **A32**, 751-767.

Sposito, G. 2004. The Surface Chemistry of Natural Particles. Oxford University Press, Oxford.

Ure A.M. and Davidson C.M. (2002) Chemical Speciation in soils and related materials by selective chemical extraction. In Chemical Speciation in the Environment, Ure, A.M.; Davidson, C.M., Eds., Blackwell Science, Oxford.

Chapter I

General Introduction :

Antimony

The main objective of the present thesis is to close some gaps in our knowledge concerning the rate of mobilisation of antimony from natural sources. In this introductory chapter, we review the atomic, physical and chemical properties, the occurrence, production, history, uses, toxicological properties and environmental speciation of antimony, as well as the available analytical techniques for the quantification of this element. Some theoretical aspects of mineral dissolution kinetics, viz. the origin of dissolution rate laws and activation energies and their interpretation are presented. Finally, crystallographic information pertaining to all the mineral phases used in the present thesis is included. In chapters II and III, the kinetics of oxidative dissolution of stibnite, the most important antimony ore and the most abundant antimony mineral will be explored in detail. In chapter IV, the effect of common low molecular weight organic ligands on stibnite dissolution kinetics is examined. The fifth chapter is dedicated to the principal weathering products of stibnite (senarmontite, valentinite and stibiconite). The dependence of their rates of dissolution on pH and temperature is investigated. In the final chapter VI, the mobilisation of Sb(V) from sediment and from pure phases representative of sediment constituents is studied. The mobilisation of antimony from contaminated soils has already been treated by Blay (2000).

I.1 Atomic Properties of Antimony

Antimony, Sb, has the atomic number 51, relative atomic mass 121.75(±3) and belongs to the 15th group of the periodic table, where it stands below arsenic and above bismuth. Its electronic configuration is $[Kr]4d^{10}5s^{2}5p^{3}$. There are two natural isotopes of Sb, of approximately equal abundance and both stable, ^{121}Sb 57.25% and ^{123}Sb 42.75% (Greenwood and Earnshaw, 1984) and at least 44 artifical and radioactive isotopes (Lide, 1996). Electronegativity values are given in table I.1, radii in table I.2 and ionization energies and electron affinities in table I.3.

Pauling	Mullikan	Allred
2.05	4.85	2.05

Table I.1 : Electronegativities of Sb (Dasent, 1982 ; Allred, 1961)

Atomic	Ionic Sb^{3+}	Ionic Sb^{5+}	Van der Waals	Covalent Sb(III)
140 pm	76 pm	60 pm	206 pm	141 pm

Table I.2 : Radii of Sb atoms and ions (Cotton and Wilkinson 1988 ; Shannon 1976) (ionic radii correspond to six-fold coordination)

1^{st} ionisation potential	2^{nd} ionisation potential	3^{rd} ionisation potential	Electron affinity
8.641 eV	16.53 eV	25.3 eV	1.05 eV

Table I.3 Ionisation potentials and electron affinity (Dasent, 1982)

I.2 Physical Properties of Antimony

Antimony exists in 4 allotropic forms:

(i) **Black antimony**, which is much more reactive than the ordinary form. It is obtained by condensing antimony vapour on clean glass surfaces in a high vacuum. There is no well defined transition

temperature of black antimony into the ordinary form. The material has semidconducting properties (positive temperature coefficient) (Krebs et al., 1955). It is oxidised by cold air and sometimes pyrophoric. On heating, it changes into ordinary antimony :

(ii) **Metallic (ordinary) antimony (α-Sb).** It is a silver grey, lustruous and brittle solid with metallic properties (from a chemical point of view, antimony has metallic and non-metallic properties, so that it is best classified as a semi-metal or metalloid). Its crystal structure is rhombohedral and consists of puckered hexagonal sheets of Sb atoms, stacked in layers perpendicular to the hexagonal c-axis. It is thus isostructural with α-As and α-Bi. α-Sb has a specific conductivity of 2.77 x 10^6 Sm^{-1} at 0°C (4.4% of that of silver). It melts at 630°C to give an opaque and conducting liquid and boils at 1325°C (Depending on the source, slightly differing values are sometimes found). Its density near room temperature is 6.697 gcm^{-3}. On solidifying, it contracts by 0.8% (Greenwood and Earnshaw, 1984), although some sources assert that an *expansion* actually occurs on solidification (Butterman and Carlin, 2004). According to Krebs and co-workers (1955), who cite an article by Hendus and Müller, the density of liquid antimony is slightly higher (6.504 gcm^{-3}) than that of the solid (6.490 gcm^{-3}).

(iii) **High pressure form I**. This is obtained from α–Sb at 50 kbar and it has a primitive cubic lattice (each Sb has 6 equidistant nearest neighbours).

(iv) **High pressure form II.** This obtained from the high pressure form I by increasing the pressure to 90 kbar. This form is hexagonally close-packed (each Sb has 12 nearest neighbours).

Both of these high pressure forms are not mentioned any more in the literature after 1950.

Yellow antimony was thought to be isostructural with white phosphorus and a separate allotrope; it is a transparent, yellow, covalent solid, soluble in CS_2. It may be prepared by the reaction of oxygen on liquid stibine at –90°C. It is very unstable. In light at –180°C and in the dark at –90°C, it changes into the black form. It was first obtained by Stock (Stock and Guttmann, 1904 ; Stock and Siebert, 1905), who took pains to show that the substance did not contain hydrogen. According to modern sources, yellow antimony is *presumably* a polymeric antimony hydride (Krebs et al., 1955 ; Lautenschläger and Schröter, 2005) and consequently no true allotrope. This view is based on the cited article by Krebs and co-workers, who fail to give crystallographic evidence, however.

Explosive antimony is obtained by high-current electrolysis of antimony trihalides. It changes explosively into the ordinary form on heating to 200°C, or sometimes on scratching. It contains some 10-15% of occluded

halide. Stock and Siebert (1905) hypothezised that this form was identical to their 'black antimony'. Krebs et al. (1955) showed that the halide is contained in chemically bound form, hence it is not a true allotrope. It is not identical to black antimony. Both yellow and explosive antimony are still sometimes listed as allotropes.

Antimony *vapour* consists of tetrahedral Sb_4 molecules, which are markedly dissociated, so that the average molecular formula is $Sb_{2.96}$ at 1572°C and $Sb_{2.68}$ at 1640°C (Greenwood and Earnshaw, 1984 ; Sidgwick 1950).

I.3 Chemical Properties of Antimony

Antimony forms compounds in the +III, +V, and –III oxidation states.

Metallic antimony is stable to air and moisture at room temperature. It is insoluble in hydrochloric and in dilute sulfuric acid. It is slowly attacked by hot concentrated sulfuric acid, yielding unstable antimonious sulfate, and it is converted by nitric acid into antimony(III)- or antimony(V)-oxide depending on the amount and concentration of the acid. The best solvent for antimony is aqua regia, which affords a solution of $[SbCl_6]^-$ (Vogel, 1937, Greenwood and Earnshaw, 1984). Sb reacts with oxygen under controlled conditions to give the oxides Sb_2O_3, Sb_2O_4 and Sb_2O_5. With chlorine, bromine and iodine, the trihalides SbX_3 are formed. Sb combines with sulfur on heating to form Sb_2S_3 ; hydrogen is without direct action (Greenwood and Earnshaw, 1984), even though the hydride

stibine (SbH_3, an exceedingly poisonous gas) exists, with Sb formally in the oxidation state –III. This can be prepared by the action of a reducing agent on aqueous solutions of Sb(III) or Sb(V). There are also antimonides such as Ag_3Sb or InSb, where Sb would have a formal oxidation state of –III. The aqueous chemistry of Sb is reviewed is chapter I.8.3

I.4 Economically Exploited Occurrences of Antimony

Antimony is concentrated in sulfide ores, along with Cu, Pb and Ag. Rarely, it occurs as native antimony associated with As, Bi or Ag. Sb also has a certain significance in gold prospecting since it is commonly associated with this element (Oelkers, 1998 and references therein) as well as with other metals of commercial importance[1] (Boyle and Jonasson, 1984). Antimony also occurs in crude oil to varying concentrations, reported to be up to 100 ppb (Shah et al., 1970; Colombo and Sironi, 1964). The most important (mined) ores of antimony are the sulfides stibnite Sb_2S_3 and jamesonite $Pb_2Sb_2S_5$, that are associated with their weathering products senarmontite and valentinite (cubic and orthorombic Sb_2O_3, respectively), stibiconite[2], cervantite[3], bindheimite ($Pb_2Sb_2O_7.xH_2O$), and

[1] Cu, Ag, Au, Zn, Cd, Hg, Ba, U, Sn, Pb, As, Bi, Se, Te, Nb, Ta, Mo, W, Fe, Ni, Co and Pt.

[2] the formula of stibiconite is sometimes given as $Sb^{III}Sb^{V}_2O_6OH$, or with substitution of Sb^{3+} by Ca^{2+} : $(Sb^{3+},Ca^{2+})_ySb^{5+}_{2-x}(O,OH,H_2O)_{6-7}$ (Vitaliano and Mason, 1952). Later, Stevens and co-workers (Stevens et al., 1993) presented a new formula for stibiconite, based on a ^{121}Sb-Mössbauer study of the mineral. Their derivation of the Sb(III)/Sb(V) ratio from areas of the Sb(III) and Sb(V) Mössbauer peaks is, however, faulty (Hoch, 2010), so that the formula originally given by Vitaliano and Mason seems preferable.

[3] Cervantite is the name given to a phase with the composition $Sb^{III}Sb^{V}O_4$. Vitaliano and Mason (1952) doubt the existence of this phase in nature, since all the alleged specimens of cervantite analysed by them turned out to be stibiconite. According to these authors, no anhydrous oxides

kermesite (Sb_2S_2O). Antimony deposits have formed from hydrothermal solutions at low temperatures and shallow depth. They typically occur as epithermal fissure or joint fillings, pegmatites, replacement lodes, or hot-spring deposits, which are not concentrated in rocks of any particular geologic age or type (Butterman and Carlin, 2004). Simple antimony deposits (consisting almost exclusively of antimony sulfide, which can be partially or completely oxidised to the above mentioned weathering products) are found in China, South Africa, the Confederation of Independent States (the former Soviet Union) and Bolivia. Complex deposits, consisting of of mixtures of antimony sulfide with sulfosalts of Fe, Cu, Pb, Hg, or Ag, are found in China, Australia, Canada and the U.S. Such deposits are often mined for other metals, but Sb can be an valuable by-product. World resources of Sb are in the range of 4 to 6 Mt ; by far the world's most important producer of Sb is China, with a production of about 10^5 tons/year, followed by the Confederation of Independent States, South Africa, Bolivia and Australia (all less than $2x10^4$ tons/year). Resources in the reserve base can provide antimony (at the rate of mine production in the year 2000) for another 30 years. (Butterman and Carlin, 2004).

---

of antimony other than senarmontite and valentinite exist in nature and they recommend that the use of the term cervantite be discontinued. Cervantite continues, however, to be a valid IMA species.

I.5 Production of Antimony

There are six methods commonly used to extract Sb from its ore. The method chosen depends on the type of ore (sulfide, oxide, or complex ore) and on its Sb concentration (Butterman and Carlin, 2004) :

(i) **Volatilization Roasting :** the sulfide is mixed with charcoal or coke and heated. Antimony oxides volatilise and are recovered. Sulfur is driven off as sulfur dioxide.

(ii) **Blast Furnace Smelting :** suitable for ore of intermediate grade and the most important process. The large amount of slag reduces losses of the metal by volatilization. The product is (impure) metal.

(iii) **Liquation :** suitable for high-grade ore (pure stibnite). The ore is heated in a reducing atmosphere to between 550 and 600°C. The molten stibnite is collected, which is used as is, or it is converted to the metal or the oxide.

(iv) **Reduction :** suitable for high-grade oxides. These are reduced under a cover of slag, which minimizes losses by volatilization and dissolves impurities. The product is (impure) metal.

(v) **Leaching & Electrowinning :** Sodium sulfide or hydroxide are used as 'solvent', which transforms the stibnite into soluble Na_3SbS_4. The leachate is then electrolysed and the metal deposited cathodically.

(vi) **Precipitation ('English process') :** molten sulfide ore or a leachate are treated by iron in a slight excess over the stoichiometrically required amount. The product is (impure) metal.

Antimony oxides produced by one of the above processes may be refined by sublimation of the crude oxide. Crude antimony metal is refined by heating the metal with stibnite or with a mixture of sodium sulfate and charcoal, which lowers iron and copper concentrations. Arsenic and sulfur levels may be reduced by covering the molten metal by a flux of sodium hydroxide or sodium carbonate and nitrate. Lead is more difficult to remove, but for a lot of applications, this is not necessary, as antimony will be alloyed with lead anyway.

A steadily decreasing amount of antimony is recovered from scrap, mostly from electrodes of scrap lead-acid batteries and other scrap lead alloys. Most secondary antimony is therefore processed at lead smelters into antimonial lead, for use in car batteries. With the advent of modern lead-acid batteries that use little or no antimony, the supply of scrap antimony has gradually decreased. US smelter production of secondary antimony has dropped from about 20000 tons/year in the 1950s to only about 8000 tons/year by 1999, when secondary antimony accounted for about 15% of the total US market supply (Butterman and Carlin, 2004).

I.6 History of Antimony

I.6.1 Discovery of antimony and etymology of the name

Antimony sulfide and the isolation of metallic antimony were already known in antiquity. An unknown object made of antimony (99% pure) dating to about 3000 BC was found at Tello (Girsu), Chaldea, which may have been either part of a vase or an item of jewellery (Shortland, 2002b), and an antimony plated copper object dating to 2500-2200 BC was found in Egypt (Kirk-Othmer, 2004). A cast antimony tube (99.7% pure), perhaps a bead, from a 3rd millennium context was found at Tell Leilan, as well as some antimony jewellery from Assur, dating to about 2000 BC, and some personal ornaments (probably buttons) from the Iron Age at Hasanlu in northwest Iran (Dyson, 1964; Shortland, 2002b). An antimony bead, consisting of 95% pure antimony, dating to 2300-2500 BC was found near Carchemish (Europus), an ancient city on the modern Turkish-syrian border (Shortland, 2002b). The bead was probably part of an item of jewellery and made by casting. Ancient antimonial bronzes (copper-antimony alloys) containing more than trace levels of antimony (i.e. showing that the addition of antimony was deliberate) are also known (Pike et al., 1996).

Finely ground stibnite was used by the Egyptians as black eye-shadow. Calcium antimony white ($Ca_2Sb_2O_7$) was used as a white pigment and opacifier, and lead antimony yellow ($Pb_2Sb_2O_7$) as a yellow pigment for glass by the Egyptians as early as 2000 BC. Both pigments were found to be synthetic. The origin of the antimony could be traced back to the Caucasus (Shortland, 2002a).

The first written account of the isolation of antimony is given by V. Biringuccio in the early sixteenth century (Biringuccio, 1540 ?). The discovery is often falsely attributed to either Georg Bauer (Latinised Georgius Agricola), who published his authoritative work on mining only in 1556 (Agricola, 1556), or to Basilius Valentinus[4], a benedictine monk and alchemist, author of the 'Triumphwagen des Antimons' (The Triumphal Chariot of Antimony) (Valentinus, 1604). In the 18th century, it became clear that B. Valentinus had never existed and that the book had been written by its editor, J. Thölde. Metallic antimony may already have been known to Abu Musa Jabir ibn Hayyan, a middle-eastern alchemist of Arab or Persian origins in the 8th century, whose works have not yet been completely translated (Dampier, 1961).

There is some uncertainty as to the etymology of the term 'antimony'. According to a very popular view, the word originates from the greek αντιμοναχοσ ('anti-monachos'), which would mean 'against the monk' or 'monk-killer'. A lot of alchemists were monks, and antimony is poisonous. Another etymology would be the hypothetical Greek αντιμονοσ, literally 'against one', meaning that antimony is not found as a (native) metal (Kirk-Othmer, 2004)[5]. According to von Lippmann (v. Lippmann, 1919-54), the word 'antimonium' is the Latinised version of the greek ανθημονιον, 'flower'. The term 'antimonium' is used in some translations of Arabic medical treatises by Constantine the African in 1050-1100 AD (v. Lippmann, 1919-54). Finally, 'antimonium' may be derived

[4] after whom the mineral valentinite (orthorhombic Sb_2O_3) is named.
[5] which is actually not the case, native antimony being a valid IMA species, with type locality Sala Silver Mine, Sala, Västmanland, Sweden.

from several different Arabic terms : « C'est le nom égyptien de l'antimoine (*mesdemet*) qui a donné lieu à la formation des noms grecs et latins de cette substance : en grec *stimmi*, en latin *stibium*, en arabe *ithmid* ou *athmoud*, transcrit *antimonium* dans les traductions barbaro-latines du moyen-âge »[6] (Sarton, 1935) (The author quotes a work by Max Meyerhof). The modern chemical symbol for antimony, Sb, was introduced by J.J. Berzelius in the 18th century, as an abbreviation for the Latin word 'stibi' (from the greek στιβι) meaning 'antimony', The adjective 'stibinus', meaning 'made of antimony' can be found in the Hieronymus Vulgate edition of the Bible, in the 1st Book of Chronicles (Biblia sacra, 1948)[7], though the word has never been translated in this sense and has, interestingly, completely disappeared from all the later editions of the Vulgate (Nova Vulgata, 1986). The word 'stibium' occurs in the 2nd book of Kings, chapter 9, verse 30 (Nova Vulgata, 1986)[8].

Historically, there is considerable confusion as to the meaning of 'antimony'. Until the late Middle Ages, 'antimony' could be taken to mean either the metal, or its sulfide (stibnite). In addition, metallic antimony was not always clearly recognised as a metal in its own right, but it was often confused with lead (Priesner and Figala, 1998).

---

[6] 'It is the Egyptian term for antimony (*mesdemet*) from which the Greek and Latin terms for that substance (*stimmi* and *stibium*, respectively) are derived. The arabic *ithmid* and *athmoud* were transcribed as *antimonium* in the Latin translations dating from the Middle-Ages.'

[7] 'ego autem (…) praeparavi impensas domus Dei mei (…) lapides onychinos et quasi stibinos et diversorum colorum (…).'

[8] 'Porro Iezabel, introitu eius audito, depinxit oculos suos stibio et ornavit caput suum et respexit per fenestram', where clearly stibnite, used as black eye shadow, is meant.

I.6.2 Early medical uses of antimony

In antiquity, antimonial preparations were used medically, in ophthalmological preparations and in salves to treat wounds and ulcers. Here, antimony acted as a bactericide. The German physician Paracelsus introduced the *internal* use of antimony compounds in the 16th century, and he thus triggered off a severe and long-lasting medical controversy. In France, for instance, antimonial preparations were officially forbidden from 1566 to 1666, when their prescription was allowed again, possibly because of an alleged cure of king Louis XIV by tartar emetic from a dangerous illness in 1657 (Thomson, 1926). Antimonials are highly toxic, but when administered in small doses and with due care, they act as laxatives, emetics and diaphoretics, and thus came to be regarded by some practitioners as something close to a panacea. Thus the physician A.J. Kirchweger (1790) stated, in his famous commentary on Basil Valentine's Triumphal Chariot, that antimony is the cure of any ailment : 'Es ist das Antimonium ein Subject, aus dem eine ganze vollständige Apotheke kann fabricieret werden, denn in ihm ist ein Vomitiv, eine Purganz, eine Blutreinigung, Schweiss- und Urinmittel. Er ist ein APERIENS und OBSTRUENS, er ist ein SOLVENS und COAGULENS, er ist ein Balsam, Unguent und Pflaster, IN SUMMA SUMMARUM, in allen und jeden Zuständen kann er appliciert werden CUM MAXIMO USU FRUCTU. Er ist ein Meister aller Krankheiten, ein Beschützer der menschlichen Natur, sofern ihn nur der Practicant recht appliciert, so ist seine VIRTUS UBIQUOTICA.' In 1866, Posner lists 12 antimonial preparations in his famous 'Handbuch' (Posner, 1886).

Commonly used antimonials included : butter of antimony ($SbCl_3$), algarot or mercurius vitae ($2SbOCl.Sb_2O_3$, an extremely violent emetic and laxative), glass of antimony (vitrum antimonii, prepared by cooling a melt of Sb_2O_3, considered to be the strongest emetic of all antimonial preparations), flowers of antimony (essentially valentinite, Sb_2O_3, formed by roasting of stibnite) and tartar emetic[9] (tartarus stibiatus, potassium antimonyl tartrate, $K_2[Sb_2(C_4H_2O_6)_2].3H_2O$) (Priesner and Figala, 1998). 'Pocula vomitoria' were tumblers made of metallic antimony, which were intended to be filled with wine and left for a while. Some antimony dissolved in the wine (no doubt in the form of tartrate complexes), which acted as an emetic when the wine was drunk. An interesting and highly entertaining description of these 'antimonyall cupps' (and other historical uses of antimony in medicine) is given by Thomson (1926). 'Pillulae perpetuae' ('perpetual pills') were metallic antimony pills which caused diarrhea when swallowed. These pills could be reused without end and often remained in a family for generations. Antimonials have also been tried againt syphilis (Filella et al., 2002a)

I.6.3 Early metallurgical uses

Stibnite was used in the separation of silver from gold. The silver-gold alloy was repeatedly molten in the presence of stibnite, to form a gold-antimony alloy in the bottom of the crucible, with concomitant formation of silver sulfide, which floated on top and could be decanted. The gold-antimony alloy was then

[9] The substance is still in use today in the treatment of schistosomiasis and leishmaniasis (Filella et al., 2002), though other organo-antimony derivatives that are better tolerated have been developed. See also the section on modern uses of antimony. It is the therapy of choice of schistosiomasis japonicum (Lauwers et al., 1990).

heated more strongly, so that the antimony was driven off as its oxide, leaving pure gold behind. Because of this use, antimony was given names such as 'lupus metallorum' ('wolf of the metals'), 'balneum regis' ('royal bath') or 'iudex ultimus' ('ultimate judge') (Priesner and Figala, 1998).

I.6.4 Antimony's importance in alchemy

Antimony and its compounds played prominent roles in alchemy, given their ability to 'purify' gold and their drastic effects when administered as a medicine. When stibnite is reduced by iron, the resulting antimony regulus often crystallizes with a typical star shaped pattern on its surface, termed 'stella antimonii' or 'antimonium stellatum'. This observation led alchemists to believe in a special relationship between antimony and the spheres of the stars. Since antimony is easily alloyed with gold, it was hoped that antimony would lead the way to the discovery of the philosopher's stone (Priesner and Figala, 1998). Common alchemical symbols for antimony are reproduced in Fig. I.1.

I.7 Contemporary Uses of Antimony

There is probably no other chemical element that has, at the same time, such an enormous technological importance, and yet is so widely unknown to the general public. A large amount of detail on antimony uses can be found in Butterman and Carlin (2004) and also Filella et al. (2002a).

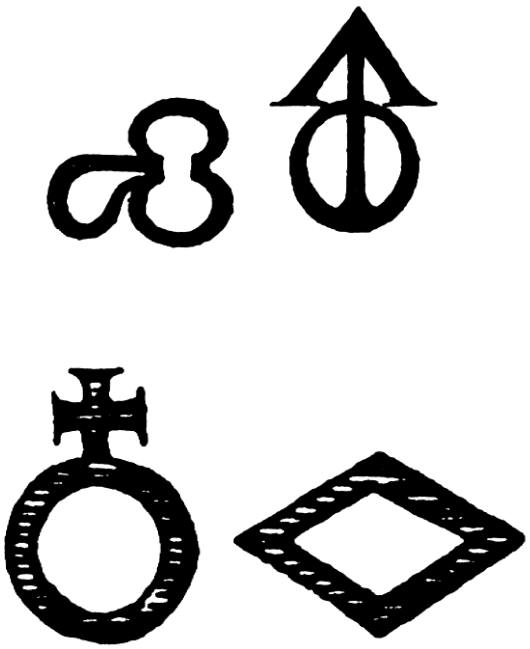

Fig I.1 Alchemical symbols for antimony (Didérot and d'Alembert, 1751-72)

I.7.1 Flame retardants

About 60% of the world consumption of primary antimony goes into the manufacture of flame retardants, where antimony(III)-oxide, antimony(V)-oxide or sodium antimonate are used. It can be found in a huge variety of goods : children's clothes, carpets, mattresses, toys, aircraft and automobile seats, fibreglass composites and differents types of plastics (e.g. PVC sheathing of cables) and even paper, to name but a few. The weight of the trioxide in polymers ranges from 1.5 to as much as 12%, in paper up to 25% and up to 30% in rubber. As a flame retardant, the antimony compounds are often combined with halogenated organic compounds. The mechanism by which antimonials act as flame retardants has not yet been elucidated. They may act by cooling by means of endothermic processes, by forming a layer of insulating

char, by diluting the reactant gases and by acting as radical scavengers and by endothermic formation of SbOCl and $SbCl_3$.

I.7.2 Metallic uses

(Butterman and Carlin, 2004) These account for some 20% of the world production. Early lead-acid automotive batteries used antimonial lead as plate grid materials. The advantages were : good strength, corrosion and creep resistance and a simplification of the casting of the grids. There were, however, also disadvantages, such as a lowering of the hydrogen overvoltage on the negative electrode. Generation of hydrogen consumed water, so that the battery needed regular topping up with water. A further problem was the increased self-discharge of the battery. In modern low-maintenance batteries, grids of calcium-lead, which does not have the above mentioned disadvantages, replace antimonial lead. In non-automotive batteries, antimonial lead grids, which contain some 11% of antimony, are still in use.

Antimony is a component in Babbitt metal alloys used for sleeve and friction bearings, it is an important constituent of soft solders, and it has long been used as a hardener for lead in small arms ammunition (containing typically 1% antimony) and in tracer ammunition and buckshot. For reasons of environmental pollution, lead in ammunition is gradually replaced by other metals (e.g. tungsten, steel, or bismuth-tin alloys) so that the use of antimony in ammunition, too, is receding.

Antimony in amounts up to 1% is alloyed with lead for the manufacture of cable sheathings, especially when the cable is intended for environments in

which it will be subjected to repeated flexing or vibration. Wrought lead-antimony containing between 8 and 12% antimony is well resistant to corrosion and finds use in building construction (flashing, gutters, moisture barrier pipes, roofing).

Industrially, alloys of lead containing up to 15% antimony are used where protection against corrosive liquids (e.g. hot sulfuric acid) is required. Lead used for radiation shielding contains 4 to 6% antimony, and collapsible tubes for the packaging of pastes contain between 1 and 4% antimony. Casting alloys consisting of tin, lead and antimony, such as pewter, Britannia metal, type metal etc. possess low melting points, good fluidity when molten, high hardness and solidify with little or no shrinkage. Fusible alloys used in fire safety devices likewise contain antimony. Very small amounts of antimony (<0.1%) are added to copper alloys such as admiralty brass, naval brass, leaded muntz metal to prevent loss of zinc. Antimony in amounts of 50 ppm nodularizes graphite in ductile iron. 0.05% antimony added to cast iron stabilises the carbide content. Antimony is added to alloys with low tin content for the manufacture of organ pipes. In the Chinese province of Keichow, a coin made of antimony was issued in 1931. Because of considerable wear, antimony never became popular as a coinage metal.

I.7.3 Non-metallic uses

These account for the remaining 20% of the world production :

I.7.3.1 Semiconductors and electronic devices.

Antimony is used in one process for the manufacture of rewritable digital video discs, as a dopant for high conductivity n-type Si wafers, in diodes, IR

detectors and Hall devices. In the 1950's, beads of lead-antimony dopant were used in the emittors and collectors of NPN alloy junction transistors. Prototypes of the novel, so-called phase change memory devices, which have not yet attained the commercial stage, are made of Ge:Te:Sb alloys in the stoichiometric proportions 2:5:2. Tin oxide doped with antimony is used to make electroconductive pigments.

I.7.3.2 Plastics additives and catalysts.

Antimony mercaptides are effective heat stabilizers for PVC. They compete with other families of stabilizers, e.g. organo-tin mercaptides, that are more efficient and insensitive to light.

A much more important use of antimony oxide, triacetate or various glyconates is as a condensation catalyst in the manufacture of PET, a large-volume commodity plastic used in drinks bottles, films, food packaging etc. Alternatives are germanium oxide, which is very expensive but gives a better transparency of the polymer, and titanium alkoxides, that cause yellowing of the product. Recent interest in the leaching behaviour of antimony from PET bottles (Shotyk et al., 2006) and from trays for ready-to-eat meals (Haldimann et al., 2007) has prompted investigations into the speciation of antimony in PET (Martin et al., 2010; Takahashi et al., 2008). PET typically contains 300 to 400 ppm antimony. XANES analysis revealed that antimony was present in both oxidation states Sb(III) and Sb(V), in variable proportions. EXAFS showed that some antimony was present as Sb_2O_3 and that nearest neighbours of Sb were oxygens with a coordination number of about three, consistent with the assumption that

Sb may be present as Sb glycolate or Sb glycolate binding to an end group of the PET polymer. No correlation between leaching behaviour and antimony speciation could be detected, suggesting that the leaching occurs as a result of the degradation of the PET itself.

I.7.3.3 Medical uses.

Antimony(V) compounds such as meglumine antimonate (trade name 'glucantime') and sodium stibogluconate ('pentostam') are the treatments of choice in major tropical protozoan diseases (e.g. leishmaniasis, schistosomiasis, ascariasis, trypanosomiasis and bilharziasis). Potassium antimonyl tartrate ('Tartar emetic') still is the treatment of choice of schistosiomasis japonicum (Lauwers et al., 1990). In veterinary practice, glucantime is also used against leihmaniasis in domestic animals. Lithium antimony thiomalate ('anthiomaline') is a skin conditioner for ruminants. Generally, antimonials have a nourishing and conditioning effect on keratinized tissue. $SbCl_3$ was used as a dehorning agent in cattle.

I.7.3.4 Other uses

These include antimony sulfide in the heads of safety matches, antimony in conjunction with Be as a startup neutron source in nuclear reactors and the use of antimony oxide in the manufacture of glass (it acts as decolouriser by countering the green tint caused by iron impurities and it protects the glass against discolouration caused by exposition to sunlight or fluorescent light). Antimony sulfide, together with other compounds, can be used as a glass colorant to yield amber, green or red glass. In the ceramic industry, mixtures of

antimony oxide with other metal oxides are used as pigments : with tin oxide, grey to blue colours, and with titanium oxide, a yellow colour are obtained. Antimony oxide or sodium antimonate, together with titanium dioxide, are used as opacifiers in vitreous enamel. Antimony oxide was used as a weathering resistant white pigment for exterior paints. Significant quantities are still used as antisolarant (colour stabilizer) in paints. Pigments made from the trisulfide and the pentasulfide are used for colouring rubber (black, yellow, orange, red). Antimony tetroxide, Sb_4O_8, is used as an oxidation catalyst, particularly for the dehydrogenation of olefins. Further, antimony sulfide is used in automotive tires and in brake linings. The latter two uses, together with the exhausts from diesel automobiles, contribute to the antimony contamination observed along motorways and in urban areas (Furuta et al., 2005; Gomez et al., 2005; Amereih et al., 2005 ; Zih-Perényi et al., 2010).

I.8 Antimony in the environment

We will briefly review the occurrence of antimony in the different geochemical compartments :

I.8.1 Rocks

Antimony is a rare element, occurring to an average of 0.2 ppm in the earth's crust. It is thus the 63rd most abundant element, ranking below Sn, As and the lanthanides, but above Bi, Hg and Ag (Butterman and Carlin, 2004). For its abundance in different types of rock, cf. Table I.4.

Ultramafic rocks	0.1 ppm
Mafic rocks	0.1-0.2 ppm
Intermediate rocks	0.x ppm
Acid rocks	0.2 ppm
Acid volcanic rocks	0.2 ppm
Argillaceous sediments	1.2-2.0 ppm
Shales	0.8-1.5 ppm
Sandstones	0.05 ppm
Limestones, dolomites	0.3 ppm

Table I.4 : Abundance of Sb in rocks

I.8.2 Soils and sediments

The estimated average abundance of Sb in soils is about 0.9 to 1 ppm (Kabata-Pendias and Pendias, 1992). In an attempt to establish background concentrations, Amereih and co-workers (Amereih et al., 2005) analysed samples from Lungau (Austria), an alpine region with negligible traffic or other sources of pollution and found averages of 0.64 to 0.81 ppm, in fair agreement with Kabata-Pendias's estimates. Concentrations in polluted areas, e.g. around mining and smelting sites, may be larger by many orders of magnitude. Thus, Hammel and co-workers (Hammel et al., 2000) found concentrations up to about 500 ppm in agricultural soils contaminated by centuries of mining activities in the Nordpfälzer Bergland (Palatinate Forest, Germany). In the soils of shooting ranges, Sb concentrations of up to 10% (!) have been measured (Scheinost et al., 2006, and references therein). Sb, along with As, appears to be weakly correlated with the fine solid phase of the deep horizons and seems to be somewhat enriched in the upper horizons (Sterckemann et al., 2004).

One of the first studies of antimony in sediments is a classic paper by Crecelius and co-workers. Analysis of surface sediment from the Puget Sound

revealed strong contamination by arsenic and antimony (and other metals) originating from a nearby copper smelter. Non-contaminated Puget Sound sediment contained 0.3-1 ppm Sb (on a dry weight basis), a range typical for fine-grained sedimentary rocks and deep sea sediment. In the contaminated area, concentrations rose up to 10000 ppm of arsenic and antimony. Chemical extractions showed that about 50% of arsenic and antimony were 'associated with extractable iron and aluminium compounds'. Antimony and arsenic were strongly correlated (Crecelius et al., 1975). Brannon and Patrick studied the release of antimony from contaminated and artificially amended (by potassium antimonyl tartrate, trivalent Sb) river sediment. They corroborated the finding of Crecelius that Sb, whether native or added, was associated with relatively immobile iron and aluminium phases. In their long-term experiments, the largest released amounts of Sb occurred early in the leaching experiments, suggesting that Sb release from contaminated sediment is more likely to occur during the first few months of the sediment-water interaction. During aerobic leaching, Sb moved in a more unavailable sediment phase. Evolution of volatile Sb species was also noted from sediments under unaerobic conditions (Brannon and Patrick, 1985). The high affinity of Sb(III) for hydrous oxides of Fe, Al and Mn was demonstrated by sorption experiments by Thanabalasingam and Pickering (Thanabalasingam and Pickering, 1990). The amount adsorbed onto each hydrous oxide phase was found to decrease strongly above pH>6. Experimental sorption capacities at pH 6-7 were 160 $mmolkg^{-1}$ for MnOOH, 45 $mmolkg^{-1}$ for FeOOH and 33 $mmolkg^{-1}$ for $Al(OH)_3$. Mok and Wal (Mok and Wal, 1990)

examined the mobilization of Sb from sediment from the Coeur d'Alene river (Idaho, US) and they found that Sb was more strongly retained in those sediments that contained more iron and manganese oxides. They also noted a pH dependence of the antimony leaching, with higher leaching being obtained at very low and at very high pH. An enrichment of Sb in crusts of manganese and iron oxides in Lake Baikal sediments has been reported (Müller et al., 2002). Finally, amorphous forms of iron and manganese oxyhydroxides were not only found to adsorb Sb(III), but also to oxidise it effectively and completely into Sb(V) within a few days (Belzile et al., 2001). The ready sorption of antimony to hydrous ferric and manganese oxides plays an important role in the natural attenuation of contaminated mine waters. In the absence of hydrous ferric oxides, contamination of rivers and streams receiving mine drainage can be expected for several kilometres to hundreds of kilometres downstream (Craw, 2008). We analysed sediment samples from the water bodies receiving the drainage from the antimony mine in Goesdorf, Luxembourg (see Appendix AII). The location of the mine and the different sampling points are shown in Fig. I.2

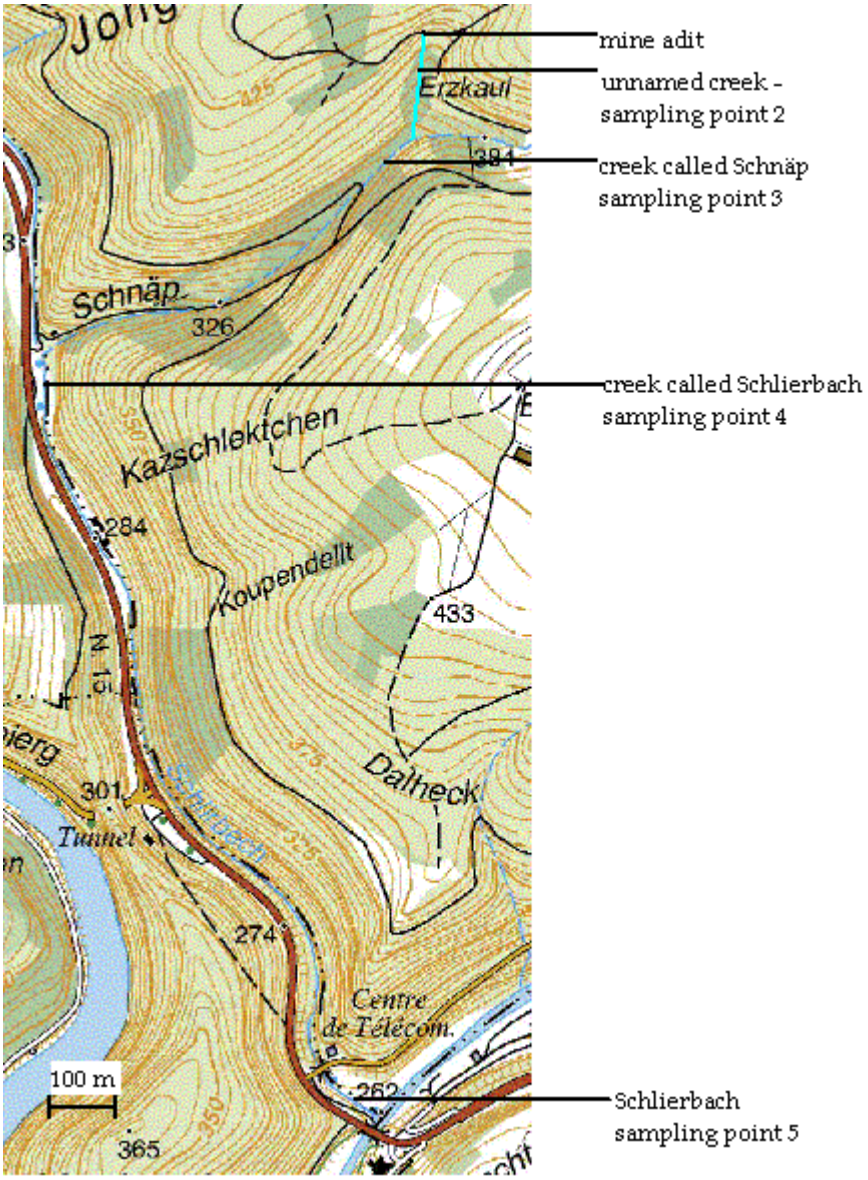

Fig. I.2 Map showing the creeks receiving the drainage from the antimony mine in Goesdorf, Luxembourg.

The analyses were carried out according to the BCR sequential extraction scheme (Ure and Davidson, 2002). Results in Fig. I.3 are the total Sb concentrations of the first three stages of the BCR extraction (i.e. *without* the so called residual fraction).

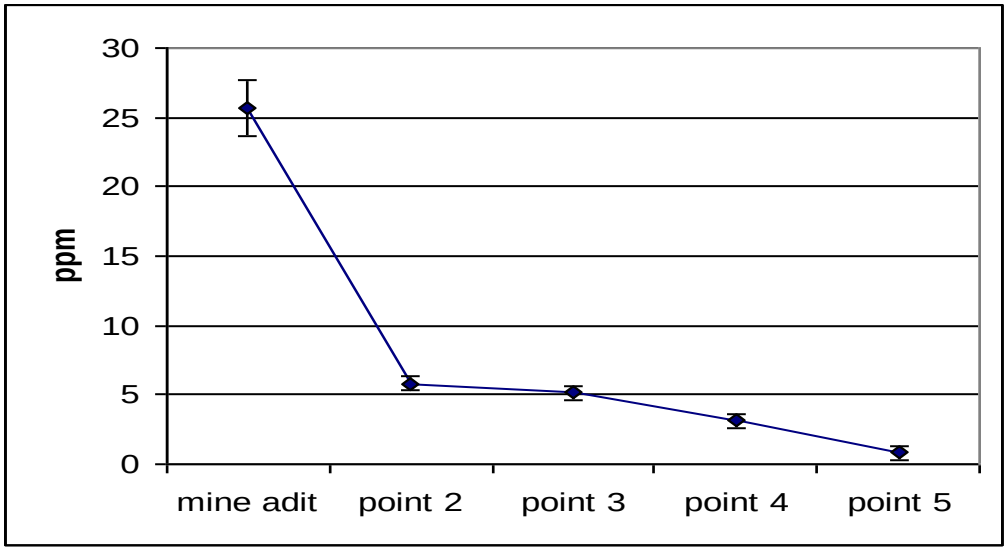

Fig. I.3 Total Sb in sediment samples in the mining area of Goesdorf, Luxembourg

As can be seen, the sediment antimony concentrations decrease with distance from the source of the pollution; the decrease being most marked over the first 100 m (from 25.7 ppm in the adit to 5.8 ppm in the unnamed creek receiving the mine drainage). At the confluence of the river Schlierbach and the river Sûre, the antimony concentration in sediment has effectively dropped to a value (0.8 ppm) close to the background (0.7 ppm) measured in a nearby similar river with no specific antimony pollution (the river Wiltz, in the north of Luxembourg, sampled in the village of Winseler). The BCR scheme was developed by the European Community's Bureau of Reference in order to improve comparability between sequential extraction results obtained by different laboratories and to simplify the extraction protocol as much as possible. The protocol was subsequently refined through two sets of interlaboratory trials. The four stages are summarized in Table I.5 :

	Extractant	**Fraction**	**Target phase(s)**
Step 1	0.11 M CH_3COOH	Exchangeable, acid and water soluble	Soil solution, exchangeable cations, carbonates
Step 2	0.1 M $NH_2OH.HCl$ at pH=2	Reducible	Fe and Mn oxyhydroxides
Step 3	H_2O_2 then 1 M CH_3COONH_4 at pH=2	Oxidisable	Organic matter and sulfides
Step 4	Aqua regia	Residual	Non-silicate minerals

Table I.5 Summary of the BCR sequential extraction protocol

The scheme is, like any other sequential extraction procedure, controversial. Thus, it was found by Fernandes and co-workers (Fernandes et al., 2004) that while the scheme was suitable for As, Pb and Cd, it was not for Co, Cu, Cr, Zn and Ni in as far as total concentrations measured by the BCR method did not agree with those obtained by INAA or total digestion methods for the latter five elements. It has also been pointed out that the scheme suffers from a certain degree of non-specificity (although the same more or less applies to all sequential extraction schemes) (Whalley and Grant, 1994; Coetzee et al., 1995) and possible analyte redistribution during the extraction steps (Raksasataya et al., 1996).

From our own study of sediments (see Appendix AII) taken from the Goesdorf site and the rivers receiving the mine waters[10], we can conclude the following :

[10] Two control samples were included in the study. In both cases, sediment from the nearby river Wiltz in northern Luxembourg was sampled. A first sample was collected in the village of Winseler, which can be regarded as essentially non-polluted. A second sample was taken in the town of Wiltz, where the river suffers mild industrial (but not specifically antimony) pollution.

- Sb in the reducible fraction (step 2) is strongly correlated to the sum of Mn+Fe in this same fraction,
- Sb in the reducible fraction is also strongly correlated to total[11] Al,
- Total Sb and total Al are very strongly correlated,
- Total Sb and total Pb are very strongly correlated,
- With one exception (sampling point 4), most of the total Sb is invariably found in the reducible (second) fraction (see fig. I.3 below)

This confirms the earlier observations by Crecelius (Crecelius et al., 1975), Brannon and Patrick (Brannon and Patrick, 1985), Blay (Blay, 2000), Müller (Müller et al., 2002), Sterckemann (Sterckemann et al., 2004) and Chen (Chen et al., 2003) that Sb is preferentially associated with Fe, Mn and Al phases.

Little is known on the actual speciation of Sb in soils and sediments. In his Ph.D. thesis in 2000, Blay investigated the sorption behaviour of both Sb(III) (as potassium antimonyl tartrate and antimonious acid) and Sb(V) (as potassium hexahydroxyantimonate) on a variety of separate soil phases and their subsequent mobilisation by natural ligands (Blay, 2000). The phases included in the study were hematite, goethite (representative of ferric oxide phases), cryptomelane (representative of manganese oxide phases) and the clay minerals montmorillonite, illite and kaolinite.

These two control samples showed the same general behaviour under the BCR scheme as the samples from the Goesdorf area.

[11] By total concentrations, we mean here the sum of the 1st three BCR fractions.

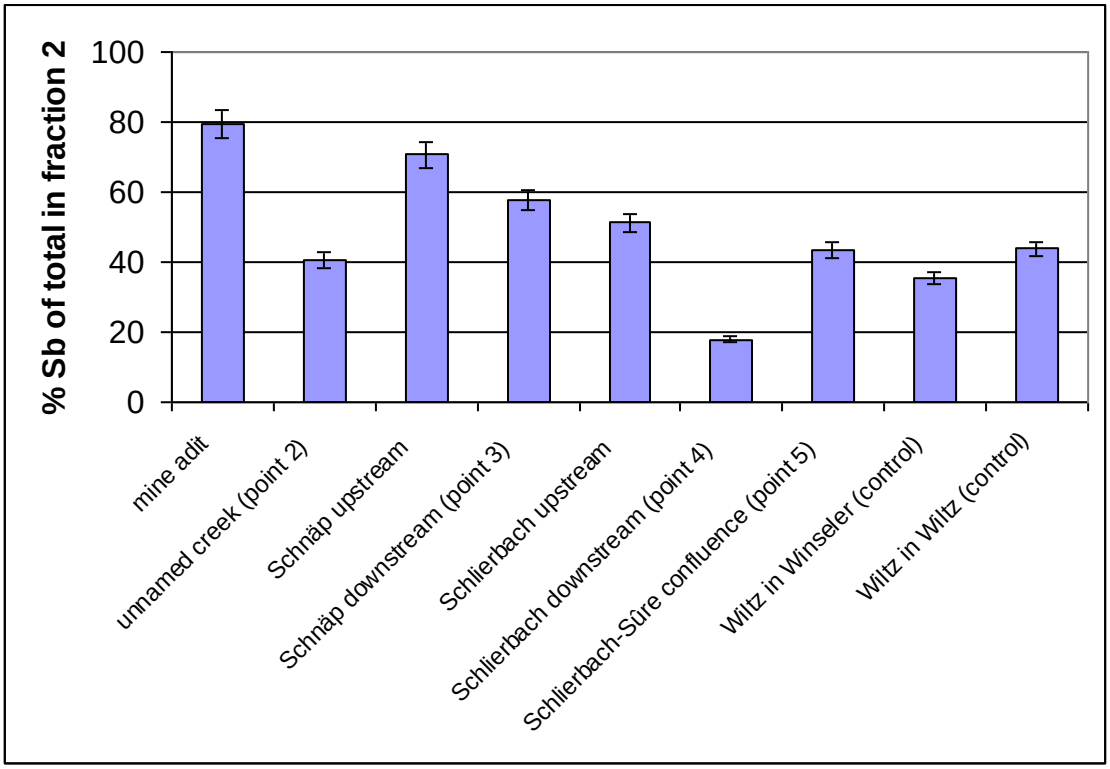

Fig. I.3 Percentage of total Sb in fraction 2 of the BCR sequential extraction.

The adsorption was modelled by Freundlich, Langmuir and Temkin isotherms and adsorption envelopes (extent of adsorption as a function of pH) were obtained. With regard to the extent of adsorption, it was found that montmorillonite adsorbed none of the antimony phases to a significant extent and that ferric oxide phases adsorbed Sb(III) most strongly. Sb(V) was adsorbed most strongly on illite. From the adsorption envelopes, Blay concluded that Sb(III) forms inner-sphere complexes with the ferric oxide phases. On montmorillonite and kaolinite, both inner-sphere and outer-sphere surfaces complexes seem to be formed, given the strong pH dependence of the adsorption on the one hand, and the fact that only part of the adsorbed antimony could be remobilised by phosphate. With regard to adsorption kinetics, adsorption from solutions of antimonyl tartrate and $K[Sb(OH)_6]$ onto ferric oxide

phases was very rapid, with equilibrium being reached after a few minutes. With regard to redox chemistry, Mn(IV) under the form of cryptomelane oxidised all of the Sb(III) to Sb(V) within a few days. Sequential extraction of contaminated soils revealed that most of the antimony was bound within the reducible fraction (in agreement with our own findings using contaminated river sediment). Finally, the mobilising capability of various organic ligands was examined, with the results that amino acids mobilised very little of the adsorbed Sb, while hydroxycarboxylic and oxocarboxylic acids mobilised much more Sb.

Sorption of Sb(III) and Sb(V) on goethite was investigated by Leuz and co-workers (Leuz et al., 2006). Sb(III) strongly adsorbs on goethite over a wide pH range (3-12) whereas maximum adsorption of Sb(V) occurs below pH 7. Within days, Sb(III) sorbed to goethite was oxidised to Sb(V).

In their EXAFS study on the speciation of antimony in shooting-range soils, Scheinost and co-workers (Scheinost et al., 2006) were able to give details on the binding of Sb to iron oxide phases : they found evidence for the presence of edge-sharing and bidentate corner-sharing linkages between $Sb^{V}(O,OH)_6$ and $Fe(O,OH)_6$ octahedra (cf. Fig. I.4). Similar structural units exist in the mineral tripuhyite ($FeSbO_4$), but the absence of Sb neighbours contradicts its presence in their soil samples. The species identified by EXAFS thus consists of inner-sphere sorption complexes with edge- and corner-sharing configurations occurring simultaneously.

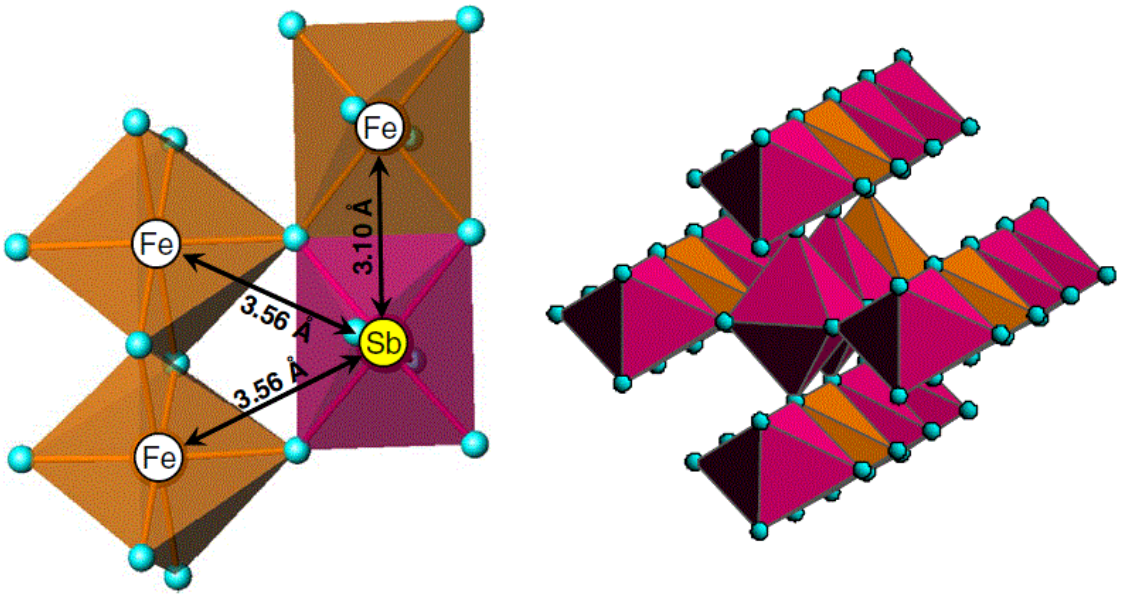

Fig. I.4 Coordination environment of Fe and Sb in the soil samples examined by Scheinost (left) and structure of tripuhyite. Image taken from Scheinost et al., 2006.

Mitsunobu and co-workers (Mitsunobu et al., 2010) essentially confirmed the formation of inner-sphere complexes of Sb(V) sorbed onto ferrihydrite and goethite (by EXAFS), but they noted that in co-precipitated samples, there were features in the EXAFS that differed from those of the adsorbed samples. The EXAFS simulation indicated that Sb(V) was actually structurally incorporated (heterovalent substitution) into the ferrihydrite or goethite matrix. They also detected such incorporations in natural samples from contaminated soils near mine tailings. Majzlan et al. (2011) give a detailed account of ternary mineral formation in a tailing impoundment and show that mobilised antimony is effectively retained by hydrous ferric oxide phases. Grains with little Sb are shown to be Goethite, those in which Sb dominates are poorly crystalline tripuhyite. The cited paper clearly demonstrates that iron oxide phases are able to decisively retard the mobilisation of Sb (in contrast to As).

A few studies exist on the interactions of Sb with humic acid. Thus, Sb(III) from either solutions of potassium antimonyl tartrate or antimonious acid was found to be adsorbed onto humic acid following a Langmuir type isotherm. Saturation capacities were estimated to be 23 μmol g^{-1} and 53 μmo lg^{-1}, for $Sb(OH)_3$ and antimonyl tartrate, respectively. The humic acid used was a commercial sample, purified according to a literature procedure (Pilarski et al., 1995). The binding of Sb(III) to commercial humic acids (of terrestrial, coal and aquatic origin) were measured by Buschmann and Sigg (Buschmann and Sigg, 2004) as a function of pH by dialysis experiments. Maximum binding to two of the humic acids (Aldrich Humic acid, of terrestrial origin, and Suwannee river humic acid) was found to occur at pH=6.1. Sorption onto Leonardite (coal-type) humic acid showed no pH dependence up to pH=6, but decreased at pH>6. Chemical modelling of the binding suggests that two types of bonding sites are involved : phenolic groups forming neutral complexes with Sb(III) and carboxylic functions forming negatively charged complexes with Sb(III). For the photosensitised oxidation of Sb(III) to Sb(V) by NOM (Buschmann et al., 2005), see also section I.8.3.5. Steely and co-workers (Steely et al., 2007) demonstrated complexation of Sb by humic acid molar mass fractions isolated from contaminated orchard soil by size-exclusion chromatography-ICP-MS and IC-ICP-MS. They also found evidence for the oxidation of Sb(III) to Sb(V) by *soil* humic acid, thus corroborating the findings of Buschmann (see above). Humic acid thus arrests the mobility of antimony in soils by complexation and contributes to its conversion into less toxic Sb(V). These findings were confirmed by Oorts and co-

workers, who found that in soil amended with Sb_2O_3, more than 70% of total Sb was present in the pentavalent form after 2 days (Oorts et al., 2008). An up-to-date review of the behaviour of antimony in soils, including comparison to its congener arsenic, was published by Wilson and co-workers (2010).

I.8.3 Natural waters

I.8.3.1 Concentrations in natural waters

In seawater, the mean antimony concentration is given as 184±45 ngl^{-1}. In unpolluted surface fresh waters, the Sb concentration is typically below 1 μgl^{-1}, although in some natural geothermal systems, concentrations up to 10% have been observed (Filella et al., 2002b). In an attempt to establish a reference level of Sb in pristine groundwater from Springwater Township, Ontario, Canada, Shotyk found a maximum concentration of 5 ngl^{-1}, and an average of 2.2±1.2 ngl^{-1} (n=34) and an Sb:Sc ratio of 1:4, which exceeds the crustal ratio (1:45) by an order of magnitude, implying a natural enrichment of Sb in pristine groundwater relative to its abundance in crustal rocks (Shotyk et al., 2005b). The studied groundwater had been in contact with dolomite and calcite. Nirel and co-workers (Nirel et al., 2008) have found a significant dependence of the antimony concentration on the lithogenic origin of the groundwater. 900 samples from the Swiss canton of Geneva had been analysed and showed that rivers draining crystalline zones carried 0.13 μgl^{-1} (median value) antimony, compared to 0.08 μgl^{-1} for waters draining carbonate-rich zones and 0.16 μgl^{-1} for waters draining molasses derived from the Alps.

I.8.3.2 Redox speciation

From a thermodynamic point of view, Sb should be entirely present in the pentavalent state in oxic solutions (cf. Figs. I.5 and I.6). However, Sb(III) is remarkably inert with respect to oxidation under oxic conditions. In a lot of natural, oxic systems (e.g. river and sea water), substantial proportions of Sb(III) are found (Quentel and Filella, 2002). This can be explained by the very slow redox kinetics of the Sb(III)/Sb(V) couple. Leuz and co-workers for instance found that no significant oxidation of trace Sb(III) by O_2 between pH 3.6 and 9.8 could be observed within 200 days (Leuz and Johnson, 2005).

Analysis of samples from the Baltic sea showed that, in sea water, low concentrations of Sb(III) are detected below the surface layer, and an increase in the anoxic zone. Sb(III) accounts for up to 44% of total Sb in the anoxic zone, only in the deepest sample does this percentage increase to 93% (Andreae and Froelich, 1984).

In aqueous solution, both Sb(III) and Sb(V)

are extensively hydrolysed. Sb(III) is present in strongly acid solution (pH up to 2) as $[Sb(OH)_2]^+$. Between pH 2 and 11, the electrically neutral 'antimonious acid' $Sb(OH)_3$ prevails, while at pH>11, the tetrahydroxyantimonite anion $[Sb(OH)_4]^-$ is formed. From acidic solutions containing Sb(III), sparingly soluble basic salts precipitate upon dilution. For Sb(V), the hexahydroxyantimonate $[Sb(OH)_6]^-$ is the dominant species at all pH values, except under very strongly acidic conditions, where $[SbO_2]^+$ exists.

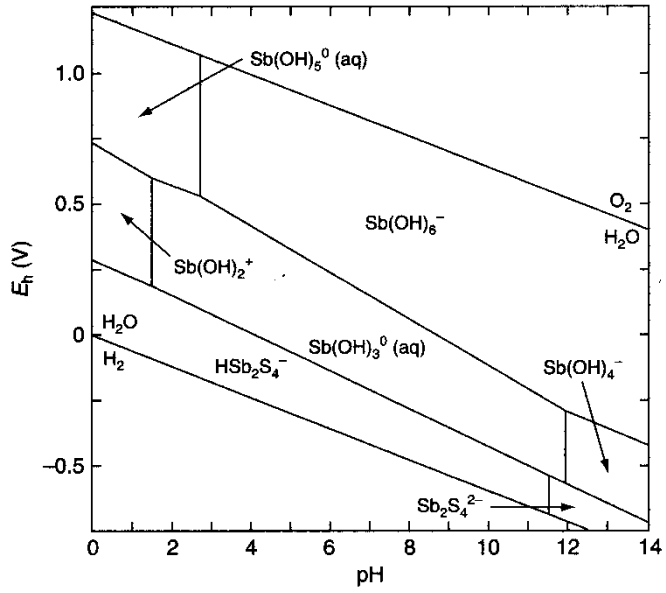

Fig. I.5 Eh-pH diagram of the aqueous speciation of Sb, calculated at 25°C and concentration of $10^{-14.6}$ moll^{-1} of total dissolved Sb. From Krupka and Serne, 2002

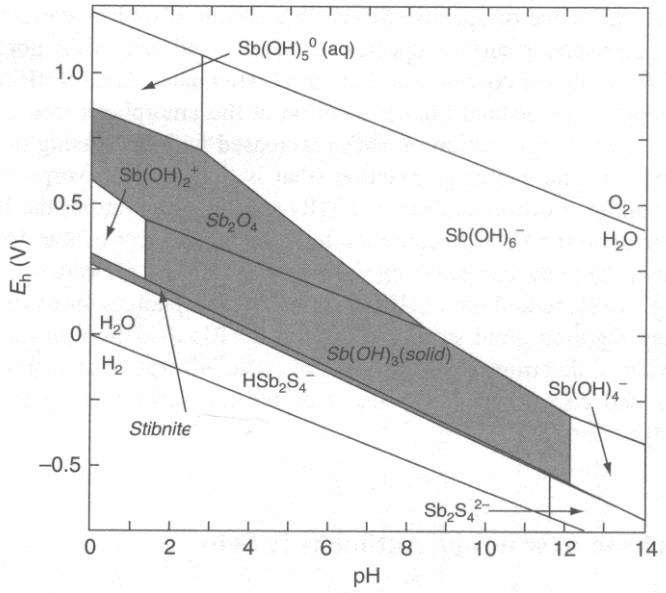

Fig. I.6 Eh-pH diagram of the aqueous speciation of Sb taking into accont important solid phases. Calculated at 25°C and 10^{-7} moll^{-1} total dissolved Sb. From Krupka and Serne, 2002.

At concentrations higher than 1 mM, Sb(V) undergoes polymerisation to form polynuclear species such as $Sb_{12}(OH)_{64}^{4-}$ and $Sb_{12}(OH)_{66}^{6-}$ (Arai, 2010). There exist, however, no polymerised species of Sb(III). The statement that Sb(V) is well soluble in oxic environments and hence that Sb(V) is a mobile element in the environment is often found and persists even in the modern literature (Arai, 2010). A report prepared for the US Department of Energy in 2002 explicity states : 'Antimony concentrations in soils under oxidizing conditions are not limited by solubility reactions. (…) Therefore, under basic pH and oxidizing conditions, antimony should be highly mobile in the geochemical environment' (Krupka and Serne, 2002). The solubility, however, *is* controlled by phases such as mopungite $Na[Sb(OH)_6]$, brandholzite $Mg[Sb(OH)_6]_2{\cdot}6H_2O$, bottinoite $Ni[Sb(OH)_6]_2{\cdot}6H_2O$, bindheimite $Pb_2Sb_2(O,OH)_7$, romeite $Ca_2Sb_2(O,OH)_7$, stetefeldtite $Ag_2Sb_2(O,OH)_7$, bismutostibiconite $BiSb_2O_6OH$, stibiconite $SbSb_2O_6OH$ and the relatively abundant tripuhyite $FeSbO_4$. Recently reported solubility products of $Ca[Sb(OH)_6]_2{\cdot}6H_2O$ and $Pb[Sb(OH)_6]_2{\cdot}6H_2O$ (Johnson et al., 2005) are in error, as any attempt to synthesize these salts yields romeite and bindheimite (Diemar, 2008). Solubility data for mopungite exist, and the solubilities of brandholzite, bottinoite, romeite and bindheimite Majzlan have recently been measured by Diemar and co-workers (Diemar et al., 2009) and it was concluded that Sb(V) is actually environmentally quite *immobile*. et al. (2011), in their study of tertiary minerals in tailings impoundments contaminated by Sb and As, also report that antimony is very effectively retained by hydrous ferric oxides, in contrast to As.

I.8.3.3 Chloro-complexes

In chloride-rich solutions, the antimony(III) speciation is dominated by complexes such as $SbCl^{2+}$, $SbCl_2^+$ and $SbCl_3$ in acidic solution (Oelkers et al., 1998). For a more recent XAFS and solubility study of the speciation of Sb(III) in saline acidic waters at high temperatures and pressures, see Pokrovski et al., 2006. These authors identified the species $Sb(OH)_3Cl^-$, $Sb(OH)_2Cl$, $Sb(OH)Cl_2$ and $SbCl_3$ in their solutions at temperatures ranging from 300 to 600°C and pressures of 600 bar, and calculated equilibrium constants for their formation.

Not much is known on the interaction of Sb(V) with chloride ; in strongly acid solution $[SbCl_x]^{-x+5}$ species seem to be formed, whereas in more dilute solutions, hydrolysed species such as $[Sb(OH)Cl_5]^-$ are most probably present.

I.8.3.4 Complexes with other ligands

In the Pearson classification of hard/soft cations, Sb(III) must be regarded as a borderline case. It interacts with both soft (e.g. thiols) or hard ligands (e.g. carboxylates). For the extensive literature on Sb(III) complexes with organic ligands, the reader is referred to the review articles by Filella et al. (2002a and 2000b). A number of stability constants of Sb(III) and Sb(V) complexes with low molecular weight ligands have been determined (Filella and May, 2005). The complexation of Sb(III) by organic ligands plays an important role in analytical methods relying on extraction/enrichment techniques of the element. Furthermore, Sb(III) is stabilised with respect to the pentavalent state by ligands such as citrate or ascorbate, hence their utility in analytical speciation techniques. Sb(V) also forms complexes with citrate (see below) and with polyhydric alcohols

and phenols. Complexation by α-hydroxyacids has been exploited in solvent extraction techniques for the quantification of Sb. Structures of dissolved Sb(III) and Sb(V) complexes with O-bearing ligands (and their stability in solution) have recently been determined using EXAFS (Tella and Pokrovsky, 2008 and Tella and Pokrovsky, 2009). Structures of various citrates in the solid state have also been determined by XRD (Smith et al., 1993). A novel Sb(V)-citrate complex has been detected in citrus juice stored in PET bottles (Hansen and Pergantis, 2006). 1:1 Sb(V)-lactate, 1:2 Sb(V)-lactate and Sb(V)-adenosine complexes were characterised in yoghourt spiked with inorganic Sb(V) by the same workers (Hansen and Pergantis, 2007). Various Sb(V)- glutathione complexes that may have a relevance in antimony biomethylation have been characterised by Wehmeier and co-workers (Wehmeier et al., 2004).

I.8.3.5 Binding to humics

Significant proportions (over 30%) of aquatic Sb(III) may be bound to natural organic matter such as humic acids (Buschmann and Sigg, 2004), which agrees with the predictions of Tella and Pokrovski (2009). Natural organic matter such as humic acid catalyses the oxidation of Sb(III) to Sb(V) (Buschmann et al., 2005). These authors used Suwannee river humic acid at 5 mgl^{-1} and found that the photosensitized oxidation was 9000 times faster than the dark reaction. There was a linear relationship between rate and DOC. Between pH 4 and 8, there was a five-fold increase in rate. Further, singlet oxygen, hydroxyl radical, hydrogen peroxide and hydroperoxyl radical/superoxide were not important oxidants in the system under investigation, while NOM derived reactive species in

excited triplet states and/or phenolic radicals seemed to play an important role. The authors presented a two binding site model : strong binding at low concentrations leading to fast oxidation kinetics and a weak binding site at high concentrations inducing slower oxidation, whereas the oxidation of non-complexes Sb(III) (as $Sb(OH)_3$) was even slower. Humic acid in soils also oxidises Sb(III) to Sb(V) (Steely et al., 2007).

I.8.3.6 Organo-antimony compounds in the environment

Organo-antimony compounds have been observed in oceanic and estuarine waters, such as methylstibonic and dimethylstibinic acid, $CH_3SbO(OH)_2$ and $(CH_3)_2SbOOH$. Methylated antimony species are present throughout the water column, with the monomethyl species being more abundant than the dimethyl species. There is a tendency toward higher levels of methylantimony species in the surface layer, and the methylated forms make up about 10% of total antimony (Andreae and Froelich, 1984, and references therein). See also section I.8.7 for biomethylation of Sb by microorganisms.

I.8.3.7 Sulfidic solutions

A very large number of different sulfide complexes of antimony has been postulated in the literature, a lot of them polymeric. It has indeed been known for a long time that Sb(III) compounds are soluble in an excess of alkaline sulfide solutions. The aqueous speciation of Sb(III) and Sb(V) in sulphidic solutions, important for the understanding of the transport of antimony in hydrothermal solutions, is quite complicated. Solubility data of Sb_2S_3 obtained by Akeret (Akeret, 1953) and data from Babko and Lisetskaya (Babko and Lisetskaya,

1956) have been tentatively interpreted by Kolpakova (Kolpakova, 1971) in terms of the species $H_2Sb_2S_4$, $HSb_2S_4^-$ and $Sb_2S_4^{2-}$. Brookins, on the basis of thermochemical calculations, asserted that SbS_3^{3-} was an important species rather than SbS_2^- or $HSbS_2^-$ (Brookins, 1972). Later work, however, did not seem to confirm his views. The stability and hydrolysis constants of the $Sb_2S_4^{2-}$ anion were determined by Dubey and Ghosh (Dubey and Ghosh, 1962). Kolpakova, in 1982, finds evidence for the existence of $HSb_2S_4^-$ from solubility studies (Kolpakova, 1982). In 1988, Krupp predicts the existence of $H_2Sb_2S_4$, $HSb_2S_4^-$ and $Sb_2S_4^{2-}$ on the basis of solubility experiments of stibnite in aqueous H_2S, as well as polymers of the general form $H_{2-x}Sb_{2n}S_{3n+1}^{x-}$ and the high temperature forms $Sb_2S_2(OH)_2$ and polymers $Sb_{2n}S_{3n-1}(OH)_2$ (Krupp, 1988). Wood essentially confirms the existence of $Sb_2S_4^{2-}$ by Raman spectroscopy (Wood, 1989) and predicts a bent SbS_2^- or pyramidal SbS_3^{3-} at lower concentrations. Tossell's ab initio quantum mechanical calculations lend support to the existence of $SbS_2(SH)^{2-}$ rather than Wood's fully deprotonated SbS_3^{3-} species. He also calculates Krupp's dimeric species $H_2Sb_2S_4$ (=$Sb_2S_2(SH)_2$) to be thermodynamically stable with respect to the monomer $Sb(SH)_3$ and the trimer $Sb_3S_3(SH)_3$. His calculations also confirm that Krupp's mixed-ligand complex $Sb_2S_2(OH)_2$ is indeed the stable species at higher temperatures (with respect to $H_2Sb_2S_4$) (Tossell, 1994). Spycher and Reed published a paper in 1989, concerning the stability constants of the complexes predicted by Krupp a few months earlier: $H_2Sb_2S_4$, $HSb_2S_4^-$ and $Sb_2S_4^{2-}$ (Spycher and Reed, 1989). Krupp violently criticised this paper; in particular, he disagreed with the way Spycher

and Reed had combined literature results (from allegedly incompatible studies) to 'generate new data', e.g. by averaging over data sets that differed from each other by more than their combined errors (Krupp, 1990). Spycher and Reed, who had been unaware of Krupp's 1988 paper, replied to this comment and justified their procedure in detail (Spycher and Reed, 1990). As far as Wood's SbS_2^- species is concerned (see above), a new experimental Raman study (Gushchina et al., 2000) confirmed its formation at high temperatures (>100°C) by depolymerisation of the low temperature (25-100°C) dimeric form $Sb_2S_4^{2-}$. There are two EXAFS studies from the year 2000 concerning the speciation of Sb(V) in sulfidic media (Sherman et al., 2000; Mosselmans et al., 2000). Sherman and co-workers conclude that the dominant species at temperatures below 150°C is $Sb(SH)_4^+$ (even though their solutions were basic and this species is fully protonated and the antimony atom bears a formal positive charge). At higher temperatures, there is evidence for four-coordinated mixed-ligand complexes $Sb(SH)^{4-n}(OH)_n^+$ which may polymerise at temperatures above 250°C to $(SH)_{4-n}(OH)_{n-1}Sb\text{-}O\text{-}Sb(OH)_{n-1}(SH)_{4-n}$. Mosselmans and co-workers worked with solutions of stibnite in deoxygenated aqueous NaSH (Mosselmans et al., 2000). They, too, found evidence for a four-coordinate species, which they formulate as SbS_4^{3-}. EXAFS does not allow an unambiguous distinction to be made between SbS_4^{3-} and Sherman's fully protonated species, but there is agreement on the question of the coordination number of Sb(V). In agreement with Sherman and co-workers, they found partial hydrolysis (substitution of SH^- by OH^-) of the complexes at higher temperatures. More importantly, their study demonstrates

that Sb(III) in the original solution *becomes oxidised* to Sb(V), since their starting material was stibnite, and that Sb(V) species exist *under reducing conditions.* According to them, the reduced species in their experiments with stibnite dissolved in aqueous NaSH would be H_2. In 2002, Helz and co-workers published an account of solubility experiments of stibnite in sulfidic solutions in the presence of elemental sulfur (Helz et al., 2002) : formation reactions and equilibrium constants are given for the mixed-valence complex $HSb_2S_5^-$ and the Sb(V) complex $Sb_2S_6^{2-}$. The presence of elemental sulfur thus significantly enhances the solubility of stibnite in anoxic, sulfidic environments. The energetics for the oxidation of the dimer $Sb_2S_4^{2-}$ to the mixed-valence dimer $Sb_2S_5^{2-}$ and from there to the all-Sb(V) dimer $Sb_2S_6^{2-}$ were calculated from first principles by Tossell (Tossell, 2003) and the results were consistent with the experimental findings.

I.8.4 Atmosphere

The presence of antimony in the atmosphere arises from natural and from anthropogenic inputs, the latter being dominant. According to estimates by Nriagu (Nriagu, 1989) natural sources account for 41% of all Sb emissions (cf. Table I.5)

	Wind-borne soil particles	Seasalt spray	Volcanoes	Forest fires	Biogenic continental particulates	Biogenic continental volatiles	Biogenic marine
Median (x 10^9 g y^{-1})	0.78	0.56	0.71	0.22	0.2	0.04	0.05

Table I.5 Inputs of antimony to the atmosphere.

Atmospheric aerosols contain <0.1 ng m^{-3} over remote oceans but up to several ng m^{-3} over industrialised areas. 0.2 ng m^{-3} is regarded as typical of the continental, and 0.45 pg m^{-3} of the marine troposphere, respectively (Austin and Millward, 1988).

Furuta and co-workers (Furuta et al., 2005) examined the trace-metal content of airborne particulate matter in the city of Tokyo and found the greatest enrichment of antimony in the size fraction <2 μm. Antimony is normally associated with the 'small' particle size fraction, as is typical for emissions from high-temperature anthropogenic processes (coal combustion, refuse incineration) (Filella et al., 2009).

I.8.5 Rain and snow

One of the first accounts of measurements of Sb in snow is by Postupolski and Golimowski (Postupolski and Golimowski, 1991), who find Sb concentrations of 0.03 μg l^{-1} (Sb(tot)) in snow collected in the unpolluted area of Szczyrk in southern Poland. The concentration rises to 5.10 μgl^{-1} (Sb(tot)) in snow from a Warsaw suburb and to 36.40 μg l^{-1} (Sb(III) only) in the city of Warsaw. The authors attribute the higher concentration in the city snow to industrial pollution, mainly from the emissions of coal-fired power stations. The analytical methodology applied was DPASV. Tripathi and Patel find concentrations ranging from 10.3 to 24.6 μg l^{-1} for rain samples collected in various locations in central India (by spectrophotometry, after preconcentration) (Tripathi and Patel, 1998). Postupolski's work shows that Sb concentrations in precipitations can vary widely (over 3 orders of magnitude), depending on local atmospheric pollution. Our own

analysis of rain collected in the village of Winseler in northern Luxembourg on 16th May 2006 yielded a concentration of 0.35±0.04 μg l^{-1}. Industrial pollution in this area can be regarded as moderate. The analysis was carried out by the DPASV method described later in section I.9 of this chapter. Determinations of Sb in polar snow and ice can be utilised to reconstruct the history of Sb pollution: see the following section.

I.8.6 Soils, peats, ice and snow as pollution 'archives'

The determination of antimony in peats, particularly ombrotrophic peats, deserves special mention, since it allows the reconstruction of the chronology of antimony deposition (Shotyk et al., 2004). Antimony was found to be effectively immobile in peat profiles. The lowest Sb concentrations (8±3 ng g^{-1}) were found in preanthropogenic peats dating from between 5320 to 8020 BP and were proportional to Sc concentrations (the ratio of Sb/Sc amounts to 0.105). This implies an Sb flux of 0.35 μg m^{-2} y^{-1}, which can be regarded as an estimate of the natural 'background' rate of deposition. Extrapolating to the Earth's land area, an estimated 51.4 T y^{-1} is deposited by natural sources to the continental land mass, or 154.2 T y^{-1} to the global atmosphere. The author concluded that natural fluxes of Sb to the atmosphere had previously been overestimated by a considerable margin. Sb was found to be significantly enriched in samples accumulated since the Roman period. Relative to preanthropogenic peats, a tenfold enrichment of Sb was seen in all of the peat cores by the end of the 19th century. Lithogenic Sb was clearly dwarfed by anthropogenic Sb in all samples.

Snow and ice may be similarly used as 'archives' documenting more recent antimony pollution (Krachler et al., 2005). Analysis of an ice-core dating from 1860 to 1996 and a snow pit from Arctic Canada revealed Sb concentrations in the range of 0.07 to 108 pgg^{-1}. The concentration of Sc, assumed to behave conservatively, showed that dust inputs had effectively remained constant over 160 y. The Sb concentrations increased rapidly from the beginning of the 20^{th} century, reflecting the growing importance of anthropogenic emissions of the element through coal burning and mining and smelting of Pb and Cu ores. A plateau was reached around 1940, and a maximum in the 1950's, probably attributable to the economic boom following WWII. Since then, Sb concentrations in the snow declined, probably owing to the use of filter technologies in coal fired power plants and emission reduction technology in modern smelters. Clearly, anthropogenic inputs dominated over natural contributions during the last 160 y.

I.8.7 Occurrence and effects in biota

In higher forms of life, antimony has no known biological function. Some bacteria derive metabolic energy from the oxidation of antimony sulfide to antimony oxide (Acidithiobacillus ferroxidans) or from the transformation of senarmontite to cervantite and stibiconite (Stibiobacter senarmontii) (Filella et al., 2007 and references therein). Sb(III) was found to inhibit the growth of soil bacteria, namely Escherichia coli, Bacillus subtilis and Streptococcus aureus, with S. aureus responding most sensitively (An and Kim, 2009). There is evidence for the reduction of antimony (and arsenic) to the trivalent form by marine phytoplankton (Andreae and Froelich, 1984). Methylated organoantimony

compounds are produced by a number of microorganisms, e.g. the fungus Scopulariopsis brevicaulis (a known methylator of arsenic, too) and consequently volatile organoantimony species have been found in landfill and sewage gases. Nonvolatile species have been found in freshwater plant extracts, seawater and sediments. (Gürleyük H. et al, 1997; Andrewes et al., 1998; Craig et al., 1999). Complexes of Sb with glutathione were identified in fermented sewage sludge and they may play a role in the biomethylation of antimony (Wehmeier et al., 2004). The accepted wisdom is that antimony is biomethylated to a far lesser extent than arsenic, for instance, although this is contradicted by recent results from Duester and co-workers (Duester et al., 2005). For very critical, modern reviews on biomethylation of antimony with more references to recent studies, see the two articles by Filella and Filella and Williams (Filella, 2010 ; Filella and Williams, 2010). The authors scrutinized 31 recent studies on biomethylation, dating from 1997 to 2003, and criticised that basic principles of chemical speciation were ignored. Their main points were the following :

- Sb(III) was sometimes added to culture media in the form of antimony(III)-oxide, and the purported dissolved antimony concentrations exceeded the solubilities of senarmontite and valentinite. Furthermore, Sb(III) was sometimes added in the form of potassium antimonyl tartrate, and it is to be expected that in concentrated solutions, Sb(III) is strongly complexed by tartrate and the concentration of the bioavailable species, $Sb(OH)_3$, may be a lot lower than the nominal total Sb(III) concentration.

- In none of the studies, any attention was given to the redox stability of Sb(III). Some experiments lasted for over a month, under oxic conditions, and it was simply assumed that all the antimony remained in the +III oxidation, even though it is well known that Sb(V) is the stable oxidation state in oxic solutions.
- In those studies that focussed on Sb(V), the element has been added as potassium hexahydroxyantimonate or commercial antimony(V)-oxide. In the latter case, the authors ignored that in neutral to acidic solutions, Sb_2O_5 was present as a metastable solution with slow equilibration to yield antimonic acid $HSbO_3.xH_2O$, stibiconite $SbSb_2OOH$ and Sb_6O_{13}. Therefore, a lot of the supposedly 'dissolved' antimony was actually present in solid phases, including amorphous or colloidal suspensions.
- The effects of the culture medium on Sb speciation were completely ignored. Culture media contain a variety of ligands that complex the element of interest. No attempts were made to take this into account, and the exact chemical composition of the media was very often not even given, thus precluding any *post hoc* speciation calculations.

These points lead the authors to conclude that it is virtually impossible to establish reliable observed effect-concentration relationships for biomethylation.

As far as ecotoxicity is concerned, we would like to quote Filella and co-workers (Filella et al., 2009): 'In the introduction of many publications, great emphasis is placed on the danger of antimony (…). However, the real environmental risk posed by antimony is still largely in need of assessment and

proof. Incidentally, careful reading of the literature shows that many authors copy other articles' introductions (...). The case of the comparison of Sb(III) vs Sb(V) is paradigmatic. In the introduction of 98 papers, it is found that "Sb(III) is more toxic than Sb(V)" and of these, 32 even go further and state that "Sb(III) is 10 times more dangerous than Sb(V)". This statement can only be wrong because toxicity depends on many parameters such as the considered organism, the route of exposure, or the presence of other contaminants. Thus, in general, no chemical species is exactly x times more toxic than another.' And :'A comprehensive compilation, review and evaluation of ecotoxicological data of antimony has never been published in a peer-reviewed paper'.

The extent to which antimony is accumulated by plants is extremely variable. A literature survey is included in Appendix AI. Some plants, even though grown on contaminated soil, scarcely accumulate any antimony at all (e.g. Daucus carota L., Beta vulgaris L., Solanum tuberosum L. and others) while others can accumulate more than 1000 $mgkg^{-1}$ (e.g. Achillea ageratum L., Plantago lanceolata L., Silene vulgaris MOENCH, (Baroni et al., 2000)). Our own investigations in the area around the abandoned antimony mine near Goesdorf, Luxembourg, showed that dewberry leaves (Rubus fruticosus agg.) growing next to the creek draining the mine, which typically carries 0.5 mg Sb per liter, tended to accumulate Sb (up to about 10 mg kg^{-1}), while Geranium robertianum L. (leaves), growing in the same spot, contained only about 0.1-0.2 mg kg^{-1}. Cirsium vulgare (SAVI) TEN. (leaves), Taraxacum officinale (WIGGERS) (leaves) and Hypericum perforatum L. (leaves), growing on a tailings heap, again showed

stronger accumulations (16.19, 46.75, 27.47 mg kg^{-1}, respectively). Trees (an apple tree, Malus domestica BORKH., growing on a tailings heap and a Common Beech, Fagus sylvatica L., growing *in* the highly contaminated creek, were sampled) did not accumulate antimony to a measurable extent in their leaves (the concentrations were below the detection limit). All the plants in the area were found to be normally developed, and an inventory of the plants established by a botanist showed a distribution typical of this habitat with no conspicuous features (Colling, 2006). This inventory is reproduced in Appendix AI. Little is known on the availability of soil antimony to plants; moreover, it is not always easily possible to distinguish between antimony taken up from the soil and antimony from atmospheric deposition (Shotyk et al., 2005a). Extraction studies by Hammel and co-workers (Hammel et al., 2000) performed on highly contaminated soils suggest that only very small proportions of total soil antimony may be available for plant uptake. Oorts and co-workers investigated the toxicity of antimony to plant growth (root elongation of barley, shoot biomass of lettuce) or to nitrification (Oorts et al., 2008). They found about 10% inhibition at soil solution concentrations of 110 μM or above (corresponding to 4.2 mmol Sb per kg of soil). Sb(V) toxicity thresholds are over 100-fold larger than estimated background values. Tschan and co-workers (2008) studied the uptake of Sb(V) by Zea mays (L.) and Helianthus annuus (L.) from nutrient solutions over a period of one week. Uptake by both species was correlated with Sb(V) in the nutrient solution. Maximum shoot concentrations for Zea mays and Helianthus annuus were 41 mg kg^{-1} and 77 mg kg^{-1}, respectively. The authors note that Sb

did not produce toxicity symptoms in the plants, unlike As used in similar experiments. They conclude that antimony uptake by these two species is unlikely to pose health risks to animals or humans.

There exists a number of studies of antimony toxicity towards aquatic species. In all of them, the effect of trivalent antimony, rather than the more common form Sb(V) in oxic waters, was assessed. Buccafusco and co-workers (Buccafusco et al., 1981) examined the toxicity of priority pollutants on bluegill (Lepomis macrochirus) and state that the LC50 over both 24 h and 96 h is higher than 530 mg Sb_2O_3/l. They note that the given concentration refers to 'undissolved solid', which probably means that in excess of 530 mg antimony oxide were added per liter of the water and the actual concentration of dissolved antimony corresponded to saturation with antimony oxide under the conditions of the experiments. This study is therefore not very illuminating. LeBlanc and Dean (LeBlanc and Dean, 1984) found that a saturated solution of Sb_2O_3 is essentially non-toxic to embryos and larvae of fathead minnows (Pimephales promelas). In 1989, Khangarot and Ray measured the 48 h -EC50[12] concentrations with respect to water fleas (Daphnia magna) of a series of metal ions in solution (Khangarot and Ray, 1989). Sb had been added in the form of Sb_2O_3 and it was found that Sb was the least toxic of all elements that had been studied. It was even less toxic than Na^+ and Mg^{2+}. However, it is again not clear if all the antimony that had been added was present in solution or if it was essentially an Sb_2O_3 saturated solution (i.e. containing about 1.3 mg Sb/l) that had been used. In a

[12] EC50 is the effective concentration at which 50% immobilization response is recorded.

1991 study of the toxicity of metals to a tubicifid worm (Tubifex tubifex), Sb(III) was again found to have little toxicity, even less than Ca^{2+} or Mg^{2+} (Khangarot, 1991). Further, Sb(III) showed little to moderate toxicity towards L-929 Fibroblasts and Tetrahymena Protozoa, which are commonly used for toxicological bioassays (Sauvant et al., 1995). The effect of $SbCl_3$ on Tilapia larvae (Oreochromis mossambicus) was examined by Lin and Hwang (1998). Antimony proved 'to be about 1000 times less toxic' than the other heavy metals studied (e.g. Cd). In a 2005 study of the toxicity of 63 elements on the freshwater amphipod Hyalella azteca, Sb(III) again exhibited surprisingly little toxicity compared with the other heavy metals: the survival rate over one week in a 1000μg l^{-1} solution was >90% (Borgmann et al., 2005). The toxicity of trivalent antimony in the form of potassium antimonyl tartrate to aquatic organisms has been studied by Nam and co-workers (2009). The substance was found to be more toxic to planktonic crustacea than to fish and green algae: larvae of Japanese medaka (Oryzias lapites) tolerated very high concentrations (24 h LC50=261 mg l^{-1}); Pseudokirchneriella subcapitata showed growth inhibition in the presence of a comparatively high Sb(III) concentration of 206 mg l^{-1} (=72 h EC50) but Simocephalus mixtus and Moina macrocopa were killed by much smaller concentrations (24 h LC50 were 4.92 mg l^{-1} and 12.83 mg l^{-1}, respectively). The study is, unfortunately, of limited use, since antimony, as an environmental contaminant, may well occur in complexed form, but not necessarily as the tartrate complex. Concentrations of 12 mg l^{-1} of potassium antimonyl tatrate are unrealistic in environmental contexts.

Ainsworth and co-workers studied the distribution of antimony in small mammals, i.e. herbivores such as the rabbit, Oryctolagus cuniculus, the short-tailed field vole, Microtus agrestis, and an insectivore, the common shrew, Sorex araneus, and invertebrates from a habitat contaminated by an antimony smelter. Despite a level of antimony in the diet constantly in excess of 10 mg kg^{-1}, all tissues of rabbits from the contaminated site had antimony levels less than 1 mg kg^{-1}. The values were elevated compared to animals from the control site, but low in relation to the difference between sites in dietary exposure. The authors conclude that the mobility of antimony in the food chain is low (Ainsworth et al., 1990). LD50 values of antimony for rabbits and mice are given as 115 mg kg^{-1} and 600 mg kg^{-1} as potassium antimonyl tartrate (WHO, 2003). If, however, potassium antimonyl tartrate is injected (ip, iv or sc), the LD50 is about an order of magnitude smaller (Gebel, 1999). The LD50 for mice exposed to gaseous stibine was 50-80 ml m^{-3}.

The toxicology of antimony in humans has been reviewed by Gebel (Gebel, 1997; Gebel, 1999). In the human body, antimony is preferentially accumulated in erythrocytes, in lung, lymph nodes and hair, but also in liver, kidney, spleen and heart. Antimony is normally present in human tissues at concentrations less than 1 $\mu g\ g^{-1}$ (Filella et al., 2002a). Mean values of Sb in body fluids are compiled in Table I.6 (Shotyk et al., 2005a).

	Urine	**Serum**	**Whole Blood**
Infants<1 year	<0.02-0.9	0.07-0.76	0.08-0.88
Healthy adults	0.19-1.8	0.8	0.3-3
Exposed subjects	5.1-8.3	n/a	0.5-17.9

Table I.6 Mean concentrations in $\mu g\ l^{-1}$ of Sb in body fluids of infants, adults and exposed workers (battery factory workers, casters, formation workers)

Krachler and Emons developed an elaborate hyphenated technique (HPLC-ICP-MS) for the speciation of antimony in urine (Krachler and Emons, 2000), which permits the determination of Sb(III), Sb(V) and trimethylantimonydichloride ($TMSbCl_2$). In non-exposed subjects' urine, typical concentrations of <0.06 $\mu g\ l^{-1}$ Sb(V), <0.025 $\mu g\ l^{-1}$ Sb(III) and 0.036 to 0.9 $\mu g\ l^{-1}$ $TMSbCl_2$ were detected. In the urine of occupationally exposed subjects (battery plant workers), concentrations were 2.0 to 5.9 $\mu g\ l^{-1}$ Sb(V), 0.025 to 0.15 $\mu g\ l^{-1}$ Sb(III) and 0.40 to 0.57 $\mu g\ l^{-1}$ $TMSbCl_2$ with total recoveries of 51 to 78%. A novel 1:1 Sb(V)-citrate complex, discovered by Hansen and Pergantis in citrus juice (Hansen and Pergantis, 2006a), could also be detected in urine. Owing to the high citrate concentrations typically present in urine, an estimated 3 to 27% of total Sb(V) should be present as Sb(V)-citrate. The measured concentrations in (spiked) urine samples confirmed this (Hansen and Pergantis, 2006b).

Antimony and its compounds have been known since the Middle Ages to be acutely toxic and they have been used in deliberate poisonings. Clinical symptoms of acute antimony poisoning somewhat resemble those of arsenic poisoning (Gebel, 1999). These include abdominal cramps, nausea, continuous vomiting, watery diarrhea, cyanosis and hematemesis. In an elderly patient, acute antimony poisoning led to multiple organ failure, cardiogenic shock, anuric renal failure, liver dysfunction, respiratory failure, thrombocytopenia, leukopenia, coagulation disorders, and metabolic acidosis (Lauwers et al., 1990) While arsenic compounds are quite effectively incorporated from the gastrointestinal tract, this does not hold for antimony. After application of inorganic Sb(III)

compounds, the biologically active species seems to be $Sb(OH)_3$. Organoantimonials such as stibogluconate and antimonyl tartrate exert their effect by continuously generating minute amounts of $Sb(OH)_3$. Pentavalent antimonials will release $[Sb(OH)_6]^-$, which will undergo reduction *in vivo* to Sb(III) to a small extent (Gebel, 1997). A recent article (Porquet and Filella, 2007) has shown that $Sb(OH)_3$ has a lot of similarities with the glycerol molecule and thus its transport in eukaryotes and prokaryotes may be facilitated by aquaglyceroporins. In contrast to arsenic, antimony does not seem to be as easily methylated and thus it is not as effectively detoxified. Both Sb(V) and Sb(III) are mainly excreted via the kidneys, Sb(V) more quickly so than Sb(III). Even if excretion of Sb(III) is slow, there is no evidence for accumulation of antimony (in experimental animals). However, not much is known on the precise reasons for the toxicity. Antimony is thought to bind to thiol moieties in amino-acids and proteins. Its affinity towards thiol groups and its potency to induce DNA-protein crosslinking seems to be lower than it is for arsenic (Gebel, 1997). Sb(III) inhibits an enzyme, gluthathione-S-transferase, in human erythrocytes, whereas Sb(V) is without action. Sb(V)-glutathione complexes possibly play a role in biomethylation (Wehmeier et al., 2004). Inhalation of antimony oxide causes lung cancer in rats, and the substance is suspected to be carcinogenic in humans. Hence antimony(III)-oxide and antimony(III)-sulfide are classed as carcinogens (group 2B and 3, respectively, by route of inhalation) by the International Agency for Research on Cancer (IARC). The mechanism of their genotoxicity is unclear; it has been proposed that Sb(III) causes DNA damage by

inhibition of DNA repair enzymes (Shotyk et al., 2005a and references therein). The mutagenicity, carcinogenicity and teratogenicity of antimony are viewed very critically by Léonard and co-workers. The evidence for mutagenicity is regarded as insufficient by these authors. The exposure in all studies that led to the conclusion of carcinogenicity allegedly also involved other, proven or likely, carcinogenic compounds. Although some studies seem to indicate that antimony(III)-oxide could interfere with embryonic or fetal development, these are not entirely conclusive. The outcome of pregnancy in women treated with antimony compounds has regrettably not yet been studied (Léonard and Gerber, 1996). Gebel, however, holds that antimonials act clastogenically without being directly mutagenic (Gebel, 1997). Pentavalent antimony, such as sodium antimony gluconate used in the treatment of tropical protozoan diseases, has a potential cardiac toxicity, which is not yet fully understood (Sundar et al., 1998). It may be due to traces of trivalent antimony present in the drug, since Sb(III) has been shown to affect intracellular free calcium in animal cardiac myocytes (Tirmenstein et al., 1995; Wey et al., 1997).

Inhalation of antimony compounds leads to irritations of the respiratory tract and even pneumoconiosis. Dusts can induce, among others, dermatitis, keratitis, conjunctivitis, suppuration of the nasal septum, and gastritis.

Moreover, antimony is regarded as a metalloestrogen (Darbre, 2006 and references therein).

In 1990, microbial generation of toxic gases, among others stibine, from flame retardants in cot mattresses, was proposed as the cause of sudden infant

death syndrome (SIDS) (Richardson, 1990; Richardson, 1994). This prompted a government inquiry, which revealed faulty and/or misinterpreted results in Richardson's study. The organism isolated from the mattresses was not a fungus (Scopulariopsis brevicaulis), as claimed by Richardson, but a mix of common environmental Bacillus species. More importantly, Richardson believed to have identified phosphine, arsine and stibine by the coloration of silver nitrate and mercuric bromide test papers. It turned out that sulfur compounds given off by the bacterial cultures were responsible for the false-positive colour tests, and hence the hypothesis that stibine generated from flame retardants in mattresses could be the cause of SIDS was rejected (Warnock et al., 1995).

There is an interesting account of elevated antimony concentrations (up to 3 mgl^{-1}, i.e. 600 times the European drinking water limit) in the drinking water in the vicinity of Schwaz, Austria. These spring waters are contaminated by dissolving ore bodies. The inhabitants have been drinking this water for centuries, without apparent adverse effects (Millen, 2001). Since the water is oxic, Sb is present mostly as Sb(V).

The mean daily uptake of antimony by respiration is estimated to about 60-460 ng d^{-1}, which is small compared to the dietary uptake of 10-70 $\mu g\ d^{-1}$ (Gebel, 1999). Gebel also compiled concentration values of antimony in foods (table I.7), revealing that Sb is mainly enriched in vegetables, meat and sea fish.

	Conc. of Sb in μg kg^{-1}	
Vegetables	0.1-200	DW
Corn	0.2-4.3	FW
Potatoe starch	8	DW
Meat (muscle)	0.3-200	DW
Milk	3	DW
Dairy products	<8	FW
Sea fish	4-200	DW
Sea food	1.1-2.8	FW
Fresh water fish	3	FW
Crustaceae	0.01-0.18	FW

Table I.7 Antimony in selected foods from Gebel, 1999
(DW=dry weight, FW=fresh weight)

Tobacco contains about 65 μg kg^{-1}, cigarette smoke contains 0.12 μg/cigarette.

I.8.8 Environmental Pollution

In section I.8.6, we have shown how the history of anthropogenic antimony pollution, beginning at Roman times, can be quite accurately reconstructed using environmental 'archives' such as peat, snow or ice. Over the last two or three decades, the main uses of antimony have shifted from its use in alloys to non-metallic applications. While scrap metals are comparatively easy to recycle, the same is not true for the numerous consumer goods, in which antimony compounds play an important role, e.g. as catalysts in plastics or flame retardant in textiles, carpets and the like. These goods are mostly disposed of after use, either by deposition in a landfill or by incineration. The use of automobile brake pads with antimony sulfide linings also significantly contributes to the dissemination of antimony in the natural environment. There are thus numerous diffuse sources of pollution that did not exist some fifty years ago, and

that are difficult to tackle. It therefore seems reasonable to assume that the environmental pollution by antimony will continue to grow in the future.

I.8.9 Environmental regulations

Both the US Environmental Protection Agency and the European Union have listed antimony and its compounds as pollutants of priority interest (United States Environmental Protection Agency, 1979 ; Council of the European Communities, 1976). Drinking water limits are 6 $\mu g\ l^{-1}$ and 5 $\mu g\ l^{-1}$ in the US and the EU, respectively. In developed countries, this regulatory requirement is met without difficulty, with very few isolated exceptions (e.g. Millen, 2001), where for local, geogenic reasons, antimony concentrations are higher. The EU requires that the sum of migration levels of Sb used in PET designed to come into contact with food and beverages does not exceed 0.04 mg kg^{-1} (EU 2005). The permissible exposure limit at the workplace defined by the US Occupational Safety and Health Administration is 0.5 mg m^{-3} (as antimony) as a time weighted average over an 8h shift (Center for Disease Control and Prevention, 2010)

I.9 Analytical chemistry and speciation of antimony

Macroscopic quantities of antimony may be determined in a variety of classical ways:

- Gravimetrically, as antimony(III)-pyrogallate,
- gravimetrically, as the trisulfide,
- coulometrically or titrimetrically by iodine,

- amperometrically or titrimetrically by bromate,
- titrimetrically by iodate or permanganate,
- spectrophotometrically by iodide. (Jefferey et al., 1989)

Numerous other classical methods of quantitative determination with literature references have been compiled by Fresenius and Jander (Fresenius and Jander, 1958). A wide variety of sometimes useful, though older, spectrophotometric techniques may be found in the classic work by Snell and Snell (1949). For the classical determination of Sb in mineral samples and their redox speciation, used in this thesis in connection with antimony oxide minerals (stibiconite, senarmontite and valentinite), see Konopik and Zwiauer (1952) and McCay (1933) (Essentially titration of Sb(III) by permanganate and determination of total antimony by reduction of Sb(V) to Sb(III) by metallic mercury, prior to titration).

Modern methodologies for the determination of antimony in environmental samples are given in the comprehensive review by Nash and co-workers (2000). Smichowski and co-workers review chemical methods (liquid-liquid and solid-liquid extraction, selective hydride generation and coprecipitation), chromatographic techniques, electrochemical techniques and kinetic methods, applicable to water samples (Smichowski et al., 1998). Particular attention to the speciation of antimony, inclusive of methylantimony compounds by hyphenated techniques, is given by Krachler and Emons (Krachler and Emons, 2001). Hansen and Pergantis have published a number of papers on the identification and quantification of novel Sb(V)-citrate and -lactate complexes by HG-ICPMS and

HPLC-ES-MS. (Hansen and Pergantis, 2006a, 2006b, 2007). The most sensitive known technique for the quantification of *total* antimony is ICP-SMS, as applied by Shotyk and co-workers with a limit of detection of 30 pg l^{-1} (Shotyk et al., 2005b) in the determination of antimony in pristine groundwaters. Given the plethora of available techniques, each with their particular strengths and weaknesses and field of applicability, we shall only describe methods used in the present thesis. For other techniques, the reader is referred to the above mentioned reviews.

For the analysis of minerals, and in some of the experiments concerning dissolution kinetics of minerals, ordinary ICP-OES was used. For a description of optical ICP spectrometry, see the monograph by Nölte (2003). A detection limit of about 4 μg l^{-1} was achieved using the Sb line at 217.58 nm on a Spectroflame Modula Instrument from Spectro Analytical Instruments, Kleve, Germany. The characteristic advantages of ICP-OES lie in the rapidity of the determination (4 replicates can be run in 3 min.) and the very large linear range of the instrument, spanning several orders of magnitude.

When a lower limit of detection was needed, or when redox speciation was desired, we used the differential pulse anodic stripping voltammetric (DPASV) technique developed by Quentel and Filella (2002).

The method was implemented on a Metrohm 797VA Computrace voltammetric analyser (Metrohm AG, Herisau, Switzerland), with a conventional three-electrode assembly, comprising a mercury drop electrode as working electrode, a platinum rod as counter-electrode, and a Ag/AgCl/3 M KCl reference

electrode. The choice of electrolyte depends on whether total antimony or only Sb(III) should be measured. A mixture of 5 ml suprapure hydrochloric acid (30%, Merck, Germany) and 5 ml circumneutral sample solution was used in the case of total Sb. A mixture of 5 ml sample solution and 5 ml of a base electrolyte (2 M HCl + 1 M NaCl, both suprapure) was used for the determination of Sb(III). The method consists of several steps, all carried out on a single, hanging mercury drop (HMDE[13], size 4): after degassing the solution by sparging for 3 min. with ultrapure nitrogen, a deposition step during which a potential of -0.45 V (against the Ag/AgCl reference electrode) is applied to the mercury drop electrode with constant stirring of the solution. The deposition time may be varied according to the desired sensitivity; 5 min. was found to be suitable. During the deposition step, Sb(III) or both Sb(III) and Sb(V), according to the chosen electrolyte, are reduced at the HMDE and the metallic antimony formed dissolves in the HMDE. After the deposition step, the stirring is stopped and, after an equilibration time of 20 s, the potential is scanned in the anodic direction from -0.45 V to -0.02 V with a sweep rate of 0.002 Vs^{-1}, leading to a reoxidation (or 'stripping') of the amalgamated Sb at characteristic potentials : -0.132 V for Sb(III) and -0.2 V for Sb(tot) in the respective electrolyte. The scan is carried out in differential pulse (DP) mode, which means that potential pulses ΔE at regular intervals are superimposed on the applied potential. The current between the working electrode and the auxiliary electrode is measured shortly *before* and *during* the applied pulse (see fig. I.7).

[13] HMDE=Hanging mercury drop electrode

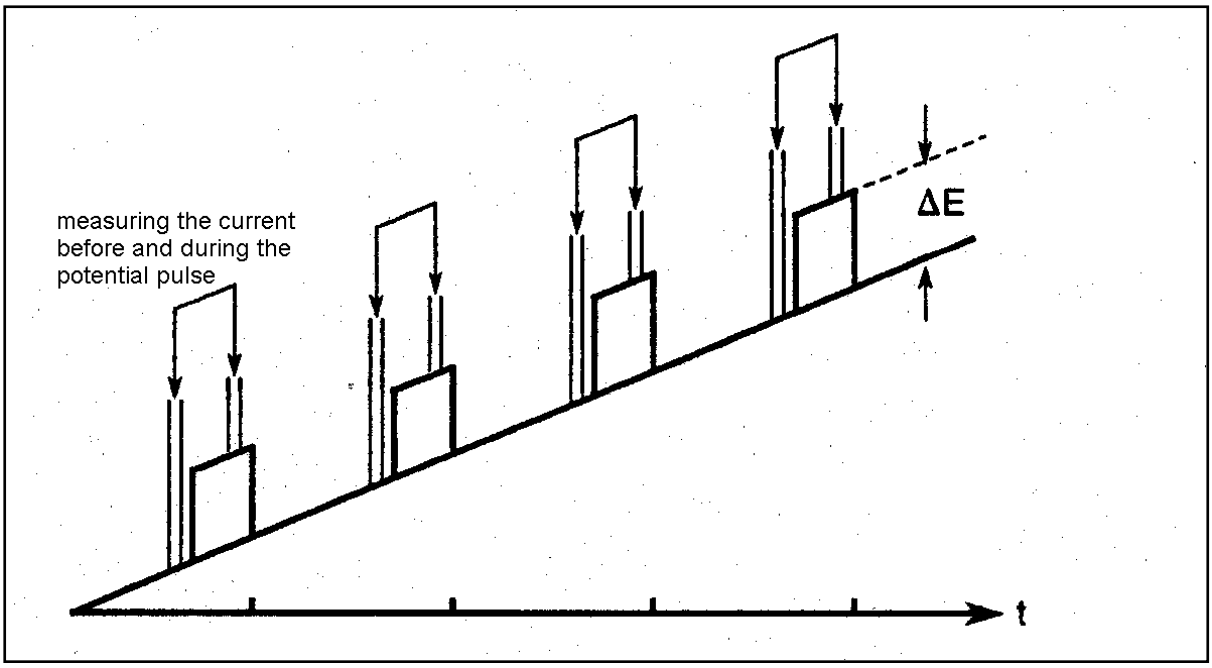

Fig. I.7 Principle of DP measurement (adapted from Neeb, 1989)

The difference between both currents is proportional to the derivative of the current-voltage profile during the scan and is termed a differential pulse voltammogram. The current-voltage curve shows inflection points whenever a species begins to be deposited at the electrode or, as is the case here, is reoxidised ('stripped') from the electrode. Thus, the DP voltammogram (cf. fig. I.8) consists of more or less symmetrical, bell-shaped curves (maxima corresponding to the inflection points of the current-voltage curve) centred around the deposition (or 'stripping') potential for each species, whose peak currents are proportional to the analyte concentration. A pulse amplitude of 0.02 V, a pulse time of 0.05 s, a potential step of 0.001 V and a step time of 0.5 s (giving rise to a sweep rate of 0.002 Vs^{-1}) were used in our method.

These peak currents are first measured in a reagent blank, then in the sample solution, and finally after several standard additions (we commonly used

2-3 standard additions of typically 10-50 μl 1 ppm Sb solution, depending on the intensity of the sample signal); see fig. I.8 for a set of voltammograms. The solution for the standard addition is freshly prepared by dilution of a 1000 ppm stock solution, prepared by dissolution of the appropriate amount of potassium antimonyl tartrate in Milli-Q water. The stock solution is stable for at least a year without special precautions. If the concentration of Sb(V) is sought, it can be obtained as the difference between Sb(tot) and Sb(III).

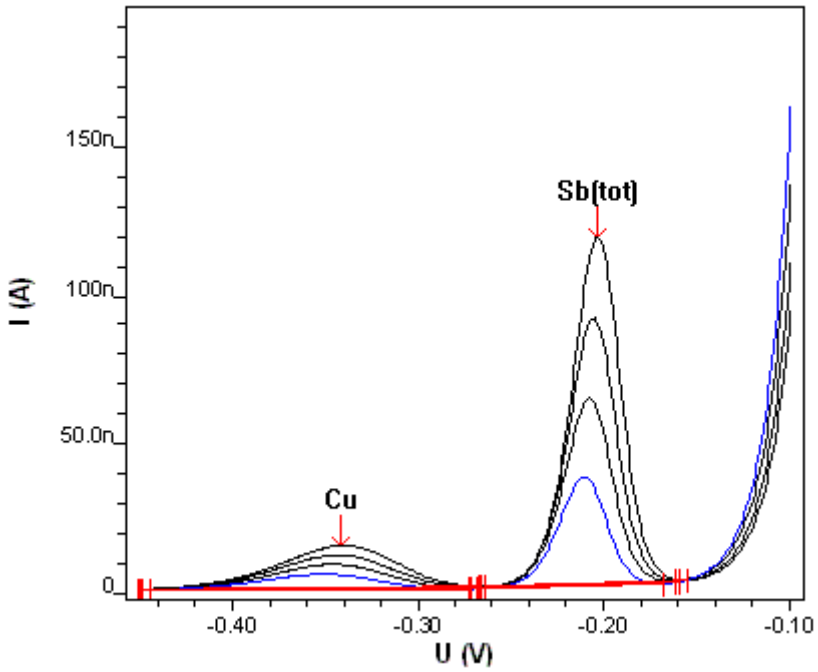

Fig I.8 Typical voltammogram for the determination of total Sb. Sample signal (bottom curve) plus 3 standard additions. Note that copper, giving a peak at -0.336 V, may be determined from the same voltammogram.

A plot of peak current vs. added concentration is linear (within a concentration range that has to be known in advance), and the analyte concentration in the sample solution may be calculated from the intersect of the regression line with the axis of abscissae (cf. fig. I.9)

As far as analytical performance is concerned, the detection limit for Sb(III) is given by the authors as 11 ngl^{-1} and 33 ngl^{-1} for Sb(V), with a deposition time of 10 min. These detection limits are comparable to those achieved by HG-ICP-MS (Nash et al., 2000), at only a fraction of the cost. The disadvantage of DPASV relative to ICP is the comparatively long time that a single determination takes (about 30 min.).

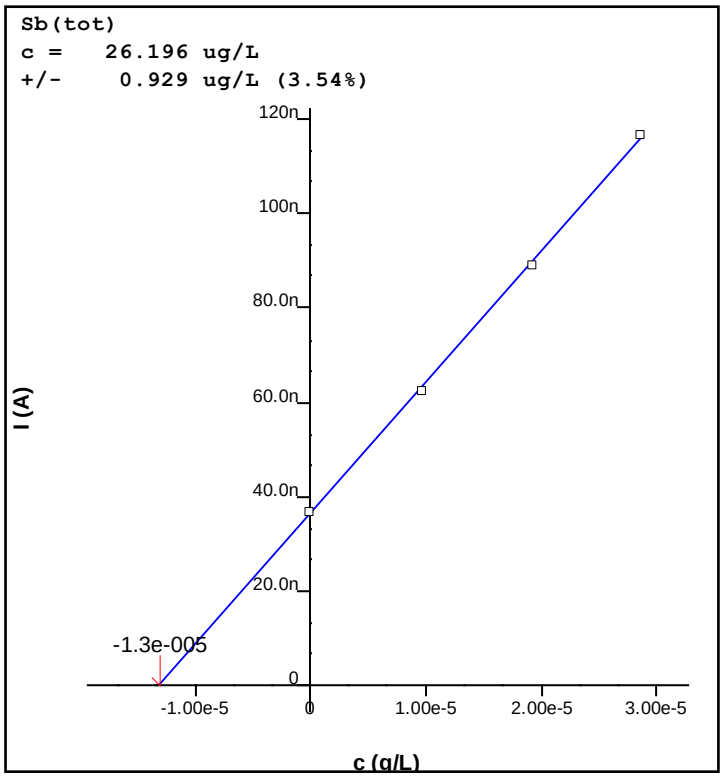

Fig. I.9 Regression line of the peak current vs. concentration for sample and standard additions from the voltammogram in fig. I.10

We tested some of the spectrophotometric methods cited in Nash's review, namely those of Tripathi and Patel (Tripathi and Patel, 1998), Sharma and Patel (Sharma and Patel, 1993) and a variant of the rhodamine-B method. The first method relies on preconcentration with cetylpyridinium chloride,

followed by extraction with the aid of Triton-X100 and complexation by brilliant green. The second method uses diphenylbenzamidine (for the extraction) and brilliant green. The authors claimed detection limits of 3 μgl^{-1} and 10 μgl^{-1} respectively. In our own experiments, we failed to achieve this sensitivity. Besides, calibration curves had poor correlation coefficients and individual measurements were not well reproducible. The third method, using rhodamine-B as a ligand, was not superior.

I.10 Important Concepts in the Kinetics of Mineral Dissolution

I.10.1 Transport vs. surface control

In the main chapters of the present thesis, frequent reference is made to mineral dissolution kinetics, e.g. to the parabolic dissolution rate. We will therefore briefly introduce the main kinetic concepts of mineral dissolution in the following :

In the early work on mineral dissolution kinetics, concerned mainly with important rock-forming oxide and silicate minerals, solute concentrations were often found to be initially proportional to the square root of time. This was first interpreted by the 'armoring precipitate' hypothesis, i.e. the assumption that dissolution products precipitate on the surface of the dissolving mineral and form an amorphous or crystalline layer. Ultimately, as the dissolution curves become linear, an equilibrium is reached between the dissolution of the precipitate itself and the diffusion of fresh material through this layer. Correns and von Engelhardt

(1938) proposed this mechanism in order to explain their experimental data on adularia dissolution. They calculated thicknesses of the surface precipitate of the order of 50 nm and diffusion coefficients of potassium in the precipitate which seemed reasonable for the diffusion of an ion through a solid at low temperature[14]. They did not, however, realise that their dissolution curves were initially parabolic.

Another, later, interpretation was the 'leached layer hypothesis' – here, the rate-limiting factor is the transport of a species through a leached layer of the mineral (Lasaga, 1984 ; Stumm and Wollast, 1990). As the layer grows in thickness, diffusion becomes harder and the rate of dissolution slows down, until the leaching rate becomes equal to the diffusion rate and the mineral dissolves at a constant rate, i.e. a steady state between the rate of diffusion through the leached layer and the rate of transport of the leached species away from the mineral surface is reached.

The origin of the initially parabolic dissolution rate can be seen as follows: Let the concentration of the leached species in the bulk of the 'fresh' mineral be c_b and the concentration at the surface be c_0. It may be verified that the solution of the diffusion equation, Fick's second law (Atkins, 1990) viz.:

$$\frac{\partial c}{\partial t} = D\frac{\partial^2 c}{\partial x^2}$$

is given by

[14] The thickness of the surface layer in potassium feldspar was later shown to be <1.7 nm (Lasaga, 1984). The diffusion coefficients of K^+ calculated by Correns and von Engeldhardt were of the order of 10^{-14} $cm^2\,day^{-1}$ for a solution pH between 3 and 11.

$$c(x,t) = c_0 + (c_b - c_0)\,\mathrm{erf}\left(\frac{x}{2[Dt]^{\frac{1}{2}}}\right) = c_0 + (c_b - c_0)\int_0^x \exp\left(\frac{-x^2}{4Dt}\right)dx$$

where c(x,t) represents the concentration of the leached species at a distance x from the surface, t is the time and D the diffusion coefficient of the species in the leached layer[15]. The flux J of the species at the surface is then obtained by Fick's first law (Atkins, 1990) :

$$J = -D\left[\frac{\partial c}{\partial x}\right]_{x=0} = -(c_b - c_0)\sqrt{\frac{D}{\pi t}}$$

The ensuing increase in concentration of the leached species in the surrounding solution is then obtained by multiplication of the flux J by the exposed surface area A and division by the solution volume V :

$$\frac{dc}{dt} = \frac{(c_b - c_0)\sqrt{D}}{\sqrt{\pi t}}\frac{A}{V}$$

Integration with respect to time yields the classic parabolic rate law[16] :

$$c(t) = (c_b - c_0)\sqrt{\frac{D}{\pi}}\frac{A}{V}\int_0^t \frac{dt}{\sqrt{t}}$$

$$= 2(c_b - c_0)\sqrt{\frac{D}{\pi}}\frac{A}{V}\sqrt{t}$$

Later, experimental methods such as XPS, Auger spectroscopy, LEED and SIMS became available which would have permitted the detection of such a leached layer on mineral surfaces. No such layer, however, was found on weathered silicates and oxides (and, of course, no 'armoring precipitate' either).

[15] This may be verified by substitution into Fick's second law, knowing that $\frac{d}{dz}\mathrm{erf}(z) = \frac{2}{\sqrt{\pi}}e^{-z^2}$ (Abramowitz and Stegun, 1965)

[16] Lasaga (1984) erroneously places the factor of 2 in the denominator of the integrated form.

The explanation for the observed non-linear kinetics stems from the sample preparation: an *apparent* parabolic rate law is obtained if preferential dissolution of fine (submicron) particles or of highly active surface sites (strained parts of the crystals, sharp edges, corners, steps and lattice defects) occurs. If the sample material is cleaned prior to the experiment, e.g. by an acid pretreatment, linear kinetics is observed from the beginning on: if the reactions at the surface are slow in comparison to diffusion into the solution or other reaction steps, the concentration of solutes adjacent to the surface will be the same as in the bulk solution. Steady-state conditions prevail at the surface and the dissolution kinetics follows a zero-order rate law :

$$\frac{dc}{dt} = kA$$

where the dissolution rate is simply proportional to the exposed surface area A of the mineral. Also, the concentrations of the dissolved reactants may reach a state of saturation with respect to new solid phases, which will precipitate on the surface of the dissolving mineral, thus limiting the increase in concentration of the precipitating elements, which in turn yields an apparently incongruent dissolution reaction and pseudoparabolic kinetics. In Chapters II and III, we shall present our investigations into the dissolution kinetics of stibnite, and it will be shown that the dissolution of this mineral is incongruent with the formation of elemental sulfur at the surface. The leached layer hypothesis, however, can be regarded as refuted in the case of oxides and silicates.

I.10.2 Rationalization of proton-promoted dissolution rates

As a result of the dissolution experiments using stibnite, and also in the case of the antimony oxide minerals, we find dissolution rate laws involving fractional powers of the hydrogen ion concentration. These may be rationalized in a variety of ways, e.g. by surface complexation models. Starting from the constant capacitance model (Stumm and Morgan, 1996), Wieland and co-workers (1988) show that the concentration of protonated sites on a metal oxide will be given by a Freundlich isotherm of the form :

$$\{= MOH_2^+\} = \frac{K_F}{[H^+]_{ZPC}^m}[H^+]^m$$

i.e.

$$[H^+] = \frac{[H^+]_{ZPC}}{K_F^{\frac{1}{m}}}\{= MOH_2^+\}^{\frac{1}{m}}$$

The substitution of this expression for the hydrogen ion concentration into the empiricial rate law of the form :

$$R_H = k_H[H^+]^n$$

yields :

$$R_H = k_H\{MOH_2^+\}^{\frac{n}{m}}\frac{[H^+]_{ZPC}^n}{K_F^{\frac{n}{m}}} = k'_H\{= MOH_2^+\}^i$$

Where $i = \frac{n}{m}$ is found to be of integer value (Wieland et al., 1988) and corresponds to the the oxidation state of the central metal ion in the crystalline lattice. This has been verified for Al(III), Fe(III), Mg(II), Be(II) and Si(IV) (Furrer and Stumm, 1986; Stumm and Wollast, 1990). Mechanistically, the proton-

promoted dissolution may be explained by the scheme in Fig. I.10 :

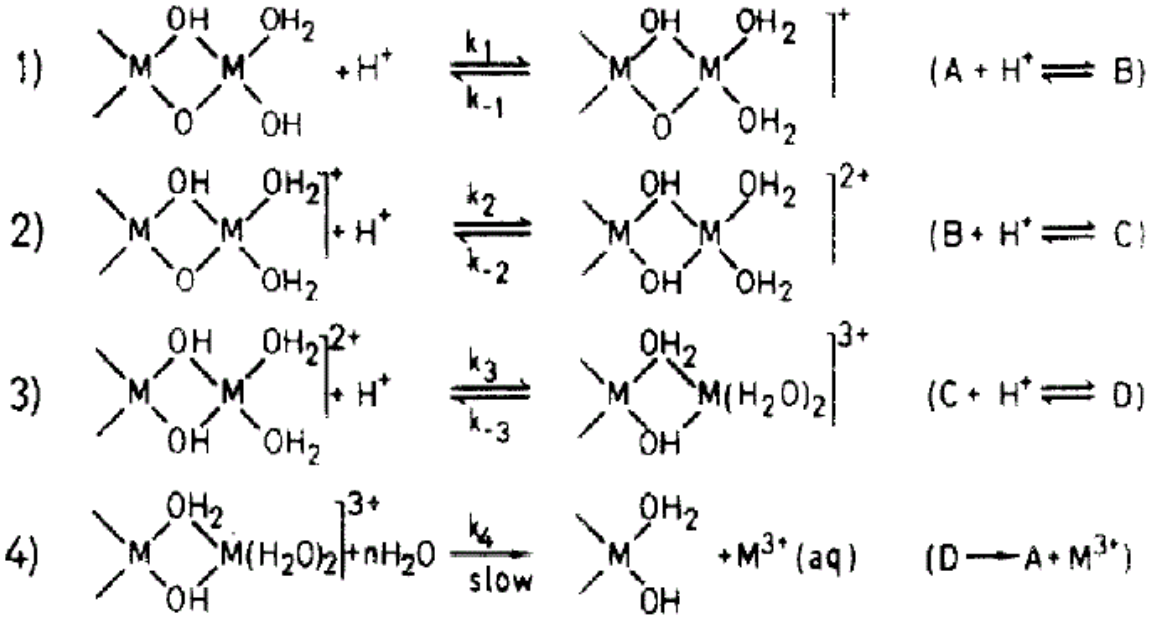

Fig. I.10 4-step mechanism for the proton-promoted dissolution of an oxide of a trivalent metal (from Furrer and Stumm, 1986).

The surface hydroxyl groups are protonated three times. These are rapid and reversible steps (the surface equilibrates with H^+ in the sourrounding solution). The 4th step is the slow, rate-limiting detachment of the metal-aqua complex from the surface induced by nucleophilic attack of water molecules at the metal ion centre, which regenerates a fresh surface layer, ready to undergo protonation.

Sposito (2008) points out that if adsorption occurs according to the generalized Langmuir-Freundlich isotherm, viz.:

$$n_i = \frac{b(Kc_i)^\beta}{1 + (Kc_i)^\beta}$$

where n_i represents the surface excess of species i, b the capacity parameter and K the Langmuir binding (or 'affinity parameter') constant and $0<\beta\leq 1$, then, at low concentrations, the approximation :

$$n_i \approx Ac_i^{\beta}$$

may hold (the so-called van Bemmelen-Freundlich isotherm), which, in our case, means that the concentration of protonated sites is proportional to a fractional concentration of H^+ :

$$\{= MOH_2^+\} = A[H^+]^{\beta}$$

Thus, if the reaction rate can be taken to be proportional to some power m of the concentration of protonated sites, i.e.

$$R_H = k\{= MOH_2^+\}^m = kA[H^+]^{m\beta} = k'[H^+]^{m\beta}$$

it becomes proportional to a fractional power of the hydrogen ion concentration.

These treatments, initially derived for oxide surfaces, may also apply to the situation of metal sulfides. Sulfides have been shown to behave in an analoguous way to oxides in that they form amphoteric hydroxo groups at their surfaces in aqueous solutions (Davis et al., 1995; Rönngren et al., 1991; Park and Huang, 1986).

I.10.3 Rationalization of ligand-promoted dissolution rates

The effects of ligands on dissolution rates have mostly been studied in the cases of (hydr-)oxides (there is an abundant literature on this topic, see for instance Furrer and Stumm (1986), Biber and Stumm (1994) and Sposito (2004) and references therein) and silicates (see Sposito (2004) and references therein, also Wieland and Stumm (1992) for kaolinite dissolution; Amrhein and Suarez

(1988) for anorthite dissolution; Welch and Ullman (1993) and Stillings et al. (1998) for plagioclase dissolution) ; studies on other mineral phases such as sulfides (Davis et al., 1995; Goyne et al., 2006) and phosphates (Martinez et al., 2004; Goyne et al., 2006; Debela et al., 2010) are much rarer.

In the presence of ligands, rates of dissolution are generally found to differ from those of pure proton-promoted dissolution. Ligands may form surface complexes by ligand exchange with surface groups; these surface complexes may either facilitate, or inhibit the detachment of metal ions from the surface. As in the case of proton-promoted dissolution, the rate determining step is usually the detachment of the surface complex along with the coordinated metal ion (Furrer and Stumm, 1986).

In the case of ligand-promotion, the actual, observed rate is a superposition of proton-promoted and ligand-promoted rates, if these occur as independent reactions.

The rate of ligand-promoted dissolution R_L is, in the general case, proportional to the surface concentration of the surface complex M-L:

$$R_L = k\{M - L\}$$

Since the surface concentration of the M-L complex depends non-linearly on the solution phase concentration of the ligand L (the two are related via an adsorption isotherm, just as in the case of proton-promoted dissolution), the rate law for R_L will have a non-integer reaction order with respect to [L] :

$$R_L = k[L]^{\beta}$$

Special cases are known in which the rate also depends on the hydrogen ion concentration, for instance if the polarizing effect of a surface chelate is insufficient to initiate detachment and an additional proton must be adsorbed to lower the activation energy (Furrer and Stumm, 1986).

Mechanistically, the process may be represented as in Fig.I.11 using the bioxalate ligand on a trivalent metal oxide as an example. In the top part of the figure, the first step is the reversible, rapid formation of a surface chelate, which in step 2 (the slow, rate-determining step) is detached by nucleophilic attack of water. Step 3 represents the rapid reprotonation of the fresh layer. In the bottom part, an alternative mechanism is proposed, in which the surface chelate, once formed, undergoes rapid reversible protonation, followed by detachment in step 3.

Ludwig and co-workers (1995) determined rate constants for the dissolution of bunsenite (NiO) by a series of aminocarboxylate ligands and they found an excellent correlation between the rate coefficient and the stability constant of the Ni^{2+} complex in solution. They conclude that the activated surface complex must resemble the dissolved complex in important ways. Such a simple relationship does no longer exist if one takes into account ligands that form inhibiting polynuclear surface complexes (cf. Chapter IV)

Ligands capable of forming five- and six-membered, *mononuclear*, chelate rings (e.g. oxalate, catechol, salicylate) with surface metal centres ordinarily enhance dissolution rates (of oxides). Monodentate ligands (e.g. benzoate) do not enhance dissolution rates. Ligands capable of forming polynuclear surface

complexes (e.g. the inorganic species phosphate, arsenate, borate, sulfate, selenite, chromate…) generally retard dissolution rates, as the concerted detachment of two metal centres from the surface is energetically disfavoured.

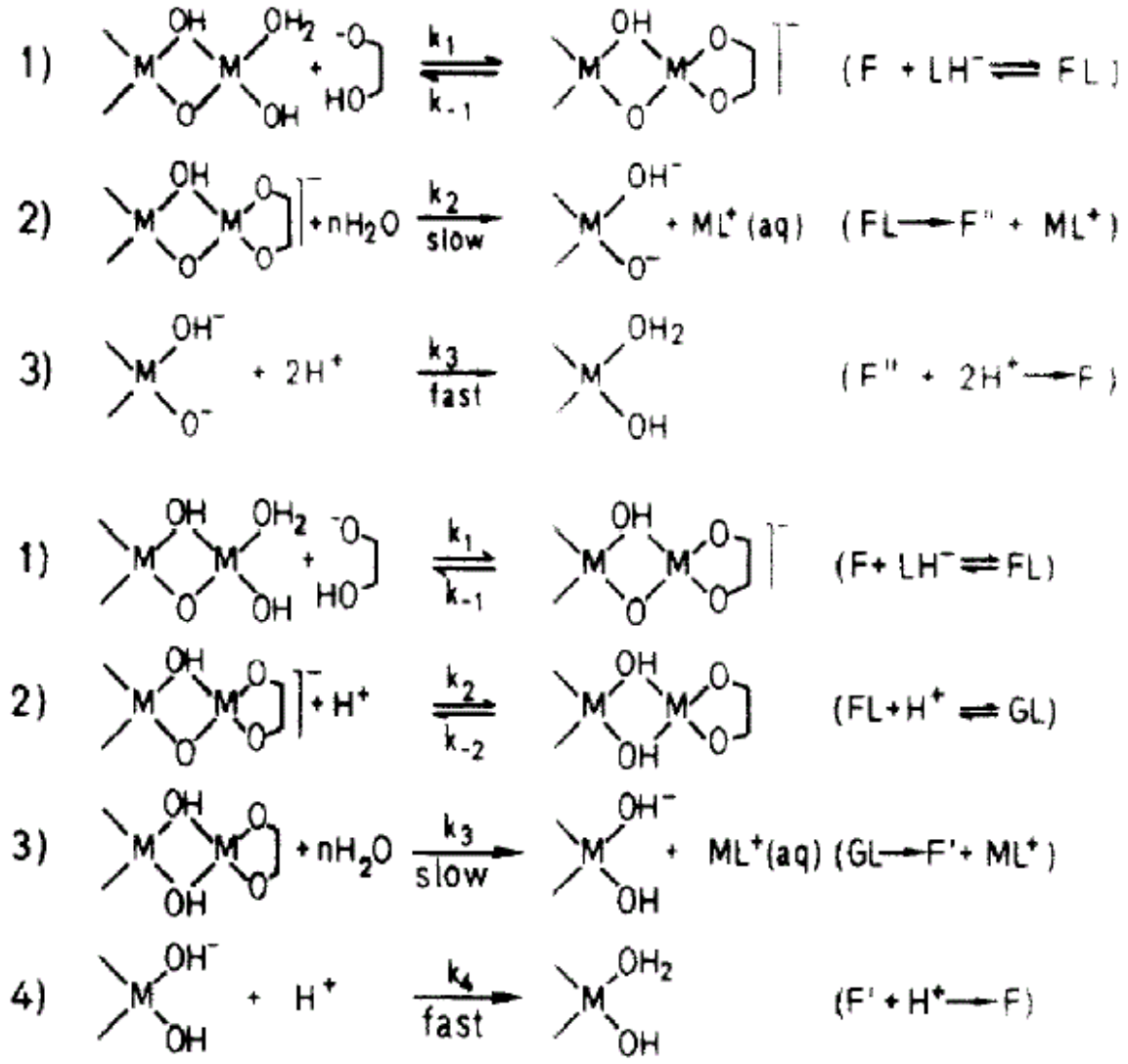

Fig. I. 11 Ligand-promoted dissolution of a trivalent metal oxide (from Furrer and Stumm, 1986)

However, these inhibiting effects are often pH dependent : phosphate, arsenate, and selenite for instance *promote* the dissolution of γ-FeOOH at pH<5, whereas above pH 5, they *inhibit* it (Bondietti et al., 1993). The reverse may also apply, for instance in the case of surface chelates. A surface chelate may become

protonated at low pH to the extent that it becomes monodentate and the rate-promoting effect of the chelate is lost (Furrer and Stumm, 1986). Ligands with large, hydrophobic moieties (e.g. long chain carboxylic acids) inhibit dissolution rates by blocking large areas of the mineral surface. Humic acids can either enhance or inhibit mineral dissolution (Martinez et al., 2004; He et al., 2007; Ravichandran et al., 1998).

The structural identity of surface complexes can be explored by modern spectroscopic techniques (surface IR, EXAFS etc.)

In chapter IV, we shall investigate the effect of various organic ligands on the dissolution rate of stibnite, and we shall see that some general principles known from oxide dissolution kinetics also appear to apply to the dissolution of stibnite.

I.10.4 Activation energies

An important parameter affecting dissolution rate constants is the temperature, which in mineral dissolution reactions, is mostly found to obey the Arrhenius equation (Laidlar, 1987):

$$k(T) = Aexp\left(-\frac{E_A}{RT}\right)$$

A lot of other ways to express the temperature dependence of rate constants exist, but the Arrhenius equation is the one that is most frequently used, because of the ready interpretation of the activation energy E_A as the energy of 'the activated complex'. Activation energies for mineral dissolution usually lie within the range 40-80 kJ mol^{-1} with an average around 60 kJ mol^{-1} (Lasaga, 1984). It must be emphasized, however, that activation energies for mineral dissolution

can be strongly pH dependent, and are usually valid only over a fairly narrow temperature range. An activation energy of about 21 kJ mol^{-1} is regarded as the boundary between transport (i.e. diffusion) controlled reactions and reactions controlled by surface phenomena, such as the formation or the dislocation of a surface complex as rate limiting steps of a reaction. Most mineral dissolution reactions have higher activation energies, which means that globally speaking, mineral dissolution is a surface controlled process. Quantum mechanical calculations of the activation energy of realgar cluster oxidation by Renock and Becker (2010) represent an interesting new development: their calculations indicate that there are two phenomena that dominate the kinetics : the spin transition of triplet oxygen to singlet oxygen, with an activation energy of 106 kJ mol^{-1}, and the subsequent dissociation of singlet oxygen, contributing 87 kJ mol^{-1}. Adsorbed hydroxide on surface in proximity to the triplet oxygen adsorption site lowers both activation barriers to 29 kJ mol^{-1} and 69 kJ mol^{-1}, respectively. Co-adsorption of other ions (carbonate, bicarbonate, sulphite and sulfate) promote the oxidation of As_4S_4 further by lowering activation energies by 5-40 kJ mol^{-1}. Their results compare favourably to the experimental data of Lengke and Tempel (2003) and they show that the rate limiting step in mineral dissolution need not necessarily be the dislocation of a surface complex.

While activation energies are, in general, distinctly larger than transport activation energies, they are clearly smaller than the range expected for bond-breaking in crystals (160-400 kJ mol^{-1}). There are, however, exceptions, such as the activation energy for stibnite dissolution in strongly acid solution (Chapter II),

which is anomalously low (5.2 kJ mol^{-1}), that of valentinite dissolution in basic solution (9.1 kJ mol^{-1}, chapter V) or that of stibiconite dissolution (Chapter V), which is even negative (-36.4 kJ mol^{-1}). Negative activation energies have been predicted by Casey and Sposito (1992), when no examples were known. In the meantime, at least three such cases have been reported : the dissolution of stibiconite (this work), the oxidative dissolution of arsenopyrite in the presence of ferric ion (Rimstidt et al., 1994), and magnesite dissolution (Saldi et al., 2010) in slightly alkaline solution. The authers offer plausible explanations, which are discussed in Chapter V.

Wieland and co-workers, and Casey and Sposito presented rationalizations of the activation energy of mineral dissolution (Wieland et al., 1988; Casey and Sposito, 1992). Wieland and co-workers applied transition state theory (activated complex theory) in the conventional way (Laidlar, 1987). If $\Delta^{\ddagger}G$ is the Gibbs free energy change in going from the initial to the activated state, then the rate constant k is given by :

$$k = \nu^{\ddagger}\exp\left(-\frac{\Delta^{\ddagger}G}{RT}\right) = \nu^{\ddagger}\exp\left(\frac{\Delta^{\ddagger}S}{R}\right)\exp\left(-\frac{\Delta^{\ddagger}H}{RT}\right)$$

where $\nu^{\ddagger}$ is a constant. Wieland et al. argue that the entropy $\Delta^{\ddagger}S$ reflected the configurational changes from a precursor structure towards the activated (surface) complex. During the monomolecular desorption of adsorbed molecules into the gaseous state, the entropy of the precursor and that of the activated complex must be very similar and thus $\Delta^{\ddagger}S$ is zero or negligibly small. The mononuclear detachment of a single metal centre from the surface of a mineral

is therefore assumed to be comparable to monomolecular desorption, and the above equation simplifies to :

$$k = A\exp\left(-\frac{\Delta^{\ddagger}H}{RT}\right)$$

Helgeson et al. (1984) showed that the enthalpy of activation may be related to the Arrhenius activation energy by :

$$\Delta^{\ddagger}H = E_A + RT$$

Since the activation energy of weathering processes is typically about 60 kJ mol^{-1} and RT at room temperature amounts to only 2.5 kJ mol^{-1}, the expression for the rate constant may be further simplified by the approximation

$$E_A \approx \Delta^{\ddagger}H$$

i.e. the Arrhenius activation energy is approximated by the enthalpy of the activated complex - unless the activation energy is exceptionally small, as in the case of stibnite dissolution in acidic solution mentioned above.

The treatment of Casey and Sposito (1992) goes one step further in that contributions from the variation with temperature of the conditional equilibrium constant for surface protonation and from the temperature dependence of the ratio of activitiy coefficients are isolated :

Let K be the equilibrium constant for surface protonation :

$$K = \frac{f_{SOH_2^+}x_{SOH_2^+}}{a(H^+)f_{SOH}x_{SOH}}$$

where f and x are the activity coefficients and mole fractions of the species in the index, respectively, and $a(H^+)$ is the hydrogen ion activity in solution. The conditional equilibrium constant K'

$$K' = \frac{x_{SOH_2^+}}{a(H^+)x_{SOH}}$$

is related to K by :

$$K' = K\frac{f_{SOH}}{f_{SOH_2^+}}$$

Solving this equation for the mole fraction of protonated sites, under the assumption that the mole fraction of negatively charged sites is negligible (i.e. the pH<pH_{PZNPC} and $x_{SOH_2^+} + x_{SOH} \approx 1$) yields :

$$x_{SOH_2^+} = \frac{a(H^+)K'}{1 + a(H^+)K'}$$

Thus,

$$\ln x_{SOH_2^+} = \ln[a(H^+)K'] - \ln[1 + a(H^+)K']$$

Differentiating with respect to $\frac{1}{T}$ gives :

$$\frac{\partial \ln x_{SOH_2^+}}{\partial\left(\frac{1}{T}\right)} = \frac{\frac{\partial K'}{\partial\left(\frac{1}{T}\right)}}{K'} - \frac{a(H^+)}{1 + a(H^+)K'}\frac{\partial K'}{\partial\left(\frac{1}{T}\right)}$$

$$= \frac{\partial \ln K'}{\partial\left(\frac{1}{T}\right)} - \frac{a(H^+)K'}{1 + a(H^+)K'}\frac{\partial \ln K'}{\partial\left(\frac{1}{T}\right)}$$

$$= \left(1 - x_{SOH_2^+}\right)\frac{\partial \ln K'}{\partial\left(\frac{1}{T}\right)}$$

On the one hand, the rate of dissolution R is proportional to some power of $x_{SOH_2^+}$:

$$R = k' {x_{SOH_2^+}}^n$$

and taking the log-derivative with respect to $\frac{1}{T}$:

$$\frac{\partial \ln R}{\partial\left(\frac{1}{T}\right)} = \frac{\partial \ln k'}{\partial\left(\frac{1}{T}\right)} + n\frac{\partial \ln x_{SOH_2^+}}{\partial\left(\frac{1}{T}\right)}$$

Substituting for $\frac{\partial \ln x_{SOH_2^+}}{\partial\left(\frac{1}{T}\right)}$ yields :

$$\frac{\partial \ln R}{\partial\left(\frac{1}{T}\right)} = \frac{\partial \ln k'}{\partial\left(\frac{1}{T}\right)} + n\left(1 - x_{SOH_2^+}\right)\frac{\partial \ln K'}{\partial\left(\frac{1}{T}\right)}$$

On the other, the temperature dependence of the rate is empirically found to obey an Arrhenius equation :

$$R = A\exp\left(-\frac{E_A}{RT}\right)$$

which is differentiated with respect to $\frac{1}{T}$:

$$\frac{\partial \ln R}{\partial\left(\frac{1}{T}\right)} = \frac{\partial A}{\partial\left(\frac{1}{T}\right)} - \frac{E_A}{R}$$

If A may be taken as temperature independent, the first term on the right of this equation vanishes. By comparison of the last two alternative equations for $\frac{\partial\, ln R}{\partial\left(\frac{1}{T}\right)}$, we finally obtain :

$$E_A = -R\frac{\partial \ln k'}{\partial\left(\frac{1}{T}\right)} - Rn\left(1 - x_{SOH_2^+}\right)\frac{\partial \ln K'}{\partial\left(\frac{1}{T}\right)}$$

From this last equation, it can be seen that the activation energy consists of three contributions: the temperature dependence of the rate coefficient k' – this corresponds to the enthalpy of the activated complex as proposed by Wieland et al. (cf. above) and two contributions from the variation with temperature of the conditional equilibrium constant for surface protonation, the first of which is, by virtue of the van't Hoff equation, proportional to the enthalpy of protonation of

the surface while the second arises from the temperature dependence of the ratio of the activity coefficients :

$$\frac{\partial lnK'}{\partial\left(\frac{1}{T}\right)} = \frac{\partial lnK}{\partial\left(\frac{1}{T}\right)} + \frac{\partial}{\partial\left(\frac{1}{T}\right)}\frac{f_{SOH}}{f_{SOH_2^+}}$$

$$= -\frac{\Delta H_{protonation}}{R} + \frac{\partial}{\partial\left(\frac{1}{T}\right)}\frac{f_{SOH}}{f_{SOH_2^+}}$$

Since in the last equation for E_A the factor in brackets in the second term is always positive, this term makes a contribution proportional to the enthalpy of protonation of the surface. This enthalpy is always negative (in the range -15 to -50 kJ mol^{-1})[17]; it may therefore be concluded that the (exothermic) protonation of the surface tends to reduce the overall activation energy and thus favours dissolution (note that conversely, the activation energy for hydroxyl-promoted dissolution would be *increased*). The contribution from the ratio of the activity coefficients $\frac{f_{SOH}}{f_{SOH_2^+}}$ arises from long range coulombic interactions between surface protons; its detailed expression depends on the chosen surface complexation model. While the exothermic contribution of the protonation enthalpy varies only slightly with pH, that of electrostatic interactions may vary by tens of kJ mol^{-1} with pH and becomes minimal near the pH_{PZNPC} and they are the principal reason for the strong pH dependence of activation energies.

An interesting prediction of Casey and Sposito's model is that the activation energy of dissolution may become negative, owing to a protonation enthalpy that outweighs electrostatic contributions among charged surface sites.

[17] These may be measured calorimetrically.

Rare instances of negative activation energies have indeed been observed, such as our example of the dissolution of stibiconite in acidic solution (Chapter V).

I.11 Crystallography of Antimony Minerals

In the present section, we will briefly present the crystal structures of the antimony minerals used in this work. Together, they represent the most abundant antimony minerals. Their macroscopic mineralogical characteristics are listed in appendix AIII.

Stibnite occurs in at least three polymorphs, the orthorhombic structure, stibnite (II), a high temperature form, stibnite(I) and a low-temperature monoclinic form, stibnite(III) (Kuze et al., 2004).

Antimony(III)-oxide has been known to occur in two polymorphs for a long time; they were described by Debray as early as 1886 (Debray, 1866). This paper even gives synthetic routes to both forms, cubic senarmontite and metastable, orthorhombic valentinite. It was later confirmed by XRD that depending on the method of precipitation, either senarmontite or valentinite can indeed be obtained from aqueous solutions (Abdullah, 2008 ; Panasenko, 2009). The transition between the two phases exhibits a strong kinetic inhibition, as both phases are structurally completely unrelated (Buerger and Hendricks, 1938). The mineral samples used in Chapter V were prepared according to the directions of Debray and Abdullah.

The structure determination of stibiconite is discussed in section I.11.4.

There are two polymorphs of the formula Sb_2O_4 : orthorhombic α-Sb_2O_4, corresponding to the mineral cervantite, and the monoclinic β-Sb_2O_4 (Stewart et al., 1972). We shall not give details on cervantite, since we did not use this phase in our experiments. Some even doubt the natural occurrence of this phase (Vitaliano and Mason (1952). Because of the difficulty in growing single crystals, the structure was determined by powder neutron diffraction, after several attempts by XRD (Thornton, 1977).

I.11.1 Stibnite (Sb_2S_3)

Only the structure of the ordinary, orthorhombic form of stibnite (stibnite(II)) will be presented here. For the other polymorphs, see the article by Kuze et al., 2004. The structure of stibnite(II) was first determined by Hofman (1933) and confirmed by Scavnicar (1960). It consists of parallel ribbon-like $(Sb_4S_6)_n$-polymers linked together by intermolecular attraction between antimony and sulfur atoms (of different ribbons), cf. Fig. I.12. A projection of the structure onto the (010) plane (Fig. I.13) shows that antimony atoms are equally distributed over two different coordination environments. One half of the antimony form trigonal SbS_3 pyramids with an Sb atom at the vertex, the other other half form SbS_5 square pyramids with an Sb atom at their centre.

Scavnicar calculates a partial ionic character of only 12% of the Sb-S bond, so that the bond may be treated as essentially covalent.

The structure was later refined by Bayliss and Nowacki (1972), and, more recently, by Kyono et al. (2002) and Kyono and Kimata (2004), who also discuss the effect of the Sb(III) lone pair.

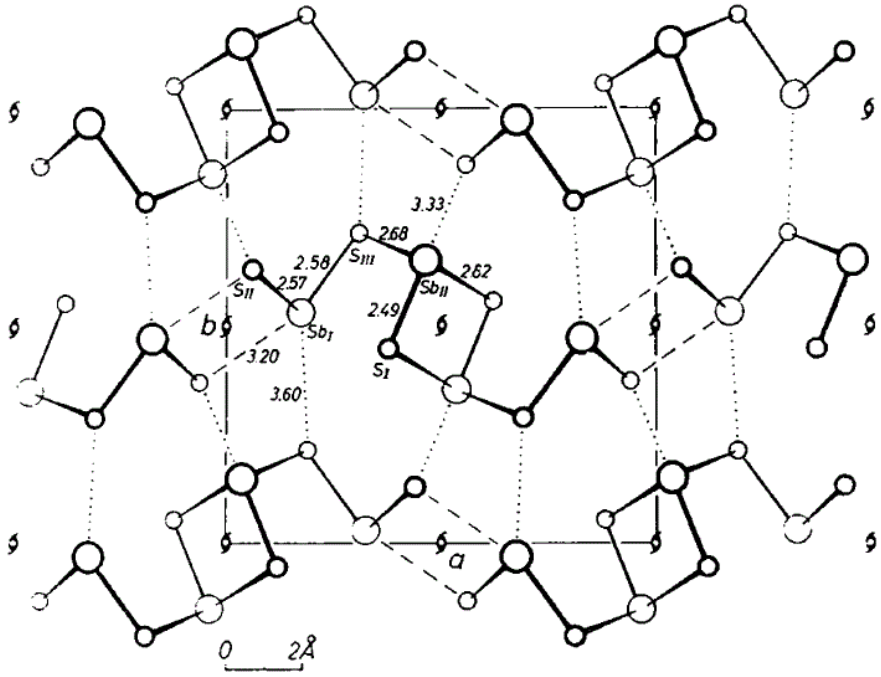

Fig. I.12 Ribbon-like structure of stibnite(II). From Scavnicar (1960)

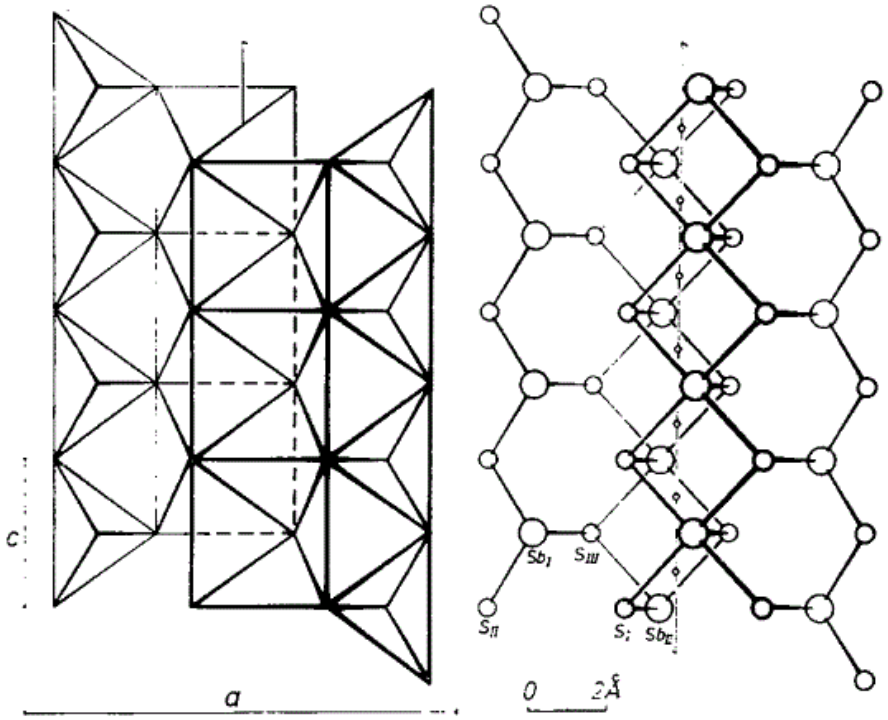

Fig. I.13 Coordination environment of Sb atoms in stibnite. From Scavnikar (1960)

I.11.2 Senarmontite (cubic Sb_2O_3)

Senarmontite forms naturally by oxidation of stibnite. It is named after the French mineralogist H. Hureau de Sénarmont (1808-1862). Senarmontite is the stable form of antimony(III)-oxide up to 570°C (Roberts and Fenwick, 1928). Its structure was first determined by Bozorth (1923), along with that of the isostructural arsenolite (As_2O_3). It consists of Sb_4O_6 groups arranged in the same way as the carbon atoms in diamond. The cubic structure is represented in Fig. I.14, taken from the original publication by Bozorth. For a refinement of the structure, see Svensson (1975). The lattice parameter given by this author is 11.1519(2) Å.

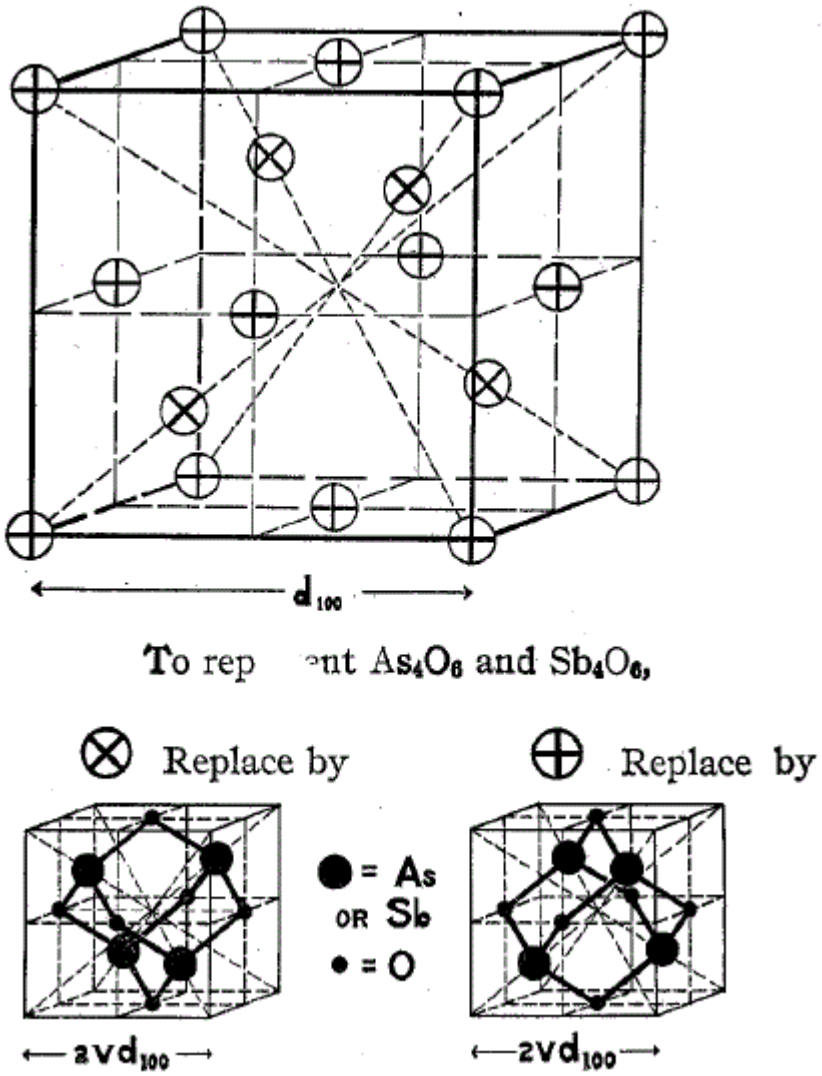

Fig. I.14 Structure of senarmontite and the isomorphous arsenolite. Taken from Bozorth, 1923.

I.11.3 Valentinite (orthorhombic Sb_2O_3)

The valentinite structure was first determined by Buerger and Hendricks (1938). It is best described as consisting of infinite $(Sb_2O_3)_\infty$ chains (Fig. I.15). 'These chains pack together (…) in such a way that a side oxygen atom of one chain butts up against a centrosymmetrically equivalent oxygen atom in the neighbouring chain. This constitutes the closest O-O approach (2.54 Å) in the structure. The vertical alignment of centrosymmetrical chain molecules is such

that the above-mentioned side oxygen comes to a position just opposite an Sb atom in the neighbouring chain. This Sb-O distance is 2.51 Å and it probably represents a weak, secondary Sb-O bond. Presumably it is this bond which is especially important in causing the chain molecules to hold together to form a crystal.' (Buerger and Hendricks, 1938). N.B. the Sb-O distance *within* the chain is 2.00 Å.

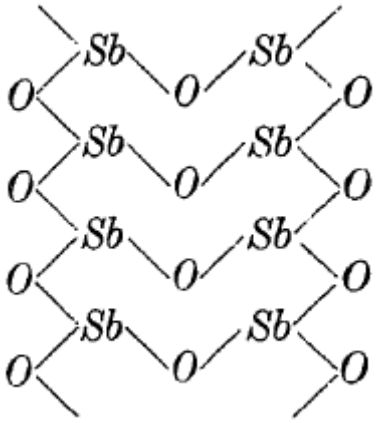

Fig. I.15 $(Sb_2O_3)_\infty$ chain in valentinite.
(From Buerger and Hendricks, 1938)

Since this structure is completely different from that of senarmontite, a large number of bonds have to be broken for the transition of one form into the other, which explains why valentinite is metastable below the transition temperature.

I.11.4 Stibiconite $Sb^{III}Sb_2{}^{V}O_6OH$

A considerable amount of confusion surrounds the characterisation of this mineral. The mineral had been known to mineralogists as 'antimony ocher' long before its first structure determination was first attempted in 1937, by Dihlström and Westgren. These authors worked with a synthetic sample, obtained by heating antimonic acid ($Sb_2O_5 \cdot x\ H_2O$) to 780°C for 3 h. They assigned the

formula given in the title to their phase and determined its structure by XRD and discussed earlier publications on the subject, trying to reconcile the contractictory data. They suggested a pyrochlore structure and claimed that it was isomorphous with synthetic $BiTa_2O_6F$, whose structure was known. The structure can be described as face-centred cubic with 8 formula units per unit cell. The lattice parameter was determined as 10.28 Å (Dihlström and Westgren, 1937). Vitaliano and Mason, in 1952, published a large study of natural stibiconite samples and they noted the wide variability in elemental composition and lattice parameter of the mineral. Total Sb was found to vary from 52.6 to 76.9 % (theory 76.37%). The natural samples always contained variable amounts of water, calcium (up to 10%) and valentinite in microscopic crystallites (up to 25%) whose presence was detected by the supernumerary reflections in the XRD. Moreover, XRD was hampered by admixture of foreign matter and poor crystallinity. Unfortunately, they did not determine the ratio Sb(III)/Sb(V) in their samples. On the basis of their experimental results, the authors suggested the general formula $(Sb^{III},Ca)_ySb^{V}_{2-x}(O,OH,H_2O)_{6-7}$ (Vitaliona and Mason, 1952). In 1972, Stewart and co-workers announced that the phase $SbSb_2O_6OH$ was nonexistent and that this composition did not correspond to the material obtained by Dihlström and Westgren's method. They proposed the composition $Sb_2O_{4.35(5)}$, equivalent to the formula Sb_6O_{13}. Their X-ray data also indicated a pyrochlore-type structure. They determined the ratio Sb(III):Sb(V) by Mössbauer spectroscopy and by chemical analysis (0.42(6) and 0.48(4), respectively) (Stewart et al., 1972). Their material thus contains 77.75% total Sb and 25.26% Sb(III) which very closely

corresponds to the composition given by Dihlström and Westgren. Our own analyses, both on natural stibnite and on the synthetic material prepared according to the directions of Dihltröm and Westgren showed higher Sb(III) contents (ca. 36% for the natural material and ca. 38% for the synthetic material). The most recent (Mössbauer) study of stibiconite ignored the work of Stewart et al. and proposed the formula $Ca_{4x}Sb^{III}_{3-8x}Sb^{V}_{1+4x}(O,OH,H_2O)_y$ with x comprised between 0 and 3/8 (Stevens et al., 1993). Hoch (2010) pointed out that a derivation of the ratio Sb(III)/Sb(V) from the relative areas of the Mössbauer peaks is not permitted because of the differing Lamb-Mössbauer factors of the two nuclei. The material used in Chapter V fits in with the data of Vitaliano and Mason, both from the point of view of elemental composition and lattice parameter.

I.12 References for chapter I

Abdulla A.H., Noor N.H.M., Ramli I., and Hashim M. (2008) Effect of precipitation route on the properties of antimony trioxide. *Materials Chemistry and Physics* **111**, 201-204

Abramowitz M. and Stegun I.A. (1965) Handbook of Mathematical Functions, Dover Publications Inc., New York.

Agricola, G. (1556) De re metallica. Minerva Verlag, Frankfurt/Main 1991.

Ainsworth N., Cooke J.A., and Johnson M.S. (1990) Distribution of Antimony in Contaminated Grassland: 2-Small Mammals and Invertebrates. *Environ. Poll.* **65**, 79-87

Akeret R. (1953) Über die Löslichkeit von Antimon(3)sulfid. PhD thesis, ETH Zürich.

Allred A.L. (1961), Electronegativity values from thermochemical data. *J. Inorg. Nucl. Chem.* **17**, 215-221

Amereih S., Meisel T., Scholger R., and Wegscheider W. (2005) Antimony speciation in soil samples along two Austrian motorways by HPLC-ID-ICP-MS. *J. Environ. Monit.* **7**, 1200-1206.

Amrhein C. and Suarez D.L. (1988) The use of a surface complexation model to describe the kinetics of ligand-promoted dissolution of anorthite. *Geochim. Cosmochim. Acta* **52**, 2785-2793

An Y.-J. and Kim M. (2009) Effect of antimony on the microbial growth and the activities of soil enzymes. *Chemosphere* **74**, 654-659

Andreae M.O. and Froelich P.N. (1984) Arsenic, antimony, and germanium biogeochemistry in the Baltic Sea. *Tellus* **36B**, 101-117

Andrewes P., Cullen W.R., Feldmann J., Koch I., Polishchuk E. and Reimer K.J. (1998) The Production of Methylated Organoantimony Compounds by *Scopulariopsis brevicaulis. Appl. Organomet. Chem.* **12**, 827-842

Arai Y., (2010) Arsenic and Antimony: in *Trace Elements in Soils,* ed. P.S. Hooda, Wiley, Chichester (UK) 2010, pp. 383-407

Atkins, P.W. (1990) Physical Chemistry, 4th ed., Oxford University Press, Oxford.

Austin L.S. and Millward G.E. (1988) Simulated effects of tropospheric emissions on the global antimony cycle. *Atmos. Environ.* **22**, 1395-1403

Babko A.K. and Lisetskaya G.S.(1956) Equilibrium in reactions of formation of thiosalts of tin, antimony and arsenic, in solution. *J. inorg. Chem.* USSR **1**, 969-980

Bayliss P. and Nowacki W. (1972) Refinement of the crystal structure of stibnite, Sb_2S_3. *Z. Kristallogr.* **135**, 308-315

Belzile N., Chen Y.-W. and Wang Z.(2001) Oxidation of antimony(III) by amorphous iron and manganese oxyhydroxides. *Chem. Geol.* **174**, 379-387

Biber M.V., Dos Santos Afonso M. and Stumm W. (1994) The coordination chemistry of weathering: IV. Inhibition of the dissolution of oxide minerals. *Geochim. Cosmochim. Acta* **58**, 1999-2010

Biblia sacra (1948) Biblia sacra iuxta latinam vulgatam versionem. Liber verborum dierum, I. Paralipomenon XXIX, 2. Romae, Typis polyglottis vaticanis MDCCCCXLVIII

Biringuccio V. (1540 ?) The pirotechnia of Vannoccio Biringuccio : the classic sixteenth-century treatise on metals and metallurgy / translated from the Italian with an introduction and notes by Cyril Stanley Smith and Martha Teach Gnudi. London : Constable, 1990

Baroni F., Boscagli A., Protano G. and Riccobono F. (2000) Antimony accumulation in *Achillea ageratum, Plantago lanceolata* and *Silene vulgaris* growing in an old Sb-mining area. *Envir. Pollut.* **109**, 347-352

Blay K. (2000) Sorption wässriger Antimon-Spezies an bodenbildende Festphasen und Remobilisierung durch natürliche Komplexbildner. PhD Thesis, Technische Universität München.

Bondietti G., Sinniger J. and Stumm W. (1993) The reactivity of Fe(III)(hydr)oxides: effects of ligands in inhibiting the dissolution. *Colloids and Surfaces A: Physicochemical and Engineering Aspects* **79**, 157-167

Borgmann U., Couillard Y., Doyle P. and Dixons G. (2005) Toxicity of sixty-three metals and metalloids to Hyalella azteca at two levels of water hardness. *Environmental Toxicology and Chemistry* **24(3)**, 641-652

Boyle R.W. and Jonasson I.R. (1984) The geochemistry of antimony and its use as an indicator element in geochemical prospecting. *J. Geochem. Explor.* **20**, 223-302

Bozorth R.M. (1923) The crystal structures of the cubic forms of arsenious and antimonious oxides. *J. Am. Chem. Soc.* **45**, 1621-1627

Brannon J.M. and Patrick W.H. Jr. (1985) Fixation and Mobilization of Antimony in Sediments. *Envir. Pollut.* **B9**, 107-126

Brookins D.G. (1972) Stability of Stibnite, Metastibnite, and Some Probable Dissolved Antimony Species at 298.15 K and 1 Atmosphere. *Econ. Geol.* **67**, 369-372

Buccafusco R.J., Elis S.J. and LeBlanc G.A. (1981) Acute Toxicity of Priority Pollutants to Bluegill (Lepomis macrochirus). *Bull. Environm. Contam. Toxicol.* **26**, 446-452

Buerger M.J and Hendricks S.B. (1938) The Crystal Structure of Valentinite (orthorhombic Sb_2O_3). *Z. Kristallogr.* **98**, 1-30

Buschmann J. and Sigg L. (2004) Antimony(III) Binding to Humic Substances: Influence of pH and Type of Humic Acid. *Environ. Sci. Technol.* **38**, 4535-4541

Buschmann J., Canonica S. and Sigg L. (2005) Photoinduced Oxidation of Antimony(III) in the Presence of Humic Acid. *Environ. Sci. Technol.* **39**, 5335-5341

Butterman W.C. and Carlin J.F. (2004) Mineral Commodity Profiles : Antimony, Open-File Report 03-019 of the U.S. Geological Survey, U.S. Department of the Interior.

Casey W.H. and Sposito G. (1992) On the temperature dependence of mineral dissolution rates. *Geochim. Cosmochim. Acta* **56**, 3825-3830

Center for Disease Control and Prevention (2010) http://www.cdc.gov/niosh/topics/antimony/ accessed on 29th December 2010

Chen Y.-W., Deng T.-L., Filella M. and Belzile N. (2003) Distribution and Early Diagenesis of Antimony Species in Sediments and Porewaters of Freshwater Lakes. *Environ. Sci. Technol.* **37**, 1163-1168

Coetzee P.P., Gouws K., Pluddemann S., Yacoby M., Howell S. and Drijver L. (1995) Evaluation of sequential extraction procedures for metal speciation in model sediments. *Water SA* **21**, 51-60

Colling G. (2006) personal communication.

Colombo U.P. and Sironi G. (1964) Systematic Neutron Activation Technique for the Determination of Trace Metals in Petroleum. *Analytical Chemistry* **36**, 802-807

Correns C.W. and von Engelhardt W. (1938) Neue Untersuchungen über die Verwitterung des Kalifeldspates. *Chemie der Erde* **12**, 1-22

Cotton F.A. and Wilkinson G. (1988) Advanced Inorganic Chemistry. 5th ed. Wiley-Interscience, New York.

Council of the European Communities (1976) Council Directive 76/464/EEC of 4 May 1976 on pollution caused by certain dangerous substances discharged into the aquatic environment of the Community. Official Journal L 129, 18/05/1976, pp. 23-29.

Craig P.J., Jenkins R.O, Dewick R. and Miller D.P (1999) Trimethylantimony generation by *Scopulariopsis brevicaulis* during aerobic growth. *The Science of the Total Environmnet* **229**, 83-88

Crecelius E.A., Bothner M.H. and Carpenter R. (1975) Geochemistries of Arsenic, Antimony, Mercury, and Related Elements in Sediments of Puget Sound. *Envir. Sci. Technol.* **9**, 325-333.

Craw, D. (2008) NZTEG 2008 Conference – Antimony in the New Zealand environment. Department of Geology, University of Otago, New Zealand.

Darbre P.D. (2006) Metalloestrogens: an emerging class of inorganic xeoestrogens with potential to add to the oestrogenic burden of the human breast. *J. Appl. Toxicol.* **26**, 191-197

Dasent W.E. (1982) Inorganic Energetics. Cambridge University Press, Cambridge.

Davis A.P., Hsieh Y.H. and Huang C.P. (1995) Photo-oxidative dissolution of CdS(s): The effect of complexing agents. *Chemosphere* **31**, 3093-3104

Debela F., Arocena J.M., Thring R.W. and Whitcombe T. (2010) Organic acid-induced release of lead from pyromorphite and its relevance to reclamation of Pb-contaminated soils. *Chemosphere* **80**, 450-456

Debray H. (1866) Ueber den Dimorphismus der antimonigen und arsenigen Säure. *J. prakt. Chemie* **98(1)**, 151-153

Didérot D. and d'Alembert J. (1751-72) Encyclopédie, ou, Dictionnaire raisonné des sciences, des arts, et des métiers, mis en ordre par MM. Diderot et d'Alembert. Paris.

Diemar G.A., Filella M., Leverett P. and Williams P.A. (2008) Dispersion of antimony from oxidising ore deposits. 13th International Symposium on Solubility Phenomena and Related Equilibrium Processes (13th ISSP), Dublin, Ireland, 27-31 July 2008.

Diemar G.A., Filella M., Leverett P. and Williams P.A. (2009) Dispersion of antimony from oxidising ore deposits. *Pure and Applied Chemistry* **81(9)**, 1547-1553.

Dihlström K. and Westgren A. (1937) Über den Bau des sogenannten Antimontetroxyds und der damit isomorphen Verbindung $BiTa_2O_6F$. *Z. allg. anorg. Chemie* **235**, 153-160

Dubey K.P. and Ghosh S. (1962) Studies on Thiosalts. IV Formation of Thiosalt from Antimonous Sulfide. *Z. Anorg. Chem.* **319**, 204-208

Duester L., Diaz-Bone R.A., Kösters J. and Hirner A.V. (2005) Methylated arsenic, antimony and tin species in soils. *J. Environ. Monit.* **7**, 1186

Dyson R.H. Jr. (1964) Sciences Meet in Ancient Hasanlu. Natural History **73**, 16-25

Dampier, W. C. (1961) A history of science and its relations with philosophy & religion. 4th ed., Cambridge University Press.

EU (2005) Commission directive 2005/79/EC

Fernandes E., Jiménez R., Lallena A.M. and Aguilar J. (2004) Evaluation of the BCR sequential extraction procedure applied for two unpolluted Spanish soils. *Envir. Pollut.* **131**, 355-364

Filella M. (2010) Alkyl derivatives of antimony in the environment. *Met. Ions Life Sci.* **7**, 267-301

Filella M., Belzile N. and Chen Y.-W. (2002a) Antimony in the environment : a review focused on natural waters. I. Occurrence *Earth-Science Reviews* **57**, 125-176 and references cited therein.

Filella M., Belzile N. and Chen Y.-W. (2002b) Antimony in the environment : a review focused on natural waters. II. Relevant Solution chemistry. *Earth-Science Reviews* **59**, 265-285 and references cited therein.

Filella M. and May P.M. (2005) Critical appraisal of available thermodynamic data for the complexation of antimony(III) and antimony(V) by low molecular mass organic ligands. *J. Environ. Monit.* **7**, 1226-1237.

Filella M., Belzile N. and Lett M.-C. (2007) Antimony in the environment : a review focused on natural waters. III. Microbiota relevant interactions. *Earth-Science Reviews* **80**, 195-217 and references cited therein.

Filella M., Williams P.A. and Belzile N. (2009) Antimony in the environment: knowns and unknowns. *Environ. Chem.* **6**, 95-105

Filella M. and Williams P.A. (2010) Antimony Biomethylation in Culture Media Revisited in the Light of Solubility and Chemical Speciation Considerations. *Environ. Toxicol.* **25**, 431-439

Fresenius W. and Jander G. (eds.) (1958) Handbuch der Analytischen Chemie. 3. Teil Quantitative Bestimmungs- und Trennungsmethoden. Band Vaγ Elemente der 5. Hauptgruppe (Arsen-Antimon-Wismut). Springer, Berlin, 1958.

Furrer G. and Stumm W. (1986) The coordination chemistry of weathering: I. Dissolution kinetics of δ-Al_2O_3 and BeO. *Geochim. Cosmochim. Acta* **50**, 1847-1860

Furuta N., Iijima A., Kambe A., Sakai K. and Sato K. (2005) Concentrations, enrichment and predominant sources of Sb and other trace elements in size classified airbone particulate matter collected in Tokyo from 1995 to 2004. *J. Environ. Monit.* **7**, 1155-1161.

Gebel, T. (1997) Arsenic and antimony : comparative approach on mechanistic toxicology. *Chemico-Biological Interactions* **107**, 131-144

Gebel, T. (1999) Umweltmedizin und Toxikologie des Metalloids Antimon. *Umweltmed. Forsch. Prax.* **4**, 259-267

Gomez D.R., Giné M.F., Sanchez Bellato A.C. and Smichowski P. (2005) Antimony : a traffic-related element in the atmosphere of Buenos Aires, Argentina. *J. Environ. Monit.* **7**, 1162-1168.

Goyne K.W., Brantley S.L. and Chorover J. (2006) Effects of organic acids and dissolved oxygen on apatite and chalcopyrite dissolution: Implications for using elements as organomarkers and oxymarkers. *Chem. Geol.* **234**, 28-45

Greenwood N.N. and Earnshaw A. (1984) Chemistry of the Elements. Pergamon Press, Oxford

Gürleyük H., van Fleet-Stalder V. and Chasteen T.G. (1997) Confirmation oft he Biomethylation of Antimony Compounds. *Appl. Organomet. Chem.* **11**, 471-483

Gushchina L.V., Borovikov A.A and Shebanin A.P. (2000) Formation of Antimony(III) Complexes in Alkali Sulfide Solutions at High Temperatures: An Experimental Raman Spectroscopic Study. *Geochemistry International* **38**, 510-513

Haldimann M., Blanc A. and Dudler V. (2007) Exposure to antimony from polyethylene terephtalate (PET) trays used in ready-to-eat meals. *Food Addit. Contam.* **24**, 860-868

Hammel W., Debus R. and Steubing L. (2000) Mobility of antimony and availabilty to plants. *Chemosphere* **41**, 1791-1798

Hansen H.R. and Pergantis S.A. (2006a) Detection of antimony species in citrus juices and drinking water stored in PET containers. *J. Anal. At. Spectrom.* **21**, 731–733

Hansen H.R. and Pergantis S.A. (2006b) Investigating the formation of an Sb(V)-citrate complex by HPLCC-ICP-MS and HPLC-ES-MS(/MS). *J. Anal. At. Spectrom.* **21**, 1240-1248

Hansen H.R. and Pergantis S.A. (2007) Identification of Sb(V) Complexes in Biological and Food Matrices and Their Stibine Formation Efficiency during Hydride Generation with ICPMS Detection. *Anal. Chem.* **79**, 5304-5311

He Z., Traina S.J. and Weavers L.K. (2007) Sonochemical Dissolution of Cinnabar (α-HgS). *Environ. Sci. Technol.* **41**, 773-778

Helgeson H.C., Murphy W.M. and Aagaard P. (1984) Thermodynamic and kinetic constraints on reaction rates among minerals and aqueous solutions. II.

Rate constants, effective surface area, and the hydrolysis of feldspar. *Geochim. Cosmochim. Acta* **48**, 2405-2432

Helz G.R., Valerio M.S. and Capps N.E.(2002) Antimony Speciation in Alkaline Sulfide Solutions: Role of Zerovalent Sulfur. *Environ. Sci. Technol.* **36**, 943-948

Hoch, C. (2010) private communication.

Hofman W. (1933) Die Struktur der Minerale der Antimonitgruppe. *Z. Kristallogr.* **86**, 225-245

Jefferey G.H., Bassett J., Mendham J. and Denney R.C. (1989) Vogel's Textbook of Quantitative Chemical Analysis, 5th Ed., Longman, 1989.

Johnson C.A., Moench H., Wersin P., Kugler P. and Wenger C. (2005) Solubility of Antimony and Other Elements in Samples Taken from Shooting Ranges. *J. Envir. Qual.* **34**, 248

Kabata-Pendias A. and Pendias H. (1992) Trace elements in soils and plants, 2nd ed., CRC Press, Boca Raton

Khangarot B.S. and Ray P.K. (1989) Investigation of Correlation between Physicochemical Properties of Metals and Their Toxicity to the Water Flea Daphnia magna Straus. *Ecotoxicology and Environmental Safety* **18**, 109-120.

Khangarot B.S. (1991) Toxicity of Metals to a Freshwater Tubicifid Worm, Tubifex tubifex (Muller). *Bull. Environm. Contam. Toxicol.* **46**, 906-912

Kirchweger, A.J. (1790) Microscopium Basilii Valentini, In: Triumphwagen des Antimons, H.G. Lenz (ed.), Buchverlag Oliver Humberg, Elberfeld, 2004

Kirk-Othmer (2004) Encyclopedia of chemical technology / executive editor, Jacqueline I. Kroschwitz ; editor, Arza Seidel. 5th ed. Wiley-Interscience. Hoboken.

Kolpakova N.N. (1971) On the speciation of antimony(III) in sulfide solutions (in Russian). In *Geochemistry of Hydrothermal Ore Deposition*. Nauka, Moscow.

Kolpakova N.N. (1982) Laboratory and Field Studies of Ionic Equilibria in the Sb_2S_3-H_2O-H_2S System. *Geochem. Int.* **19**, 46-54

Konopik N. and Zwiauer J. (1952) Über Antimontetroxyd. *Monatshefte für Chemie* **83**, 189-195

Krachler M. and Emons H. (2000) Urinary antimony speciation using HPLC-ICP-MS. *J. Anal. At. Spectrom.* **16**, 20-25

Krachler M. and Emons H. (2001) Speciation of antimony for the 21st century: promises and pitfalls. *Trends in analytical chemistry* **20**, 79-89.

Krachler M., Zheng J., Koerner R., Zdanowicz C., Fisher D. and Shotyk W. (2005) Increasing atmospheric antimony contamination in the northern hemisphere: snow and ice evidence from Devon Island, Arctic Canada. *J. Environ. Monit.* **7**, 1169-1176

Krupka K.M. and Serne R.J. (2002) Geochemical Factors Affecting the Behavior of Antimony, Cobalt, Europium, Technetium and Uranium in Vadose Sediments; Pacific North West Laboratory, Richland, Washington.

Krupp R.E. (1988) Solubility of stibnite in hydrogen sulfide solutions, speciation, and equilibrium constants, from 25 to 350°C. *Geochim. Cosmochim. Acta* **52**, 3005-3015

Krupp R.E. (1990) Comment on "As(III) and Sb(III) sulfide complexes: An evaluation of stoichiometry and stability from existing experimental data" by N.F. Spycher and M.H. Reed. *Geochim. Cosmochim. Acta* **54**, 3239-3240

Kuze S., Du Boulay D., Ishizawa N., Saiki A. and Pring A. (2004) X-ray diffraction evidence for a monoclinic form of stibnite, Sb_2S_3, below 290 K. *Am. Mineral.* **89**, 1022-1025

Kyono A., Kimata M., Matsuhisa M., Miyashita Y and Okamoto K. (2002) Low-temperature crystal structure of stibnite implying orbital overlap of Sb $5s^2$ inert pair electrons. *Phys. Chem. Minerals* **29**, 254-260

Kyono A. and Kimata M. (2004) Structural variations induced by difference of the inert pair effect in the stibnite-bismuthinite solid solution series $(Sb,Bi)_2S_3$. *Am. Mineral.* **89**, 932-940

Laidlar K.J. (1987) Chemical Kinetics. Harper Collins, New York

Lasaga A.C. (1984) Chemical Kinetics of Water-Rock Interactions. *J. Geophys. Res.* **89**, 4009-4025

Lautenschläger K.H and Schröter W. (2005) Taschenbuch der Chemie. Verlag Harri Deutsch, 20th ed., Frankfurt/Main.

Lauwers L.F., Roelants A., Rossel P.M., Heyndrickx B. and Baute L. (1990) Oral antimony intoxication in man. *Crit. Care Med.* **18**, 324-326

LeBlanc G.A. and Dean J.W. (1984) Antimony and Thallium Toxicity to Embryos and Larvae of Fathead Minnows (Pimephales promelas). *Bull. Environm. Contam. Toxicol.* **32**, 565-569.

Lengke M.F. and Tempel R.N. (2003) Natural realgar and amorphous AsS oxidation kinetics. *Geochim. Cosmochim. Acta* **67**, 859-871

Léonard A. and Gerber G.B. (1996) Mutagenicity, carcinogenicity and teratogenicity of antimony compounds. *Mutation Res./Rev. Genetic Toxicol.* **366**, 1-8

Leuz A.-K. and Johnson C.A. (2005) Oxidation of Sb(III) to Sb(V) by O_2 and H_2O_2 in aqueous solution. *Geochim. Cosmochim. Acta* **69**, 1165-1172

Leuz A.-K., Mönch H. and Johnson C.A. (2006) Sorption of Sb(III) and Sb(V) to Goethite: Influence on Sb(III) Oxidation and Mobilization. *Environ. Sci. Technol.* **40**, 7277-7282

Lide D. (ed.) (1996) CRC Handbook of Chemistry and Physics, 77th ed. CRC Press, Boca Raton

v. Lippmann E.O. (1919-1954) Enstehung und Ausbreitung der Alchemie. Bd.I Berlin 1919, Bd.II Berlin 1931, Bd.III Weinheim 1954.

Lin H.C. and Hwang P.P. (1998) Acute and Chronic Effects of Antimony Chloride ($SbCl_3$) on Tilapia (Oreochromis mossambicus) Larvae. *Bull. Environ. Contam. Toxicol.* **61**, 129-134.

Ludwig C., Casey W.H. and Rock P.A. (1995) Prediction of ligand-promoted dissolution rates from the reactivities of aqueous complexes. *Nature* **375**, 44-47

Majzlan J., Lalinska B, Chovan M., Bläss U., Brecht B., Göttllicher J., Steininger R, Hug K., Ziegler S. and Gescher J. (2011) A mineralogical, geochemical, and microbiological assessment of the antimony- and arsenic-rich neutral mine drainage tailings near Pezinok, Slovakia. *American Mineralogist* **96**, 1-13

Martin R.R., Shotyk W., Naftel S.J., Ablett J.M. and Northrup P. (2010) Speciation of antimony in polyethylene terephtalate bottles. *X-Ray Spectrom.* **39**, 257-259

Martinez C.E., Jacobsen A.R. and McBride M.B. (2004) Lead Phosphate Minerals: Solubility and Dissolution by Model and Natural Ligands. *Environ. Sci. Technol.* **38**, 5584-5590

McCay L.W. (1933) Reduction of Antimonic Acid in Hydrochlorid Acid Solution with Mercury. *Ind. Eng. Chem. Anal. Ed.* **5**, 1-3

Millen B.M.J. (2001) Aspects of the Hydrogeology of a Mining Region with a Focus on the Antimony Content of a Spring-Water, Eiblschrofen Massif, Schwaz, Tyrol, Austria. *Mitt. Österr. Geolog. Gesell.* **94**, 139-156.

Mitsunobu S., Takahashi Y., Terada Y. and Sakata M. (2010) Antimony(V) Incorporation into Synthetic Ferrihydrite, Goethite, and Natural Iron Oxides. *Environ. Sci. Technol.* **44**, 3712-3718

Mok W.-M. and Wal C.M. (1990) Distribution and Mobilization of Arsenic and Antimony Species in the Coeur d'Alene River, Idaho. *Environ. Sci. Technol.* **24**, 102-108

Mosselmans J.F.W, Helz G.R., Pattrick R.A.D., Charnock J.M. and Vaughan D.J. (2000) A study of speciation of Sb in bisulfide solutions by X-ray absorption spectroscopy. *Appl. Geochem.* **15**, 879-889

Müller B., Granina L., Schaller T., Ulrich A. and Wehrli B. (2002) P, As, Sb, Mo, and other Elements in Sedimentary Fe/Mn Layers of Lake Baikal. *Environ. Sci. Technol*. **36**, 411-420

Nam S.H., Yang C.-Y. and An Y.-J. (2009) Effects of antimony on aquatic organisms (Larva and embryo of Oryzias latipes, Moina macrocopa, Simocephalus mixtus and Pseudokirchneriella subcapitata). *Chemosphere* **75**, 889-893

Nash M.J., Maskall J.E. and Hill S.J. (2000) Methodologies for determination of antimony in terrestrial environmental samples. *J. Environ. Monit.* **2**, 97-109

Neeb R. (1989) Stripping voltammetry. Monograph published by Metrohm AG, Herisau, Switzerland.

Nirel P.A., Pomian-Srzednicki I., Meyer M. and Filella M. (2008) Dissolved antimony concentrations in contrasted watersheds: the importance of lithogenic origin. *J. Envir. Monit.* **10**, 256-260

Nölte, J. (2003) ICP Emission Spectrometry. A Practical Guide. Wiley-VCH, Weinheim, 2003.

Nova Vulgata (1986) Bibliorum sacrorum editio, Libreria editrice vaticana.

Nriagu J.O. (1989) A global assessment of natural sources of atmospheric trace metals. *Nature* **338**, 47-49

Oelkers E.H., Sherman D.M., Ragnasdottir K.V. and Collins C. (1998) An EXAFS spectroscopic study of aqueous antimony(III)-chloride complexation at temperatures from 25 to 250°C. *Chem. Geol.* **151**, 21-27

Oorts K., Smolders E., Degryse F., Buekers G.G., Cornelis G. and Merstens J. (2008) Solubility and Toxicity of Antimony Trioxide (Sb_2O_3) in Soil. *Environ. Sci. Technol.* **42**, 4378-4383

Panasenko A.E., Zemnukhova L.A., Ignat'eva L.N., Kaidalova T.A., Kuznetsov S.I., Polyakova N.V. and Marchenko Y.V. (2009) *Inorganic Materials* **45**, 402-408

Park S.W. and Huang C.P. (1986) The surface acidity of hydrous CdS(s). *J. Colloid Interf. Sci.* **117**, 431-441

Pike A.W.G., Cowell M. and Curtiss J.E. (1996) The Use of Antimony Bronze in the Koban Culture. *Historical Metallurgy* **30**, 11-16

Pilarski J., Waller P. and Pickering W. (1995) Sorption of Antimony Species by Humic Acid. *Water, Air and Soil Pollution* **84**, 51-59

Pokrovski G.S., Borisova A.Y., Roux J., Hazemann J.-L., Petdang A., Tella M. and Testemale D. (2006) Antimony speciation in saline hydrothermal fluids: A combined X-ray absorption fine structure spectroscopy and solubility study. *Geochim. Cosmochim. Acta* **70**, 4196-4214

Porquet A. and Filella M. (2007) Structural Evidence of the Similarity of $Sb(OH)_3$ and $As(OH)_3$ with Glycerol: Implications for Their Uptake. *Chem. Res. Toxicol.* **20**, 1269-1276

Posner L. (1866) Handbuch der klinischen Arzneimittellehre, A. Hirschfeld, Berlin.

Postupolski A. and Golimowski J. (1991) Trace Determination of Antimony and Bismuth in Snow and Water Samples by Stripping Voltammetry. *Electroanalysis* **3**, 793-797

Priesner C. and Figala K. (1998) Alchemie. Lexikon einer hermetischen Wissenschaft. Verlag C.H. Beck, München.

Quentel F. and Filella M. (2002) Determination of inorganic antimony species in seawater by differential pulse anodic stripping voltammetry: stability of the trivalent state. *Anal. Chim. Acta* **452**, 237-244.

Ravichandran M., Aiken G.R., Reddy M.M. and Ryan J.N. (1998) Enhanced Dissolution of Cinnabar (Mercuric Sulfide) by Dissolved Organic Matter isolated from the Florida Everglades. *Environ. Sci. Technol.* **32**, 3305-3311

Renock D. and Becker U. (2010) A first principles study of the oxidation energetics and kinetics of realgar. *Geochim. Cosmochim. Acta* **74**, 4266-4284

Richardson B.A. (1990) Cot mattress biodeterioration and SIDS. *The Lancet* **335**, 670

Richardson B.A. (1994) Sudden infant death syndrome: a possible primary cause. *J. Forens. Sci. Soc.* **34**, 199-204

Rimstidt J.D., Chermak J.A. and Gagen P.M. (1994) Rates of Reaction of Galena, Sphalerite, Chalcopyrite, and Arsenopyrite with Fe(III) in Acidic Solutions. In *Environmental Geochemistry of Sulfide Oxidation, ACS Symposium Series 550* (eds. C.N. Alpers and D.W. Blowes) American Chemical Society, Washington, chapter 1.

Roberts E.J. and Fenwick F. (1928) The antimony-antimony trioxide electrode and its use as a measure of acidity. *J. Am. Chem. Soc.* **50**, 2125-2147

Rönngren L., Sjöberg S., Sun Z., Forsling W. and Schindler P. (1991) Surface reactions in aqueous metal sulfide systems. 2. Ion exchange and acid/base reactions at the ZnS-H_2O interface. *J. Colloid Interf. Sci.* **145,** 396-404

Saldi G.D., Schott J., Pokrovsky O.S. and Oelkers E. (2010) An experimental study of magnesite dissolution rates at neutral to alkaline conditions and 150 and 200°C as a function of pH, total dissolved carbonate concentration, and chemical affinity. *Geochim. Cosmochim. Acta* **74**, 6344-6356

Sarton, G. (1935). Max Meyerhof.-(*Al-morchid fi'l-kohhl*) ou *Le guide d'oculistique*. *Isis* **22**, 539-542.

Sauvant M.P., Pépin D., Grolière C.A. and Bohatier J. (1995) Effects of Organic and Inorganic Substances of the Cell Proliferation of L-929 Fibroblasts and Tetrahymena pyriformis GL Protozoa used for Toxicological Bioassays. *Bull. Environ. Contam. Toxicol.* **55**, 171-178.

Scavnicar S. (1960) The crystal structure of stibnite. A redetermination of atomic positions. *Z. Kristallogr.* **114**, 85-97

Scheinost A.C., Rossberg A., Vantelon D., Xifra I., Kretzschmar R., Leuz A.-K., Funke H. and Johnson C.A. (2006) Quantitative antimony speciation in shooting-range soils by EXAFS spectroscopy. *Geochim. Cosmochim. Acta* **70**, 3299-3312

Shah K.R., Filby R.H. and W.A. Haller (1970) Determination of Trace Elements in Petroleum by Neutron Activation Analysis. *J. Radioanal. Chem.* **6**, 413-422

Shannon R.D. (1976) Revised effective ionic radii and systematic studies of interatomic distances in halides and chalcogenides. *Acta Cryst.* **A32**, 751-767

Sharma M. and Patel K.S.(1993) Determination and Speciation of Antimony in Waters. *International Journal of Environmental Analytical Chemistry* **50**, 63-71

Sherman D.M., Ragnarsdottir K.V. and Oelkers E.H. (2000) Antimony transport in hydrothermal solutions : an EXAFS study of antimony(V) complexation in alkaline-sulfide and sulfide-chloride brines at temperatures from 25°C to 300°C at P_{sat}. *Chem. Geol.* **167**, 161-167.

Shortland A.J. (2002a) The use and origin of antimonate colorants in early egyptian glass. *Archaeometry* **44(4)**, 517-530

Shortland A.J. (2002b) An antimony bead from Jerablus-Tahtani. *Historical Metallurgy* **36(1)**, 1-5.

Shotyk W., Krachler M. and Chen B. (2004) Antimony in recent, ombrotrophic peat from Switzerland and Scotland: Comparison with natural background values (5,320 to 8,020 ^{14}C yr BP) and implications for the global atmospheric Sb cycle. *Global Biogeochemical Cycles* **18**, GB1016.

Shotyk W., Krachler M. and Chen B. (2005a) Anthropogenic Impacts on the Biogeochemistry and Cycling of Antimony. in *Biogeochemistry, Availability, and Transport of Metals in the Environment,* ed. A. Sigel, H. Sigel, R.K.O.

Sigel, M. Dekker, **Vol. 44** of *Metal Ions in Biological Systems*, New York, 2005, pp. 172-203

Shotyk W., Krachler M., Chen B. and Zheng J. (2005b) Natural abundance of Sb and Sc in pristine groundwaters, Springwater Township, Ontario, Canada, and implications for tracing contaminations by landfill leachates. *J. Envir. Monit.* **7**, 1238-1244

Shotyk W., Krachler M. and Chen B. (2006) Contamination of Canadian and European bottled waters with antimony from PET containers. *J. Environ. Monit.* **8**, 288-292

Sidgwick N.V. (1950) The Chemical Elements and their Compounds. Clarendon Press, Oxford.

Smichowski P., Madrid Y. and Camara C. (1998) Analytical Methods for antimony speciation in waters at trace and ultratrace levels. A review. *Fresenius J. Anal. Chem.* **360**, 623-629

Smith G., Sagatys D.S., Bott R.C. and Lynch D.E. (1993) Group 15 Complexes with carboxylic acids-VI. *Polyhedron* **12**, 1491-1497.

Snell F.D. and Snell C.T. (1949) Colorimetric Methods of Analysis, 3rd ed., vol. II, D. van Nostrand, New York (1949).

Sposito G. (2004) The Surface Chemistry of Natural Particles, Oxford University Press, Oxford.

Sposito G. (2008) The Chemistry of Soils, Oxford University Press, Oxford.

Spycher N.F. and Reed M.H. (1989) As(III) and Sb(III) sulfide complexes : An evaluation of stoichiometry and stability from existing experimental data. *Geochim. Cosmochim. Acta* **53**, 2185-2194

Spycher N.F. and Reed M.H. (1990) Reply to comment by R.E. Krupp on "As(III) and Sb(III) sulfide complexes: An evaluation of stoichiometry and stability from existing experimental data. *Geochim. Cosmochim. Acta* **54**, 3241-3243

Steely S., Amarasiriwardena D. and Xing B. (2007) An investigation of inorganic antimony species and antimony associated with soil humic acid molar mass fractions in contaminated soil. *Env. Poll.* **148**, 590-598

Sterckeman T., Douay F., Baize D., Fourrier H., Proix N. and Schwartz C. (2004) Factors affecting trace element concentrations in soils developed on recent marine deposits from northern France. *Appl. Geochem.* **19**, 89-103

Stewart D.J., Knop O.K., Ayasse C. and Woodhams F.W.D. (1972) Pyrochlores. VII. The Oxides of Antimony: an X-ray and Mössbauer study. *Canadian Journal of Chemistry* **50**, 690-700

Stevens J.G., Etter R.M. and Setzer E.W. (1993) ^{121}Sb Mössbauer spectroscopy study of the mineral stibiconite. *Nuclear Instruments and Methods in Physics Research* **B76**, 252-253

Stillings L.L., Drever J.I. and Poulson S.R. (1998) Oxalate Adsorption at a Plagioclase (An_{47}) Surface and Models for Ligand-Promoted Dissolution. *Environ. Sci. Technol.* **32**, 2856-2864

Stock A. and Guttmann O. (1904) Über den Antimonwasserstoff und das gelbe Antimon. *Chem. Ber.* **37**, 885-900

Stock A. and Siebert W. (1905) Die Modificationen des Antimons. *Chem. Ber.* **38**, 3837-3844

Stumm W. and Morgan J.J. (1996) Aquatic Chemistry, 3rd ed., Wiley-Interscience, New York

Stumm W. and Wollast R. (1990) Coordination Chemistry of Weathering : Kinetics of the Surface-Controlled Dissolution of Oxide Minerals. *Rev. Geophys.* **28**, 53-69

Sundar S., Sinha P.R., Agrawal N.K., Srivastava R., Rainey P.M., Berman J.D., Murray H.W. and Singh V.P. (1998) A cluster of cases of severe cardiotoxicity among kala-azar patients treated with a high-osmolarity lot of sodium antimony gluconate. *Am. J. Trop. Med. Hyg.* **59(1)**, 139-143

Svensson C. (1974) The crystal structure of orthorhombic antimony trioxide, Sb_2O_3. *Acta Cryst.* **B30**, 458-461

Svensson C.(1975) Refinement of the crystal structure of cubic antimony trioxide, Sb_2O_3. *Acta Cryst.* **B31**, 2016-2018

Takahashi Y., Sakuma K., Itai T., Zheng G. and Mitsunobo G. (2008) Speciation of Antimony in PET Bottles Produced in Japan and China by X-ray Absorption Fine Structure Spectroscopy. *Environ. Sci. Technol.* **42**, 9045-9050

Thanabalasingam P. and Pickering W.F. (1990) Specific sorption of antimony(III) by the hydrous oxides of Mn, Fe and Al. *Water, Air, and Soil Pollution* **49**, 175-185

Thomson S. (1926) Antimonyall Cupps: Pocula Emetica or Calices Vomitorii. *British Medical J.* **1** (no 3406, April 10th, 1926) 669-671

Tella M. and Pokrovsky G.S. (2008) Antimony(V) complexing with O-bearing organic ligands in aqueous solution: an X-ray absorption fine structure spectroscopy and potentiometric study. *Min. Mag.* **72**, 205-209

Tella M. and Pokrovsky G.S. (2009) Antimony(III) complexing with O-bearing organic ligands in aqueous solution: an X-ray absorption fine structure spectroscopy and solubility study. *Geochim. Cosmochim. Acta* **73**, 268-290

Thornton G. (1977) A neutron diffraction study of α-Sb_2O_4. *Acta cryst*. **B33**, 1271-1273

Tirmenstein M.A., Plews P.I., Walker C.V., Woolery M.D., Wey H.E. and Toraason M.A. (1995) Antimony-Induced Oxidative Stress and Toxicity in Cultured Cardiac Myocytes. *Toxicology and Applied Pharmacology* **130**, 41-47

Tossell J.A. (1994) The Speciation of antimony in sulfidic solutions : A theoretical study. *Geochim. Cosmochim. Acta* **58**, 5093-5104

Tossell J.A. (2003) Calculation of the energetics for the oxidation of Sb(III) sulfides by elemental S and polysulfides in aqueous solution. *Geochim. Cosmochim. Acta* **67**, 3347-3354

Tripathi A.N. and Patel K.S.(1998) Determination of antimony in rainwater at the nanogram level with surfactant and brilliant green. *Fresenius J. Anal. Chem.* **360**, 270-272

Tschan M., Robinson R. and Schulin R. (2008) Antimony uptake by *Zea mays* (L.) and *Helianthus annuus* (L.) from nutrient solution. *Environ. Geochem. Health* **30**, 187-191

United States Environmental Protection Agency (1979) Water Related Fate of the 129 Priority Pollutants, vol. 1. USEPA, Washington, DC, USA, EP-440/4-79-029A.

Ure, A.M. and Davidson, C.M. (2002) Chemical Speciation in soils and related materials by selective chemical extraction. In Chemical Speciation in the Environment, Ure, A.M.; Davidson, C.M., Eds., Blackwell Science, Oxford.

Valentinus B. (1604) Triumphwagen des Antimons, H.G. Lenz (ed.), Buchverlag Oliver Humberg, Elberfeld, 2004

Vitaliano C.J. and Mason B. (1952) Stibiconite and Cervantite. *Am. Min.* **37**, 982-999.

Vogel A.I. (1937) A Text-Book of Qualitative Chemical Analysis Including Semimicro Qualitative Analysis. Longmans, Green and Co., London

Wehmeier S., Raab A. and Feldmann J. (2004) Inverstigations into the role of methylcobalamin and glutathione for the methylation of antimony using isotopically enriched antimony(V). *Appl. Organomet. Chem.* **18**, 631-639

Welch S.A. and Ullman W.J. (1993) The effect of organic acids on plagioclase dissolution rates and stoichiometry. *Geochim. Cosmochim. Acta* **57**, 2725-2736

Whalley C. and Grant A. (1994) Assessment of the phase selectivity of the European Community Bureau of Reference (BCR) sequential extraction procedure for metals in sediment. *Anal. Chim. Acta* **291**, 287-295

Wieland E., Wherli B. and Stumm W. (1988) The coordination chemistry of weathering: III. A generalization on the dissolution rates of minerals. *Geochim. Cosmochim. Acta* **52**, 1969-1981

Wieland E. and Stumm W. (1992) Dissolution kinetics of kaolinite in acidic aqueous solutions at 25°C. *Geochim. Cosmochim. Acta* **56**, 3339-3355

Wilson S.C., Lockwood P.V., Ashley P.M. and Tighe M. (2010) The chemistry and behaviour of antimony in the soil environment with comparison to arsenic: A critical review. *Environmental Pollution* **158**, 1169-1181

Warnock D.W., Delves H.T., Campbell C.K., Croudace I.W., Davey K.G., Johnson E.M. and Sieniawska G. (1995) Toxic gas generation from plastic mattresses and sudden infant death syndrome. *The Lancet* **346**, 1516-1520

Wey H.E., Richards D., Tirmenstein M.A., Mathias P.I. and Toraason M. (1997) The Role of Intracellular Calcium in Antimony-Induced Toxicity in Cultured Cardiac Myocytes. *Toxicology and Applied Pharmacology* **145**, 202-210

WHO (2003) Antimony in Drinking-Water. Background Document for Development of WHO Guidelines for Drinking-Water Quality. WHO/SED/WSH/03.04.

Wood S.A. (1989) Raman spectroscopic determination of the speciation of ore metals in hydrothermal solutions : I. Speciation of antimony in alkaline sulfide solutions at 25°C. *Geochim. Cosmochim. Acta* **53**, 237-244.

Zih-Perényi K., Neurohr K., Nagy G., Balla M. and Lasztity A. (2010) Selective extraction of traffic-related antimony compounds for speciation analysis by graphite furnace atomic absorption spectrometry. *Spectrochimica Acta Part B* **65**, 847-851

Chapter II :

Experimental Studies of Stibnite (Sb_2S_3) Dissolution Kinetics: Effects of pH, Dissolved Oxygen, Ferric Iron and Temperature.

Part I : Acidic Solutions.

Abstract - The kinetics of oxidative dissolution of natural stibnite (Sb_2S_3) in perchloric acid solutions is investigated. The effects of hydrogen ion concentration (pH=1 to 5), dissolved oxygen saturation (partial pressures from 0 to 0.8 atm), ferric iron (10^{-5} to 10^{-3} M) and temperature (25° to 40°C) on the reaction rate were studied using a mixed flow reactor. The stibnite dissolution rate was found to be proportional to a fractional power of hydrogen ion concentration, while the rate dependence on dissolved oxygen is best described in terms of Langmuir adsorption, with saturation occurring at oxygen partial pressures in excess of 0.2 atm:

$$r = k\left[H^+\right]^{\alpha} \frac{K\left[O_2\right]}{1+K\left[O_2\right]}, \text{ where}$$

$k=1.14\times10^{-10} \pm 0.09\times10^{-10}$; $\alpha=0.125 \pm 0.006$; $K=2.13\times10^{4} \pm 0.26\times10^{4}$ mol^{-1} l.

The activation energy at pH=3 in the temperature range 25-40°C is 5.2 ± 0.4 kJ mol^{-1}, suggesting a mixed adsorption and diffusion controlled mechanism. Ferric iron strongly catalyses the dissolution, with an acceleration of the rate by approximately an order of magnitude for $[Fe^{3+}] = 10^{-3}$ M at pH = 2. The kinetics is again best described in terms of Langmuir adsorption of Fe^{3+} on the stibnite surface, with saturation occurring above ca. 4×10^{-3} M,

$$r = r_{\max} \frac{K\left[Fe^{3+}\right]}{1+K\left[Fe^{3+}\right]}, \text{ where}$$

$r_{max}= 4.6\times10^{-10} \pm 0.3\times10^{-10}$ mol s^{-1} m^{-2}; $K=1.4\times10^{4} \pm 0.5\times10^{4}$ mol^{-1} l.

Aluminium ion, which has an ionic radius (54 pm) almost identical to that of ferric iron (55 pm), produces a similar rate enhancement. The effect of

cationic radius on the dissolution rate of stibnite was evaluated using Ce^{3+} (114 pm) which increased the rate even more.

Stibnite dissolution is incongruent to varying degrees, with elemental sulfur forming a residual surface layer. In the presence of high concentrations of ferric iron, the dissolution becomes highly incongruent, with a substantial accumulation (7 to 13 atomic layers) of elemental sulfur. In contrast to Fe^{3+}, neither Ce^{3+} nor Al^{3+} has an effect on the formation of elemental sulfur, clearly demonstrating the important role played by Fe^{3+} in the oxidation of sulfide to elemental sulfur.

II.1 Introduction

The oxidative dissolution of pyrite, the single most abundant sulfide mineral, leads to the net release of protons, a phenomenon known as acid mine or acid rock drainage. The increased acidity of surface waters reported in extreme cases are illustrated by pH values as low a -3.6 (Nordstrom et al., 2000). Subsequent weathering and leaching of other minerals by acidic drainage waters causes elevated concentrations of a broad range of potentially toxic elements, especially chalcophile elements such as Cd and Pb which are enriched in metal sulfides. The elevated concentrations of these "heavy metals" and the predominance of their generally more harmful, cationic forms at low pH, present serious risks to all forms of life in receiving water bodies. There is an abundant literature on sites affected by acid mine drainage (Edwards et al., 2000; Domènech et al., 2002; Moncur et al., 2005; Moncur et al., 2009; Asta et al., 2010a) and comprehensive reviews are available (Nordstrom, 2000; Akcil, 2006), which also cover microbiological aspects of sulfide weathering and methods of remediation. Anomalous acidity and elevated metal concentrations in surface waters may also arise naturally, as a consequence of acid rock drainage in areas devoid of mining activities (Kwong et al., 2009; Verplanck et al., 2009).

While the mechanism of pyrite oxidation has been extensively studied and is comparatively well understood (Rimstidt and Vaughan, 2003), the same cannot be said about other sulfide minerals. Clearly, it is difficult if not impossible to apply the pyrite model to constitutionally and structurally differing sulfide minerals. There is a number of kinetic and surface studies on the weathering of

other sulfides: orpiment and amorphous As_2S_3 (Lengke and Tempel, 2001 and 2002), realgar and amorphous AsS (Lengke and Tempel, 2003), galena (Giudici et al., 2005), arsenopyrite (Nesbitt et al., 1995; Walker et al., 2006; Corkhill and Vaughan, 2009; Asta et al., 2010b), galena, chalcopyrite and sphalerite (Abraitis et al., 2004) and mackinawite (Jeong et al., 2010). A review of chalcopyrite dissolution rate laws was presented by Kimball et al., (2010) and theoretical studies of realgar dissolution by Renock and Becker (2010). However, despite the growing economic importance of antimony and its compounds and alloys (Filella et al., 2002), kinetic and mechanistic aspects of the weathering of stibnite (Sb_2S_3), the single most important antimony ore, have not yet received any attention. Given the growing recognition of antimony as an emerging contaminant and globally important atmospheric pollutant (Fillela et al., 2002), there is a real need to develop a better understanding of the geochemistry of this fascinating element in the weathering zone, beginning with its release from its predominant source, stibnite.

The aim of the present work is to study the abiotic oxidative dissolution of stibnite and to establish a kinetic rate law under acid conditions (pH 1 to 5). These studies have been undertaken, taking into account the effects of dissolved oxygen (from partial pressures ranging from 0.05 atm to 0.8 atm) , cations (Fe^{3+}, Al^{3+}, Ce^{3+}) and temperature (over the range 25°C to 40°C). The formation of elemental sulfur on the surface of dissolving stibnite is duly considered, using an analytical method for measuring elemental sulfur developed for this task.

Oxidative dissolution of stibnite under basic conditions will be dealt with in Chapter III.

II.2. Materials and Methods

II.2.1 Sample Origin and Pretreatment

Stibnite from the Goesdorf deposit, Luxembourg (Europe) was used in the experiments. The geology of this deposit has been described by Fillela and co-workers (Fillela et al., 2009). Elemental analysis (ICP-OES) showed the mineral to be >98% Sb_2S_3, the major impurities being Fe, Pb and silica. A large mineral fragment was broken with a steel hammer; pieces free of superficial oxidation products were crushed in a steel percussion mortar and ground to powder in an agate mortar. The powder was sieved and the fraction between 0.122 and 0.062 mm was retained for the experiments. In order to remove finer particles, portions of approx. 2 g were covered with about 50 ml of analytical grade ethanol (96% v/v) and sonicated for 30 min at 100W. The dark supernatant was removed by suction and the sonication process repeated twice. The mineral was rinsed with ethanol and dried *in vacuo* at room temperature. Electron micrographs of samples before and after this pre-treatment show that the sonication in ethanol removes most, but not all of the fine particles adhering to the mineral grains (Figs.II.1 and 2). This is, however, of little consequence, as the experiments are designed so as to measure steady-state dissolution rates, which are reached only after virtually all of the fine particles will have dissolved.

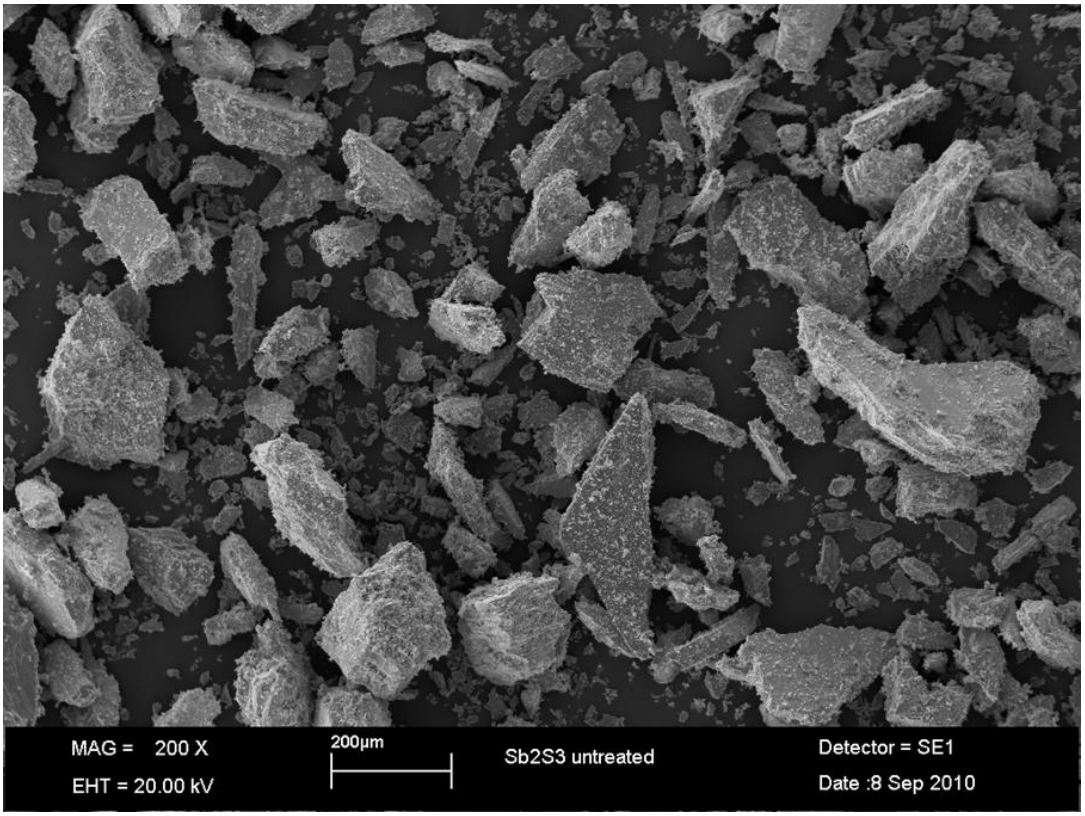

Fig. II.1 SEM micrograph of gold-coated stibnite sample before sonication in ethanol

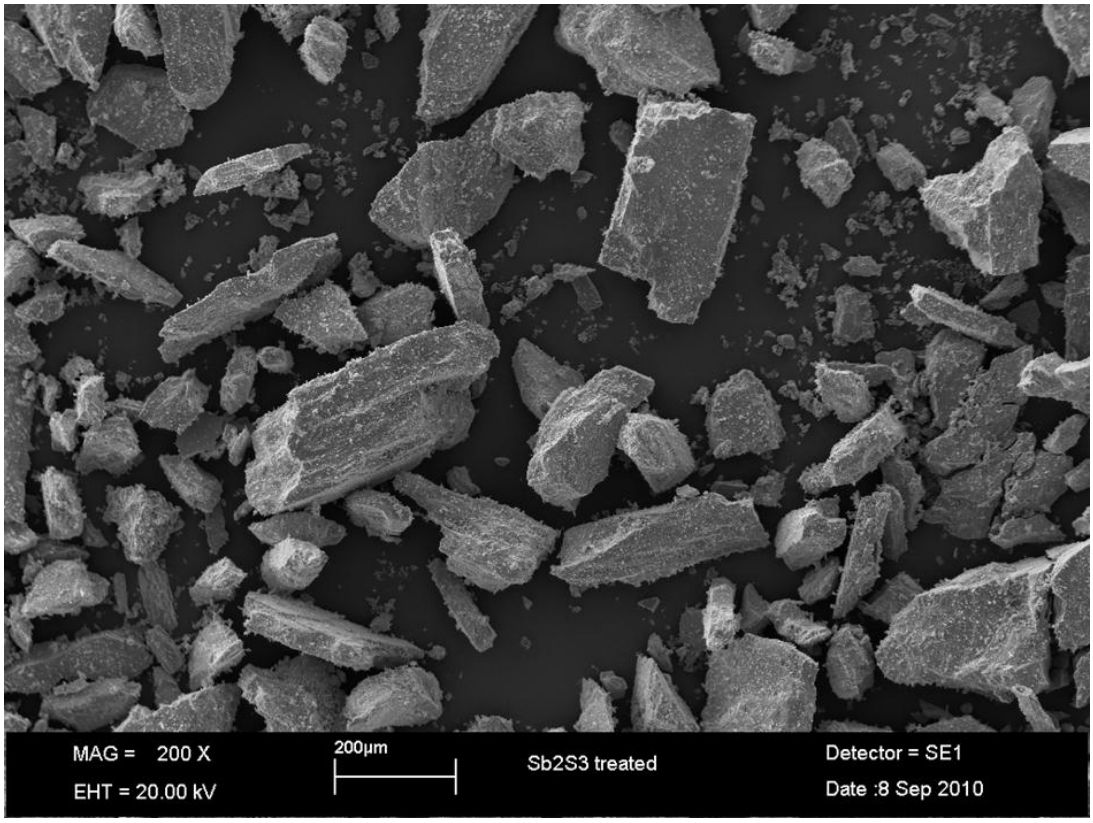

Fig. II.2 The same material as in Fig. II.1 after sonication in Ethanol

II.2.2 Measurement of rates of dissolution

II.2.2.1. Experimental design

Dissolution rates were measured using a mixed flow reactor. The application of the mixed flow reactor in the study of mineral dissolution kinetics and its advantages over other experimental designs were first described and discussed by Rimstidt and Dove (1986) and it has since become a well established technique.

The feed solutions (perchloric acid solutions of pH 1, 2, 3, 4, and 5) were prepared by dilution of conc. perchloric acid ('supra' quality) from C. Roth, Germany, with ultrapure water from a Milli-Q water purification unit. The ionic strength of the feed solutions was adjusted to 0.01 M by $NaClO_4$ (p.a. ACROS), except for solutions of pH 1 and 2. The feed solution was sparged with oxygen-nitrogen mixtures (5%, 10%, 20%, 40%, 60% and 80% O_2) in order to achieve different concentrations of dissolved oxygen. An experiment under anoxic conditions was also made; the feed solution was sparged with >99.999% nitrogen. The gases and gas mixtures prepared from >99.999% pure gases were purchased from L'Air Liquide SA, Luxembourg. In some experiments, feed solutions containing Fe^{3+}, Al^{3+}, Ce^{3+} at pH=2 were used. These were prepared by dissolution of the corresponding perchlorates and perchloric acid in Milli-Q water. Perchloric acid and perchlorate salts were chosen for several reasons: the use of sulfuric acid would have precluded the determination of dissolved sulfur species in the effluent, while the formation of antimony chloro-complexes that could have affected reaction rates ruled out the use of hydrochloric acid. Moreover, the

perchlorate anion only forms extremely weak complexes in aqueous solution (Johansson, 1974).

The feed solution was pumped into the reactor (a Millipore Amicon Ultrafiltration Cell, Model 8200, of nominal volume 200 ml) containing approx.1.5 g (accurately weighed) of the mineral by a variable speed peristaltic pump. The reactor contents were mixed by means of a magnetic stirrer bar suspended from the lid, to avoid grinding of the mineral. The reactor was wrapped in aluminium foil (to avoid photochemical reactions) and immersed in a constant temperature water bath. All connections between the components of the experimental setup were made with glass and semi-rigid FEP tubing. The effluent from the ultrafiltration cell passed through a large Erlenmeyer flask that could be fitted with dissolved oxygen (DO) and pH probes (Hanna Instruments MI 9146 oxymeter and Metrohm pH Meter Model 632, respectively). The flow rate was measured using a graduated cylinder and a stopwatch. Samples were taken after ca. 8 h, then ca. every hour after a 24 h equilibration period. A stationary state with respect to total antimony concentration was generally reached after 24 to 36 h. Some experiments took longer to reach a steady state and ran for 48 h or longer, as required.

II.2.2.2. Analytical Methods

Total Sb and Sb(III) concentrations were measured in the effluent using voltammetric techniques (Quentel and Filella., 2002) implemented on a Metrohm VA797 Computrace voltammetric analyser. Sodium chloride solution was used as the bridging electrolyte in the reference electrode to avoid clogging of the

diaphragm by $KClO_4$ which would precipitate if a solution high in perchlorate is measured with KCl as the bridge electrolyte. Antimony concentrations ranged between 10 and 500 µg l^{-1}, so that samples had to be diluted by injecting volumes of 50 to 500 µl into 10 ml of the voltammetric base electrolyte (15% Suprapur HCl for Sb(tot), 0.5 M NaCl and 0.5 M HCl for Sb(III)). The reported detection limits are 33 ng l^{-1} for Sb(tot) and 11 ng l^{-1} for Sb(III). Samples for Sb(III) analysis (10 ml) were collected in PP vials containing 50 mg ascorbic acid, to inhibit oxidation to Sb(V), and were frozen immediately. It was verified in an independent experiment that ascorbic acid at this concentration did not reduce any Sb(V) to Sb(III), and that solutions of Sb(III) in stoppered vials were indeed stable for several days under these conditions.

Dissolved sulfur concentrations were measured using ICP-OES (Spectroflame Modula, Spectro Analytical Instruments) with a detection limit of 5 µg l^{-1}.

Elemental sulfur formed on the mineral surface was quantitatively determined using UV photometry (cf. Appendix AIV). Sulfur dissolved in cyclohexane has an absorption maximum at 206.3 nm with a specific extinction coefficient of 0.238 ± 0.037 l mg^{-1} cm^{-1} (useful conc. range : 0 to 4 mg l^{-1}). The reacted stibnite samples were recovered from the reactor after the experiment, washed once with dionized water and vacuum dried. An accurately weighed amount (50-100 mg) was introduced into a PTFE centrifuge tube and extracted with 10 ml spectroscopic grade cyclohexane (C. Roth, Germany) on a tumbler for

ca. 8 h. The tubes were centrifuged and the absorption of the clear supernatant measured in quartz cells, after dilution with cyclohexane if necessary.

Specific surface areas of the mineral samples were estimated from multiple-point N_2 BET adsorption isotherms (Gemini VII 2390, Micromeritics GmbH, Aachen, Germany) and ranged between 0.24 to 0.45 m^2g^{-1} (between 8 to 10 data points were gathered). The relative error in this determination was always better than 0.6%.

II.3 Results and Discussion

From the flow rate Q of the solution through the reactor, the measured total antimony concentration [Sb(tot)] and the surface area A of the sample, the rate of stibnite dissolution is obtained as

$$r = -\frac{d[Sb_2S_3]}{dt} = \frac{[Sb(tot)]Q}{2A}$$

(Nagy et al., 1991). In a typical experiment, the dissolution rate exhibits a maximum shortly after the start of the experiment and gradually slows down to a constant value. The reason for the early maximum is most likely the 'excessively reactive surface [of the freshly ground material] due to adhering small grains, sharp edges, and stressed areas that react more rapidly than the bulk solid' (Rimstidt and Dove, 1986). After the rapid dissolution of ultrafine grains, an essentially constant surface area is eventually reached and the mineral dissolves at a constant rate. In our experiments, this steady state was assumed to have been reached whenever a series of successive measurements gave a constant

product [Sb(tot)]Q, with standard deviations less than 10%; in most experiments, the standard deviations were much better.

With respect to dissolved sulfur species, the standard deviations in the steady state concentrations were always larger. Moreover, the detection limit of S by ICP-OES (5 µg l^{-1}) is larger than that of the electrochemical Sb determination (33 ng l^{-1}), and the correlation coefficients in the log-log plots used to determine the experimental rate orders were not as good as those based on Sb measurements. The fact that zerovalent sulfur could be detected on the reacted mineral surface showed that the dissolution was to varying degrees incongruent. Given these circumstances and observations, the total Sb concentration in solution was considered a more reliable reaction progress variable.

Four types of experiments were carried out, with the aim of establishing an empirical rate law of the form :

$$r = -\frac{d[Sb_2S_3]}{dt} = \frac{1}{2}\frac{d[Sb(tot)]}{dt} = k\left[H^+\right]^{\alpha}\left[O_2\right]^{\beta}$$

First, the pH was varied between 1 and 5, keeping temperature and oxygen saturation constant. Secondly, the oxygen concentration was varied at constant pH and temperature. Thirdly, different concentrations of Fe(III) were applied at constant pH, oxygen concentration and temperature. Fourthly, the temperature was varied and all other parameters kept constant. The ionic strength of all solutions was adjusted to 0.01 M with $NaClO_4$, except in experiments at pH=1 and pH=2.

II.3.1 Effect of hydrogen ion

The hydrogen ion concentrations were calculated from the measured pH values using a modified Debye-Hückel equation (Hückel, 1925) employing the known ionic strengths of the solutions and a radius parameter for H^+ of 4.78 Å (Merkel and Planer-Friedrich, 2008) The experiments were carried out at constant temperature T=298.16 K and dissolved oxygen concentration $[O_2]=2.69\times10^{-4}$ mol l^{-1}, which corresponds to saturation with oxygen under atmospheric conditions. The logarithm of the rate depends linearly on the logarithm of hydrogen ion concentration (Fig. II.3).

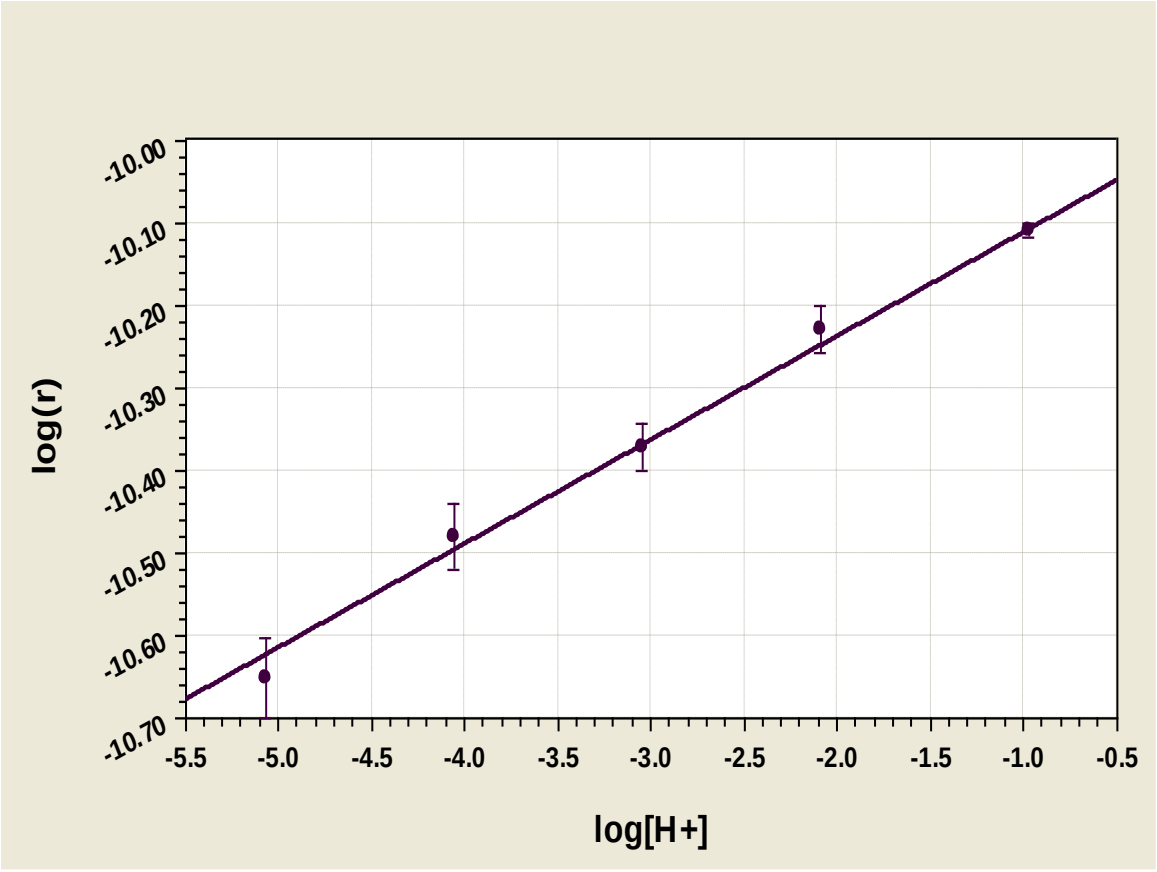

Fig. II.3 Logarithm of rate vs. log[H^+], T=298.16 K, $[O_2]=2.69\times10^{-4}$ $moll^{-1}$

From the slope of the straight line, the rate of dissolution was found to increase as $[H^+]^{0.125\pm0.006}$ with a correlation coefficient r>0.996. Rationalizations of fractional orders with respect to hydrogen ion concentrations are offered by Wieland and co-workers in terms of surface complexation models (Wieland et al., 1988) and Sposito (2008) in terms of the van Bemmelen-Freundlich isotherm. The actual rates varied from 7.84×10^{-11} mol $s^{-1}m^{-2}$ at pH=1.08 to 2.26×10^{-11} mol $s^{-1}m^{-2}$ at pH=5.10, corresponding to time scales of dissolution (Sposito, 2004) for 1 g of material between 2.6 and 9.1 years. The rate of dissolution based on dissolved sulfur concentrations varied as $[H^+]^{0.181\pm0.008}$ with r>0.989. As noted above, however, because the dissolution of stibnite is incongruent, with elemental S residually enriched at the surface of the reacting mineral, the Sb concentration in solution is a more robust and reliable indicator of reaction progress.

II.3.2 Effect of dissolved oxygen

At constant temperature and pH (T=298.16 K, pH=3), the concentration of dissolved oxygen was varied from 6.51×10^{-5} mol l^{-1} (equilibration of the feed solution with 5% oxygen in nitrogen) to 2.69×10^{-4} mol l^{-1} (equilibration with 20% oxygen). When the feed solution was equilibrated with gas mixtures that contained more than 20% oxygen, no increase in reaction rate was observed. This suggests that surface adsorption of oxygen may be a limiting step and that the surface becomes saturated at a partial pressure of 0.2 atm of oxygen above the influent solution. The data can, however, be fitted to a rate law involving a fractional power of $[O_2]$, with a correlation coefficient r>0.992 (Fig. 4a). From

the slope of this line, a dependence on $[O_2]^{0.26\pm0.04}$ is calculated. Combining the regressions in Figs II.3 and II.4a yields a rate constant $k=1.17\times10^{-9} \pm 0.01\times10^{-9}$. The oxygen dependence in basic solution is the same (within experimental error), while the rate constant is about two orders of magnitude smaller (Part II of this paper, in chapter III). Since there is saturation of the surface at partial pressures of O_2 greater than 0.2 atm, it may be more appropriate to regard the rate as proportional to the surface coverage θ as given by a Langmuir isotherm (Langmuir, 1916) :

$$r = k\left[H^+\right]^{\alpha}\theta = k\left[H^+\right]^{\alpha}\frac{K\left[O_2\right]}{1+K\left[O_2\right]},$$

where K is the equilibrium constant for adsorption of dissolved O_2 on stibnite. This equation can be rearranged into :

$$\frac{\left[O_2\right]}{r} = \frac{1}{k\left[H^+\right]^{\alpha}K} + \frac{\left[O_2\right]}{k\left[H^+\right]^{\alpha}}$$

and a plot of $[O_2]/r$ vs. $[O_2]$ is linear with $r>0.999$ (Fig. II.4b). Using this graph, $k[H^+]^q$ and K can be obtained from the intercept and slope: $K=2.13\times10^4 \pm 0.26\times10^4$ mol^{-1} l, $k=1.14\times10^{-10} \pm 0.09\times10^{-10}$. The equilibrium constant K is of the same magnitude as the one found for arsenopyrite ($K=1\times10^4$ mol^{-1} l) by Asta et al., (2010b). A similar saturation effect was observed in the oxygen dependence of the rate of pyrite oxidation, although in basic solution (Nicholson, 1987) as well as in the dissolution of arsenopyrite (Asta et al., 2010b). An experiment was also conducted under completely anoxic conditions; in this case, the feed solution was sparged with pure nitrogen until no dissolved oxygen could be detected, and the dissolution rate tended toward zero.

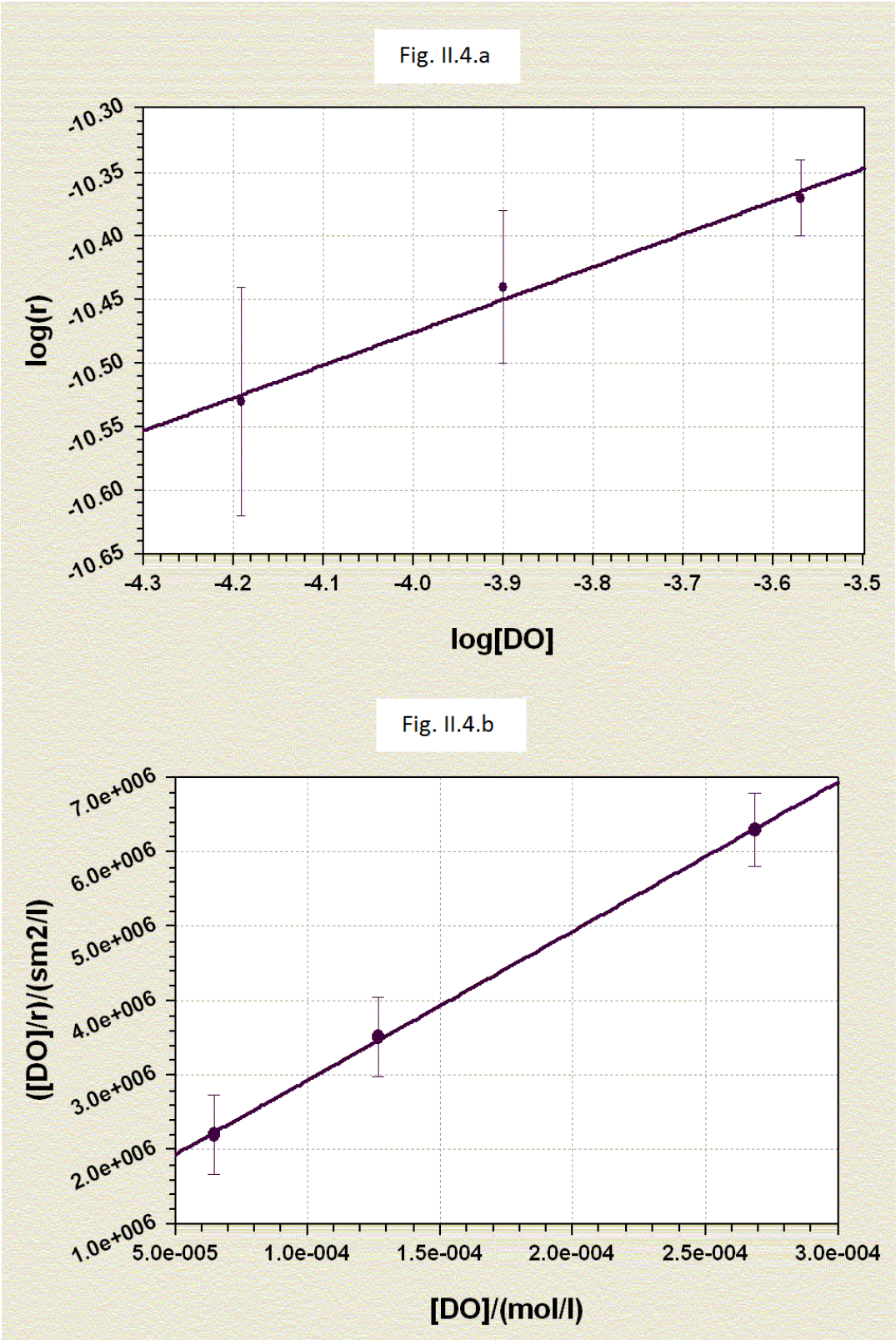

Figs II.4. Rate dependence on dissolved oxygen: log-log plot (a), Langmuir plot (b)

II.3.3. Effect of ferric iron and other cations

Experiments were carried out at pH=2 and 298.16 K and saturation with 0.2 atm O_2. Ferric ion (Fe^{3+}) was found to strongly catalyse the dissolution. Thus, a concentration of 10^{-5} mol l^{-1} (0.56 mg l^{-1}) increased the rate by a factor of about 3, and a concentration of 10^{-3} mol l^{-1} (55.8 mg l^{-1}) increased the rate by roughly an order of magnitude. The absolute rates are given in table II.1. The dependence of the rate on the concentration of ferric ion is well described by assuming Langmuir behaviour of the rate determining adsorption of ferric ion on the stibnite surface :

$$r = r_{\max} \frac{K[Fe^{3+}]}{1 + K[Fe^{3+}]}$$

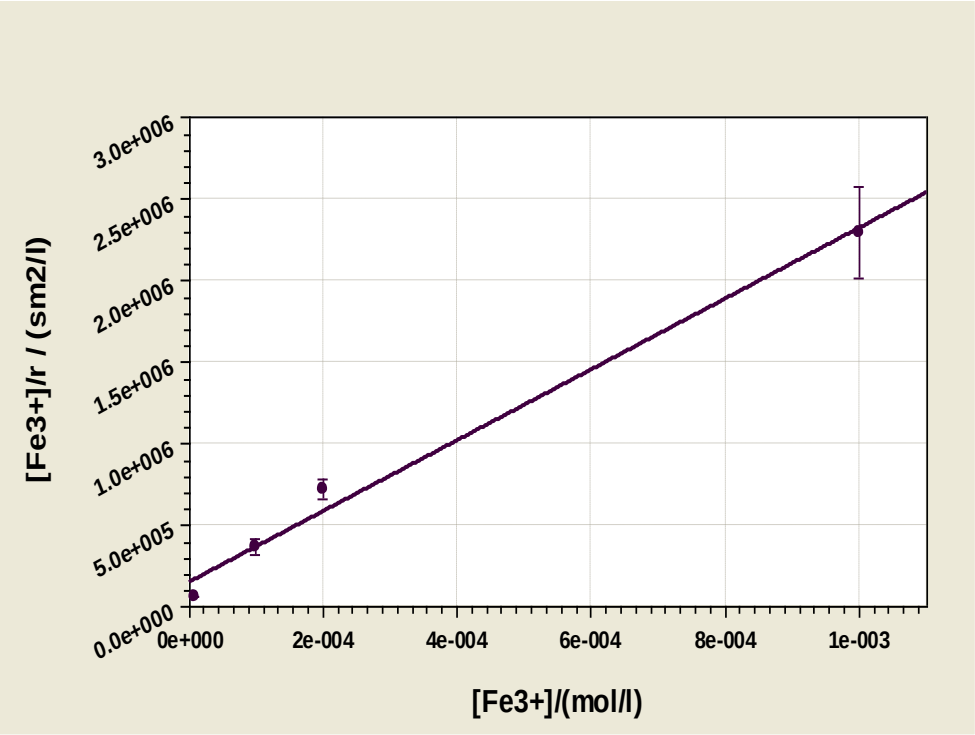

Fig. II.5. A plot of $[Fe^{3+}]/r$ vs. $[Fe^{3+}]$, which is linear with a correlation coefficient r>0.994.

$[Fe^{3+}]$ / mol l^{-1}	Rate / mol m^{-2} s^{-1}
10^{-5}	$1.6\times10^{-10} \pm 0.1\times10^{-10}$
10^{-4}	$2.6\times10^{-10} \pm 0.3\times10^{-10}$
10^{-3}	$4.3\times10^{-10} \pm 0.5\times10^{-10}$

Table II.1 : Dissolution rate at various iron(III) conc.

The maximum rate that can be reached with Fe^{3+} as catalyst is estimated to be $r_{max}= 4.6\times10^{-10} \pm 0.3\times10^{-10}$ mol $s^{-1}m^{-2}$ for $[Fe^{3+}] \geq 4\times10^{-3}$ mol l^{-1}. The adsorption constant is $K=1.4\times10^{4} \pm 0.5\times10^{4}$ mol^{-1} l (obtained from the regression in fig. II.5), which is of the same order of magnitude as the adsorption constant for dissolved oxygen (cf. section II.3.2).

In order to test whether Fe^{3+} catalyses the dissolution only by virtue of its oxidising nature, experiments were repeated under the same conditions using Al^{3+} or Ce^{3+} at concentrations of 10^{-4} mol l^{-1} instead of Fe^{3+}. The cations had been added to the feed solution in the form of their perchlorates. Aluminium and cerium were chosen because Al^{3+} has almost the same ionic radius (54 pm) as Fe^{3+} (55 pm), while that of Ce^{3+} is much larger (114 pm) (Shannon, 1976), and both cations are redox-inactive under the conditions of the experiment. With aluminium, a rate of $2.5\times10^{-10} \pm 0.1\times10^{-10}$ mol $s^{-1}m^{-2}$ was found, which is insignificantly smaller than that for ferric ion under the same conditions ($2.6\times10^{-10} \pm 0.3\times10^{-10}$ $mols^{-1}m^{-2}$). With cerous ion, however, the observed rate was $3.3\times10^{-10} \pm 0.1\times10^{-10}$ mol $s^{-1}m^{-2}$, which is significantly greater than the rate for ferric ion. Cerous ion, owing to its much larger radius, would be expected to adsorb more strongly to the surface than either ferric or aluminium ion. Therefore, the observation that redox-inactive cations catalyse the dissolution of

stibnite in the order of their strength of adsorption, leads us to conclude that the rate promoting effect of metal cations is not be due to their participation in redox reactions at the surface, but rather a case of metal-promoted dissolution (Sposito, 2004). The observation of rate inhibition by multivalent cation adsorption in acidic solution is, however, a much more common phenomenon, at least in the case of oxide minerals (Biber et al., 1994). As will be shown below, ferric ion has an additional, and more important catalytic effect, in that it is also involved in the oxidation of sulfide to elemental sulfur.

II.3.4 Effect of temperature

The effect of temperature was studied over the range 25-40°C. Since activation energies of mineral dissolution reactions usually exhibit a more or less pronounced pH dependence, we opted for a measurement at an intermediate pH of 3, and saturation with oxygen at its atmospheric partial pressure. A plot of ln(r) vs. 1/T is linear with slope $-E_A/R$ and correlation coefficient $r>0.999$, yielding a calculated activation energy of $E_A=5.2 \pm 0.4$ kJ mol^{-1} (Fig. II.6). This very small value is well below the maximum value (21 $kJmol^{-1}$) indicative of diffusion controlled chemical processes (Lasaga, 1984). For comparison, the activation energy for self-diffusion of water is 19.16 kJ mol^{-1} (Wang, 1951), that for diffusion of oxygen dissolved in water is 17.9 kJ mol^{-1} (van Stroe et al., 1993) and that for diffusion of the hydrated proton is estimated to be between 8.87-12.55 kJ mol^{-1} (Agmon 1995). Considering that in stirred solution, transport activation energies are approximately reduced by a factor of 5/6 (Berner 1978),

our activation energy (5.2 ±0 .4 kJmol^{-1}) is closest to the lower estimate of that of the proton in stirred solution (6.97 kJ mol^{-1}).

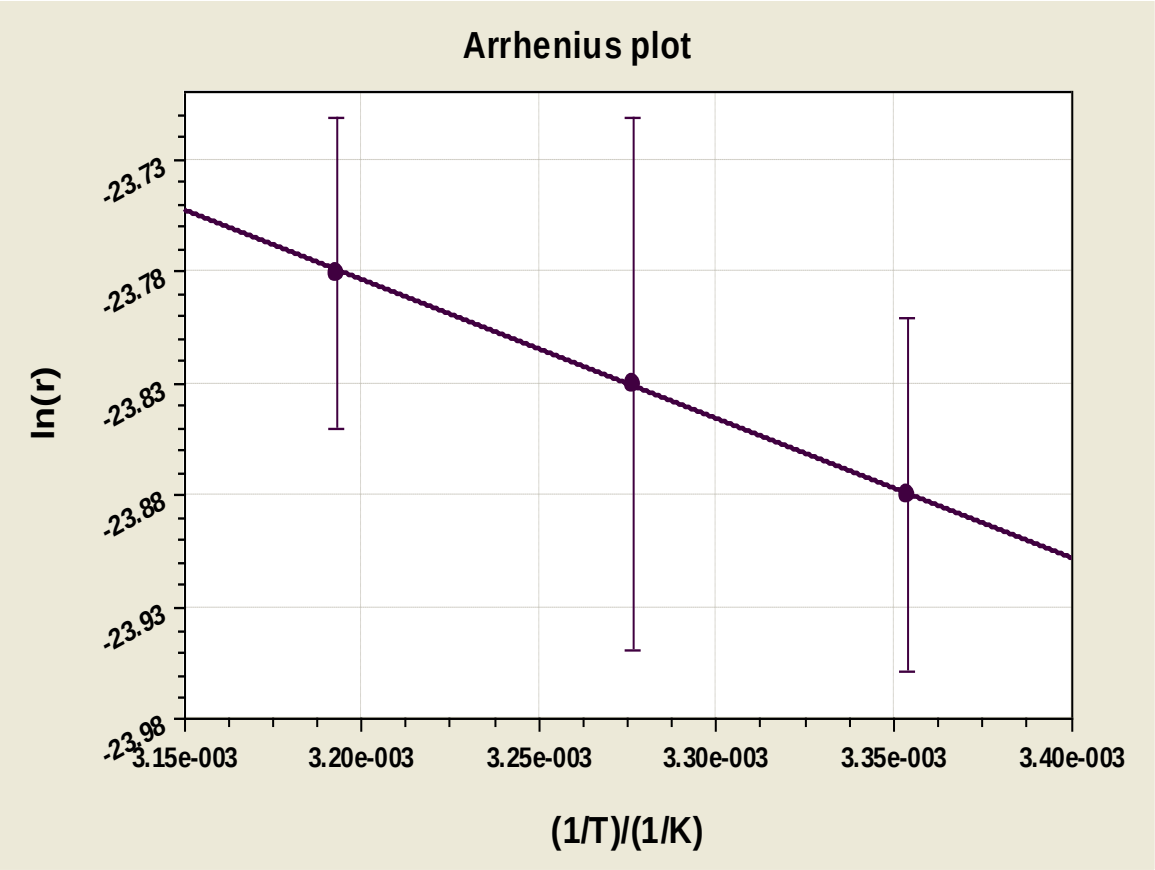

Fig. II.6 Arrhenius plot (ln(r) vs. 1/T) for the temperature range 25-40°C

II.3.5 Formation of elemental sulfur on the surface of dissolving stibnite

The higher the pH of the feed solution, the more elemental sulfur could be recovered from the weathered surface: ca. 1.5 µmol/m^2 at pH 1 and ca. 2.5 µmol/m^2 at pH 3 after an approximate duration of the experiments of ca. 36 h. Using a density of 2070 kg m^{-3} for orthorhombic α-S_8 (Rettig and Trotter, 1987), the amount recovered at pH 1 corresponds to an average layer thickness of 2.3×10^{-11} m; as this is only about one tenth of the van der Waals radius (180 pm) of a sulfur atom, the stibnite surface reacting under these conditions cannot

even be covered by a monolayer. In the iron catalysed experiments, the amount of sulfur formed per unit surface area (experiments lasting ca. 36 h) depends linearly on the stationary state reaction rate (Fig.II.7, r>0.997) and is much higher, and significant, compared to the iron-free experiments.

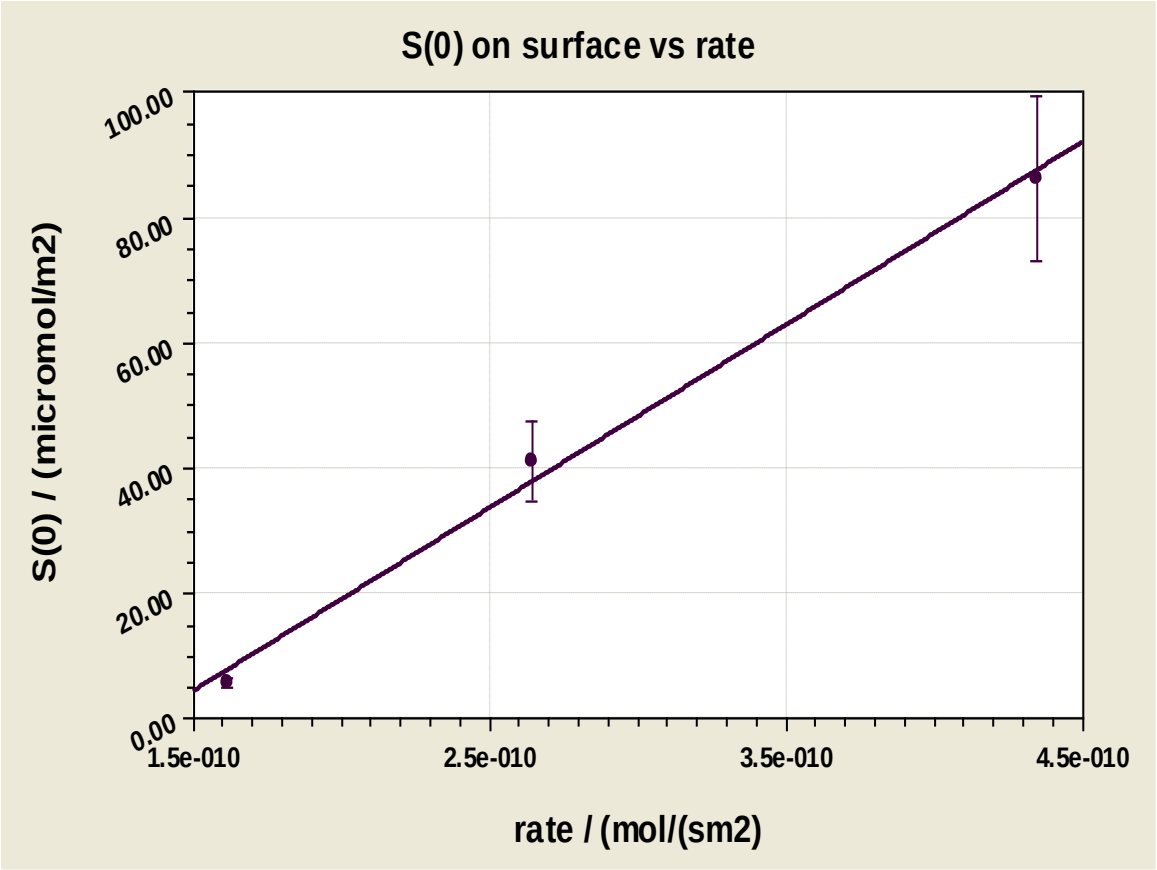

Fig. II.7 Elemental sulfur formed at the mineral surface as a function of steady state dissolution rate (iron catalysed experiments, duration of the experiments ca. 36 h)

At $[Fe^{3+}]=10^{-3}$ mol l^{-1}, ca. 86.4 µmol/m^2 were recovered, corresponding to an average layer thickness of about 1.4 nm or 7 to 13 sulfur atomic layers (estimated using the covalent radius of 102.5 pm, and van der Waals radius of 180 pm, respectively). Cerium and aluminium cations had no effect on the amount of superficial sulfur formed: 1.2 µmol/m^2 for $[Ce^{3+}] = 10^{-4}$ mol l^{-1} and 1.0 µmol/m^2 for $[Al^{3+}] = 10^{-4}$ mol l^{-1}. For comparison, a solution at pH=2 containing

neither Ce^{3+} nor Al^{3+} yielded 1.1 µmol/m^2. The comparisons presented here indicate that ferric ion is involved in the oxidation of sulfide to elemental sulfur, while cerous and aluminium ion are not.

II.3.6 Redox speciation of Sb

No clear trend could be observed in the evolution of the redox state of Sb in solution over the course of the experiments. In an experiment at pH=3 under saturation with atmospheric oxygen, an average of 77% of total Sb was present as Sb(III) (n=14, σ=21.2, range 37 to 100%). In a similar experiment using an iron(III) concentration of 10^{-3} M at pH=2, Sb(III) accounted for 88% of the total Sb (n=6, σ=12.7, range 77 to 100%). We conclude (a) that Fe^{3+}(aq) does not oxidise Sb(III) on the timescale of the experiment, and (b) that oxidation of Sb(III) by dissolved oxygen is slow on the timescale of the experiment, which is in agreement with the findings of Leuz (Leuz et al., 2006; Leuz and Johnson, 2005) and (c) that the oxidation of solution-phase Sb(III) has no effect on the dissolution rate of Sb_2S_3.

II.4 Summary and Conclusions

A rate law for the dependence of stibnite dissolution under acidic conditions was established from experiments in a mixed flow reactor. The rate is proportional to a fractional power of the hydrogen ion concentration, whereas the dependence on dissolved oxygen is best described by Langmuir adsorption of oxygen on the stibnite surface, with a saturation occurring at partial pressures

above ca. 0.2 atm. Rates are of the order of 10^{-11} to 10^{-10} $mols^{-1}m^{-2}$. The activation energy was found to be in the range of diffusion controlled processes. Diffusion and adsorption of the oxidant onto the surface seem to be the rate limiting steps. Ferric ion strongly catalyses the dissolution; the dependence of the rate on ferric ion is well described by Langmuir adsorption of ferric ion onto the surface. A maximum rate is attained at about 4×10^{-3} mol l^{-1} of ferric ion, corresponding to an acceleration of the rate by about an order of magnitude. Dissolution is incongruent in the sense that a layer of elemental sulfur forms on the mineral surface; the rates of dissolution were consequently measured in terms of the rates of Sb release to the solution phase. The amounts of S(0) formed on the surface were quantified by UV spectrometry and found to increase with pH and vary linearly with the concentration of ferric ion.

In the absence of iron, other trivalent and redox-inactive ions, such as Al^{3+} and Ce^{3+}, also increase the dissolution rate, without increasing the production of elemental sulfur, which suggests that Fe^{3+} must be involved in the oxidation of sulfide to elemental sulfur, while the reaction rate increase is, at least partially, due to charge effects on the stibnite surface. These findings are directly relevant for the study of sulfide weathering in the field, for pH values below 2 with high iron loads (up to nearly 0.01 mol l^{-1}) are conditions which are frequently found in environments affected by acid mine or acid rock drainage (Rimstidt et al., 1994, and references therein). The general finding that low pH and high ferric iron concentrations accelerate the mobilisation of metals from

sulfide minerals is confirmed here, on a quantitative basis, in the special case of stibnite.

II.5 Acknowledgement

We thank Drs H.P. Meyer and A. Varychev for assistance with the SEM.

II.6 References for chapter II

Abraitis P.K., Pattrick R.A.D., Kelsall G.H. and Vaughan D.J. (2004) Acid leaching and dissolution of major sulfide ore minerals: processes and galvanic effects in complex systems. *Mineral. Mag.* **68**, 343-351

Agmon N. (1995) The Grotthuss mechanism. *Chem. Phys. Lett.* **244**, 456-462

Akcil A. and Koldas S. (2006) Acid Mine Drainage (AMD) : causes, treatment and case studies. *J. Clean. Product.* **14**, 1139-1145

Asta M.P., Ayora C., Roman-Ross G., Cama J., Acero P., Gault A.G., Charnok J.M. and Bardelli F. (2010a) Natural attenuation of arsenic in the Tinto Santa Rosa acid stream (Iberian Pyritic Belt, SW Spain): The role of iron precipitates. *Chem. Geol.* **271**, 1-12

Asta M.P., Cama J., Ayora C., Acero P. and De Giudici G. (2010b) Arsenopyrite dissolution rates in O_2-bearing solutions. *Chem. Geol.* **273**, 272-285

Berner R.A.(1978) Rate Control of Mineral Dissolution under Earth Surface Conditions. *Am. J. Sci*. **278**, 1235-1252

Biber M.V., Dos Santos Afonso and Stumm W. (1994) The coordination chemistry of weathering: IV. Inhibition of the dissolution of oxide minerals. *Geochim. Cosmochim. Acta* **58**, 1999-2010

Biver M. and Shotyk W. (2011) *Geochim. Cosmochim. Acta* submitted

Corkhill C.L. and Vaughan D.J. (2009) Arsenopyrite oxidation – a review. *Appl. Geochem.* **24**, 2342-2361

De Giudici G., Rossi A., Fanfani L. and Lattanzi P. (2005) Mechanisms of galena dissolution in oxygen-saturated solutions : Evaluation of pH effect on apparent activation energies and mineral-water interface. *Geochim. Cosmochim. Acta* **69**, 2321-2331

Domènech C., de Pablo J. and Ayora C. (2002) Oxidative dissolution of pyritic sludge from the Aznallcóllar mine (SW Spain). *Chem. Geol.* **190**, 339-353

Edwards K.J., Bond P.L., Druschel G.K., McGuire M.M., Hamers R.J. and Banfield J.F. (2000) Geochemical and biological aspects of sulfide mineral dissolution: lessons from Iron Mountain, California. *Chem. Geol.* **169**, 383-397

Filella M., Belzile N. and Chen Y.-W. (2002) Antimony in the environment : a review focused on natural waters. I. Occurrence. *Earth Science Reviews* **57**, 125-176

Filella M., Chanudet V., Philippo S. and Quentel F. (2009) Particle size and mineralogical composition of inorganic colloids in waters draining the adit of an abandoned mine, Goesdorf, Luxembourg. *Appl. Geochem.* **24**, 52-61

Hückel E. (1925) Zur Theorie konzentrierter wässeriger Lösungen starker Elektrolyte. *Physikalische Zeitschrift*, **26**, 93-149

Kimball B.E., Rimstidt J.D. and Brantley S.L. (2010) Chalcopyrite dissolution rate laws. *Appl. Geochem.* **25**, 972-983

Kwong Y.T., Whitley G. and Roach P. (2009) Natural acid rock drainage associated with black shale in the Yukon Valley, Canada. *Appl. Geochem.* **24**, 221-231

Jeong H.Y., Han Y., Park S.W. and Hayes K.F. (2010) Aerobic oxidation of mackinawite (FeS) and its environmental implication for arsenic mobilization. *Geochim. Cosmochim. Acta* **74**, 3182-3198

Johansson L. (1974) The role of the perchlorate ion as ligand in solution. *Coordination Chemistry Reviews*, **12**, 241-261

Langmuir I. (1916) The Constitution and Fundamental Properties of Solids and Liquids. *J. Am. Chem. Soc.* **38**, 2221-2295

Lasaga A.C. (1984) Chemical Kinetics of Water-Rock Interactions. *J. Geophys. Res.* **89(B6)**, 4009-4025

Lengke M.F. and Tempel R.N. (2001) Kinetic rates of amorphous As_2S_3 oxidation at 25 to 40°C and initial pH of 7.3 to 9.4. *Geochim. Cosmochim. Acta* **65**, 2241-2255

Lengke M.F. and Tempel R.N. (2002) Reaction rates of natural orpiment oxidation at 25 to 40°C and pH 6.8 to 8.2 and comparison with amorphous As_2S_3 oxidation. *Geochim. Cosmochim. Acta* **66**, 3281-3291

Lengke M.F. and Tempel R.N. (2003) Natural realgar and amorphous AsS oxidation kinetics. *Geochim. Cosmochim. Acta* **67**, 859-871

Leuz A.K. and Johnson C.A. (2005) Oxidation of Sb(III) to Sb(V) by O_2 and H_2O_2 in aqueous solutions. *Geochim. Cosmochim. Acta* **69**, 1165-1172

Leuz A.K., Hug S.J., Wehrli B. and Johnson C.A (2006) Iron Mediated Oxidation of Antimony(III) by Oxygen and Hydrogen Peroxide Compared to Arsenic(III) Oxidation. *Environ. Sci. Technol.* **40**, 2565-2571

Merkel B.J. and Planer-Friedrich B.(2008) Groundwater Geochemistry. 2nd ed., edited by D.K. Nordstrom. Springer, Berlin

Moncur M.C., Ptacek C.J., Blowes D.W. and Jambor J.L. (2005) Release, transport and attenuation of metals from an old minings impoundment. *Appl. Geochem.* **20**, 639-659

Moncur M.C, Jambor J.L., Ptacek C.J. and Blowes D.W. (2009) Mine drainage from the weathering of sulfide minerals and magnetite. *Appl. Geochem.* **24**, 2362-2373

Nagy K.L, Blum A.E. and Lasaga A.C. (1991) Dissolution and precipitation kinetics of kaolinite at 80°C and pH 3: the dependence on solution saturation state. *Am. J. Science* **291**, 649-686.

Nesbitt H.W., Muir I.J. and Pratt A.R. (1995) Oxidation of arsenopyrite by air and air-saturated, distilled water and implications for mechanism of oxidation. *Geochim. Cosmochim. Acta* **59**, 1773-1786

Nicholson R.V., Gillham R.W. and Reardon E.J. (1987) Pyrite oxidation in carbonate-buffered solution : 1. Experimental kinetics. *Geochim. Cosmochim. Acta* **52**, 1077-1085

Nordstrom D.K, Alpers C.N., Ptacek C.J. and Blowes D.W. (2000) Negative pH and Extremely Acidic Mine Waters from Iron Mountain, California. *Environ. Sci. Technol.* **34**, 254-258

Nordstrom D.K. (2000) Advances in the Hydrogeochemistry and Microbiology of Acid Mine Waters. *Int. Geol. Rev.* **42**, 499-515

Quentel F. and Filella, M. (2002) Determination of inorganic antimony species in seawater by differential pulse anodic stripping voltammetry : stability of the trivalent state. *Anal. Chim. Acta* **452**, 237-244

Renock D. and Becker U. (2010) A first principles study of the oxidation energetics and kinetics of realgar. *Geochim. Cosmochim. Acta* **74**, 4266-4284

Rettig S.J. and Trotter J. (1987) Refinement of the structure of orthorhombic sulfur, α-S_8. *Acta Crystallographica* **C43**, 2260-2262

Rimstidt J.D. and Dove P.M. (1986) Mineral/solution reaction rates in a mixed flow reactor: Wollastonite hydrolysis. *Geochim. Cosmochim. Acta* **50**, 2509-2516

Rimstidt J.D., Chermak J.A. and Gagen P.M. (1994) Rates of Reaction of Galena, Sphalerite, Chalcopyrite, and Arsenopyrite with Fe(III) in Acidic Solutions. In *Environmental Geochemistry of Sulfide Oxidation, ACS Symposium*

Series 550 (eds. C.N. Alpers and D.W. Blowes) American Chemical Society, Washington, chapter 1.

Rimstidt J.D. and Vaughan D.J. (2003) Pyrite Oxidation : A state-of-the-art assessment of the reaction mechanism. *Geochim. Cosmochim. Acta* **67**, 873-880

Shannon, R.D. (1976) Revised Effective Ionic Radii and Systematic Studies of Interatomic Distances in Halides and Chalcogenides. *Acta Cryst.* **A32**, 751-767.

Sposito G. (2004) *The Surface Chemistry of Natural Particles*. Oxford University Press, Oxford/New York.

Sposito G. (2008) *The Chemistry of Soils.* Oxford University Press, Oxford/New York.

Van Stroe A.J. and Janssen L.J.J. (1993) Determination of the diffusion coefficient of oxygen in sodium chloride solutions with a transient pulse technique. *Anal. Chim. Acta* **279**, 213-219

Verplanck P., Nordstrom D.K., Bove D.J., Plumlee G.S. and Runkel R.L. (2009) Naturally acidic surface and ground waters draining porphyry-related mineralized areas of the southern Rocky Mountains, Colorado and New Mexico. *Appl. Geochem.* **24**, 255-267

Walker F.P., Schreiber M.E. and Rimstidt J.D. (2006) Kinetics of arsenopyrite oxidative dissolution by oxygen. *Geochim. Cosmochim. Acta* **70**, 1668-1676

Wang J.H. (1951) Self-Diffusion and Structure of Liquid Water. I. Measurement of Self-Diffusion of Liquid Water with Deuterium as a Tracer. *J. Am. Chem. Soc.* **73**, 510

Wieland E., Wehrli B., and Stumm W. (1988) The coordination chemistry of weathering: III. A generalization on the dissolution rates of minerals. *Geochim. Cosmochim. Acta* **52**, 1969-1981

Chapter III :

Experimental Study of Stibnite Dissolution Kinetics: Effect of pH, Dissolved Oxygen, Temperature, and Alkaline-Earth Metal Cations.

Part II. Alkaline Solutions and Field Implications.

Abstract – This is the second of two papers dealing with the rates of dissolution of stibnite (Sb_2S_3). While Part I was concerned with the dissolution under acid conditions (chapter II), the rate of dissolution in alkaline solutions (carbonate-buffered as in the case of the Goesdorf mine, Luxembourg) is examined here. The effect of hydrogen ion concentrations, dissolved oxygen concentrations, temperature, and alkaline-earth metal cations (Mg^{2+} and Ca^{2+}) are studied.

The empirical rate law may be written as :

$$r = k\left[H^+\right]^{-0.13\pm0.01}\frac{K\left[O_2\right]}{1+K\left[O_2\right]}$$

with $k=6.3\times10^{-13} \pm 0.7\times10^{-13}$ and $K=7.8\times10^{4} \pm 2.0\times10^{4}$ mol^{-1} l at 25°C with 8 < pH < 11, and dissolved oxygen saturation between 0 and 4 atm. In contrast to acidic solutions, the dissolution rate in alkaline solution did not reach a maximum when the atmospheric partial pressure of oxygen was achieved. The temperature dependence of the rate between 25°C and 48°C leads to an apparent activation energy of the reaction of 51.8 ± 0.5 $kJmol^{-1}$ at pH=9.9, indicative of a surface-controlled mechanism; this E_A values is approximately one order of magnitude greater than in acidic solutions where a diffusion-controlled mechanism had been suggested. A laboratory simulation of the weathering conditions found in an abandoned antimony mine in Goesdorf (Luxembourg) was carried out, which revealed that the rate was also critically dependent on the concentrations of alkaline-earth cations. Magnesium and calcium were found to increase the dissolution rates substantially (calcium had a stronger effect than magnesium), which is, to our knowledge, the first description of metal-promoted dissolution of

a sulfide mineral. The amounts of elemental sulfur formed at the weathered stibnite surface were also measured and found to correlate with reaction rate.

III.1. Introduction

The kinetics of the oxidative dissolution of stibnite (Sb_2S_3) in acidic solutions was presented earlier (Chapter II). Those results are relevant to situations of acid mine drainage, a common environmental problem in mining areas. A brief introduction to the published studies of acid mine drainage can be found in Part I (Chapter II). Mine drainage can, however, also be neutral or even basic, depending on the mineralogy of the site (Lindsay et al., 2009). Acid drainage can be naturally attenuated if rocks or minerals, in particular carbonates such as calcite and dolomite, are present which provide sufficient acid neutralising capacity. An example (the tailing impoundments near Pezinok, Slovakia) is described in detail by Majzlan et al. (2011). The abandoned antimony mine near Goesdorf, Luxembourg, is such an example: dolomite, ankerite, and, to a lesser extent, calcite, are among the important gangue minerals, so that the drainage waters are alkaline (pH close to 8), yet they carry elevated loads of antimony (up to 1 mg l^{-1}). The antimony mineralisation consists of high quality stibnite, along with pyrite and a large number of less important minerals (Philippo and Hanson, 2007). Here, we investigate the effects of pH, dissolved oxygen and temperature on stibnite weathering kinetics in basic solution.

In addition, a laboratory experiment was designed to measure the rate of stibnite dissolution under the conditions simulating those found in the Goesdorf mine. This experiment revealed that the high concentration of alkaline-earth cations found in the mine water leads to an increased rate of mobilisation of antimony, the rate being proportional to the Langmuir coverage of the surface by Mg^{2+} ions. The effect of Ca^{2+} was even more pronounced. A 0.3 mM solution of Ca^{2+} caused approximately the same increase in dissolution rate as a 3 mM solution of Mg^{2+}. To our knowledge, this is the first observed case of metal-promoted dissolution of a sulfide mineral. The quantity of elemental sulfur formed on the mineral surface during the leaching experiments was determined spectrophotometrically as described in appendix AIV. It was found that the amount of sulfur formed at the surface after a 36 h duration of the experiment correlated with reaction rate, both in the absence and presence of Mg^{2+}.

III.2 Materials and Methods

The materials and methods used here were identical to those used in the companion paper and described it detail elsewhere (Chapter II), except where noted below.

III.2.1 Sample origin and pretreatment

The stibnite sample was taken from the abandoned antimony mine of Goesdorf, Luxembourg and it was treated as described in Chapter II.

III.2.2 Measurements

A mixed flow reactor, immersed in a thermostated water bath, was used in the experiments, with gases and gas mixtures used to adjust the feed solutions to the different dissolved oxygen concentrations also as described previously (Chapter II).

Feed solutions were carbonate buffers of constant total ionic strength I=0.01 $moll^{-1}$ prepared by dissolving analytical grade sodium bicarbonate and sodium carbonate (C. Roth, Germany) in Milli-Q water in proportions such that the desired pH and ionic strength were approximately reached. There was thus no need to adjust the ionic strength by addition of sodium perchlorate. Exact pH values were recorded during the experiments. The tank used for storing the feed solutions was protected from atmospheric CO_2 by a soda-lime guard tube.

In order to examine the effect of hydrogen ion concentration, both in the presence and absence of carbonate, the feed solutions were equilibrated with 0.2 atm O_2 and the temperature of the reactor kept at 298.15 K. For the study of the rate dependence on dissolved oxygen (DO), carbonate buffered solutions of pH=9.9 were used, also at 298.15 K. The effect of temperature was investigated by heating the water bath to 25°C, 32°C, 40°C and 48°C while keeping the other parameters (oxygen saturation corresponding to 0.2 atm and pH=9.9) constant. The effect of magnesium and calcium ions was investigated using sodium bicarbonate solutions spiked with variable concentrations of magnesium or calcium perchlorate, respectively.

The mineral was recovered from the reactor after each experiment and the amount of sulfur formed at its surface was determined spectrophotometrically (Appendix AIV). Calcium determinations were carried out by flame-AAS on a Pye-Unicam SP90.

Specific surface areas were determined using multiple-point N_2 adsorption isotherms according to the BET method (Gemini VII 2390, Micromeritics GmbH, Aachen, Germany). The results varied between 0.24 to 0.45 m^2g^{-1} with the relative error being 0.6% or better.

III.3. Results and Discussion

III.3.1 Dependence on hydrogen ion concentration

Rates were first measured in the four carbonate-buffered solutions from pH 8.85 to 10.63. The measured pH values were converted to logarithms of hydrogen ion concentration using the extended Debye-Hückel formula (Hückel, 1925) for activity coefficients, with a radius parameter of 4.78 Å for H^+ (Merkel and Planer-Friedrich, 2008) and an ionic strength I=0.01 mol l^{-1}. Experiments were run at 298.16 K and $[O_2]=2.66\times10^{-4}$ mol l^{-1} (corresponding to a partial pressure of 0.2 atm). As can be seen from a log-log plot (Fig.III.1) the rate increases with decreasing hydrogen ion concentration (correlation coefficient>0.993) as $[H^+]^{-0.13\pm0.01}$.

Note that in acid solution, an inverse trend, i.e. an increase of the rate with increasing hydrogen ion concentration, is observed. The actual rates varied

from $9.29\times10^{-11} \pm 0.18\times10^{-11}$ mol $s^{-1}m^{-2}$ (dissolution time scale (Sposito, 2004) for 1 g of material : 2.2 y) at pH=8.85 to $1.55\times10^{-10} \pm 0.10\times10^{-10}$ mol $s^{-1}m^{-2}$ (dissolution time scale for 1 g : 1.32 y) at pH 10.63.

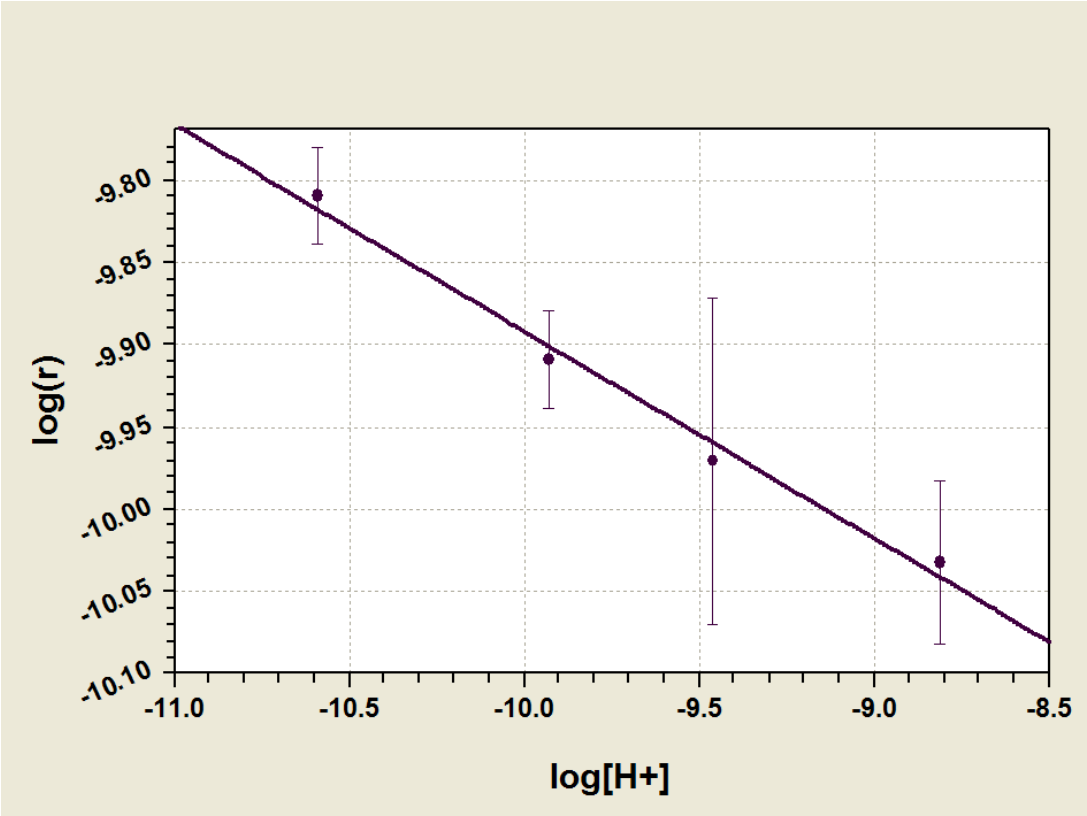

Fig. III.1 Dependence of the logarithm of the rate on the logarithm of hydrogen ion concentration

The smallest dissolution rate in basic solution (at pH 8.85) is still greater than the fastest rate in acid solution, namely $7.84\times10^{-11} \pm 0.18\times10^{-11}$ mol $s^{-1}m^{-2}$ at pH 1.08, dissolution time scale 2.6 y (Chapter II). Thus, it seems that even under very drastic acid drainage conditions, Sb is not as rapidly mobilised as under relatively mild basic conditions. The waters emanating from the Goesdorf mine have elevated Sb concentrations (up to 1 mg l^{-1}) and an approximate pH of

8. Water in chemical equilibrium with calcite and atmospheric P_{CO2} is expected to have a pH of 8 (Faure, 1998), so the pH of the waters from the Goesdorf mine can be explained by equilibria with dolomite and calcite, important gangue minerals in the area. Despite the high pH provided by the chemical weathering of dolomite and calcite, the rate of Sb release from stibnite is sufficiently rapid that elevated concentrations of Sb are achieved in the drainage waters.

III.3.2 Dependence on dissolved oxygen

At fixed pH=9.8 (carbonate-buffered, I=0.01 mol l^{-1}), four experiments were carried out in which the concentration of dissolved oxygen was varied between 2.66×10^{-4} mol l^{-1} (partial pressure 0.2 atm O_2) and 28.29×10^{-4} mol l^{-1} (partial pressure 0.8 atm O_2). Up to this concentration, the reaction rate increased (from $1.07\times10^{-10} \pm 0.43\times10^{-10}$ mol $s^{-1}m^{-2}$ under 0.2 atm O_2 to $1.52\times10^{-10} \pm 0.43\times10^{-10}$ $mols^{-1}m^{-2}$ under 0.8 atm O_2) without leveling off; this contrasts with the observations made in acidic solutions where the reaction rate achieved a plateau as P_{02} reached atmospheric values ie 0.21 atm (chapter II). A log-log plot (Fig. III.2.a) showed that the rate varied as $[O_2]^{0.296\pm0.054}$ (correlation coeff. > 0.965), which is similar (within experimental error) to the dependence on dissolved oxygen of orpiment oxidation in mildly alkaline carbonate solution ($[O_2]^{0.36\pm0.09}$ (Lengke and Tempel, 2002)). It is also very close to the oxygen dependence of stibnite dissolution in acid solution ($[O_2]^{0.26\pm0.04}$ (Chapter II).

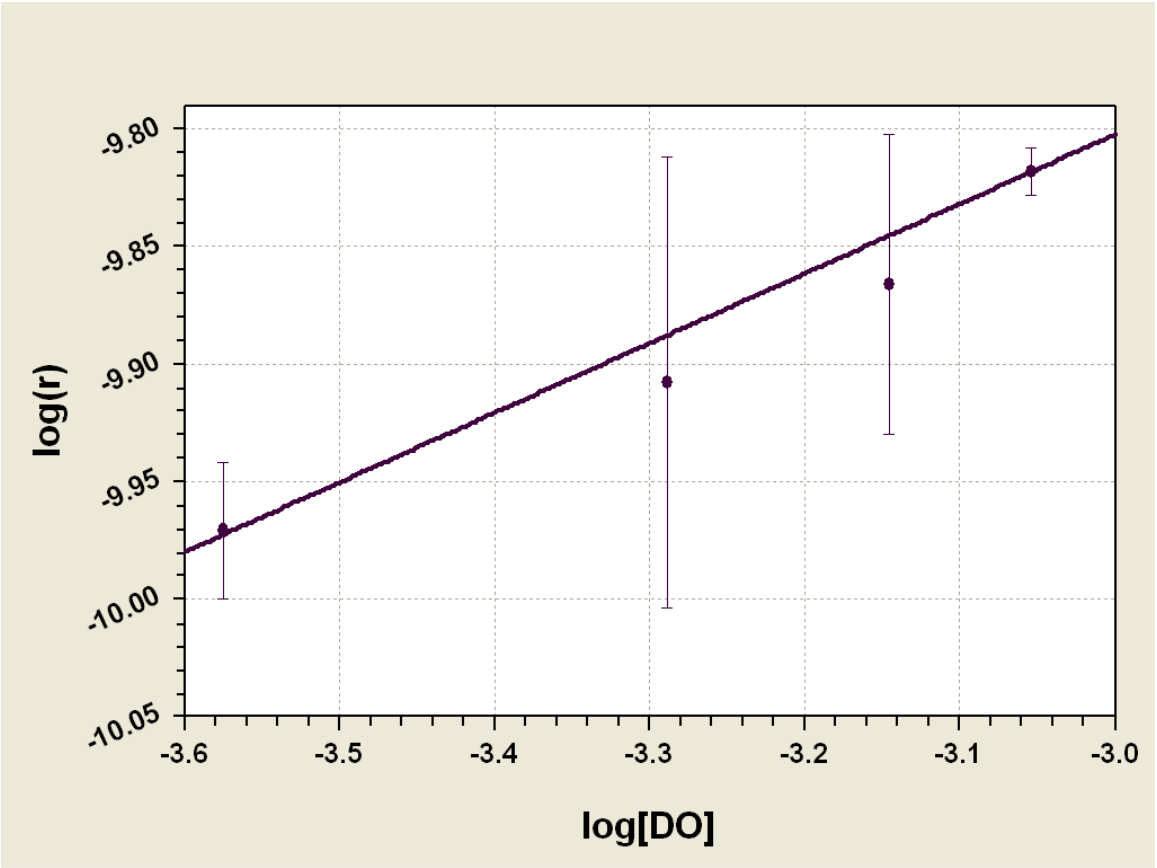

Fig. III.2.a Rate dependence on dissolved oxygen: log-log plot

Combining the regressions in Figs.III.1 and III.2.a, we obtain the rate constant $k=1.12\times10^{-11} \pm 0.14\times10^{-11}$, which is about two orders of magnitude smaller than the corresponding constant in acid solution ($1.17\times10^{-9}\pm0.01\times10^{-9}$), so that the rate law may be written as

$$r = k\left[H^+\right]^{-0.13\pm0.01}\left[O_2\right]^{0.296\pm0.054}$$

with $k=1.12\times10^{-11} \pm 0.14\times10^{-11}$. Nevertheless, a Langmuir fit of the form :

$$r = k\left[H^+\right]^{-0.13\pm0.01}\frac{K\left[O_2\right]}{1+K\left[O_2\right]}$$

proves to be more successful. If we plot $[O_2]/r$ vs $[O_2]$, a straight line with correlation coefficient > 0.991 is obtained (Fig.III.2.b). From its slope and intercept, we calculate $k=6.3\times10^{-13} \pm 0.7\times10^{-13}$ and the adsorption equilibrium

constant $K=7.8\times10^{4} \pm 2.0\times10^{4}$ mol^{-1} l. The adsorption constant is thus about three times as large as in acid solution (chapter II), while the rate constant is about 200 times smaller ($K=2.13\times10^{4} \pm 0.26\times10^{4}$ $mol^{-1}l$, $k=1.14\times10^{-10} \pm 0.09\times10^{-10}$). By extrapolation, we predict that the surface becomes saturated at concentrations in excess of 5×10^{-3} mol l^{-1}, corresponding to an oxygen partial pressure of nearly 4 atm, and a maximum reaction rate of about 1.8×10^{-10} mol $s^{-1}m^{-2}$. Again, this contrasts with the situation in acidic solutions, where the saturation occurs at exactly atmospheric oxygen partial pressure.

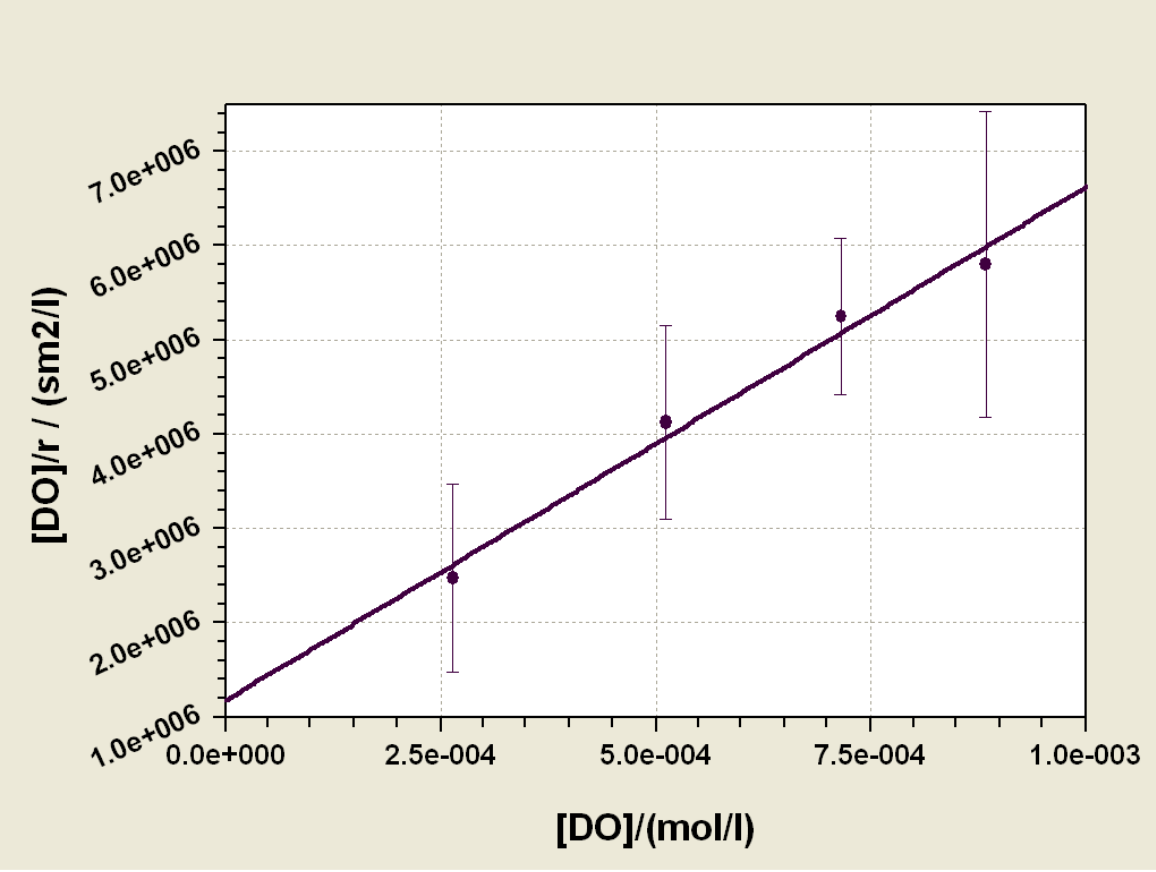

Fig. III.2.b Rate dependence on dissolved oxygen : Langmuir plot

III.3.3 Effect of temperature

The reaction rates were measured at pH 9.9 and $[O_2]=2.66\times10^{-4}$ mol l^{-1} at the following temperatures : 25°C, 32°C, 40°C and 48°C. An Arrhenius plot of ln(r) vs. 1/T is linear (Fig.III.3) with a correlation coefficient > 0.994 and from the slope an activation energy of 51.8 ± 0.5 $kJmol^{-1}$ is obtained. This value is about an order of magnitude greater than the activation energy in acidic

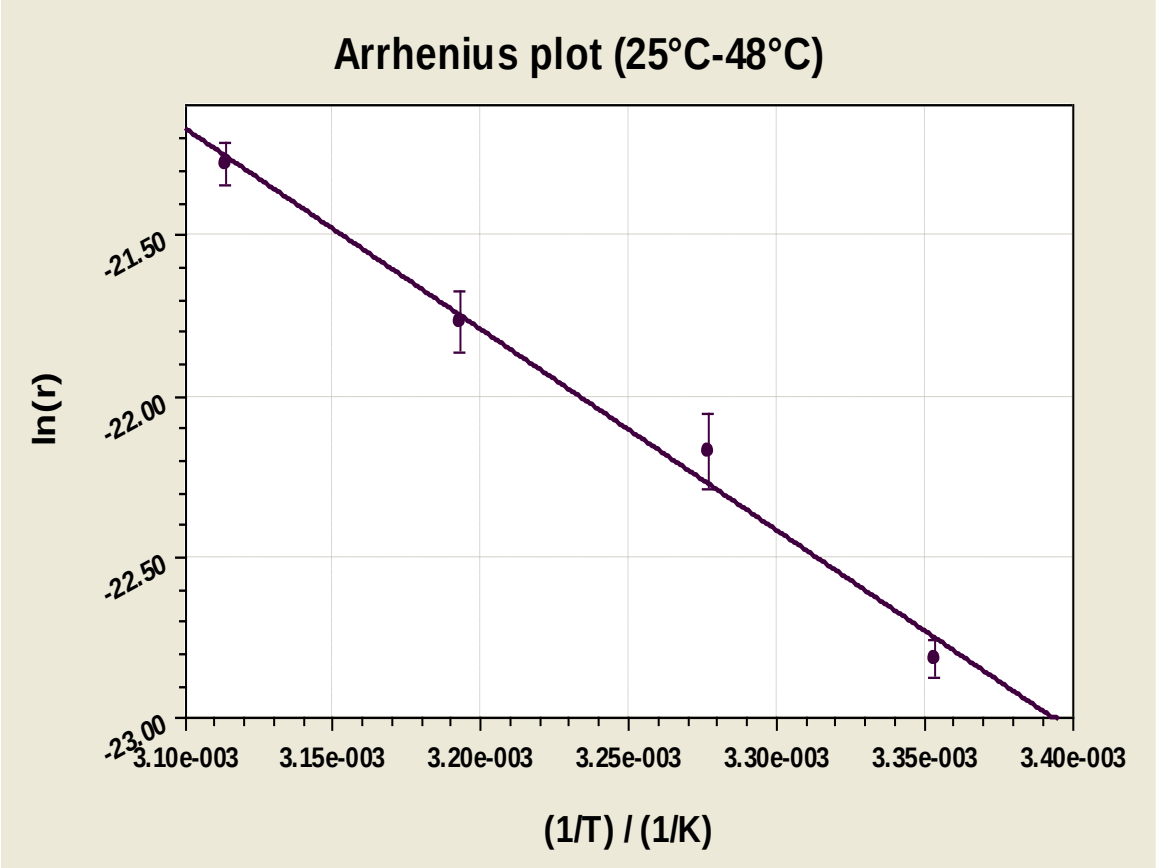

Fig. III.3 Arrhenius plot for the temperature range 25°C to 48°C.

solutions (E_A=5.2 ± 0.4 kJ mol^{-1} (Chapter II). Moreover, the E_A reported here is far greater than the value which is generally given (ca. 20 $kJmol^{-1}$ or less) for chemical reaction rates controlled by diffusion (Lasaga, 1984). The activation energy reported here, however, is similar to the one for orpiment dissolution (59.1±0.4 $kJmol^{-1}$) published by Lengke and Tempel (2002) and for realgar

dissolution (64.2±9.8 $kJmol^{-1}$) presented by Lengke and Tempel (2003). A similar change from low to high activation energies on going from acidic to basic solutions was observed for galena (De Giudici et al., 2005), also implying a change from a diffusion to a surface controlled reaction mechanism.

III.3.4 Experiment with synthetic drainage water

Water samples were taken at several times between 2006 and 2007 and their major ion chemistry as well as trace element concentrations were determined. The samples were taken at the deepest point of the mine adit, where water percolates from the tunnel ceiling and through the tunnel walls. This water has a high concentration of antimony (typically close to 1 mgl^{-1}). The major ion chemistry is remarkably uniform in the course of time; all analyses fall into area 5 of the Piper diagram (Piper, 1944) with the waters dominated by alkaline-earth cations and bicarbonate (Fig. III.4). Values in table III.1 represent the average of 7 analyses. Magnesium, bicarbonate and sulfate are dominant.

Synthetic drainage water (without antimony) was prepared by dissolving 8.4722 g $NaHCO_3$, 1.8557 g $CaSO_4 \cdot 2H_2O$, 0.2070 g K_2SO_4, 1.8431 g $MgSO_4$, 1.788 g $Mg(NO_3)_2 \cdot 6H_2O$ and 10.0455 g $MgCl_2 \cdot 6H_2O$ in Milli-Q water, adjusting the pH with a little $HClO_4$ to a value close to 8 and completing to a total volume of 22 l. The measured stibnite dissolution rate in this solution, at pH=8.10 and 25°C, was $2.03 \times 10^{-10} \pm 0.15 \times 10^{-10}$ mol $s^{-1}m^{-2}$. On the basis of the solution pH, temperature and oxygen saturation, a rate of 7.31×10^{-11} mol $s^{-1}m^{-2}$ had been expected. The actual rate was therefore about 2.8 times faster than the predicted one. One of the principal differences between the synthetic mine water

and the carbonate buffers used in the kinetic study is the presence of elevated concentrations of alkaline-earth metal cations in the former. These findings naturally lead to additional experimental studies of the effects of magnesium and calcium ions on the dissolution rate of stibnite.

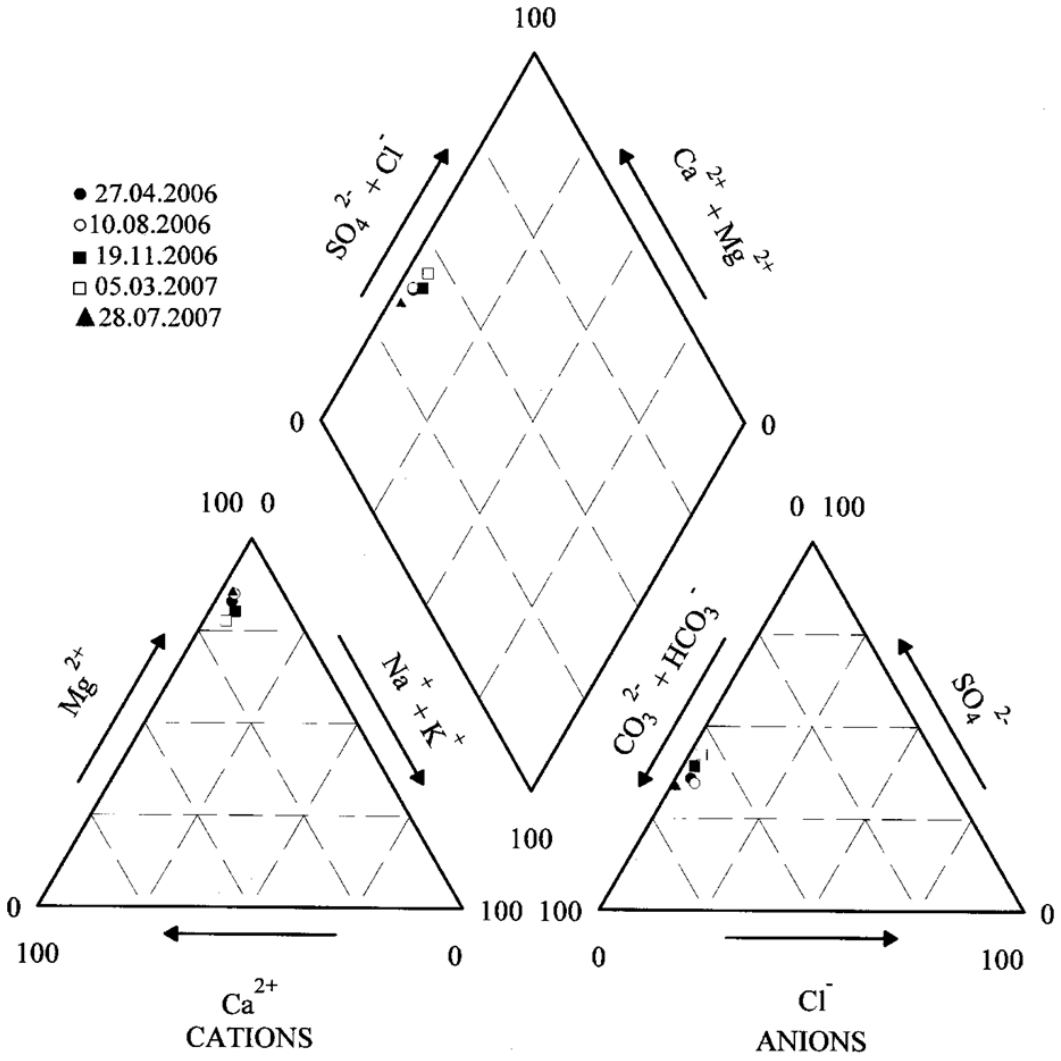

Fig.III.4 Piper diagram of the drainage water in the Goesdorf antimony mine.

pH	7.92	Conduct.	635.4 $mScm^{-1}$
Temp.	10.7°C	O_2	87.2%
HCO_3^-	4.464 $mmoll^{-1}$	Na^+	0.207 $mmoll^{-1}$
Cl^-	0.242 $mmoll^{-1}$	K^+	0.108 $mmoll^{-1}$
NO_3^-	0.634 $mmoll^{-1}$	Mg^{2+}	3.260 $mmoll^{-1}$
SO_4^{2-}	1.240 $mmoll^{-1}$	Ca^{2+}	0.490 $mmoll^{-1}$

Table III.1 Mean analytical composition of the drainage water

III.3.5 Effect of magnesium and calcium ion

The dissolution rate was measured in sodium bicarbonate solutions spiked with concentrations of Mg^{2+} ranging from 3×10^{-4} to 4.5×10^{-3} mol l^{-1}, keeping the ionic strength and the pH=8.7 constant. The alkaline-earth cations had been added as magnesium or calcium perchlorate, respectively. The calcium solution in bicarbonate buffer was supersaturated with respect to calcite, but it was verified that no precipitation occurred over the duration of the experiment by periodically determining Ca^{2+} in the feed solution. In the presence of 3 mM Mg^{2+}, a concentration representative of the Goesdorf mine water, the stibnite dissolution rate was indeed accelerated by a factor of approx. 2.9 with respect to the pure carbonate buffer (actual rate $2.55\times10^{-10} \pm 0.14\times10^{-10}$ mol $s^{-1}m^{-2}$ vs. 8.71×10^{-11} $mols^{-1}m^{-2}$ predicted). The measured dissolution rates at different Mg^{2+} concentrations (ranging from 0.3 mM to 3 mM) were fitted to a rate law of the form :

$$r = r_{\max} \frac{K\left[Mg^{2+}\right]}{1+K\left[Mg^{2+}\right]},$$

i.e. assuming that the rate is proportional to the Langmuir coverage of the surface with Mg^{2+}. A plot of $[Mg^{2+}]/r$ vs. $[Mg^{2+}]$ was indeed linear ($r>0.997$),

with $r_{max}=2.83\times10^{-10}\pm0.21\times10^{-10}$ mol $s^{-1}m^{-2}$ and $K=7.00\times10^{3}\pm0.43\times10^{3}$ mol^{-1} l. This seems to indicate that sorption of magnesium cations to the mineral surface promotes the dissolution rate of stibnite, presumably by imparting positive charge to the surface, which makes it more susceptible to attack by H_2O and/or O_2.

The effect of calcium ion was investigated in a single experiment with the same bicarbonate concentration and 0.3 mM calcium ion. The measured rate was again higher than that predicted on the basis of pH, temperature and $[O_2]$ alone, and comparable to that produced by 3 mM Mg^{2+}, i.e. the cations catalyse the dissolution in the order of their expected strength of adsorption which reflect, in turn, the ratio of charge to size: the ionic radius of Mg^{2+} is 72 pm and that of Ca^{2+} is 100 pm (Shannon, 1976). This is, to our knowledge, the first instance of metal-promoted dissolution of a sulfide mineral to be reported. In acid solution (chapter II), a similar effect was observed with ferric, cerous and aluminium cations. Multivalent cation adsorption is known to accelerate rates of dissolution of oxide minerals in basic solution (Biber et al., 1994, cf. Table 1 in that paper).

In the context of the Goesdorf mine drainage water, we note that the observed rate is close to the maximum rate predicted by the above equation. With respect to stibnite leaching kinetics, the composition of the Goesdorf water is a particularly unlucky coincidence of basic pH and high load of alkaline-earth metals, which both contribute to accelerate the rate.

III.3.6 Elemental sulfur recovered from the mineral surface.

The amounts of recovered sulfur formed on the surface of stibnite after 36 h of reaction were of comparable magnitude to those obtained under acid conditions, but generally an order of magnitude smaller than those obtained in the presence of ferric ion (cf. chapter II). Specifically, 1.0 ± 0.1 μmol/m^2 of elemental sulfur was found at pH 8.8 and 1.9 ± 0.1 μmol/m^2 at pH 10.6. In the presence of Mg^{2+}, these amounts increased to 4.3 ± 0.1 μmol/m^2 at [Mg^{2+}]=1.5 mM and 4.9 ± 0.1 μmol/m^2 at [Mg^{2+}]=3 mM. There is an excellent correlation (r>0.996) between the reaction rate and amount of elemental sulfur at the surface (Fig. III. 5).

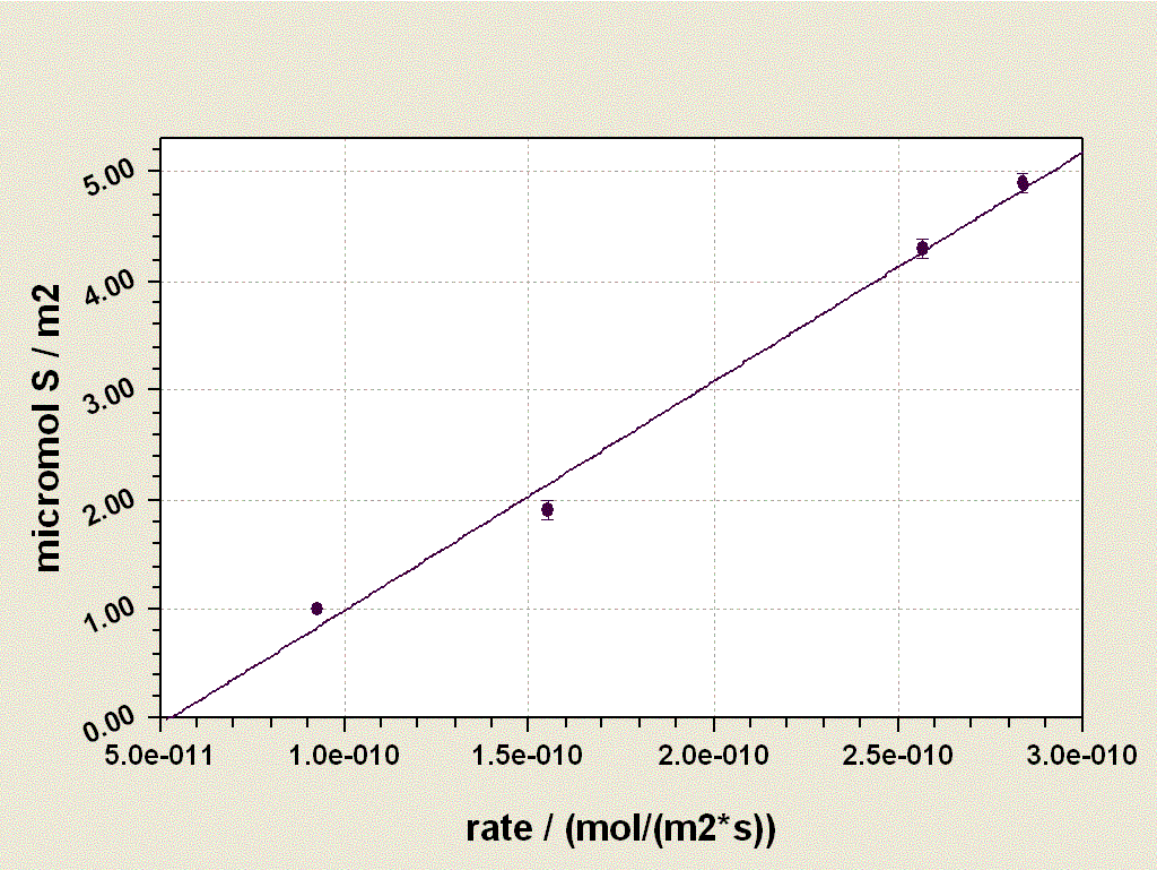

Fig. III.5 Recovered amount of S vs dissolution rate in the presence of Mg^{2+}

III.4 Summary and Conclusions

Mixed-flow reactor experiments were used to derive the rate law for the dissolution of stibnite in alkaline (carbonate-buffered) solutions. The rate was found to be inversely proportional to a fractional power of the hydrogen ion concentration and proportional to a fractional power of the dissolved oxygen concentration. The rate could also be successfully modelled by assuming proportionality to the Langmuir coverage of the mineral surface by molecular oxygen. Unlike in acidic solution, no saturation effect at a partial oxygen pressure corresponding to atmospheric conditions was observed; by extrapolation, saturation was predicted to occur at oxygen partial pressures in excess of 4 atm. The measured activation energy at pH=9.9 is indicative of surface, rather than diffusion control, which contrasts with the behaviour in acidic solution where the activation energy is smaller by an order of magnitude and the dissolution is diffusion controlled.

Comparison of the reaction rate measured in a laboratory simulation of alkaline mine drainage to the one predicted on the basis of pH and oxygen saturation alone, revealed that alkaline earth cations, contained in the mine water, significantly affected the rate: a magnesium concentration of 3 mmol l^{-1} increased the rate by a factor of nearly three, while calcium had the same effect at a concentration of only 0.3 mmol l^{-1}. When comparing the rates in basic solution (even in the absence of alkaline earth cations) to the ones measured in acidic solution in chapter II, we note that even in mildly basic solution

(pH=8.85), the mobilisation of antimony is faster than under very strongly acidic conditions (pH=1.08). This may help to explain the antimony anomalies discovered by Wolkersdorfer in waters draining Sb ore bodies in Tyrol, Austria (Wolkersdorfer and Wackwitz, 2004). The antimony concentrations in waters from five distinct lithological units, each containing Sb mineralization in the form of fahlore, were measured, and those in waters originating from a dolomitic environment were the highest. Quite generally, we would expect, on the basis of our results, the mobilisation of antimony from stibnite to be faster under conditions of neutral and alkaline mine drainage than under acid mine drainage conditions. Dissolution in basic solution was incongruent, and the amounts of elemental sulfur recovered from the reacted mineral surfaces were comparable to those obtained in acidic solution and much smaller than those obtained in the presence of ferric iron. In the presence of Mg^{2+}, the amounts of elemental sulfur increased in proportion to the increase in reaction rate.

III.5 References for Chapter III

Biber M.V., Dos Santos Afonso M. and Stumm W. (1994) The coordination chemistry of weathering: IV. Inhibition of the dissolution of oxide minerals. *Geochim. Cosmochim. Acta* **58**, 1999-2010

Biver M. and Shotyk W. (2011) *Geochim. Cosmochim. Acta* submitted.

De Giudici G., Rossi A., Fanfani L. and Lattanzi P. (2005) Mechanisms of galena dissolution in oxygen-saturated solutions : Evaluation of pH effect on apparent activation energies and mineral-water interface. *Geochim. Cosmochim. Acta* **69**, 2321-2331

Faure, G. (1998) *Principles and Applications of Geochemistry*. Prentice-Hall, Upper Saddle River, NJ.

Hückel E. (1925) Zur Theorie konzentrierter wässeriger Lösungen starker Elektrolyte. *Physikalische Zeitschrift*, **26**, 93-149

Lasaga A.C. (1984) Chemical Kinetics of Water-Rock Interactions. *J. Geophys. Res.* **89(B6)**, 4009-4025

Lengke M.F. and Tempel R.N. (2002) Reaction rates of natural orpiment oxidation at 25 to 40°C and pH 6.8 to 8.2 and comparison with amorphous As_2S_3 oxidation. *Geochim. Cosmochim. Acta* **66**, 3281-3291

Lengke M.F. and Tempel R.N. (2003) Natural realgar and amorphous AsS oxidation kinetics. *Geochim. Cosmochim. Acta* **67**, 859-871

Lindsay M.B.J., Condon P.D., Jambor J.L., Lear K.G., Blowes D.W. and Ptacek C.J. (2009) Mineralogical, geochemical, and microbial investigation of a sulfide-

rich tailings deposit characterised by neutral drainage. *Appl. Geochem.* **24**, 2212-2221

Majzlan J., Lalinska B, Chovan M., Bläss U., Brecht B., Göttllicher J., Steininger R, Hug K., Ziegler S. and Gescher J. (2011) A mineralogical, geochemical, and microbiological assessment of the antimony- and arsenic-rich neutral mine drainage tailings near Pezinok, Slovakia. *American Mineralogist* **96**, 1-13

Merkel B.J. and Planer-Friedrich B.(2008) Groundwater Geochemistry. 2nd ed., edited by D.K. Nordstrom. Springer, Berlin

Philippo S. and Hanson A. (2007) Inventaire minéralogique du Luxembourg: Stolzembourg, Schimpach, Goesdorf. *Ferrantia* **49**, 111-146

Piper A.M. (1944) A graphic procedure in the geochemical interpretation of water analysis. *Trans. Am. Geophys. Union* **25**, 914-928

Shannon R.D. (1976) Revised Effective Ionic Radii and Systematic Studies of Interatomic Distances in Halides and Chalcogenides. *Acta Cryst.* **A32**, 751-767.

Sposito G. (2004) *The Surface Chemistry of Natural Particles*. Oxford University Press, Oxford/New York.

Wolkersdorfer C. and Wackwitz T. (2004) Antimony anomalies around abandoned silver mines in Tyrol/Austria. In *Proceedings International Mine Water Association Symposium 1* (eds. A.P. Jarvis, B.A. Dudgeon and P.L. Younger) University of Newcastle, Newcastle-upon-Tyne, pp. 161-167

Chapter IV

Experimental Study of the Kinetics of Ligand-Promoted Dissolution of Stibnite (Sb_2S_3)

Abstract. Batch reactor experiments were carried out in order to investigate the influence of organic ligands in aqueous solution on the rate of dissolution of stibnite (Sb_2S_3). Ligands that may be regarded as representative of those occurring naturally in the soil solution were chosen, namely acetic, oxalic, citric, and salicylic acids, EDTA, glycine, cysteine, glucose, catechol, desferrioxamine-B, and standardized natural chestnut leaf litter extract. Millimolar concentrations of the ligands dissolved in inert buffers at pH=4, 6, and 8 were added to powdered stibnite in a stirred, thermostatted reactor (25°C) and the rate of increase in antimony concentration over time was monitored by ICP-OES. Dissolution rates were initially parabolic and settled into a linear regime. Comparison of initial and steady state rates achieved with different ligands with the blank experiments gives a very complex picture. Both rate enhancements and retardations are observed, and in some cases the net effect of a ligand at a given pH may be either an increased or a decreased mobilization with respect to the blank experiment, depending on the time of contact of the solution with the mineral. Rationalisations in terms of known principles of surface complexation are attempted. The extent of solution phase complexation of Sb(III) with the ligand under investigation is not found to be a decisive factor in the cases of those systems for which complexation constants are known.

IV.1 Introduction

In earlier papers, we investigated the rates of oxidative dissolution of stibnite (Sb_2S_3), the most important antimony ore, in acidic and in basic solution. The aim of the present work is to extend the study to the effect of low molecular weight organic acids (LMWOA) on the rates of stibnite dissolution. Ligand-promoted dissolution of oxides and silicates has been studied extensively (Furrer and Stumm, 1986; Biber et al., 1994; Sposito, 2004 and references therein), while fewer data exist on the dissolution of sulfides (Davis et al., 1995). The same general principles are expected to hold, since surfaces of sulfides behave in a similar way to those of oxides, forming amphoteric surface hydroxo groups (Davis et al., 1995; Rönngren et al., 1991). LMWOA occur in soils as a result of microbial breakdown of humic substances, leaching of plant detritus, and root exudation. Commonly found LMWOA in the soil solution comprise carboxylic acids, e.g. formic and acetic acids (2-5 $mmoll^{-1}$), oxalic and tartaric acids (0.05-1 $mmoll^{-1}$), citric acid (<0.05 $mmoll^{-1}$), aromatic acids (0.05-0.3 $mmoll^{-1}$), amino acids (e.g. glycine, alanine, aspartic acid, glutamic acid, arginine, lysine, 0.05-0.6 $mmoll^{-1}$) and carbohydrates (e.g. glucose, glucosamine, galactose, mannose, xylose), which, together with their polymerised forms, can account for up to one half of a soil's organic carbon (Sposito, 2008). Davis and co-workers examined the effect of citric, oxalic, benzoic, salicylic, phthalic acids, as well as EDTA, NTA and catechol on the photo-oxidative rate of dissolution of cadmium sulfide (Davis et al., 1995). The effect of citric, oxalic, phthalic and salicylic acids on the

dissolution of chalcopyrite was studied by Goyne and co-workers (2006), without analysis of the reaction kinetics. Antimony(III) is known to form complexes with all of the above mentioned organic acids, and for some of them complexation constants are known (Anderegg and Malik, 1970; Filella and May, 2005, Tella and Pokrovski, 2009). It also forms a complex with guanosine (Klüfers and Mayer, 1997), which suggests that carbohydrates may have an effect on the rate of dissolution of stibnite. A special class of biomolecules found in soils are the siderophores. These are synthesised by bacteria, fungi and graminaceous plants under conditions of iron deficiency in oxic environments, where the bioavailability of iron is severely limited by the poor solubility of Fe(III) containing minerals. Siderophores form soluble Fe(III) complexes, in which form the Fe(III) becomes accessible to organisms. Some 500 siderophores have been characterised today (Sposito, 2008). They are typically tetradentate to hexadentate ligands that contain some combination of hydroxamate, catecholate or (amino-)carboxylate moieties, with a high specificity for Fe^{3+}. Siderophores are present at concentrations from 10-100 $nmoll^{-1}$ in all oxic environments, including marine, fresh waters, and soils. In the rhizosphere, the local concentration of siderophores may be orders of magnitude higher than in the surrounding soil (Duckworth et al., 2009b). Historically, siderophores with hydroxamate and catecholate functionalities were discovered first. The first aminocarboxylate siderophore to be discovered was rhizobactin (Smith et al., 1985), mugineic acid secreted from barley roots (Ma et al., 1993) being another example (Fig. IV.1).

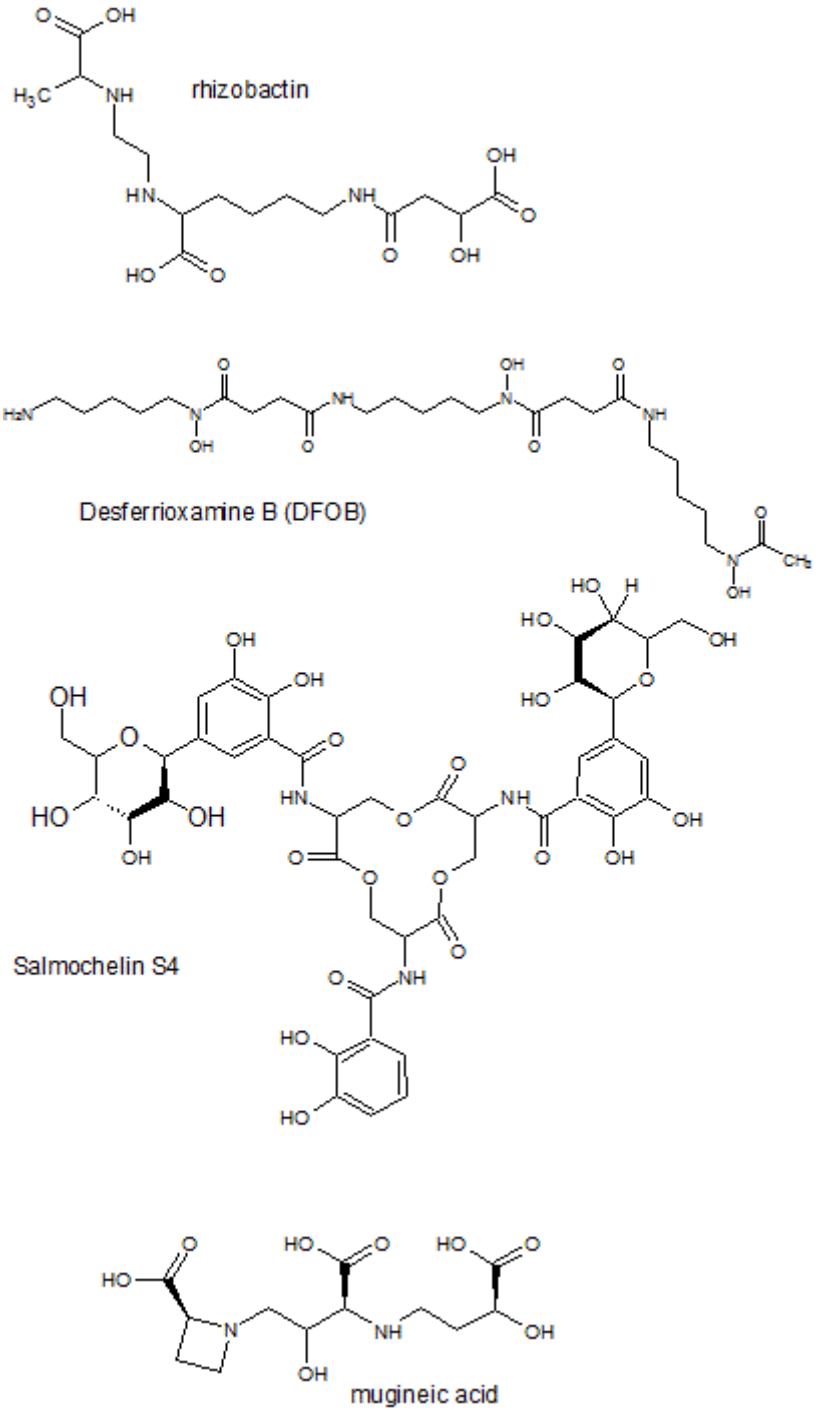

Fig. IV.1 Structures of some siderophores

Salmochelin (Fig. IV.1) is an example of a catecholate siderophore (Müller et al., 2009). The most extensively studied siderophore is desferrioxamine-B (DFOB, deferoxamine), a trihydroxamic acid (Fig. IV.1). DFOB is commercially

available as the mesylate salt under the trade name Desferal (Novartis). It is medicinally used in the treatment of iron poisoning. DFOB has been shown to promote the dissolution of the iron minerals goethite, α-FeOOH, (Simanova et al., 2010), hematite, α-Fe_2O_3, (Hersman et al., 1995), but also manganite, γ-MnOOH (Duckworth and Sposito, 2005b), hausmannite, Mn_3O_4 (Pena et al., 2007), and cobalt hydroxides (Bi et al., 2010) by forming an exceptionally stable Co(III) complex (more stable than the Fe(III) complex) (Duckworth et al., 2009a). Similarly, Mn(III) is stabilised in aqueous solution by complexation with DFOB (Duckworth ans Sposito, 2005a). A large number of stability constants of DFOB-metal complexes is known (Anderegg et al., 1963; Hernlem et al., 1996), unfortunately, no constant is available for antimony. Cornejo-Garrido and coworkers (2008) conducted a kinetic study on the effect of DFOB on arsenopyrite and galena dissolution.

We thus chose a number of representative substances, which either occur as such in the soil solution, or which may serve, by virtue of structural and functional similarities, as proxy compounds for a class of common soil solution components (Table IV.1 and Fig. IV.2). An experiment was also carried out using DFOB in conjunction with citric acid, as synergistic kinetic effects had been reported between DFOB and LMWOA (Duckworth et al., 2009b and references therein ; Cheah et al., 2003). A synergistic kinetic effect between a reductant (ascorbate) and a chelator (oxalate) in the dissolution of hematite has also been reported (Banwart et al., 1989)

Class	**Representative Substance**	**Concentration in the experiment**	**Concentration in the soil soln.**
Carboxylic acids	Acetic acid	1 mM	2-5 mM
	Oxalic acid	1 mM	0.05-1 mM
	Citric acid	1 mM	<0.05 mM
Aminocarboxylic acids, aminocarboxylate siderophores	EDTA	1 mM	
Aromatic acids	Salicylic acid	1 mM	0.05-0.3 mM
Amino Acids	Glycine	1 mM	0.05-0.6 mM
S-bearing amino acid	Cysteine	1 mM	
Carbohydrates	Glucose	1 mM	
Phenols, catecholate siderophores	Catechol	1 mM	Nanomolar, up to 0.25 mM in the rhizosphere
Hydroxamic Siderophores	Desferrioxamine-B (DFOB)	1 mM	
	DFOB + citric acid	1 mM each	
Leaf Litter extract		1 mM total acidity	

Table IV.1 List of ligands used in the kinetic experiments

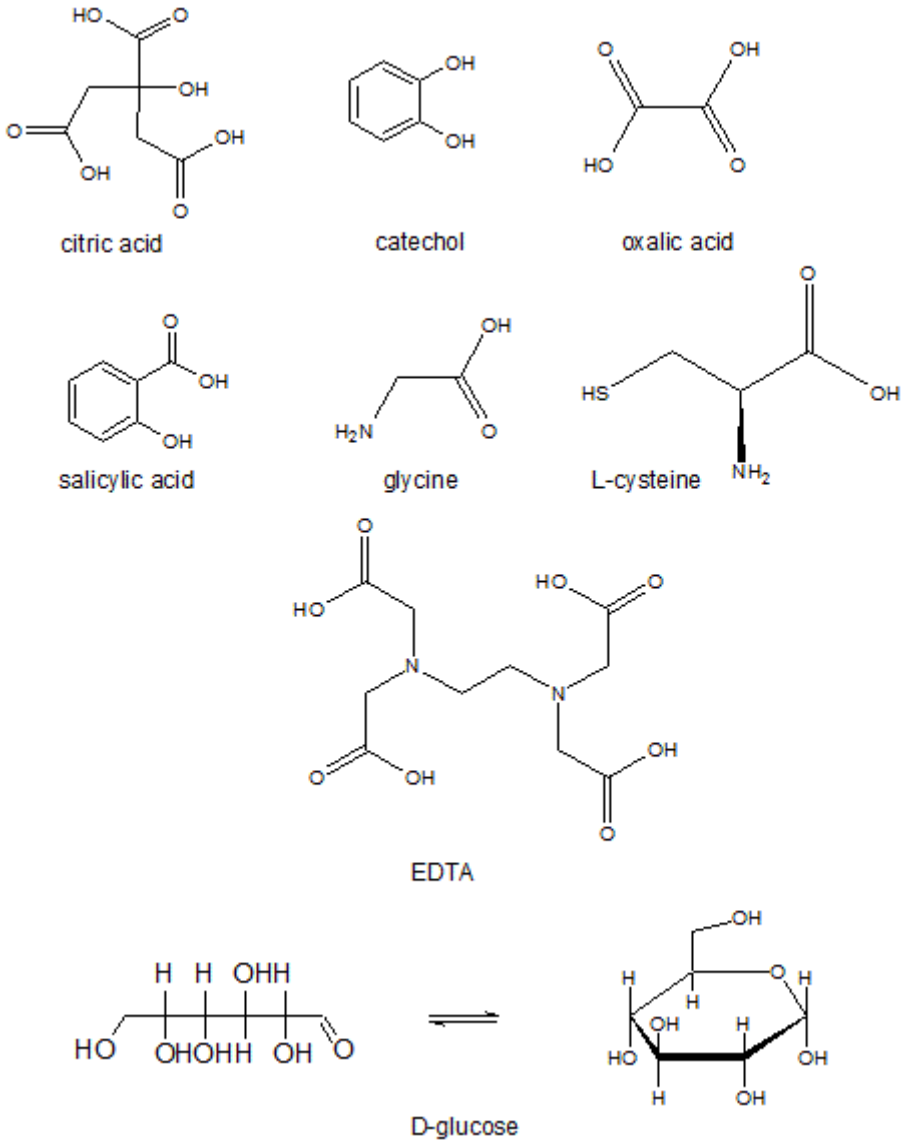

Fig. IV. 2 Structures of the ligands used in the kinetic experiments

IV.2 Experimental

Rates of dissolution of stibnite were measured in a batch reactor. This consisted of a conventional, 1 L two-necked, round-bottom flask immersed in a constant temperature water bath set to 25°C. Through the central neck, a ground glass stopper with a plastic axle carrying a magnetic stirrer bar was fitted, so that the stirrer did not touch the bottom of the flask, in order to avoid grinding

of the mineral. The second neck remained open to the atmosphere and was used as a sampling port. The following buffer agents were used : pH 4: sulfanilic acid (pK_a=3.3), pH 6: MES (2-(N-morpholino)-ethanesulfonic acid, pK_a=6.2) and pH 8: MOPS (3-(N-morpholino)-propanesulfonic acid, pK_a=7.2). The so called 'Good's buffers' MES and MOPS were chosen because they are known to complex metal ions to a negligible extent (Good et al., 1966). The suitability of sulfanilic acid for the present purpose was tested by control experiments at pH=4 without buffer, showing that a sulfanilic acid/sulfanilate buffer did neither promote nor inhibit the stibnite dissolution rate. The total buffer concentrations were 0.05 M and the pH adjusted to the desired value with 1 M NaOH solution under potentiometric control (pH Meter: Model 632, Metrohm, Switzerland, calibrated using NIST-traceable standards from Hanna Instruments, Hungary). Each solution contained one of the ligands in table IV.1 (Structural formulae in Figs. IV.1 and IV.2) to a final concentration of 1 mM. The ionic strength of each solution was adjusted to 0.1 M by addition of the calculated amount of $NaClO_4$. This ionic strength was chosen because it corresponds to the conditions most frequently encountered in the literature (Ludwig et al., 1995; Furrer and Stumm, 1986) on ligand-promoted kinetics. Blank experiments were carried out using a buffer solution without added ligand. For every run, 1 L of the buffer solution was introduced into the reactor, and, once thermal equilibrium was established, an accurately weighed mass of about 100 mg commercial Sb_2S_3 was added. The solutions were stirred magnetically. 10 ml samples were taken in 5 minute intervals for 90 minutes, using disposable PP/PE syringes (Brown, Germany) fitted with CME 0.45 µm

hydrophilic syringe filters (Millipore, US) and a short length (about 10 cm) of silicone tubing (C.Roth, Germany). All reagents used were p.a. grade or better. Sulfanilic acid, citric acid, sodium salicylate, oxalic acid, cysteine and glucose were from Merck, Germany. Catechol, glycine, EDTA, sodium acetate, MES and MOPSO were from C. Roth, Germany. DFOB-mesylate was from Novartis, Switzerland. The aqueous leaf litter extract (LLE) was prepared according to the directions of Blaser and co-workers (1984) from chestnut (Castanea sativa L.) leaves (Heinrich Klenk GmbH, Germany). Briefly, the leaves were cut to powder in a blender and mixed with distilled water; the solid-to-liquid ratio was 2.5 g/100 ml. The suspension was stirred magnetically for 12 h and the extract was filtered over ashless paper of medium porosity. The filtrate was a dark brown liquid, clear and transparent, turning to yellow on dilution, with an initial pH of 4.51. The total acidity (0.0176 M) of the leaf litter extract was determined by conductimetric titration with 0.01 M NaOH, following the protocol in Blaser's paper. 25 ml of the LLE had been diluted to 200 ml with distilled water prior to titration. The dry solid matter content was determined by evaporation of 100 ml LLE and amounted to 0.49% (w/v), close to the value of 0.50% (w/w) found by Blaser. The extract was diluted to give a total acidity of 1 mM in buffer solution before use. The LLE was stored in a refrigerator at 2°C and kept for no longer than 3 days. Antimony sulfide and sodium perchlorate were from Acros, Germany. The identity and structure (stibnite) of the antimony sulfide were confirmed by powder X-ray diffraction (Cu Kα1 radiation, Debye-Scherrer geometry). The specific BET-surface area of the stibnite samples (0.8333±0.0089 m^2g^{-1}) was determined by

multiple-point N_2 adsorption using a Gemini VII 2390 instrument (from Micromeritics, Germany). The stibnite powder was used as supplied. Total antimony concentrations in the samples were determined by ICP-OES (Spectroflame Modula, Spectro Analytical Instruments, Kleve, Germany). The instrument had been calibrated using a commercial single-element antimony standard (Alfa-Aesar, Germany) and a detection limit of 4.6 µg l^{-1} had been achieved.

IV.3 Results and Discussion

At the beginning of the experiments, the release of antimony from the mineral to solution can be seen to follow a parabolic rate law, which becomes linear after 20-50 min. (Lasaga, 1984; Stumm and Wollast, 1990). As an example, the amount of Sb (normalised with respect to the surface area of the sample) as a function of time is plotted in Fig. IV.3 at pH=4 and 1 mM DFOB and 1 mM LLE respectively.

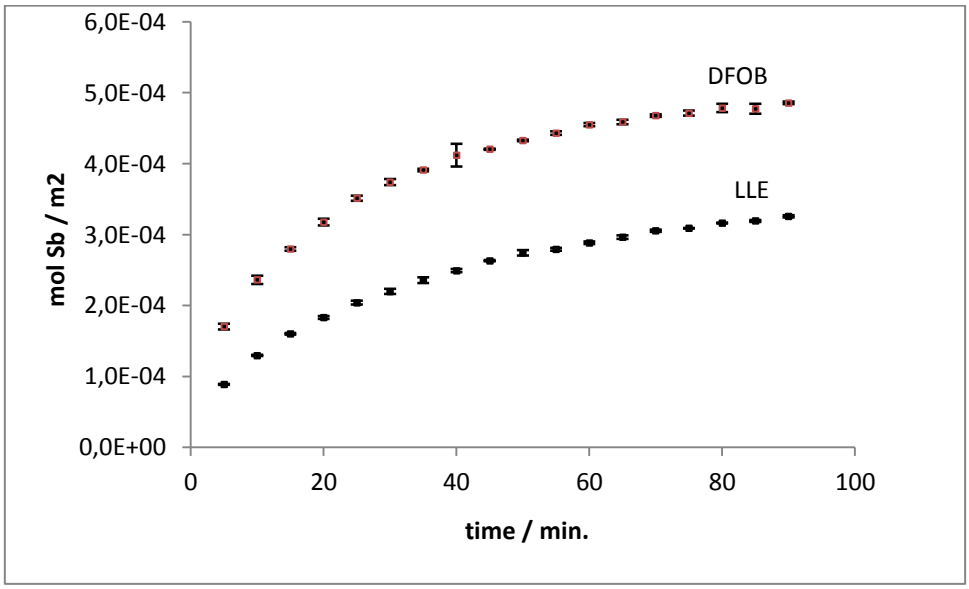

Fig. IV.3 Surface-normalised amount of Sb mobilised at pH 4 by DFOB and LLE

IV.3.1 Initial rates

The initial rates of dissolution (Fig. IV. 4) were evaluated using the amount of mobilised antimony after the first 5 min. of the experiment. All the measured rates significantly differed from the blank, except in the case of glycine at pH=6. The only three substances that promoted the intial rate at *any* pH were citrate, EDTA and oxalate. Catechol had a promoting effect only at pH>4, and cysteine at pH>6. Six out of the 13 ligands (acetate, DFOB, DFOB+citrate, glucose, LLE and salicylate) inhibited the initial rate at any pH. In the blank experiments, the intial rate was found to decrease on going from pH 4 to pH 8. In the presence of acetate, citrate, DFOB+citrate, EDTA, oxalate and salicylate, the same qualitative trend could be observed: the rates in the presence of acetate, DFOB+citrate, and salicylate were smaller than the blank rates while an increase with respect to the blank was observed in the case of citrate, EDTA and oxalate. The LLE was the only substance that caused an increase in the initial dissolution rate with increasing pH; however, there was a significant inhibition of the rate with respect to the blank at any pH. In the remaining cases (catechol, cysteine, DFOB, glucose and glycine), the rates did not vary monotonically with pH.

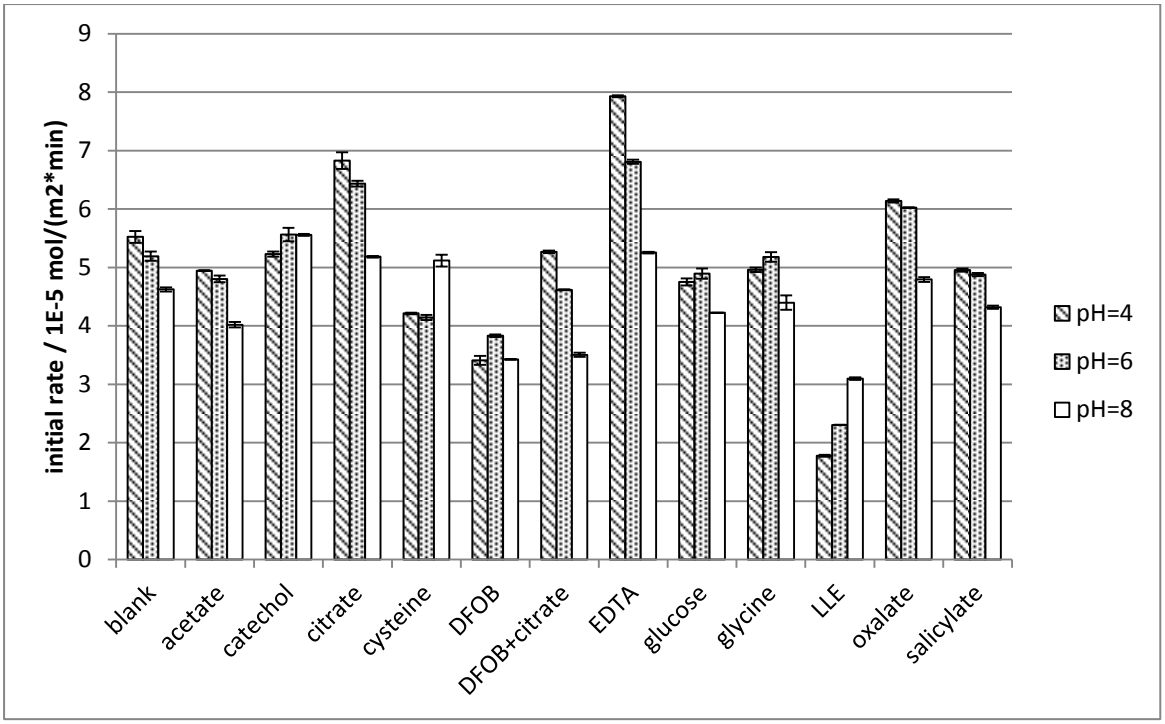

Fig. IV. 4 Initial rates of dissolution (after 5 min.) at pH=4, 6, 8

Initial rates (numerical data) are supplied in Appendix AV.

IV.3.2 Steady state rates

Straight lines were fitted to the linear portions of the graphs and the rates of dissolution corresponding to a steady state condition at the mineral surface were estimated from their slopes (Fig. IV.5-7). Correlation coefficients were between 0.97 and 0.99 at pH=4, between 0.94 and 0.99 at pH=6 and between 0.92 and 0.997 for pH=8.

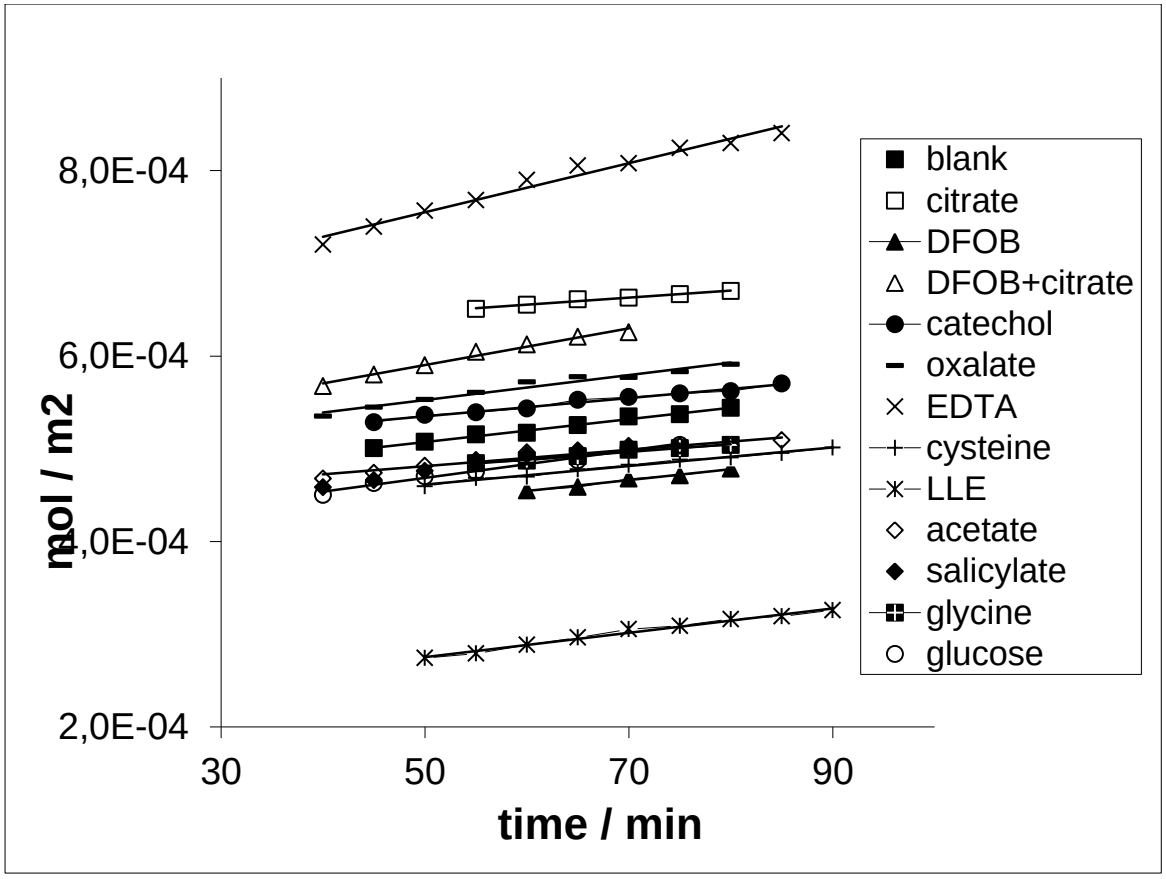

Fig.IV.5 Amount of Sb mobilised as function of time at pH 4 for various ligands. Error bars omitted for clarity.

The resulting rates are represented in Figs. IV.8-10. Ligands with similar behaviour were grouped together. In the absence of organic ligands, the rates (of pure proton-promoted dissolution) decrease in going from acidic (pH=4) to basic (pH=8) solution. The stibnite surface, with a pH(pzc)=2.0 (Healy and Fuerstenau, 2007), can be considered to bear a net negative charge over the whole pH domain covered by our experiments.

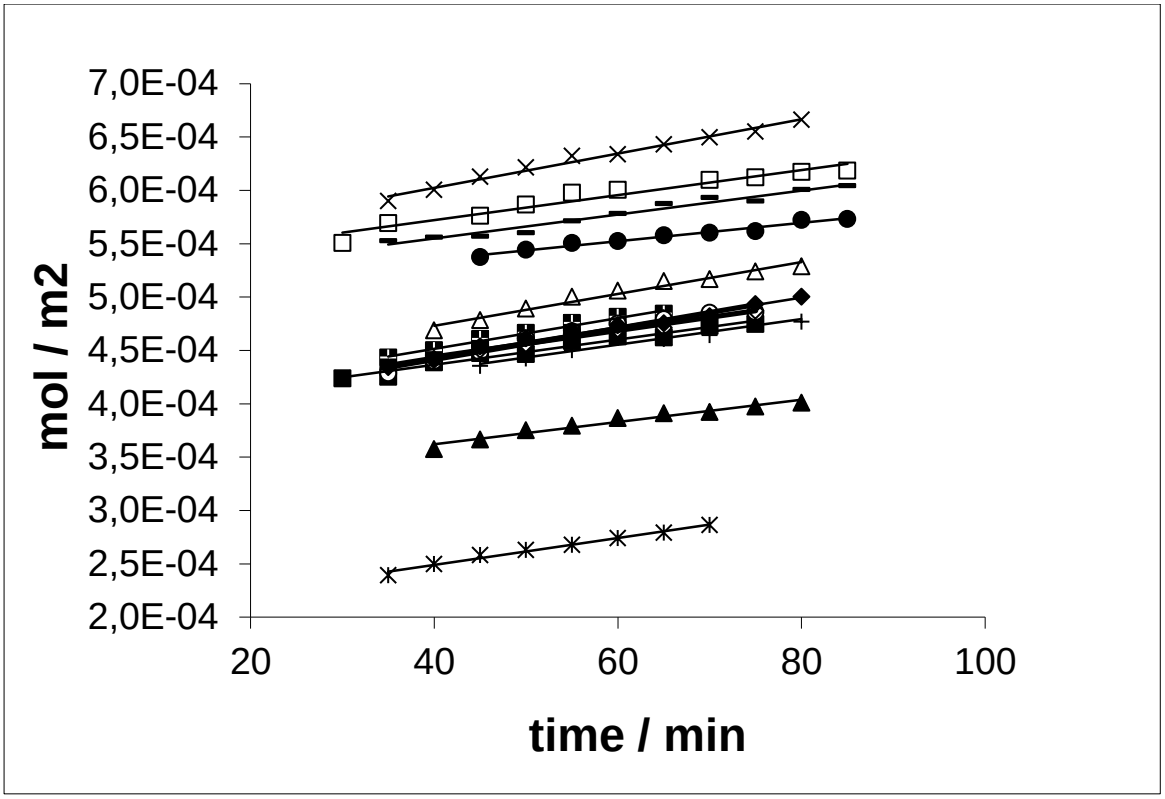

Fig. IV.6 Amount of Sb mobilised as function of time at pH 6 for various ligands. Error bars omitted for clarity. Legend as in Fig. 5.

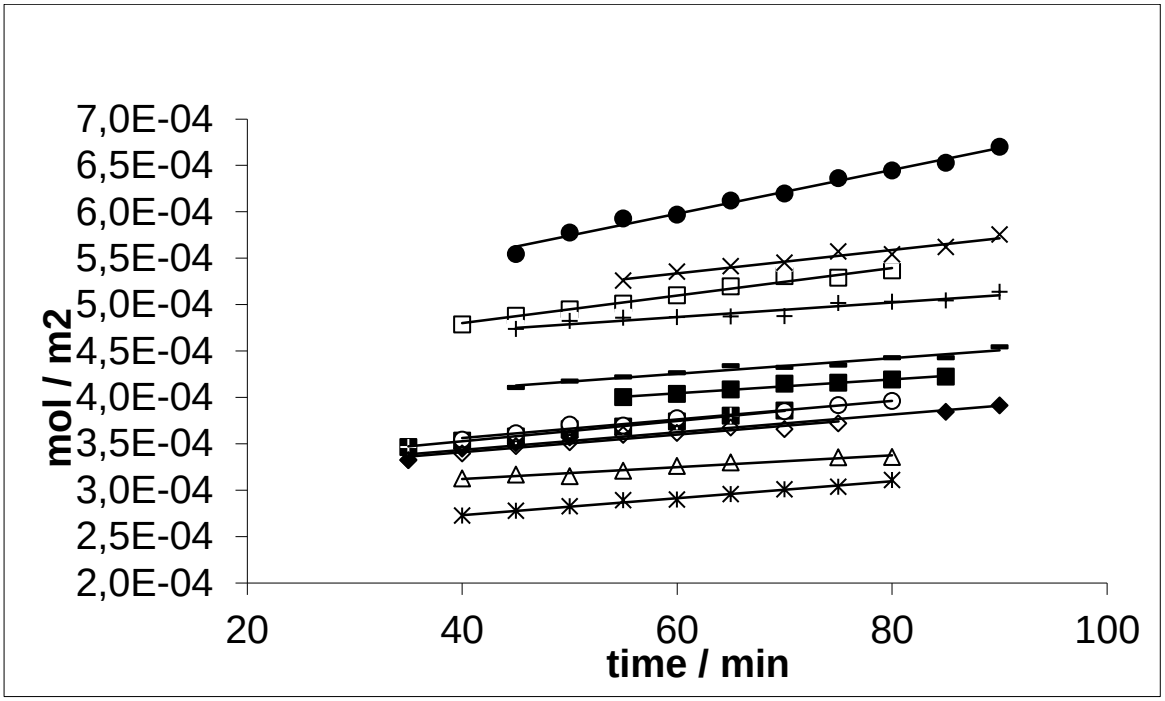

Fig.IV.7 Amount of Sb mobilised as function of time at pH 8 for various ligands. Error bars omitted for clarity. Legend as in Fig. IV.5.

In Fig.IV.8, the rates vary monotonically with pH. The general trend is a decrease in rate with increasing pH, parallel to that of the pure, proton-promoted dissolution, which may reflect the decreasing equilibrium adsorption of ligands with increasing negative charge on the surface. Citrate is an exception in that it has a passivating effect in acid solution at pH=4. At pH=6, it has virtually no effect and it strongly promotes the rate in basic solution. At pH=4, only the first protolysis of citric acid is virtually complete (pK_{a1}=3.16, pK_{a2}=4.76), so that it cannot act as multidentate chelator. It rather acts as a monodentate ligand at this pH. This is similar to glycine, cysteine and acetate (monodentate ligands), which all inhibit the rate of dissolution at pH=4 (Fig.IV.10). This is in agreement with Furrer and Stumm's observation (1986) that monodentate ligands, although they adsorb readily, they do not enhance and even inhibit rates of dissolution (by blocking the access to the surface). Salicylate, however, with much a lower pK_{a1} of 2.75, seems to be able enhance the dissolution by formation of a surface chelate. The phenol function of salicylic acid (pK_a=12.38) does not need to be deprotonated for this. The same may be true for oxalate, even though the difference with respect to the blank is not significant at pH=4. Salicylate, LLE and glucose promote the rate over that of pure proton-promoted dissolution at every pH with respect to the blank, while the overall effect of oxalate is comparatively small (no significant effect at pH=4 and 6, promotive in basic solution). In the case of glucose, there is little

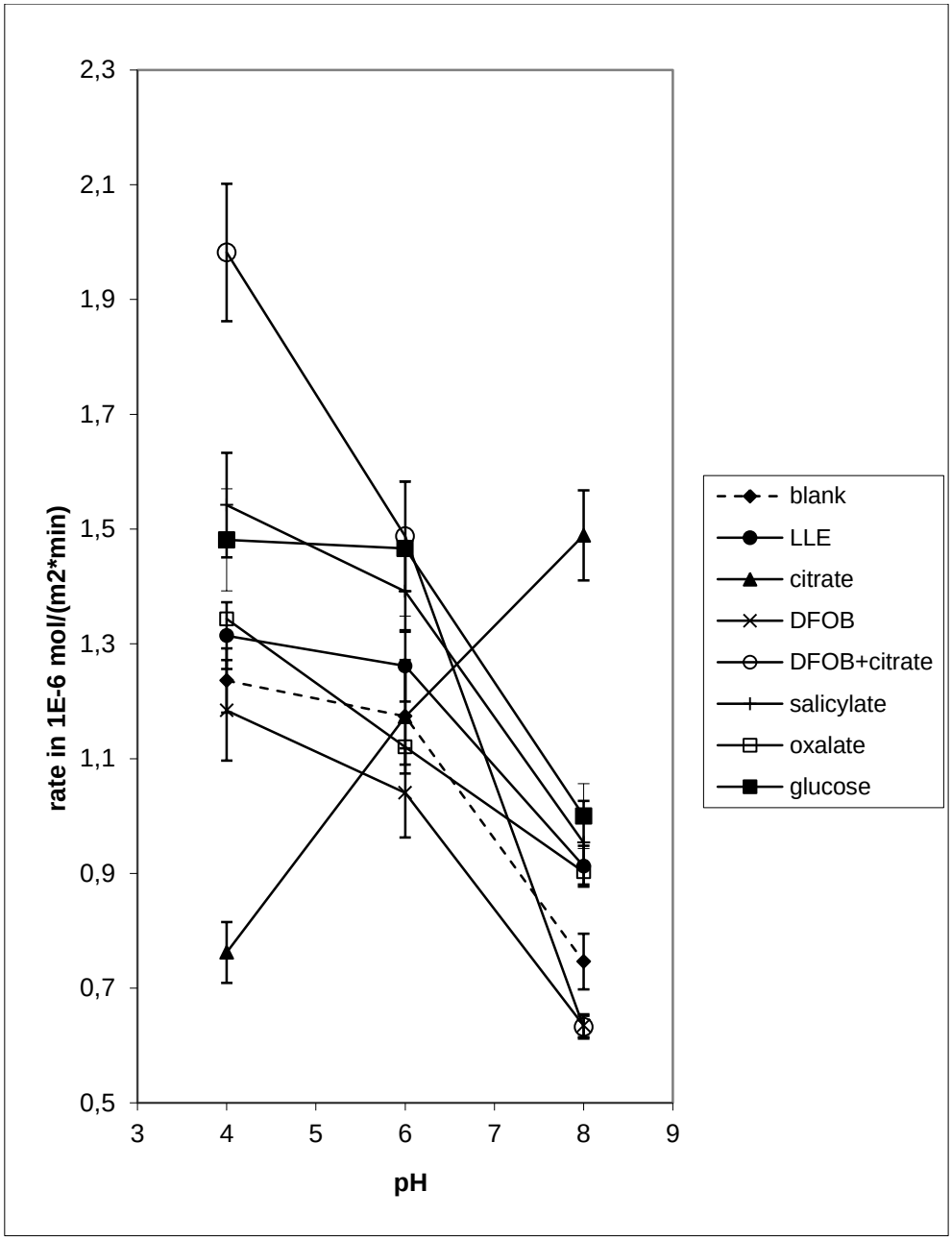

Fig. IV.8 Rates varying monotonically with pH

difference in the rate at pH=4 and pH=6, but it is considerably reduced at pH=8, although the overall effect in comparison to the blank remains promotive. The siderophore DFOB inhibits the rate at all pH values, but at pH=4 and pH=6, there is a very strong synergistic effect between citrate and DFOB leading to an overall promotion of the rate. Note that both citrate and DFOB *on their own*

inhibit the rate in acid solution, but *in combination* they strongly promote it. The usual interpretation of the synergistic effect of siderophores in the presence of LMWOA is that the LMWOA is able to form a surface complex with metal ions in the mineral surface, leading ultimately to the dislocation of the metal ion from the crystal and the transfer of the LMWOA-metal ion complex to the solution phase, where it acts as a prey for the siderophore. The siderophore, whose complex with the metal is more stable than the LMWOA complex, scavenges the metal ion from the latter and releases the LMWOA, which can then again react at the mineral surface. A similar effect was observed by Cheah and co-workers (2003) between DFOB and oxalic acid in the dissolution of goethite. These authors actually hypothesise that this synergistic effect is the principal reason for the siderophores' efficacy in mobilising iron from insoluble minerals. The siderophore *on its own*, i.e. in the absence of LMWOA, would have to be present in much larger (unrealistic) concentrations in order to fulfil its function effectively. In our experiment, the DFOB actually inhibits the dissolution on its own. This passivation is most probably due to the formation of multinuclear surface complexes. DFOB (Fig.IV.1) possesses several functionalised moieties, capable of coordinating a metal ion, that are far enough apart to span several metal ions on the mineral surface. The simultaneous, concerted detachment of three metal ions is an unlikely process with a high activation energy and thus kinetically disfavoured. At high pH, it appears likely that even in the presence of citrate, the surface is saturated with polynuclear DFOB complexes, so that access to the surface is completely blocked and citrate remains without effect.

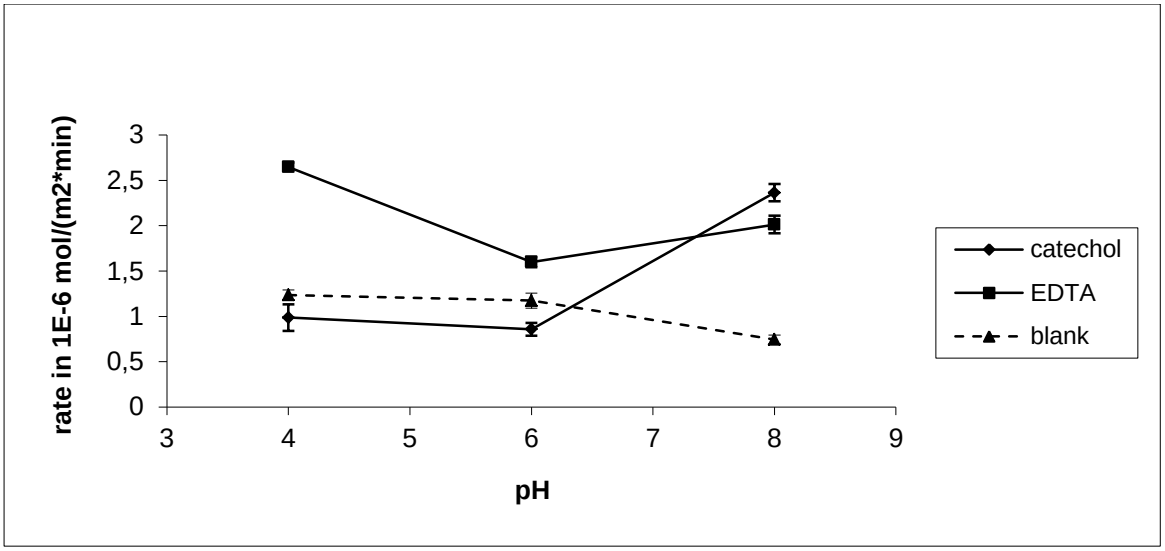

Fig IV.9 Rates having a minimum at intermediate pH

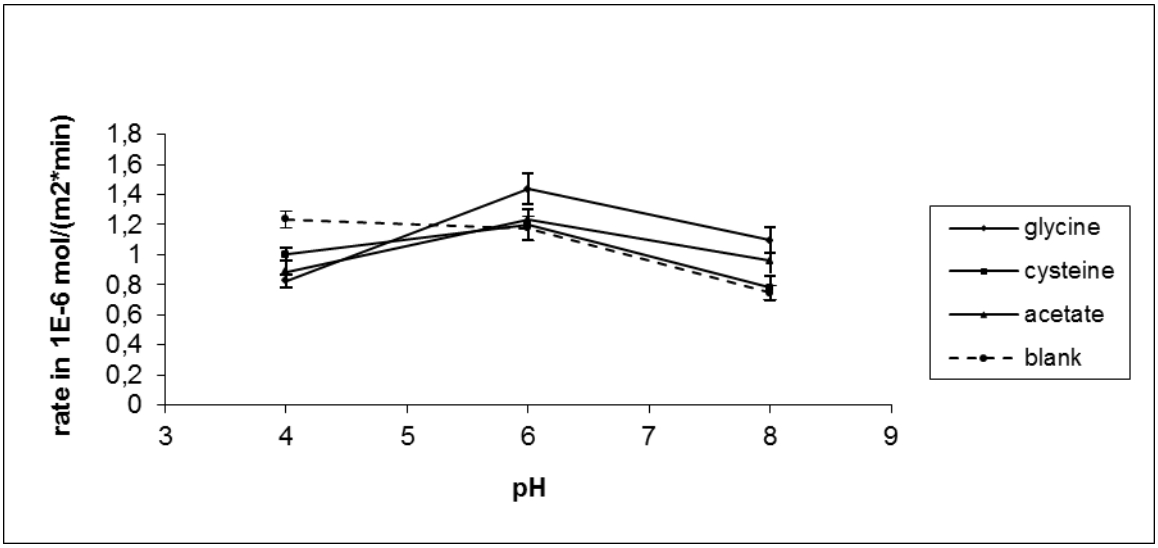

Fig. IV.10 : Rates having a maximum at intermediate pH

The effects of the remaining ligands are somewhat more complicated : the rate in the presence of catechol and EDTA goes through a minimum at pH=6 (Fig. IV.9). Catechol inhibits the dissolution at pH=4 and pH=6, while it promotes it in basic solution. The reason for this may lie in the relatively high pK_{a1} of the 1st (phenolic) protolysis of catechol (pK_{a1}=9.85). As in the case of salicylate above, it seems that at least one of the chelating functions must be, at least

partially, deprotonated, so that catechol can exert its chelating ability only as the 1st pK_a is approached. At pH=4 and 6, catechol seems to behave as a monodentate ligand with the retarding effect on the rates of dissolution described below (case of acetate, glycine and cysteine). The effect of EDTA is always a promotive one. This may be understood by looking at the 1st two pK_a values (pK_{a1}=2.0 and pK_{a2}=2.7) of the acid, which are both well below 4, so that even at pH=4, two fully deprotonated carboxyl groups are available for multidentate chelation. The decrease in dissolution rate up to pH=6 reflects the growing negative charge on the surface, while nothing changes in the extent of deprotonation of the ligand. It is only above pH 6 that one more carboxyl function becomes deprotonated (pK_{a3}=6.16) and available for chelation, which explains the increasing reaction rate at pH=8. Rates in the presence of the amino-acids glycine and cysteine, and acetate have a maximum at pH=6 (Fig. IV.10). In acid solution, at pH=4, all these ligands retard the dissolution. At pH=6, cysteine and acetate are without significant effect and only glycine acts promotively. At pH=8, glycine and acetate promote the rate and cysteine is without significant effect. As pointed out by Furrer and Stumm, monodentate ligands frequently have no significant promotive effect, or they may even retard dissolution by blocking access to the surface.

For acetate, EDTA, oxalate, catechol and citrate, stability constants for the Sb(III)-ligand complexes exist (Anderegg and Malik, 1970 ; Filella and May, 2005 ; Tella and Pokrovski, 2009). No correlation was found between the extent of complexation in solution and the reaction rate. For instance, EDTA, oxalate and

citrate all complex the available antimony to virtually 100% under the conditions of the experiments, yet the dissolution rates and the observed trends of the rates as a function of pH differ widely for these three ligands. Complexes taken into account were $[Sb(acetate)]^{2+}$, $[Sb(acetate)_2]^{+}$, $[Sb(EDTA)]^{-}$, $[Sb(oxalate)_2]^{-}$, [Sb(citrateH)], [Sb(catechol)(OH)] and $[Sb(catechol)_2]^{-}$. The simple principle of a correlation between dissolution rate and the stability of the dissolved complex (Ludwig et al., 1995) may not be generally applicable: the concept of the similarity between the surface complex and the aqueous complex present in solution, for instance, does not at all take into account the possibility of surface passivation resulting from polynuclear surface complexes, which may be of similar stability as the aqueous complexes, but quite reluctant to detach from the surface.

There is, however, a strong correlation between the reaction rates at pH=8 and the pK_a of the dissociation step of a polyprotic acid believed to be relevant for complex formation (Fig. IV.11), i.e. catechol : pK_{a2}=12.8, citrate : pK_{a3}=6.396, cysteine : pK_{a1}=1.71 (carboxylate), EDTA : pK_{a4}=10.26, glycine : pK_{a1}=2.34 (carboxylate), oxalate : pK_{a1}=1.24, salicylate : pK_{a1}=2.75 (carboxylate), acetate pK_a=4.75.

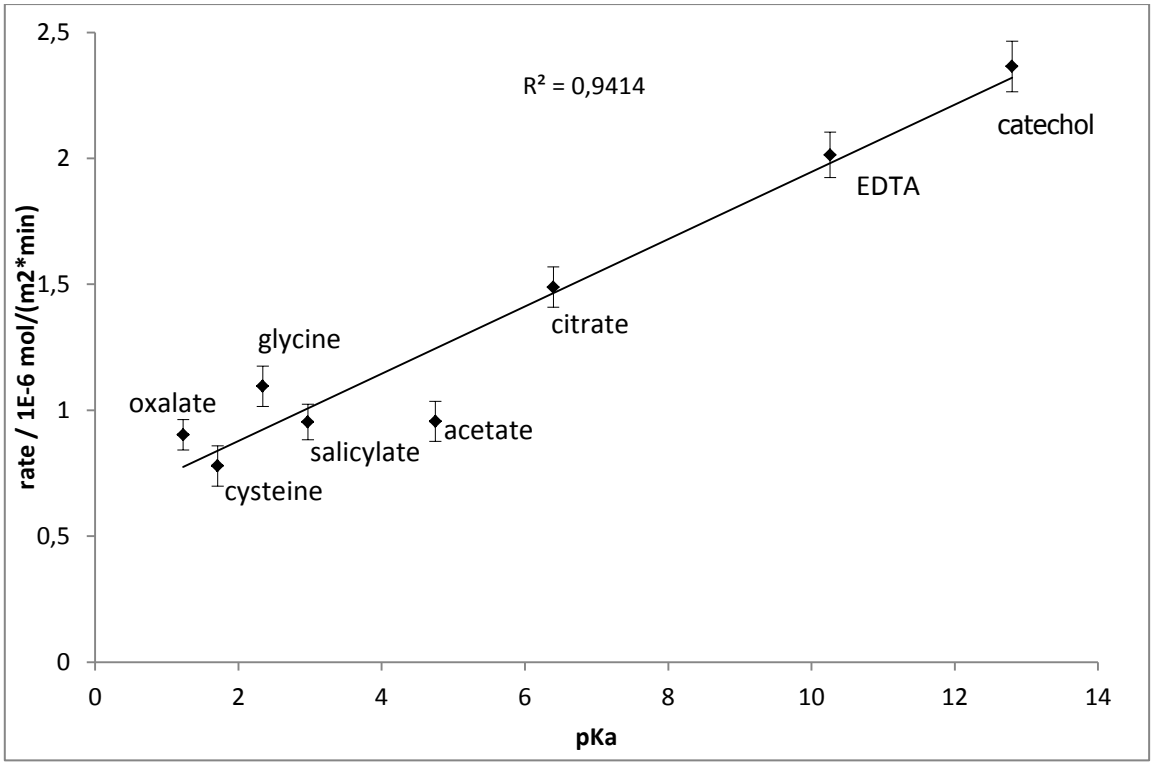

Fig. IV.11 Correlation between dissolution rate and pK_a at pH=8

The reason why such a correlation is not observed at a lower pH is that the proton-promoted dissolution, whose contribution to the total, measured rate, is apparently not simply additive, only makes a negligible contribution at pH=8: for six out of the eight considered ligands in this correlation, a *promoting* effect of the ligands only becomes apparent at pH≥6.

When comparing our data to the results with the same ligands available in the literature, we note that Goyne and co-workers (2006) also found that citrate had the strongest mobilising effect on chalcopyrite (more so than salicylate), although their work was carried out at a single pH (5). Oxalate and DFOB are both known to promote the dissolution of iron (hydr)oxide phases, whereas in our experiments, oxalate had little effect on stibnite and DFOB even an inhibiting one. A Table with the calculated rates is supplied in Appendix AV.

In order to recognise the geochemical implications of the observations made in this chapter, initial rates as well as the rates under steady state conditions at the surface need to be taken into account. The leaf litter extract, for instance, has an overall promotive effect at pH=8 under steady conditions, but the *initial* rate in the presence of LLE is much smaller than in the blank experiment. Whether LLE will eventually mobilise more antimony than in the blank experiment is therefore critically dependent on *the contact time* of the solution with the mineral. If this time is short, less antimony will be mobilised in the presence of LLE than in its absence. If the contact time is, however, long enough for the system to compensate for the initially inhibited rate by its larger rate under steady state conditions, then more antimony will be released in the presence of LLE than in its absence. The same reasoning must be applied to the case of citrate, at pH=4. Here, the initial rate is higher than the blank and the rate decreases until a steady state rate is reached, which is smaller than in the blank experiment. In this case, too, the ligand can either mobilise more antimony than the blank solution (if the contact time is short enough), or less (if the contact time is long enough). The only unambiguous cases are those in which both intial rate and steady state rate are either smaller than in the blank experiment, in which case less antimony is mobilised, or those in which both rates are higher than in the blank experiment, in which case more antimony will be mobilised. To complicate matters further, one and the same ligand can fulfil both conditions, depending on the pH. Catechol is an illustrative example: at pH=4, both intial and steady state rate are below the blank value, which means

that under these conditions the mobilisation will be less than in the absence of catechol, whatever the contact time. At pH=8, the reverse is true. Both rates are higher than the blank, and more antimony will be mobilised than in its absence, whatever the contact time is (at pH=6, the intial rate is higher than the blank value and the steady state rate is lower, as in the case of citrate at pH=4, so that the contact time becomes important). The behaviour of every individual ligand at the three pH values studied is summarised in Table IV.2, which can be used to predict what the overall effect of a given ligand at a given pH will be.

Ligand	pH	Initial rate vs. blank	Steady state vs. blank	Net mobilisation vs. blank
Acetate	4	<	<	<
	6	<	≈	<
	8	<	>	t-dep.
Catechol	4	<	<	<
	6	>	<	t-dep.
	8	>	>	>
Citrate	4	>	<	t-dep.
	6	>	≈	>
	8	>	>	>
Cysteine	4	<	<	<
	6	<	≈	<
	8	<	≈	<
DFOB	4	<	≈	<
	6	<	≈	<
	8	<	<	<
DFOB +citrate	4	<	>	t-dep.
	6	<	>	t-dep.
	8	<	<	<
EDTA	4	>	>	>
	6	>	>	>
	8	>	>	>
Glucose	4	<	>	t-dep.
	6	<	>	t-dep.
	8	<	>	t-dep.
Glycine	4	<	<	<
	6	≈	>	>
	8	<	>	t-dep.
LLE	4	<	≈	<
	6	<	≈	<
	8	<	>	t-dep.
Oxalate	4	>	≈	>
	6	>	≈	>
	8	>	>	>
Salicylate	4	<	>	t-dep.
	6	<	>	t-dep.
	8	<	>	t-dep.

Table IV.2 Mobilisation behaviour of organic ligands with respect to blank solutions. '≈' means 'not significantly different from' and 't-dep.' means that the mobilisation effect is dependent on the contact time

IV.4 Acknowledgements

Dr Jörg Luster, of the Swiss Federal Institute for Forest, Snow and Landscape Research, is acknowledged for providing a reference sample of Chestnut leaf litter. Dr Constantin Hoch, of the Max Planck Institute for Solid State Research, Stuttgart, recorded the X-ray diffractogram of stibnite.

IV.5. References for chapter IV

Anderegg G., L'Eplattenier F. and Schwarzenbach G. (1963) Hydroxamatkomplexe II. Die Anwendung der pH Methode. *Helv. Chim. Acta* **46**, 1400-1408

Anderegg G. and Malik S. (1970) Die Komplexbildungstendenz des dreiwertigen Antimons in wässriger Lösung. *Helv. Chim. Acta* **53**, 577-600

Banwart S., Davies S. and Stumm, W. (1989) The role of oxalate in accelerating the reductive dissolution of hematite (α-Fe_2O_3) by ascorbate. *Colloids and Surfaces* **39**, 303-309

Bi Y., Hesterberg D.L. and Duckworth O.W. (2010) Siderophore-promoted dissolution of cobalt from hydroxide minerals. *Geochim. Cosmochim. Acta* **74**, 2915-2925

Biber M.V, Dos Santos Afonso M. and Stumm W. (1986) The coordination chemistry of weathering: IV. Inhibition of the dissolution of oxide minerals. *Geochim. Cosmochim. Acta* **58**, 1999-2010

Blaser P., Sposito G. and Holtzclaw K.M. (1984) Composition and Acidic Functional Group Chemistry of an Aqeous Chestnut Leaf Litter Extract. *Soil Sci. Soc. Am. J.* **48**, 278-283

Cheah S.F., Kraemer S.M., Cervini-Silva J., Sposito G. (2003) Steady-state dissolution kinetics of goethite in the presence of desferrioxamine B and oxalate ligands: implications for the microbial acquisition of iron. *Chem. Geol.* **198**, 63-75

Cornejo-Garrida H., Fernandez-Lomelin P., Guzman J. and Cervini-Silva J. (2008) Dissolution of arsenopyrite (FeAsS) and galena (PbS) in the presence of desferrioxamine-B at pH 5. *Geochim. Cosmochim. Acta* **72**, 2754-2766

Davis A.P., Hsieh Y.H. and Huang C.P. (1995) Photo-oxidative dissolution of CdS(s): The effect of complexing agents. *Chemosphere* **31**, 3093-3104

Duckworth O.W., Bargar J.R., Jarzecki A.A., Oyerinde O., Spiro T.G. and Sposito G. (2009a) The exceptionally stable cobalt(III)-desferrioxamine B complex. *Marine Chemistry* **113**, 114-122

Duckworth O.W., Bargar J.R. and Sposito G. (2009b) Coupled biogeochemical cycling of iron and manganese as mediated by microbial siderophores. *Biometals* **22**, 605-613

Duckworth O.W. and Sposito G.(2005a) Siderophore-Manganese(III) Interactions. I. Air-Oxidation of Manganese(II) Promoted by Desferrioxamine B. *Environ. Sci. Technol.* **39**, 6037-6044

Duckworth O. W. and Sposito G. (2005b) Siderophore-Manganese(III) Interactions. II. Manganite Dissolution Promoted by Desferrioxamine B. *Environ. Sci. Technol.* **39**, 6045-6051

Filella M. and May P.M. (2005) Critical appraisal of available thermodynamic data for the complexation of antimony(III) and antimony(V) by low molecular mass organic ligands. *J. Environ. Monit.* **7**, 1226-1237

Furrer G. and Stumm W. (1986) The coordination chemistry of weathering: I. Dissolution kinetics of δ-Al_2O_3 and BeO. *Geochim. Cosmochim. Acta* **50**, 1847-1860

Good N.E., Winget G.D., Winter W., Connolly T.N., Izawa S. and Singh R.M.M. (1966) Hydrogen Ion Buffers for Biological Research. *Biochemistry* **5**, 467-477

Goyne K.W., Brantley S.L. and Chorover J. (2006) Effects of organic acids and dissolved oxygen on apatite and chalcopyrite dissolution: Implications for using elements as organomarkers and oxymarkers. *Chem. Geol.* **234**, 28-45

Healy T.W. and Fuerstenau D.W. (2007) The isoelectric point/point-of zero-charge of interfaces formed by aqueous solutions and nonpolar solids, liquids and gases. *J. Colloid Interface Sci.* **309**, 183-188

Hernlem B.J., Vane L.M. and Sayles G.D. (1996) Stability constants for the complexes of the siderophore desferrioxamine B with selected heavy metal cations. *Inorganica Chimica Acta* **244**, 179-184

Hersman L., Lloyd T. and Sposito G. (1995) Siderophore-promoted dissolution of hematite. *Geochim. Cosmochim. Acta* **59**, 3327-3330

Klüfers P. and Mayer P. (1997) Polyol-Metall Komplexe. 27[1] Bis-diolato-antimonate(III) mit Guanosin als Diol. *Z. anorg. Allg. Chemie* **623**, 1496-1498

Lasaga A.C. (1984) Chemical Kinetics of Water-Rock Interactions. *J. Geophys. Res.* **89(B6)**, 4009-4025

Ludwig C., Casey W.H. and Rock P.A. (1995) Prediction of ligand-promoted dissolution rates from the reactivities of aqueous complexes. *Nature* **375**, 44-47

Ma J.F, Kusano G., Kimura S. and Nomoto, K. (1993) Specific recognition of mugineic acid-ferric complex by barley roots. *Phytochemistry* **34**, 599-603

Müller S.I., Valdebenito M. and Hantke K. (2009) Salmochelin, the long-overlooked catecholate siderophore of *Salmonella*. *Biometals* **22**, 691-695

Pena J., Duckworth O.W., Bargar J.R. and Sposito G. (2007) Dissolution of hausmannite (Mn_3O_4) in the presence of the trihydroxamate siderophore desferrioxamine B. *Geochim. Cosmochim. Acta* **71**, 5661-5671

Simanova A.A., Persson P. and Loring J.S. (2010) Evidence for ligand hydrolysis and Fe(III) reduction in the dissolution of goethite by desferrioxamine-B. *Geochim. Cosmochim. Acta* **74,** 6706-6720

Sposito G. (2004) *The Surface Chemistry of Natural Particles*. Oxford University Press, Oxford/New York.

Sposito (2008) *The Chemistry of Soils.* Oxford University Press, Oxford/New York.

Stumm W. and Wollast R. (1990) Coordination chemistry of weathering: Kinetics of the surface-controlled dissolution of oxide minerals. *Reviews of Geophysics* **28**, 53-69

Smith M.J., Shoolery J.N., Schwyn B., Holden I. and Neilands J.B. (1985) Rhizobactin, a structurally novel siderophore from *Rhizobium meliloti*. *J. Am. Chem. Soc.* **107**, 1739-1743

Tella M. and Pokrovski G.S. (2009) Antimony(III) complexing with O-bearing organic ligands in aqeous solution: An X-ray absorption fine structure spectroscopy and solubility study. *Geochim. Cosmochim. Acta* **73**, 268-290

Chapter V

Experimental Study of the Kinetics of Proton-Promoted Dissolution of the Secondary Antimony Minerals Stibiconite, Senarmontite and Valentinite under Environmentally Relevant Conditions

Abstract. Batch reactor experiments were carried out in order to derive rate laws for the proton promoted dissolution of the main natural antimony oxide phases, namely stibiconite (idealized composition $SbSb_2O_6OH$), senarmontite (cubic Sb_2O_3) and (metastable) valentinite (orthorhombic Sb_2O_3) over the range $2 \leq pH \leq 11$, under standard conditions and ionic strength $I=0.01$ mol l^{-1}. The rates of antimony release by stibiconite were $r=(1.5\pm0.2)\times10^{-9}$ $[H^+]^{0.12\pm0.02}$ mol m^{-2} s^{-1} for $2.00 \leq pH \leq 4.74$ and $r=(2.31\pm0.02)\times10^{-10}$ $[H^+]^{-0.049\pm0.004}$ mol m^{-2} s^{-1} for $4.74 \leq pH \leq 10.54$. The rates of dissolution of senarmontite were $r=(4.6\pm2.6)\times10^{-7}$ $[H^+]^{0.54\pm0.05}$ mol m^{-2} s^{-1} for $2.00 \leq pH \leq 6.93$ and $r=(1.7\pm0.3)\times10^{-14}$ $[H^+]^{-0.52\pm0.07}$ mol m^{-2} s^{-1} for $6.93 \leq pH \leq 10.83$. The rates of dissolution of valentinite were $r=(3.7\pm0.9)\times10^{-7}$ $[H^+]^{0.32\pm0.04}$ mol m^{-2} s^{-1} for $1.97 \leq pH \leq 4.05$. Above pH=4.58, valentinite was found to dissolve at a constant rate of $r=(3.47\pm0.15)\times10^{-8}$ mol m^{-2} s^{-1}. Activation energies were determined at selected pH values in the acidic and basic domain, over the temperature range 25-50°C. The values for stibiconite are -36.4±1.6 kJ mol^{-1} (pH=2.00) and 58±18 kJ mol^{-1} (pH=8.7). For senarmontite, we found 36±5 kJ mol^{-1} (pH=3.0) and 68±6 kJ mol^{-1} (pH=9.9) and for valentinite 53.5±3.6 kJ mol^{-1} (pH=3.0) and 9.1±2.7 kJ mol^{-1} (pH=9.9). These activation energies are interpreted in the text. The solubility of stibiconite at 25°C in the pH domain from 2 to 10 was determined; solubilites decrease from 452.0 µg l^{-1} (as Sb) at pH=2.00 to 153.2 µg l^{-1} at pH=7.55 and increase again in the basic region, up to 176.6 µg l^{-1} at pH=9.92. A graphical synopsis of all the kinetic results, including those of stibnite (Sb_2S_3) from earlier work, is presented. This allows an easy comparison between the dissolution rates of stibnite and the

minerals examined in the present work. The geochemical implications for the weathering of antimony oxide minerals and stibnite, with particular reference to the mobilization of antimony in the context of an abandoned antimony mine (Goesdorf, Luxembourg), are discussed.

V.1. Introduction

Antimony is a toxic trace element, occurring naturally in the Earth's crust to an average of 0.2 ppm. The increased use of its compounds, e.g. as flame retardants in textiles and plastics, as catalysts in the manufacture of PET, in automobile brake pads and in numerous other industrial applications, has led to a growing dispersion of antimony in the natural environment, so that antimony is the most enriched trace element in urban aerosols today (Furuta et al., 2005), and the quantification of antimony in peat bogs (Shotyk et al., 2004) has demonstrated that antimony emissions have grown since Roman times. While emissions of lead have fortunately declined for the last decades, those of antimony still increase, as has been shown by analysis of snow and ice samples from the high Arctic (Krachler et al., 2005). The adverse effects of antimony on human health have been reviewed in a number of papers (Gebel, 1997 and 1999). The growing concern with antimony pollution is exemplified by the classification of antimony as a priority pollutant by the USEPA and the EU (United States Environmental Protection Agency, 1979 ; Council of the European

Communities, 1976). Important aspects of the geochemistry of antimony have been reviewed by Filella et al. (2002a and 2002b)

The most important natural source of antimony is the ore mineral stibnite (Sb_2S_3), which, in the supergene environment, is associated with its principal weathering products senarmontite (cubic Sb_2O_3) , valentinite (orthorhombic Sb_2O_3), and stibiconite (Sb_3O_6OH), along with (minor) sulfo-salts and sulfates such as kermesite (Sb_2S_2O) , coquandite ($Sb_6O_8SO_4 \cdot H_2O$), klebelsbergite ($Sb_4O_4(OH)_2SO_4$) and peretaite ($CaSb_4O_4(OH)_2(SO_4)_2 \cdot 2\ H_2O$) (Filella et al., 2009). The kinetics of the mobilization of antimony from stibnite has been studied in detail by Biver and Shotyk (2011a and 2011b). With regard to the main, naturally occurring antimony oxide phases, however, only thermodynamic solubility data are available on senarmontite and valentinite (Zotov et al., 2003), while nothing is known on their kinetics of dissolution. Yet the dissolution of these phases is thought to contribute significantly to the antimony pollution in waters draining zones with known stibnite mineralisation (Filella et al., 2009). In the abandoned antimony mine in Goesdorf (Luxembourg), Filella and co-workers found that valentinite and senarmontite were dominant among the secondary minerals, with relative occurrences of 70% and 15%, respectively, whereas sulfates accounted for 12% and other minor phases for 3%. Szakall and co-workers (2000) conducted an extensive survey of all the known occurrences of stibnite and fahlore in Hungary (a total of 22 sites), and they noted that 'stibiconite proved to be ubiquitous', whereas senarmontite and valentinite were very rare in the Hungarian ore deposits. The purpose of the present paper,

therefore, is the kinetic study of proton-promoted dissolution of those secondary antimony oxides that appear to be the most important, i.e. stibiconite, senarmontite and valentinite. Our data also allow the determination of the solubility of stibiconite, since in the batch experiments described in detail below, equilibrium was reached at the end.

Stibiconite had been known to mineralogists, a long time before its structure was elucidated by Dihlström and Westgren (1937), as 'antimony ochre'. There was some controversy over the determination of its structure, further complicated by the fact that natural samples of 'antimony ochres' can broadly vary in their elemental composition and in the dimensions of their unit cell. Natural samples are often earthy, poorly crystalline materials, admixed with foreign matter, which complicates their crystallographic characterisation (Vitaliano and Mason, 1952). These authors analysed 33 samples from different locations and found antimony contents ranging from 52.6 to 76.9% and combined water ranging from 1.63 to 9.20%. A frequent impurity was calcium (up to 10%). Valentinite, revealed by extra lines in the diffractograms, was present in extremely small grains, that could not be detected optically, in amounts up to 25%. The lattice parameter was found to vary from 10.262 to 10.282 Å. Their structural and chemical data suggest that homogeneous material of antimony ochre is best interpreted in terms of the formula $(Sb^{III},Ca)_ySb^{V}_{2-x}(O,OH,H_2O)_{6-7}$. Stevens and co-workers proposed an alternative formula, based on their Mössbauer studies of 5 different stibiconite samples (Stevens et al., 1993). Whether their formula is to be preferred, is, however, very debatable,

because the ratio of the Sb(III) and Sb(V) Mössbauer peaks does not necessarily reflect the ratio of the amounts of Sb in both oxidation states, owing to the differing Lamb-Mössbauer factors of both nuclei. Dihlström and Westgren's (1937) structure determination was carried out on synthetic material with the composition $Sb^{III}Sb^{V}_2O_6(OH)$, a formula often quoted as the 'ideal' composition of stibiconite. Its structure is of the pyrochlore type. It can be described as face-centred cubic with 8 $SbSb_2O_6(OH)$ formula units per unit cell.

Antimony trioxide, Sb_2O_3, naturally occurs in two polymorphs, one cubic (senarmontite), and the other orthorhombic (valentinite), whose structures were refined by Svensson (1974; 1975). Senarmontite is the stable phase up to 570°C, above which temperature valentinite is stable. Valentinite is, however, metastable and can actually be prepared below 570°C. The standard Gibbs free enthalpy of formation of senarmontite is -151.4±0.6 kJ mol^{-1}, that of valentinite is -149.6±0.3 kJ mol^{-1} (Zotov et al., 2003).

V.2. Materials and Methods

All chemicals were analytical reagent grade or better.

V.2.1 Stibiconite

A large specimen (ca. 117 g) of stibiconite (a pseudomorph after stibnite) from the Catorce mine, state of San Luis Potosi, Mexico, was used. The specimen was broken with a steel hammer, crushed in a percussion mortar, and ground to powder in an agate mortar. The powder was sieved and the fraction

between 0.122-0.263 mm was retained for the experiments. Total Sb determined by ICP-OES (after dissolution in boiling conc. sulfuric acid) was 64.97 ± 0.23 %. The main impurities were Ca (1.4%) and Mg (0.14%). X-ray diffraction revealed the expected pyrochlore structure, with a refined lattice parameter of 10.2752 Å. This is in excellent agreement with the data of Vitaliano and Mason (1952), who give a lattice parameter of 10.275 Å for material containing 65.4% Sb. There was evidence for small amounts of a second phase, forming extremely small cristallites within the stibiconite matrix. This was most probably valentinite, which is frequently found embedded in natural stibiconite. Sb(III) was determined by redox titration with standard potassium permanganate solution (Konopik et al., 1952) and found to account for 36.77% (25.46% in pure Sb_3O_6OH). Its specific surface area, determined according to the BET method, was 0.2350 ± 0.0140 m^2g^{-1}. Electron microscopy revealed the absence of individual crystals from the material.

V.2.2 Senarmontite and valentinite

These were prepared according to literature procedures, as no natural samples of sufficient size could be found. Senarmontite was prepared by titration of a solution of potassium antimonyl tartrate (tartar emetic) by sodium hydroxide (Abdullah et al., 2008). Briefly, 500 ml of a 0.1 molar (with respect to antimony) solution of potassium antimonyl tartrate was placed on a magnetic stirrer and an equal volume of 0.1 molar sodium hydroxide was added dropwise from a buret. After about 2/3 of the base had been added, the solution became opalescent and senarmontite began to precipitate. The precipitate was washed three times by

decantation, filtered, and dried for 6 h at 100°C. The yield of the synthesis was 80%. The product was assayed by titration with potassium permanganate and it was found to be >98% pure. The BET surface area was 0.8433 ± 0.0055 m^2g^{-1}.

Electron micrographs show that the sample consists of octahedral crystals that are several μm long. (Fig. V.1)

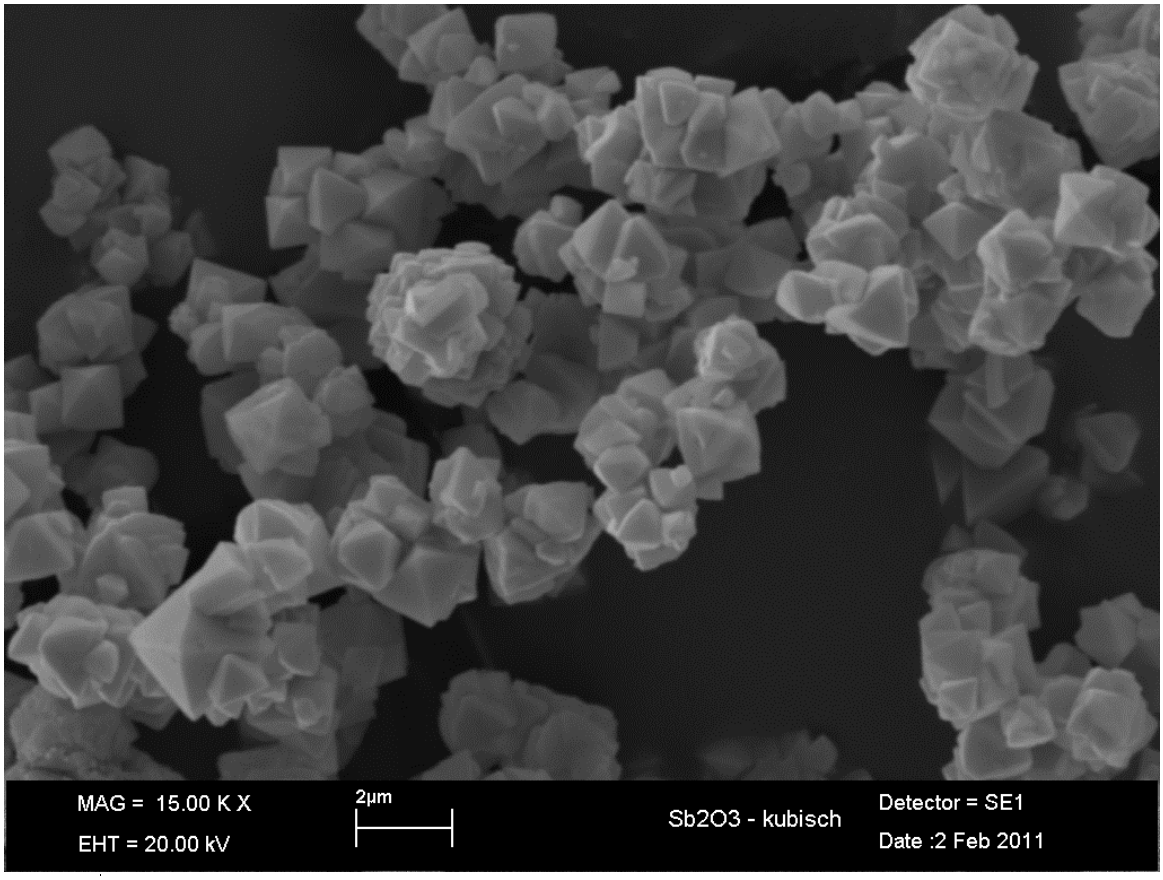

Fig. V.1 Octahedral senarmontite crystals (synthetic).

Valentinite was prepared by precipitation of a solution of antimony trichloride with boiling sodium carbonate solution (Debray, 1866). 217 g of sodium carbonate were dissolved in approx. 1 l of distilled water and the solution was brought to boiling. 150 ml of distilled water were added to 15.7 g of antimony trichloride in a separate flask. A dense, white precipitate of antimony oxychloride formed. Fuming hydrochloric acid was added to the stirred

suspension until the precipitate redissolved (ca. 40 g acid needed). This solution was also heated to boiling, and added dropwise to the boiling sodium carbonate solution. The precipitate of valentinite was left to settle and washed three times by decantation. The last portion of water was exempt of chloride and carbonate (silver nitrate test). The precipitate was filtered and dried for 6 h at 100°C. The yield of the synthesis was 89%. Assay by redox titration showed the product to be 99-100% pure and it had a BET surface area of 0.3250 ± 0.0082 m^2g^{-1}. In the electron micrographs (Fig.V.2), needle-shaped crystals up to 40 µm long and 2-5 µm wide can be seen. Very rare octahedra are also visible (Fig.V.3), which show that some senarmontite has also formed in the course of the synthesis.

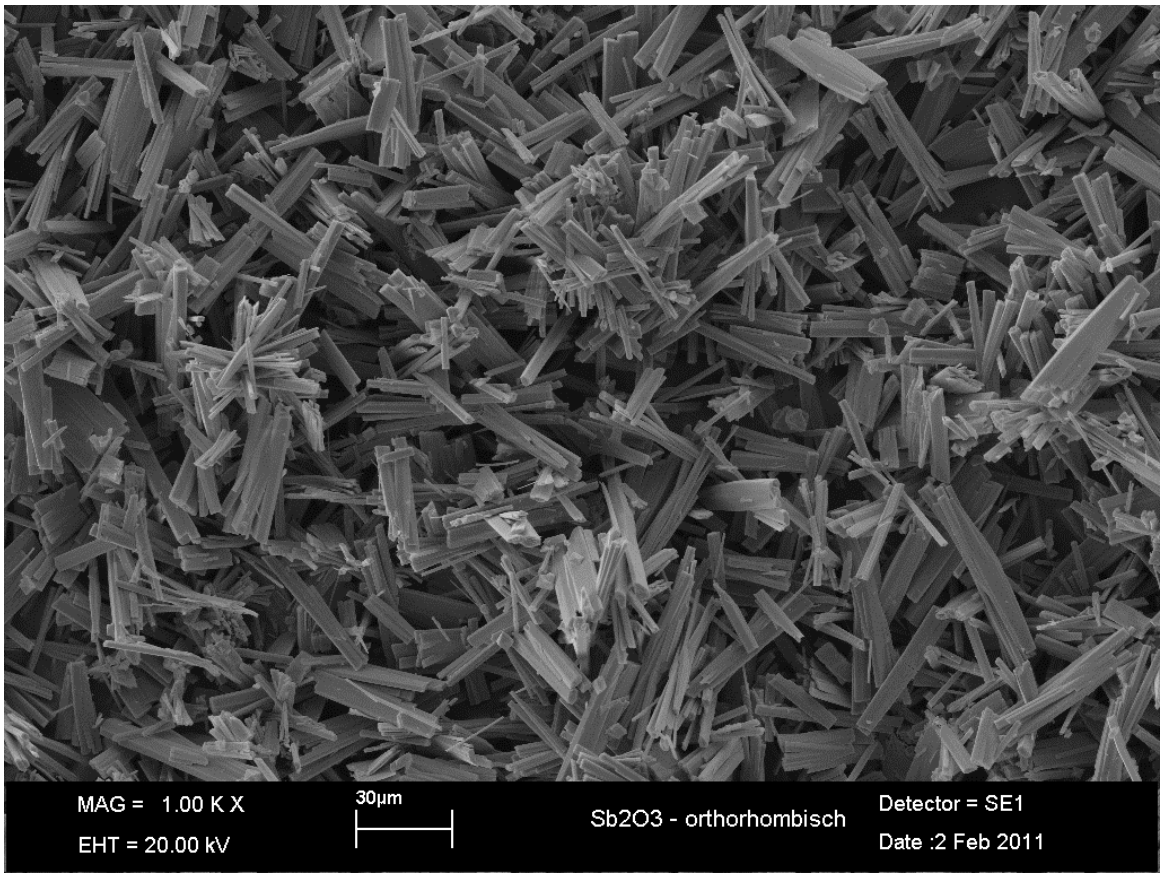

Fig.V.2 Needle-shaped crystals of valentinite (synthetic)

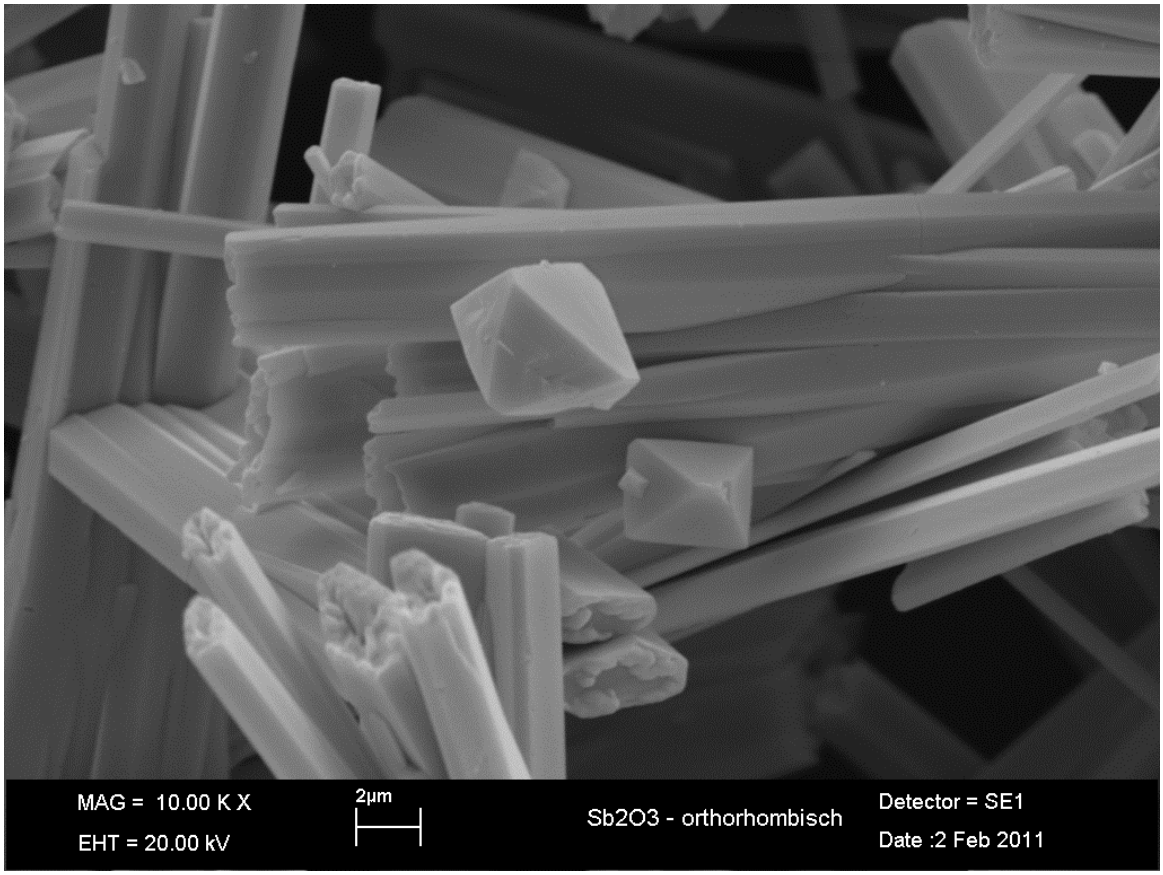

Fig. V.3 Senarmontite contamination on valentinite needles.

V.2.3 Analytical methods and instrumentation

Antimony determinations were carried out on a Spectroflame Modula ICP-OES spectrometer (Spectro Analytical Instruments, Germany) calibrated with a commercial standard (Alfa-Aesar, Germany). A detection limit of 5 µg l^{-1} was achieved. BET surface areas were measured by multiple-point N_2 adsorption with a Gemini VII 2390 Instrument (Micromeritics, Germany). A Model 632 pH meter (Metrohm, Switzerland) was used, and calibrated with commercial, NIST-traceable buffers (Hanna, Romania).

V.2.4 Batch experiments

Rates of dissolution were measured in a batch reactor. This consisted of a conventional, 1 L two-necked, round-bottom flask immersed in a constant temperature water bath set to 25°C. Through the central neck, a ground glass stopper with a plastic axle carrying a magnetic stirrer bar was fitted, so that the stirrer did not touch the bottom of the flask, in order to avoid grinding the solid. The second neck remained open to the atmosphere and was used as a sampling port. The masses of mineral (accurately weighed) used in each experiment were as follows : ca. 100 mg of stibiconite, ca. 50 mg of valentinite and ca. 50 mg of senarmontite, except at pH=6.01, pH=6.93 and pH=8.74, where ca. 500 mg senarmontite were used because the rate of dissolution was so slow that 50 mg did not suffice to measure it. Acidic leaching solutions consisted of aqueous perchloric acid, with the ionic strength adjusted to 0.01 mol l^{-1} by addition of sodium perchlorate. The basic solutions were mixtures of sodium carbonate and sodium bicarbonate in varying proportions. The amounts of both salts were chosen so as to give a total ionic strength of 0.01 mol l^{-1}. Solutions with a pH between 6 and 7 were buffered by the addition of 1 mmol l^{-1} MES ((2-(N-Morpholino)-ethanesulfonic acid, pKa=6.2), the pH was adjusted by addition of sodium hydroxide solution and the ionic strength adjusted to 0.01 mol l^{-1} with sodium perchlorate. In order to determine activation energies, experiments were repeated at higher temperatures (32°C, 40°C and 50°C) at selected pH values. The solutions and mineral samples were introduced into the batch reactor, stirred continuously so that all the solid remained in suspension, and samples were

taken at regular intervals by means of disposable PP syringes (10 ml) (Brown, Germany), fitted with 0.45 µm hydrophilic CME filters (Millipore) and a short length of silicone tubing. Experiments ran for 12 h, with sampling every hour, in the case of stibiconite. Senarmontite and valentinite were more reactive, so that these experiments ran for 4 h, with sampling every 20 min. At the end of the experiments, the concentrations of Sb in the samples were measured using ICP-OES. Of each sample, 4 replicates were measured.

At the beginning of the experiments, the rate of reaction could be seen to follow a parabolic rate law, which became linear after a while, typically after 3-4 h in the stibiconite experiments, after 140 min. at the latest in the senarmontite experiments and somewhat faster in the valentinite experiments : after 80 min. at the latest. Straight lines were fitted to the linear portions of the graphs in order to determine the rates of dissolution when steady state conditions prevailed at the reacting mineral surface. As an example, two complete curves showing the mass of released antimony by dissolving valentinite as a function of time are reproduced in Fig. V.4.

It can be seen that ultimately, the curves form a plateau corresponding to the dissolution equilibrium. The origin of the parabolic and zero-order rate laws in mineral dissolution kinetics is explained by Lasaga (1984) and a detailed discussion given by Stumm and Wollast (1990). Proton-promoted dissolution of oxides and silicates is discussed by Sposito (2004, and references therein).

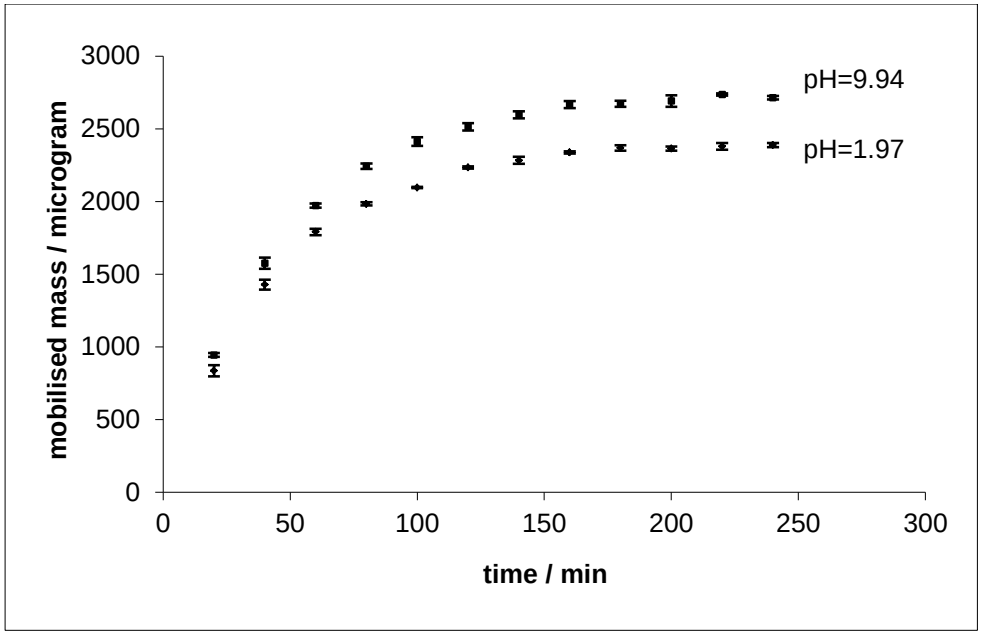

Fig.V.4 Mobilized mass of valentinite as a function of time. Parabolic and zero-order kinetics.

V.3 Results and Discussion

V.3.1 Stibiconite

For the experiments at constant temperature (25°C) and varying pH, the mobilised Sb mass is plotted as a function of time. The linear portions, corresponding to steady state dissolution at the mineral surface are shown in Fig.V.5 (the correlation coefficients R^2 range from 0.9612 to 0.9911).

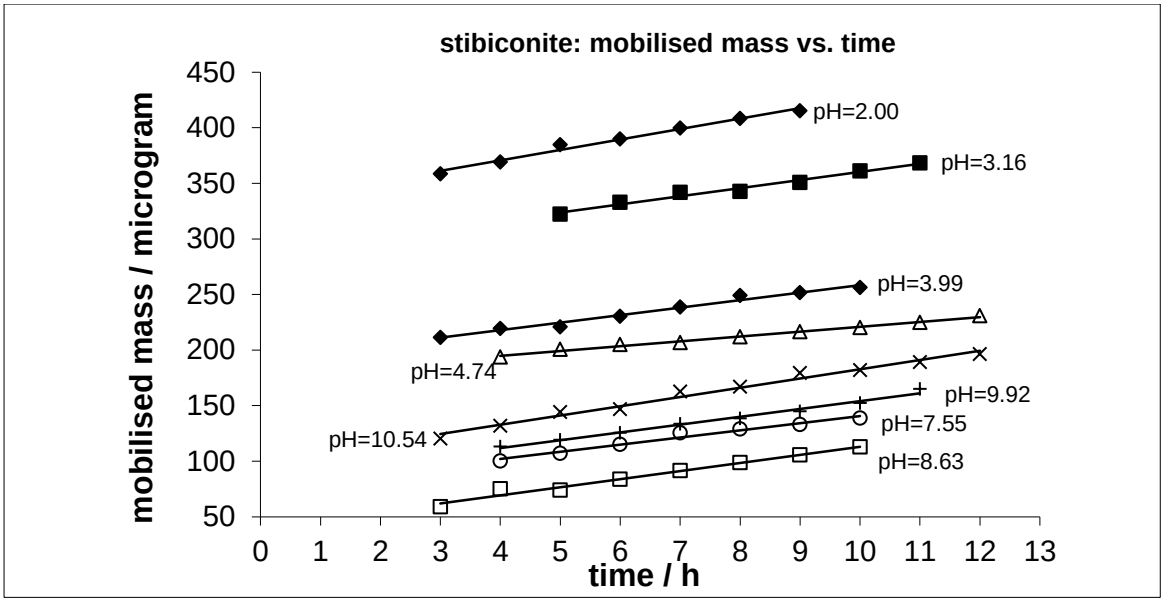

Fig.V.5 mobilized mass as a function of time, stibiconite. The line for pH=6.75 is not shown as it coincides with that for pH=4.74. Error bars omitted for clarity.

From the slopes of these lines, the rates at which the Sb concentration in solution increases may be calculated. Note that we do not convert these into rates of dissolution of the mineral, since the material that was used in the experiments deviates from the ideal stoichiometry of stibiconite. In order to model the rates by an equation of the form

$$r = \frac{d[Sb]}{dt} = k[H^+]^{\alpha}$$

the logarithm of the rates, expressed in mol m^{-2} s^{-1}, was plotted against the logarithm of the hydrogen ion concentrations (Fig.V.6). Hydrogen ion concentrations were obtained from the measured activities by the modified Debye-Hückel formula. From the slopes in Fig.V.6, k and α were obtained as $k=(1.5\pm0.2)\times10^{-9}$ and $\alpha=0.12\pm0,02$ for $2.00\leq pH\leq4.74$ ($R^2=0.9509$) and $k=(2.31\pm0.02)\times10^{-10}$ and $\alpha=-0.049\pm0.004$ for $4.74\leq pH\leq10.54$ ($R^2=0.9720$) .

The maximum and minimum rates were observed at pH=2.00, r=(8.5±0.5)×10^{-10} mol m^{-2} s^{-1} and at pH=4.74, r=(3.9±0.1)×10^{-10} mol m^{-2} s^{-1}, respectively.

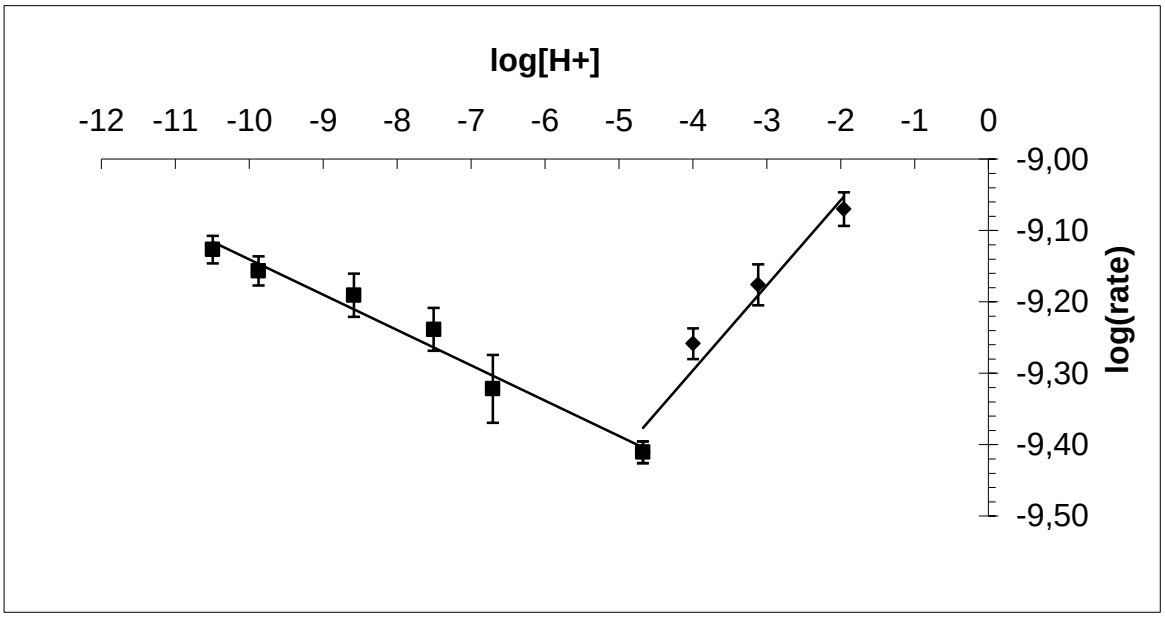

Fig. V.6 : logarithm of rate vs logarithm of H^+ concentration, stibiconite.

The temperature dependence of the rate was investigated in acid solution at pH=2 and in basic solution at pH=8.7 for temperatures ranging from 25°C to 50°C, and the results plotted in Fig.V.7 (natural logarithm of the rate constant vs inverse absolute temperature). The activation energies obtained from the slopes are -36.4±1.6 kJ mol^{-1} at pH=2 (R^2=0.9962) and 58±18 kJ mol^{-1} at pH=8.7 (R^2=0.9140) . The value in basic solution indicates that dissolution is a surface-controlled process (Lasaga, 1984 ; Berner, 1978). The negative activation

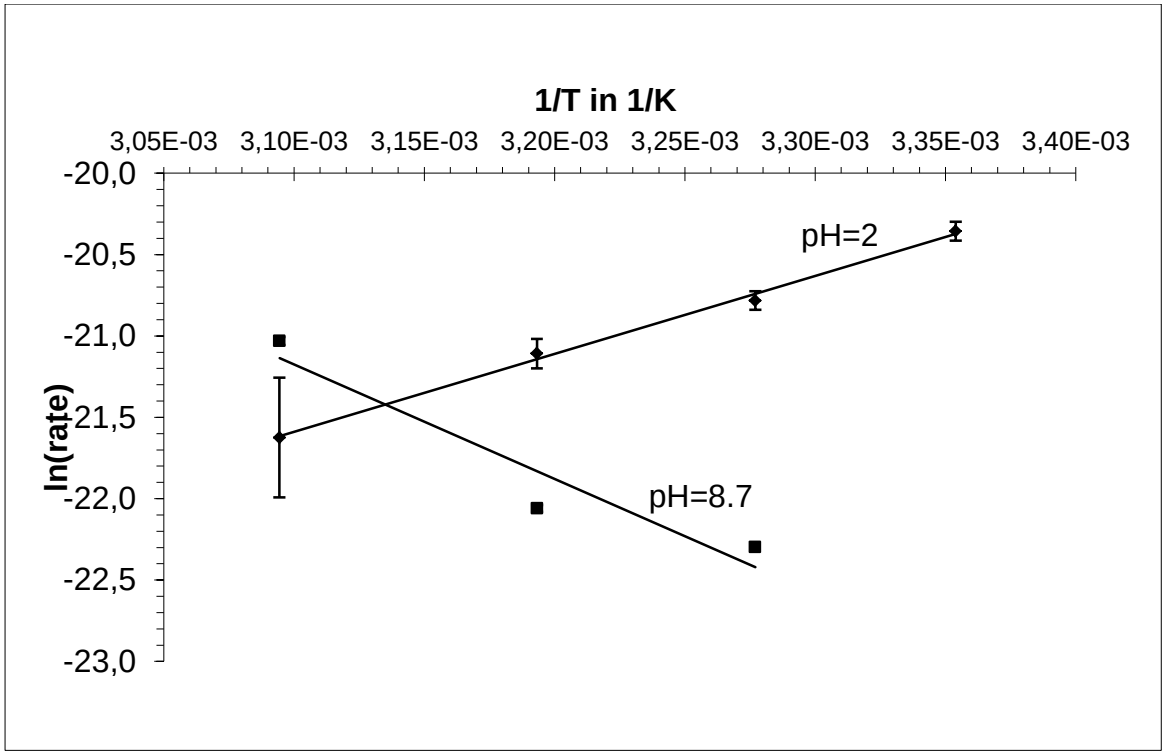

Fig.V.7 Arrhenius plot (ln(k) vs 1/T) for stibiconite in acidic and in basic solution.

energy in acid solution is a much rarer observation. Rimstidt found a negative activation energy (-6 kJ mol^{-1}) for the oxidative dissolution of arsenopyrite in the presence of ferric ion (Rimstidt et al., 1994). A negative activation energy could result from the passivation of the mineral surface by surface precipitation of a reaction product. However, it is not obvious which phase could precipitate at the surface in our present case. Rimstidt and co-workers suggest another possible reason, in that the dissolution is governed by 'a sequence of reactions that contains a branch where one reaction path is dominant at all temperatures, while the less vigorous side reaction that produces an inhibitor of the rate-limiting step becomes increasingly important at higher temperatures.' Very recently, a negative activation energy was reported in the case of dissolving magnesite under neutral to alkaline conditions (Saldi et al., 2010). The authors successfully

explain their findings by a decrease in reactive (protonated) surface sites with increasing temperature. The possible occurrence of negative activation energies in mineral dissolution reactions was predicted by Casey and Sposito in (1992), when examples of negative activation energies in mineral dissolutions were still unknown. The activation energy is the sum of enthalpies of similar magnitude but different sign – the enthalpy of proton adsorption and a contribution that arises from long-range electrostatic interaction among charged surface groups. Specifically, the enthalpy of proton adsorption is exothermic, and can, at least in theory, outweigh the other, endothermic contribution, leading to an overall negative activation energy (Proton adsorption enthalpies range from -10 to -50 kJ mol^{-1}). This is concordant with Saldi's view, for if proton adsorption is exothermic, it will be disfavoured with increasing temperature, and the number of reactive, protonated surface sites should decrease.

In our batch experiments with stibiconite, dissolution equilibrium was attained at the end as the concentrations of dissolved antimony did not vary any more within experimental error (typically over the last two to four hours of the experiment). In table V. 1, we report the measured equilibrium concentration of antimony in solution and the dissolved mass of stibiconite, based on the empirical composition of our material rather than the idealised one.

pH	[Sb] / µg l^{-1}	[stibiconite] / µg l^{-1}	N
2.00	452.0±1.0	695.8±1.5	4
3.16	412.6±1.9	635.1±2.9	2
3.99	297.6±3.2	458.1±4.9	2
4.74	257.1±2.2	395.7±3.4	2
6.75	245.1±0.6	377.2±1.0	2
7.55	153.2±4.1	235.9±6.3	4
8.63	166.7±0.1	256.5±0.1	4
9.92	176.6±12.1	271.9±18.7	3

Table V.1 Equilibrium concentration of Sb in aqueous solution in contact with stibiconite and mass of dissolved stibiconite per liter at equilibrium (at 25°C, ionic strength I=0.01 $moll^{-1}$). Error margins reflect the 95% confidence level.

V.3.2 Senarmontite

The data for senarmontite dissolution were analysed in exactly the same way as above; a linear regime was reached after 140 min. at the latest, in most cases much earlier. The mobilised masses of antimony vs time at steady state are plotted in Fig.V.8 (correlation coefficients range from R^2=0.9556 to 0.9980) and the logarithms of the rates (expressed as mol m^{-2} s^{-1}) vs the logarithms of the hydrogen ion activities in Fig.V.9. Since the stoichiometry of the senarmontite corresponds to the theoretically required one, we may calculate actual rates of dissolution of the mineral, from the rate of appearance of Sb in the solution :

$$r = -\frac{d[Sb_2O_3]}{dt} = \frac{1}{2}\frac{d[Sb(tot,aq)]}{dt} = k[H^+]^{\alpha}$$

The maximum and minimum rates were observed at pH=2.01, r=(2.4±0.4)×10^{-8} mol m^{-2} s^{-1} and at pH=6.93, r=(9.60±0.3)×10^{-11} mol m^{-2} s^{-1}, respectively. For the pH range 2.00≤pH≤6.93, k=(4.6±2.6)×10^{-7} and α=0.54±0.05 (R^2=0.9655). For the range 6.93≤pH≤10.83, we obtain

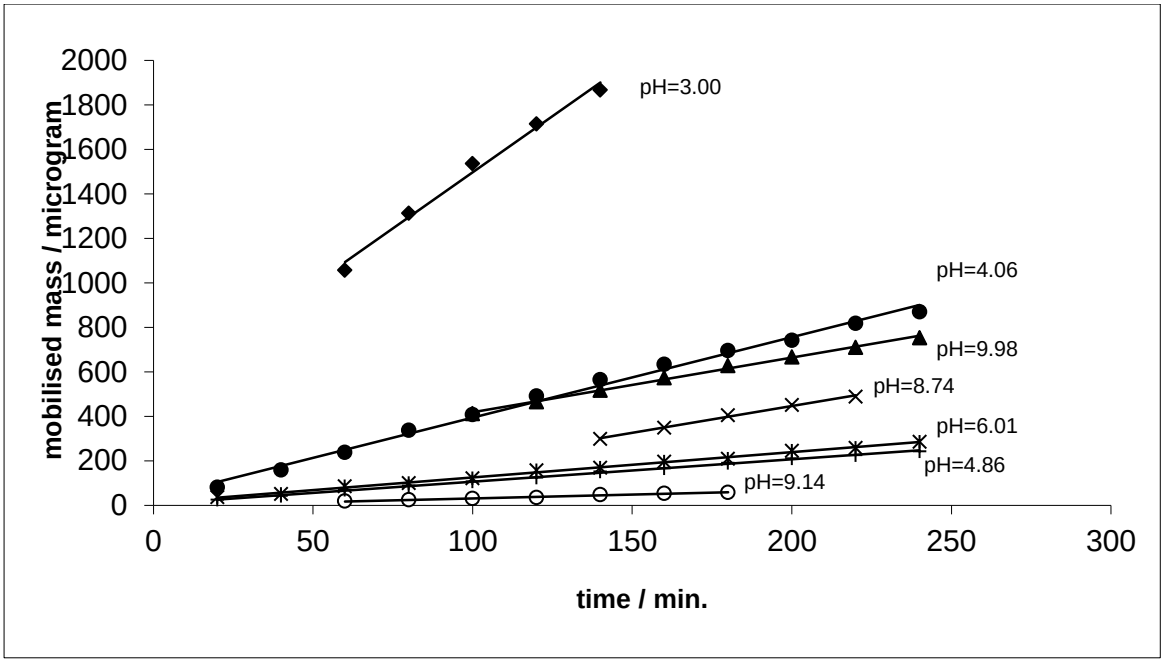

Fig.V.8 mobilized mass as a function of time, senarmontite. Error bars omitted for clarity.

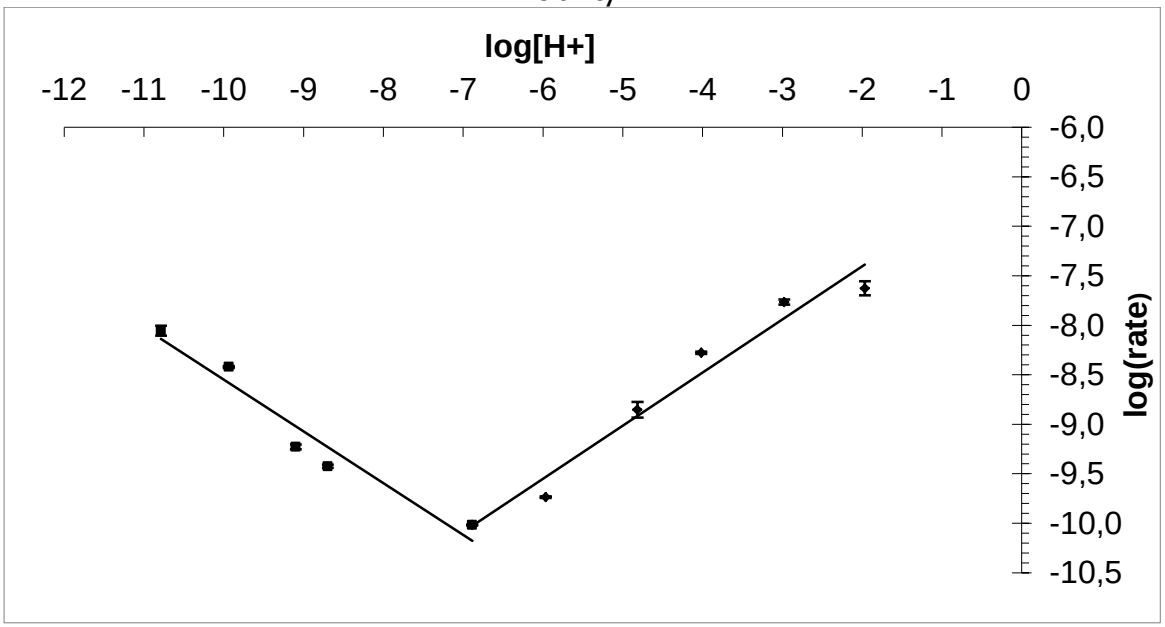

Fig. V.9 : logarithm of rate vs logarithm of H^+ concentration, senarmontite.

$k=(1.7\pm0.3)\times10^{-14}$ and $\alpha=-0.52\pm0.07$ ($R^2=0.9444$). The temperature dependence was investigated in acidic solution at pH=3.0 and in basic solution at pH=9.9. The corresponding Arrhenius plots are shown in Fig.V.10. From these, we obtain the activation energies at pH=3.0 as 36±5 kJ mol^{-1} (R^2= 0.9607) and

68±6 kJ mol^{-1} (R^2=0.9828) at pH=9.9. Both of these activation energies are in the range expected for surface-controlled dissolution reactions.

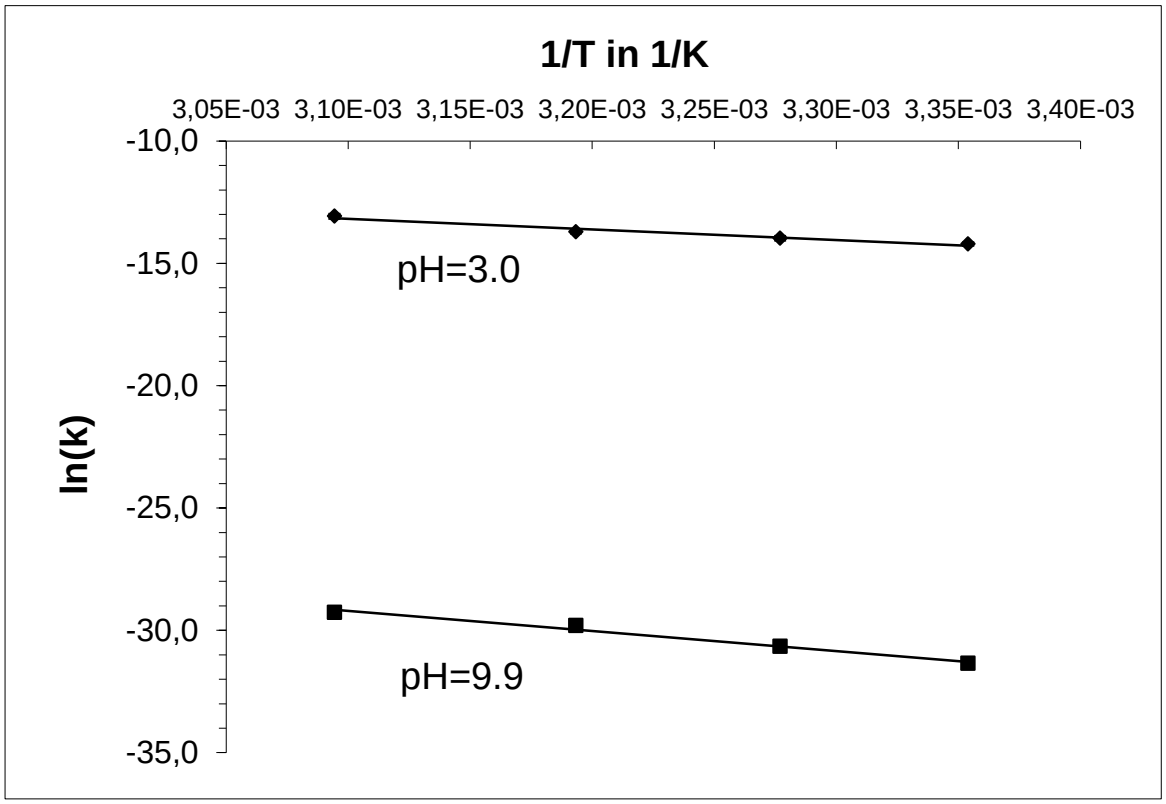

Fig.V.10 Arrhenius plot (ln(k) vs 1/T) for senarmontite in acidic and in basic solution. Error bars not visible; the relative error in ln(k) is always better than 0.7%.

V.3.3 Valentinite

The experimental protocol for valentinite was exactly the same as in the senarmontite experiments. Generally, the linear regime was observed earlier as in the case of senarmontite. Some of the data from which the steady state dissolution rates were computed are shown in Fig.V.11. Correlation coefficients were of the order of 0.98 to 0.99, except for the experiments at pH=9.94 (R^2=0.8978) and pH=10.70 (R^2=0.9155).

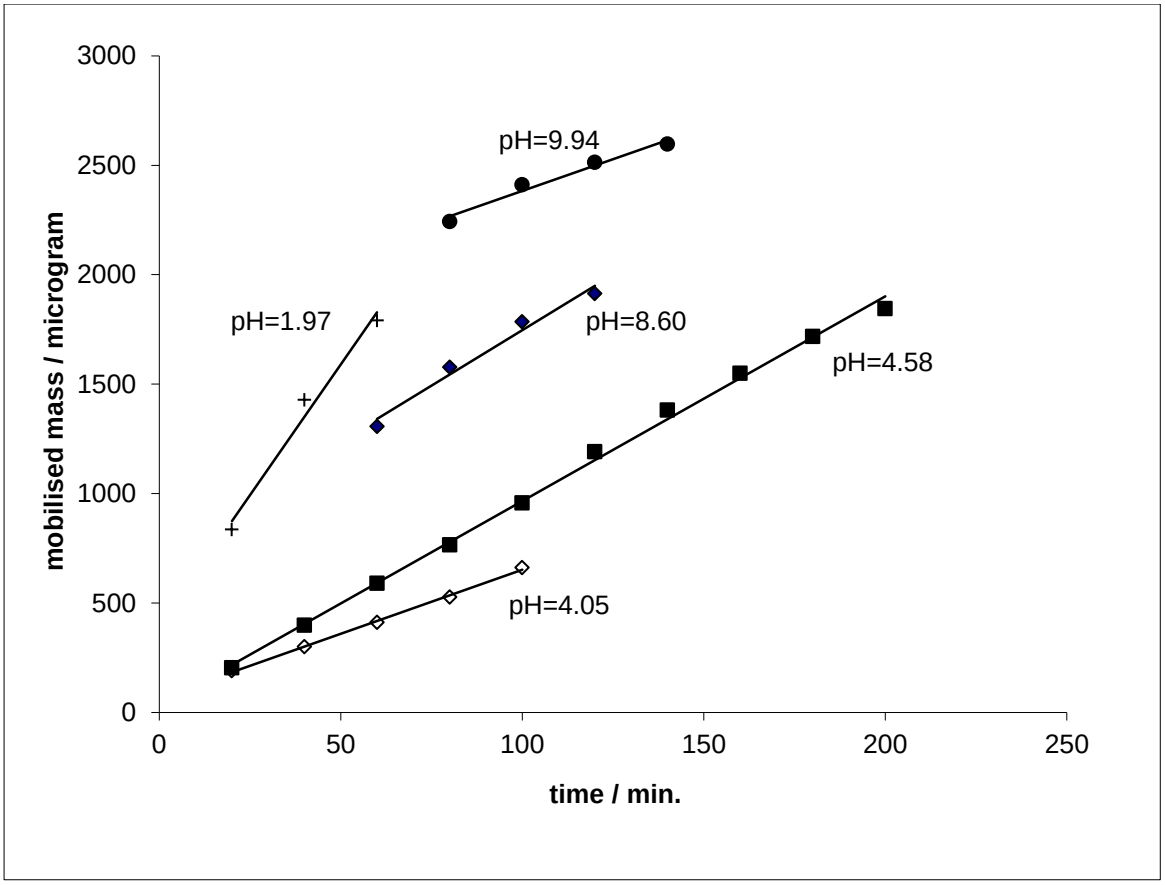

Fig.V.11 : mobilized mass as a function of time, valentinite. Error bars omitted for clarity. The curves corresponding to pH=3.00 ; 5.45 and 6.85 are not shown as they coincide with the line for pH=4.58.

In acidic solution, there is sharp increase of the dissolution rate with decreasing pH, while above pH=4.58, the rate is independent of pH to within experimental error (Fig.V.12). Note than even though a constant rate of dissolution is found above pH=4.58, the *initial* rates varied over nearly one order of magnitude, as can be seen in Fig.V.13 : at pH=4.58, the initial rate was $r_0=(3.8\pm 0.2)\times10^{-8}$ mol m^{-2} s^{-1} and this had increased to $r_0=(2.23\pm0.02)\times10^{-7}$ mol m^{-2} s^{-1} at pH=10.70. Consequently, the total mobilized amounts of antimony varied widely over this pH range, so that we are led to conclude that the equilibrium solubility of valentinite is not independent of pH.

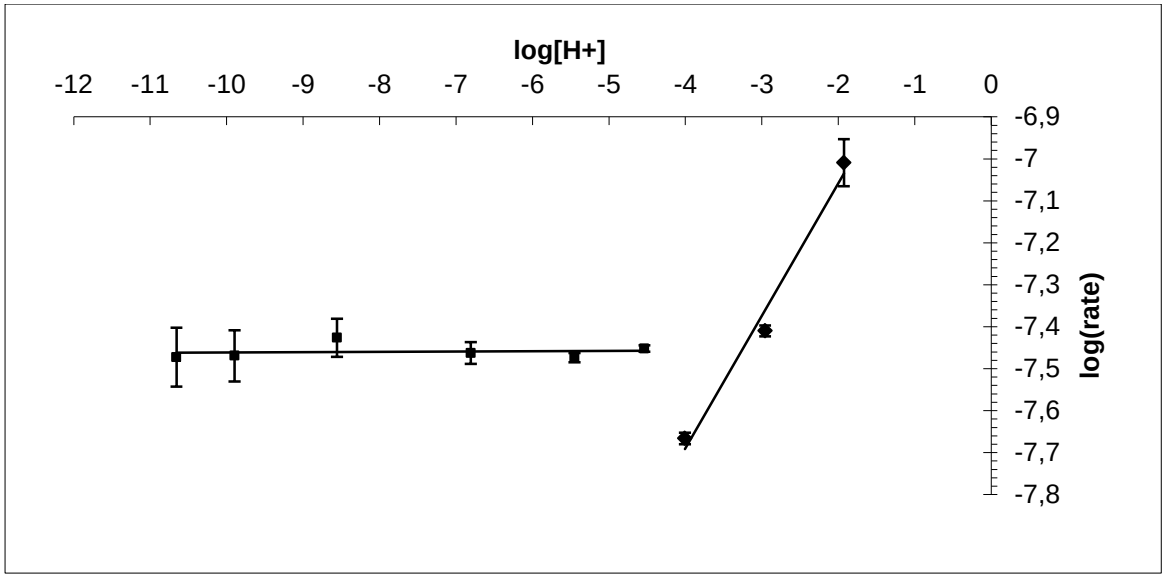

Fig.V.12 logarithm of rate vs. logarithm of H^+ concentration, valentinite.

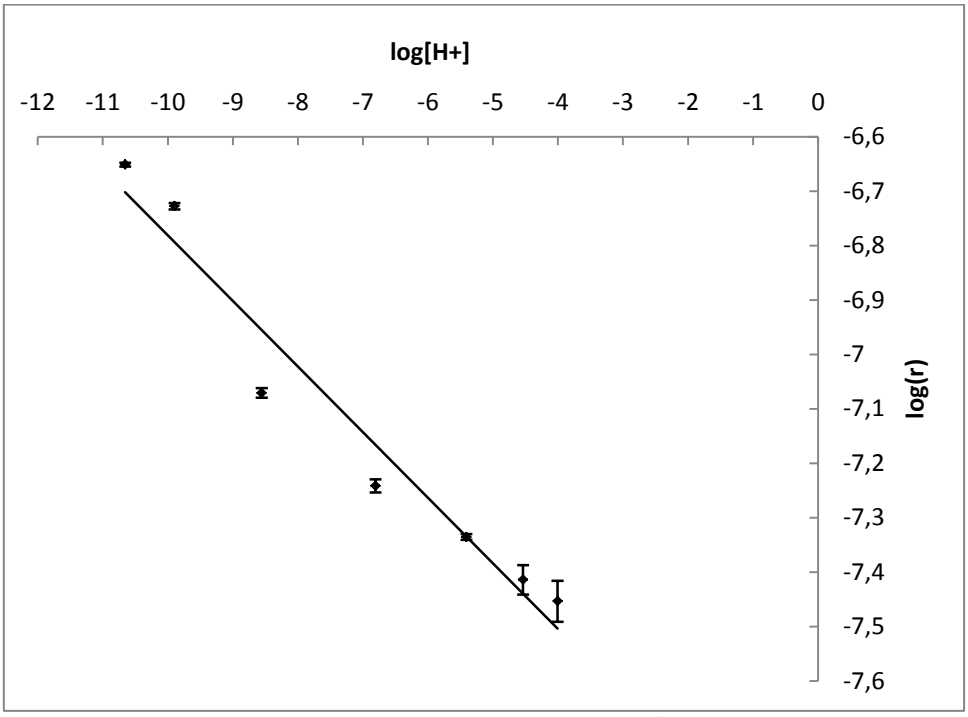

Fig.V.13: logarithm of initial rate vs. logarithm of H^+ concentration, valentinite. Error bars reflect the 95% confidence margins, R^2>0.9540.

For the range 1.97≤pH≤4.05, the kinetic rate constant is k=(3.7± 0.9)×10^{-7}, which is comparable to the rate constant of senarmontite dissolution in acidic solution. The order with respect to the hydrogen ion concentration is α=0.32±0.04 (R^2=0.9827) , i.e. the dependence on the hydrogen ion

concentration is less marked than in the case of senarmontite. The mean rate above pH 4.58 is r=(3.47±0.15)×10^{-8} mol m^{-2} s^{-1}, which is one to two orders of magnitude faster than the dissolution of senarmontite in basic solution. The maximum rate was observed at pH=1.97, r=(9.8±1.3)×10^{-8} mol m^{-2} s^{-1} and the minimum rate at pH=4.05, r=(2.16±0.05)×10^{-8} mol m^{-2} s^{-1}. The activation energies were determined by measuring the rate constants at 25°C, 32°C, 40°C and 50°C at pH=3.0 and at pH=9.9. The corresponding Arrhenius plots are shown in Fig.V.14.

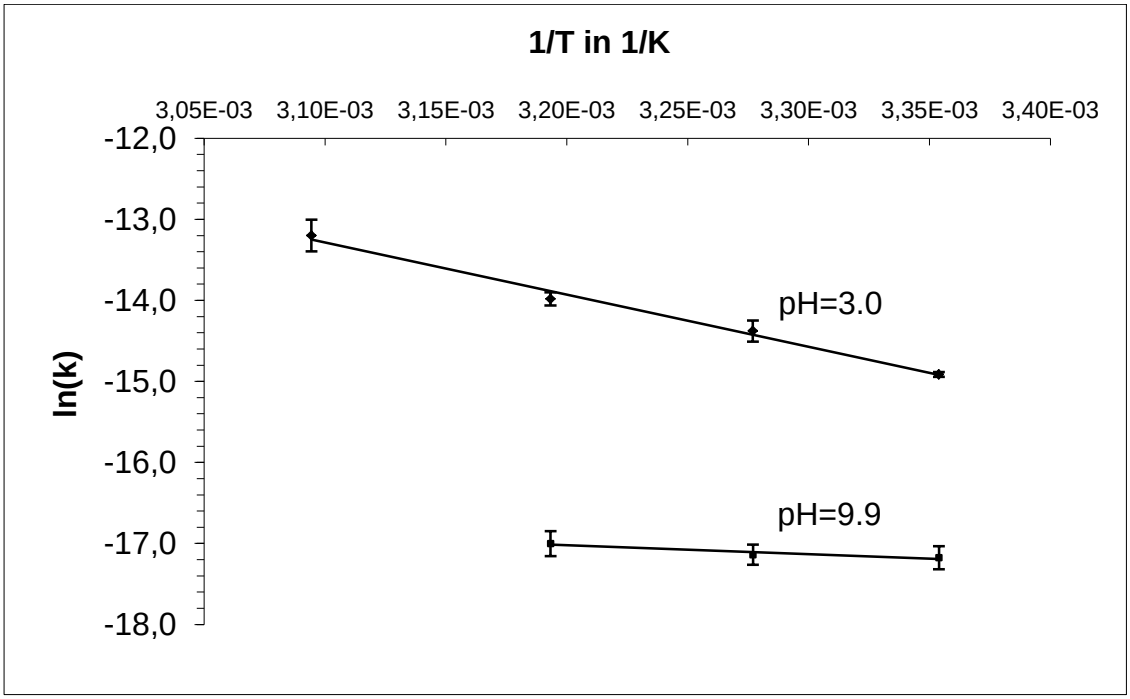

Fig.V.14 Arrhenius plot (ln(k) vs 1/T) for valentinite in acidic and basic solution.

At pH=3.0 and pH=9.9, activation energies of 53.5±3.6 kJ mol^{-1} (R^2=0.9910) and 9.1±2.7 kJ mol^{-1} (R^2=0.9174) are obtained. The activation energy at pH=3.0 is higher than that of senarmontite under the same conditions and still typical of surface controlled processes. The very low activation energy at pH=9.9 indicates that a diffusion controlled mechanism appears likely.

V.4 Summary and conclusion

We derived rate laws for the proton-promoted dissolution of stibiconite, senarmontite and valentinite over the pH range 2 to 11. The stibiconite experiments allowed the calculation of the equilibrium solubility of this mineral at different pH values. Activation energies determined at selected pH values in the acid and basic regions are such that the dissolution of these minerals appears to be a surface-controlled process, except for stibiconite, which exhibits a negative activation energy in acid solution (possible interpretations of this phenomenon are given above) and valentinite, which has an activation energy smaller than ≈20 kJ mol^{-1} in basic solution, normally taken as indicative of diffusion control. Moreover, the behaviour of valentinite in solutions above pH 4.5 is anomalous in that the rate of dissolution becomes independent of pH. A possible explanation would be that surface phenomena such as the extent of surface protonation are not rate-limiting, in contrast to the transport of detached ions from the surface into the solution phase, a view which is also supported by the measured activation energy.

A synopsis of all the measured rates and their pH dependence is given in Fig.V.15. The rates for stibiconite dissolution are based on the rates of release of Sb to solution and the idealised composition Sb_3O_6OH. For comparison, we also included the rates of stibnite (Sb_2S_3) dissolution determined in earlier work.

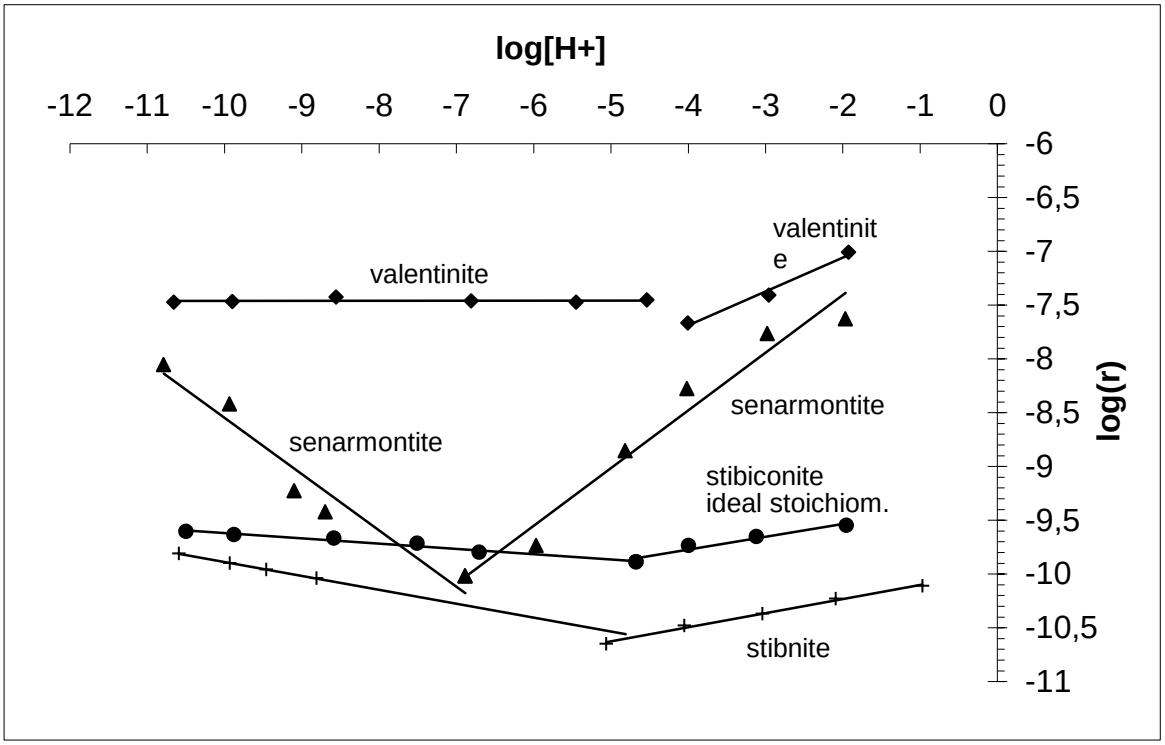

Fig.V.15: logarithm of rates of dissolution of antimony oxide minerals and stibnite. The data for stibiconite are based on the idealized composition Sb_3O_6OH. The data for stibnite are taken from chapters II & III. Error bars omitted for clarity.

It appears that the metastable oxide phase, valentinite, dissolves fastest, followed by senarmontite and stibiconite. The dissolution of stibnite is still about half an order of magnitude slower than that of stibiconite over the whole considered pH range. We attribute this to the higher degree of covalency in bonding in the sulfide than in the oxide minerals. It is further interesting to note that the rates of dissolution of valentinite, stibiconite and stibnite all have a minimum between pH 4 and 5, whereas that of senarmontite is close to pH=7.

In the introduction, we mentioned that thermodynamic solubility data were available for senarmontite and valentinite. Filella and co-workers (Filella et al., 2009) give the solubility of senarmontite under standard conditions as ≈1.3 mg Sb / l. This value is extrapolated from an equation given by Zotov and co-

workers (Zotov et al., 2003), the equation was derived for temperatures above 80°C. It is also claimed that the solubility of senarmontite is independent of pH in the region 4≤pH≤10. Our own experiments at pH<4 show that the solubility of senarmontite was considerably higher at pH=2.01 (2.9 mg Sb / l) and at pH=3.00 (2.6 mg Sb/l). In our experiments at 4≤pH≤10, the solubility given by Filella was indeed never exceeded, but the broadly varying initial rates of dissolution make it appear likely that the solubility is not completely pH independent. This is certainly a point that deserves further experimental study. As far as the solubility of valentinite is concerned, Zotov and co-workers cite data by Gayer and Garrett (1952), from which a solubility of 6.33 mg Sb / l can be calculated. In our experiments, the dissolved antimony concentration never exceeded this value. It thus appears that the phase with the higher solubility (the metastable valentinite) is also the one that dissolves fastest.

In an environment of weathered stibnite, the oxide phases studied would generally be expected to make the dominant contribution to the antimony mobilization, since their rates of dissolution are higher than that of stibnite by several orders of magnitude. However, this difference in reactivity could be outweighed by the relative magnitudes of the exposed stibnite and secondary mineral surfaces, especially when owing to their faster rate of dissolution, the available oxides will be consumed earlier (and new oxides may not readily form in a submerged vein) , leaving 'clean' stibnite surfaces behind. We also showed in our earlier papers (Chapters II and III) that there are factors which dramatically enhance the reactivity of stibnite, such as the presence of other metal ions (Fe^{3+}

in acid solution, which is always present in acid mine/rock drainage, or Mg^{2+} and Ca^{2+} in basic solution). In environments similar to the antimony mine in Goesdorf, Luxembourg (i.e. the case studied by Filella et al.), which is characterized by slightly alkaline drainage (pH≈7.9) due to the dissolution of dolomitic gangue material, the rates of dissolution of senarmontite and stibnite become very similar (Fig.V.15), and that of stibnite is further enhanced by the high concentration of alkaline-earth cations. It seems possible that, if senarmontite were a dominant phase in such an environment, the rate of mobilization of Sb would actually be controlled by the weathering of stibnite rather than that of senarmontite.

An estimate of the rate of release of Sb by the Goedorf mine, based on the assumption that *only valentinite and senarmontite* contribute (in the relative proportions given by Filella and co-workers) , a mean pH=7.92 (Biver and Shotyk, 2011b) and the rate laws derived in this paper, amounts to 5.72×10^{-8} mol m^{-2} s^{-1}. The rate of mobilization by *stibnite alone*, under oxic conditions, and taking into account the presence of magnesium ion (which was found to increase the rate), amounts to 5.10×10^{-10} mol m^{-2} s^{-1} (Chapter III). This second rate is roughly two orders of magnitude smaller than the first one, which means that if the exposed surface area of stibnite is larger than that of the oxide minerals by a factor of 100 or more, stibnite will make the dominant contribution. In the light of this finding, it would be highly interesting to know how large the exposed areas of the different minerals are in relation to one another.

V.5 Acknowledgment

The expert help of Dr Constantin Hoch, Max-Planck Institut für Festkörperforschung, Stuttgart, in the crystallographic characterization of our natural stibiconite sample, is gratefully acknowledged. Drs Hans-Peter Meyer and Alexander Varychev helped to take the electron micrographs.

V.6 References

Abdulla A.H., Noor N.H.M., Ramli I., Hashim M. (2008) Effect of precipitation route on the properties of antimony trioxide. *Materials Chemistry and Physics* **111**, 201-204

Berner R.A.(1978) Rate Control of Mineral Dissolution under Earth Surface Conditions. *Am. J. Sci*. **278**, 1235-1252

Biver and Shotyk (2011a) Chapter II of the present work.

Biver and Shotyk (2011b) Chapter III of the present work.

Casey W.H. and Sposito G. (1992) On the temperature dependence of mineral dissolution rates. *Geochim. Cosmochim. Acta* **56**, 3825-3830

Council of the European Communities (1976) Council Directive 76/464/EEC of 4 May 1976 on pollution caused by certain dangerous substances discharged into the aquatic environment of the Community. Official Journal L 129, 18/05/1976, pp. 23-29.

Debray H. (1866) Ueber den Dimorphismus der antimonigen und arsenigen Säure. *J. prakt. Chemie* **98(1)**, 151-153

Dihlström K. and Westgren A. (1937) Über den Bau des sogenannten Antimontetroxyds und der damit isomorphen Verbindung $BiTa_2O_6F$. *Z. allg. anorg. Chemie* **235**, 153-160

Filella M., Belzile N., Chen Y.-W. (2002a) Antimony in the environment : a review focused on natural waters. I. Occurrence *Earth-Science Reviews* **57**, 125-176 and references cited therein.

Filella M., Belzile N., Chen Y.-W. (2002b) Antimony in the environment : a review focused on natural waters. II. Relevant Solution chemistry. *Earth-Science Reviews* **59**, 265-285 and references cited therein.

Filella M., Philippo S., Belzile N., Chen Y., and Quentel F. (2009) Natural attenuation processes applying to antimony: A study in the abandoned antimony mine in Goesdorf, Luxembourg. *Science of the Total Environment* **407**, 6205-6216

Furuta N., Iijima A., Kambe A., Sakai K., Sato K. (2005) Concentrations, enrichment and predominant sources of Sb and other trace elements in size classified airbone particulate matter collected in Tokyo from 1995 to 2004. *J. Environ. Monit.* **7**, 1155-1161.

Gayer K. H. and Garrett A. B. (1952) The equilibria of antimonous oxide (rhombic) in dilute solutions of hydrochloric acid and sodium hydroxide at 25°. *J. Am. Chem. Soc.* **74,** 2353–2354

Gebel, T. (1997) Arsenic and antimony : comparative approach on mechanistic toxicology. Chemico-Biological Interactions **107**, 131-144

Gebel, T. (1999) Umweltmedizin und Toxikologie des Metalloids Antimon. Umweltmed. Forsch. Prax. **4**, 259-267

Konopik N. and Zwiauer J. (1952) Über Antimontetroxyd. *Monatshefte für Chemie* **83**, 189-196

Krachler, M., Zheng J.,Koerner R., Zdanowicz C., Fisher D., and Shotyk W. (2005) Increasing atmospheric antimony contamination in the northern hemisphere : snow and ice evidence from Devon Island, Arctic Canada. *J. Environ. Monit.* **7**, 1169-1176

Lasaga A.C. (1984) Chemical Kinetics of Water-Rock Interactions. *J. Geophys. Res.* **89(B6)**, 4009-4025

Rimstidt J.D., Chermak J.A., Gagen P.M. (1994) Rates of Reaction of Galena, Sphalerite, Chalcopyrite, and Arsenopyrite with Fe(III) in Acidic Solutions. In *Environmental Geochemistry of Sulfide Oxidation, ACS Symposium Series 550* (eds. C.N. Alpers and D.W. Blowes) American Chemical Society, Washington, chapter 1.

Saldi G.D., Schott J., Pokrovsky O.S. and Oelkers E. (2010) An experimental study of magnesite dissolution rates at neutral to alkaline conditions and 150 and 200°C as a function of pH, total dissolved carbonate concentration, and chemical affinity. *Geochim. Cosmochim. Acta* **74**, 6344-6356

Shotyk W., Krachler M., and Chen B. (2004). Antimony in recent, ombrotrophic peat from Switzerland and Scotland: Comparison with natural background values (5,320 and 8,020 14C yr BP) and implications for the global atmospheric Sb cycle. *Global Biogeochemical Cycles* **18**, BG1016.

Sposito G. (2004) *The Surface Chemistry of Natural Particles*. Oxford University Press, Oxford/New York.

Stevens J.G., Etter R.M. and Setzer E.W. (1993) ^{121}Sb Mössbauer spectroscopic study oft he mineral stibiconite. *Nuclear Instruments and Methods in Physics Research* **B76**, 252-253

Stumm W. and Wollast R. (1990) Coordination chemistry of weathering: Kinetics of the surface-controlled dissolution of oxide minerals. *Reviews of Geophysics* **28**, 53-69

Svensson C. (1974) The crystal structure of orthorhombic antimony trioxide, Sb_2O_3. *Acta Cryst.* **B30**, 458-461

Svensson C.(1975) Refinement of the crystal structure of cubic antimony trioxide, Sb_2O_3. *Acta Cryst.* **B31**, 2016-2018

Szakall S., Papp G., Sajo I. and Kovacs A. (2000) Antimony oxide minerals from Hungary. *Acta Mineralogica-Petrographica, Szeged,* **XLI**, 31-62

United States Environmental Protection Agency (1979) Water Related Fate of the 129 Priority Pollutants, vol. 1. USEPA, Washington, DC, USA, EP-440/4-79-029A.

Vitaliano C.J and Mason B. (1952) Stibiconite and Cervantite. *American Mineralogist* **37**, 982-999

Zotov A.V., Shikina N.D., Akinfiev N.N. (2003) Thermodynamic properties of the Sb(III) hydroxide complex $Sb(OH)_{3\ (aq)}$ at hydrothermal conditions. *Geochim. Cosmochim. Acta* **67**, 1821-1836

Chapter VI :

The Desorption of Sb(V) from Sediments, Hydrous Oxides and Clay Minerals by Carbonate, Phosphate, Sulfate, Nitrate and Chloride

Abstract. The desorption of Sb(V) from two sediment samples by phosphate, carbonate, sulfate, chloride and nitrate at pH=8 was examined. One strongly contaminated sediment sample was taken from an antimony mine (Goesdorf, Luxembourg), the other one was the certified reference material PACS-2 (marine sediment). Phosphate was found to have a strong mobilising ability, while that of carbonate was in general weaker. For comparison, and to better understand the possible importance of individual components of the sediments, desorption experiments were also carried out on pure phases, namely hydrous oxides of Fe, Mn and Al, and the clay minerals kaolinite and montmorillonite. In the cases of hydrous metal oxides, Sb(V) was most effectively desorbed by phosphate, followed by carbonate. Phosphate also desorbed Sb(V) from the clay minerals, while carbonate had no effect. Envelopes showing the extent of adsorption of Sb(V) as a function of pH in the absence and presence of carbonate revealed that adsorption densities were higher (except in the case of montmorillonite) in the absence of carbonate, suggesting a competition between carbonate and $[Sb(OH)_6]^-$ for surface sites generally, and a lowering of surface charge in the case of hydrous aluminium oxide. Desorption experiments on sediments with varying concentrations of phosphate and carbonate demonstrated that at environmentally relevant concentrations, desorption by phosphate is negligible while the effect of carbonate is not. Sulfate, chloride and nitrate generally had little effect. The proportion of antimony desorbed in blank experiments coincides with that mobilized in the first fraction

of the BCR sequential extraction (easily exchangeable and carbonate-bound fraction).

VI.1. Introduction

There is a growing awareness of the emerging importance of antimony as a global pollutant. A chalcophile trace element lacking any physiological function, this semi-metal, its alloys and compounds are very widely used and today in a broad range of industrial and commercial applications (Emsley, 2001). The fugitive emissions of this element into the natural environment via the atmosphere are recorded as pronounced enrichments in the surface, recent layers of peat cores collected in ombrotrophic (ie rain-fed) bogs from western and northern Europe (Cloy et al. 2005; Shotyk et al. 2005). With its extensive use in automobile brake pads, plastics, textiles, and a broad range of other products which are eventually disposed, often through incineration, Sb is the most highly enriched trace metal in urban aerosols today (Furuta, 2005; Gomez et al., 2005; Weckwerth, 2001; Weckwerth 2010). Whereas atmospheric Pb concentrations have been declining during the past decades thanks to the elimination of leaded gasoline, snow and ice in the remote high Arctic of Canada indicate that the enrichments of Sb have actually been increasing during the same period (Krachler et al., 2005). While Sb may be viewed as an emerging contaminant, Sb has been used by man for thousands of years (Emsley, 2001) and evidence of atmospheric Sb contamination has been traced back at least two thousand years

using peat bogs (Shotyk et al., 2004) and three thousand years using Arctic ice (Krachler et al., 2008) With antimony trioxide a suspected carcinogen, for this and many other reasons, Sb is considered as a pollutant of priority interest by the USEPA (United States Environmental Protection Agency, 1979) and the EU (European Union Council of the European Communities, 1976).

Despite the recent awareness of the environmental significance of Sb, compared to other potentially toxic trace elements such as As, Cd, Pb and Hg, there have been remarkably few studies of the transformations, behaviour, and fate of Sb in soils, waters, and sedimentary environments (see the reviews by Boyle and Jonasson, 1984; Filella et al., 2002; Shotyk et al., 2005). Soils and sediments are the ultimate receptors of Sb released to the environment, yet relatively little is known about the behaviour of antimony at the Earth's surface. To a large extent, the bioaccessibility of anthropogenic Sb, and its bioavailability, will be governed by the chemical reactions and transformations taking place in soils and sediments, with the secondary minerals and related amorphous phases contained therein being especially important (Adriano et al., 1994; Sigel et al., 2005; Sposito, 2008). Thus, the fate of Sb in soils and sediments, represents the vital link in our understanding of the overall cycling of antimony in the natural environment and in effect, will ultimately define the significance of human impacts. The aim of the present work is to illustrate the leaching behaviour of Sb from sediments and sedimentary materials using environmentally realistic concentrations of relevant anions.

Antimony (Z = 51, atomic weight 121.75) lies between As and Bi in the periodic table, with the electronic configuration [Kr] $4d^{10}5s^{2}5p^{3}$. Antimony commonly exhibits four formal oxidation states: (V), (III), (0) and (–III). Antimony readily loses either three or five electrons, yielding Sb^{3+} and Sb^{5+} which, upon hydrolysis, yield $[Sb(OH)_3]^o$ and $[Sb(OH)_6]^-$, respectively; these are the predominant aqueous species within the Eh and pH range of most natural waters. Given the redox potential of most soils, therefore, Sb(V) should be the most important oxidation state and the migration of Sb is likely to be controlled by the formation of sparingly soluble antimonates and the adsorption of $[Sb(OH)_6]^-$ (Diemar et al., 2008; Johnson et al., 2005; Tighe et al., 2005). Strong sorption of Sb (V) onto hydrous oxide surfaces in soils may help to explain why recent groundwaters from artesian flow systems can contain such exceedingly low Sb concentrations (ca. 1 ng/l) relative to the elevated concentrations in atmospheric inputs (30 - 66 ng/l) in the same region (Shotyk et al., 2010). Taking advantage of the appearance of ^{125}Sb (half-life 2.73 years) created by the Chernobyl nuclear reactor accident, studies of the chemical speciation of Sb in lakes confirm that $[Sb(OH)_6]^-$ is the predominant species in surface waters (Lindner et al., 1993). The purpose of the present study is to quantify the desorption of Sb (V) from secondary mineral phases that are commonly found in soils and sediments, by commons anions, as well as the competitive sorption of Sb (V) onto these surfaces.

Unlike the case of Sb, there has been a number of studies of the leaching behaviour of As which are helpful by comparison. Carbonate species, for

example, have been shown to effectively leach As from rocks and sediments (Kim et al., 2000; Kim et al., 2006; Anawar et al., 2004; Appelo et al., 2002) With bicarbonate effective in replacing arsenate on the surface of iron and manganese oxyhydroxides, an analogous circumstance could reasonably be expected for Sb(V). Carbonate species are also known to play a part in the mobilization of uranium(VI) from soils. On the one hand, this is due to the formation of soluble anionic complexes that do not adsorb to soil constituents under normal conditions, on the other, there is competition between anionic uranium and carbonate species for adsorption sites at high alkalinity (Duff et al., 1996). There is a decrease in chromate adsorption onto goethite in the presence of carbonate (Zachara et al., 1987) and a marked competition between the adsorption of carbonate on the one hand, and sulfate and selenate on the other, on both goethite (Wijnja and Schulthess, 2002) and aluminium oxide (Wijnja and Schulthess, 2000). In the latter two cases, the matter is further complicated by the interesting observation that at low concentrations, carbonate does not inhibit, but rather *promotes* the adsorption of sulfate and selenate.

Phosphate is also known to mobilize arsenic from sediments through substitution of arsenate at mineral surfaces (Keon et al., 2001). Arsenate and phosphate have been shown to compete for adsorption sites on kaolinite and montmorillonite (Manning and Goldberg, 1996). Moreover, phosphate has been shown to mobilize antimony from soils (Nakamura et al., 2006; Blay, 1999). Given that carbonate is ubiquitous in natural waters, and that phosphate is a common pollutant in waters impacted by industrial, domestic wastewaters, and

agriculture, the leaching behaviour of Sb from soils and sediments must duly consider the importance of these two anions.

The purpose of the present study was to quantify the effects of bicarbonate and phosphate on the desorption of Sb(V) from contaminated sediment, from spiked synthetic amorphous iron, manganese and aluminium hydroxides, and from clays. Clays are common constituents of soils and sediments, and the hydrous metal oxides frequently occur as coatings on soil and sediment particles. Further, the mobilizing ability of phosphate and carbonate are compared to the mobilizing ability of the other common anions such as chloride, nitrate and sulfate at pH 8.

Isotherms and envelopes for the adsorption of antimony onto important soil phases have been established by Blay (Blay, 1999). The effect of carbonate species on the adsorption envelopes is examined in the present work. Both carbonate and phosphate are, in general, found to mobilize antimony strongly, but here we also investigate these effects at environmentally relevant concentrations.

Since Sb(V) is the dominant Sb species in oxic water and sediment (Filella et al., 2002), only Sb(V) is considered in this paper.

VI.2. Materials and Methods

VI.2.1 Sediments

A strongly contaminated sediment sample for the present study was obtained from the drainage adit of an abandoned antimony mine near Goesdorf, in Luxembourg (Europe). The geological setting of the mine is described by Filella and co-workers (Filella et al., 2009). As a consequence of the weathering of dolomite, the most important gangue mineral of this deposit, the drainage waters from which the sediment is taken are alkaline (typical pH between 7.5 and 8.5 with an average total alkalinity of about 5 mmol/L and a total sulfate concentration ranging between 1 and 1.5 mmol/L). A large quantity of superficial sediment was collected by hand using a PE container, next to the exit of the drainage gallery of the mine. The sediment was air-dried and sieved. The fraction <0.263 mm was retained for the experiments and well homogenised. This sediment contained a total of 312±10 ppm Sb (INAA, n=6) and 322±31 ppm (n=3) could be mobilized in an aqua regia attack, carried out according to the ISO 11466 protocol. In a sequential extraction scheme following the BCR protocol (Ure and Davidson, 2002), 3.0% of the total Sb content were found in the first (easily mobile and carbonate-bound) fraction and 8.0% of total Sb in the second (reducible) fraction.

The second sediment to be used in the present work was the certified reference material (marine sediment) PACS-2 from the Canadian National

Research Council, with a certified total of 11.3±2.6 ppm Sb, of which 9.4±0.7 ppm could be mobilized by the ISO 11466 aqua regia attack.

VI.2.2 Hydrous oxide phases

Pure hydrous oxide phases were prepared by the precipitation of the corresponding perchlorate salts with ammonia (in the case of iron and aluminium) or potassium hydroxide and hydrogen peroxide (in the case of manganese). Perchlorate was chosen for its very weak coordinating properties and its weak affinity towards oxide surfaces (Rietra et al., 2000) in order to keep the surfaces as free as possible from interfering anionic ligands, and for the negligible effect that perchlorate exerts on the ordering of water molecules at the solid-liquid interface (Tejedor-Tejedor and Anderson, 1986). For the same reasons, the desorption experiments were carried out in an ammonia/ammonium perchlorate buffer.

Powder X-ray diffraction (Cu Kα1 radiation in Debye-Scherrer geometry) showed that all the prepared phases were perfectly amorphous. It was verified that the hydroxides were soluble in 0.1 M oxalate solution adjusted to pH=2, which is normally interpreted as indicative of lack of crystallinity.

VI.2.3 Clays

Commercial kaolinite and montmorillonite (from ACROS, Germany) were used. Kaolinite was used as supplied. Montmorillonite was washed four times by decantation with 10 times its weight of ultrapure water, until a circumneutral suspension pH was achieved. The material was filtered off and dried overnight at 80°C.

VI.3. Experimental

VI.3.1 Desorption : Sediment samples

About 250 mg of sediment PACS-2 or 100 mg of Goesdorf sediment were accurately weighed into 15 ml PP centrifuge tubes. 10 ml of a 1 M ammonia/ammonium perchlorate buffer of pH=8 and 2.0 ml of one of the following electrolyte solutions were added :

- 0.5 M potassium monohydrogenphosphate,
- 0.5 M sodium hydrogencarbonate,
- 0.5 M sodium chloride,
- 0.5 M sodium nitrate,
- 0.5 M sodium sulfate,
- ultrapure water as a blank.

All the salts were of analytical grade from Carl Roth, Germany, and all solutions were prepared with ultrapure water from a TKA GenPure purification unit (TKA, Germany). The concentration of each electrolyte thus amounted to 0.083 M. The buffer solution was prepared by adding 5.5 ml (0.1 mol) of concentrated ammonia solution (35% Trace Analysis Grade, Fisher Scientific) to about 70 ml of ultrapure water and adjusting the pH to the desired value by dropwise addition of concentrated perchloric acid (70% suprapure, Merck, Germany). The pH was measured by means of a pH Meter (Model 632 from Metrohm, Switzerland). The final volume of the buffer was made up to 100 ml. The suspensions were mixed for either 1 h or 24 h on an end-over-end tumbler

set at 0.5 revolutions per second. The pH of the suspensions was measured before and after the desorption step to verify that it was held constant by the buffer. The tube was centrifuged and the supernatant filtered (0.45 µm CME hydrophilic syringe filters, Millipore) and analysed for Sb(V). The analysis was carried out by differential pulse anodic stripping voltammetry (DPASV), following the method of Quentel and Filella (Quentel and Filella, 2002). The original method was modified in the sense that a 3 M NaCl liquid junction was used in the reference electrode (instead of a 3 M KCl solution) in order to avoid precipitation of potassium perchlorate which would have clogged up the diaphragm of the electrode. The voltammetric method was implemented on a Metrohm 797 VA Computrace voltammetric analyser (Metrohm, Switzerland) interfaced to a laptop computer. 35% Suprapure hydrochloric acid (Merck, Germany) was needed as a reagent. The analysis was done by standard addition. To this effect, a 1000 ppm Sb stock solution was prepared by dissolution of the appropriate amount of potassium antimonyl tartrate trihydrate (analytical grade, Alfa-Aesar, Germany) and a 1 ppm working solution was freshly prepared (on a daily basis) by dilution of the stock solution. The detection limit is given by the authors as 11 ng/ml.

All experiments and analyses were carried out at room temperature (20±2 °C) under aerobic conditions.

VI.3.2 Desorption : Amorphous oxyhydroxides

Amorphous iron oxyhydroxide was prepared in small portions in 15 ml PP centrifuge tubes, by addition of 300 µl concentrated ammonia (trace analysis grade, Fisher Scientific, Germany) to 5 ml of a 0.1 M solution of iron(III)-

perchlorate hexahydrate (Alfa-Aesar, Germany). The resulting suspension was shaken a few times and immediately submitted to centrifugation for 30 min at 6000 rpm. The supernatant was decanted and discarded and the solid was resuspended in 10 ml of a 48.7 ppb (4×10^{-7} M) Sb(V) solution. This solution was prepared by dilution of a 0.01 M stock solution of potassium hexahydroxyantimonate(V) trihydrate (Alfa-Aesar, Germany) and analysed shortly before use to determine its actual concentration. The suspension was mixed on a tumbler for 1 h. The supernatant was separated by centrifugation and analysed for Sb(V) as above. The analysis revealed that an equilibration time of 1 h was sufficient for Sb(V) to be quantitatively adsorbed onto the iron hydrous oxide precipitate. The subsequent desorption procedure was analogous to the one outlined above.

Amorphous aluminium hydroxide was prepared in centrifuge tubes, as above, by addition of 300 µl ammonia solution to 5 ml of 0.1 M aluminium perchlorate (analytical grade, Acros, Germany) solution. The supernatant was separated by centrifugation and discarded. The remaining solid was resuspended in 10 ml of the Sb(V) solution and equilibrated for 6 h. After centrifugation, the supernatant was analysed for Sb, since the adsorption of Sb(V) onto the aluminium hydroxide surface was only complete to 80-90%. The difference in concentration between the initial Sb(V) solution and the supernatant was used to calculate the amount of Sb actually adsorbed. The subsequent procedure was analogous to the one described above.

Amorphous hydrous manganese(IV) oxide was prepared by addition of 5 ml 1 M potassium hydroxide solution (analytical grade, Roth, Germany) and 20 drops of 3% hydrogen peroxide (Fischar, Germany) to 5 ml of a 0.1 M managanese(II)-perchlorate hexahydrate (Acros, Germany) solution in a centrifuge tube. The tube was shaken and the supernatant separated by centrifugation and discarded. The subsequent procedure was analogous to the one outlined above for the iron(III) oxyhydroxide.

VI.3.3 Desorption : Clay minerals

About 500 mg of each clay sample were accurately weighed into centrifuge tubes and 10 ml of 48.7 ppb Sb(V) solution was added. The suspensions were mixed for 24 h. The suspensions were centrifuged, and in each case, the supernatant solutions were filtered (0.45 µm) and analysed for Sb(V) in order to calculate the adsorbed amount of Sb(V). Adsorption densities were lower for kaolinite (ca. 0.3 µg Sb/g) than for montmorillonite (ca. 1 µg Sb/g) , where the adsorption was very nearly quantitative. The desorption experiments were then conducted as described under 3.1.

VI.3.4 Adsorption envelopes : Hydrous ferric oxide

5 ml of 0.1 M ferric perchlorate solution was added to about 5 ml ultrapure water contained in a 15 ml PP centrifuge tube. 300 µl concentrated ammonia solution was added and the resulting precipitate separated immediately from the mother liquor by centrifugation. The precipitate was equilibrated for 24 h with a buffer solution of the desired pH (PIPES 0.25 M for pH=6 and 7, ammonia/ammonium perchlorate buffer for pH=8, 9, 10, 11). The precipitate

was separated from the buffer by centrifugation and equilibrated for 24 h with 10 ml of *either* aqueous $NaClO_4$ 0.01 M adjusted to the desired pH (by addition of KOH or $HClO_4$) *or* with aqueous $NaClO_4$ 0.01 M + $NaHCO_3$ 0.01 M, adjusted to the desired pH, as before. 20 µl of Sb(V) 0.01 M was added to each batch, leading to an initial concentration of 2.43 ppm Sb. After another equilibration period of 24 h, the pH of the suspension was measured and its Sb(V) concentration measured by DPASV. The extent of adsorption of Sb was calculated as the difference between the initial amount and the amount present in solution after adsorption and the result expressed as µg of adsorbed Sb per mg Fe in the solid (adsorbent) phase.

VI.3.5 Adsorption envelopes : Hydrous aluminium oxide

5 ml of 0.1 aluminium perchlorate solution were introduced into a 15 ml PP centrifuge tube.

300 µl of concentrated ammonia solution was added and the resulting precipitate separated from the solution by centrifugation. The subsequent procedure was analogous to the one described for hydrous ferric oxide. As some dissolution of the hydroxide phase seemed to take place at very high or very low pH values, the precipitate was dissolved in hydrochloric acid and its amount determined by ICP-OES.

VI.3.6 Adsorption envelopes : Kaolinite and Montmorillonite

Approximately 1 g of kaolinite was accurately weighed into a centrifuge tube. 10 ml of buffer solution (as in the case of hydrous ferric oxide) was added and the mixture equilibrated for 24 h. The subsequent procedure was analogous

to the one described under 3.4 for hydrous ferric oxide, except that 100 µl of Sb(V) 1.21 ppm was added, so that the initial concentration of Sb amounted to 12 ppb Sb.

The montmorillonite experiments were carried out in a similar fashion, with an approximate mass of 0.4 g mineral equilibrated with a suitable buffer, followed by 10 ml of the electrolyte solution, spiked with 400 µl of Sb(V) 1.21 ppm, giving an initial concentration of 47 ppb Sb(V).

VI.3.7 Desorption of Sb(V) from sediment : dependence on phosphate and carbonate concentrations

About 250 mg of PACS-2 or 100 mg of Goesdorf sediment were accurately weighed into centrifuge tubes and mixed with solutions of KH_2PO_4 of different concentrations (5×10^{-3}, 1×10^{-3}, 5×10^{-4}, 1×10^{-4} $molL^{-1}$) that were adjusted to pH=8 with 0.1 M ammonia/ammonium perchlorate buffer. The solutions were mixed for 17 h on a tumbler.

A similar experiment was carried out using about 500 mg of PACS-2 or 50 mg of Goesdorf sediment and sodium hydrogencarbonate solutions (5×10^{-3}, 1×10^{-3}, 5×10^{-4}, 1×10^{-4} $molL^{-1}$) that were adjusted to pH=8 with 0.1 M ammonia/ammonium perchlorate buffer. The solutions were mixed for 17 h on a tumbler. The Goesdorf sediment had previously been washed by stirring a suspension of 3 g of sediment in 250 ml ultrapure water overnight, followed by gravity filtration and air-drying.

After the mixing period, the suspensions were centrifuged and the supernatant analysed for Sb(V). The proportion of desorbed Sb relative to the total amount present in the sediment was calculated.

VI.4. Results and Discussion

VI.4.1 Desorption from sediment samples

The desorbed amount of Sb is reported as % of the total S As expected, phosphate ion displays the strongest desorbing effect. Bicarbonate desorption is nearly as strong as that of phosphate, yet the effect of bicarbonate seems to depend on the type of sediment : its desorbing effect on PACS-2 is significantly higher than that of the blank solution, while in the case of Goesdorf sediment, the difference is only marginal. b (as obtained after aqua regia extraction) present in the sediment (fig. VI.1).

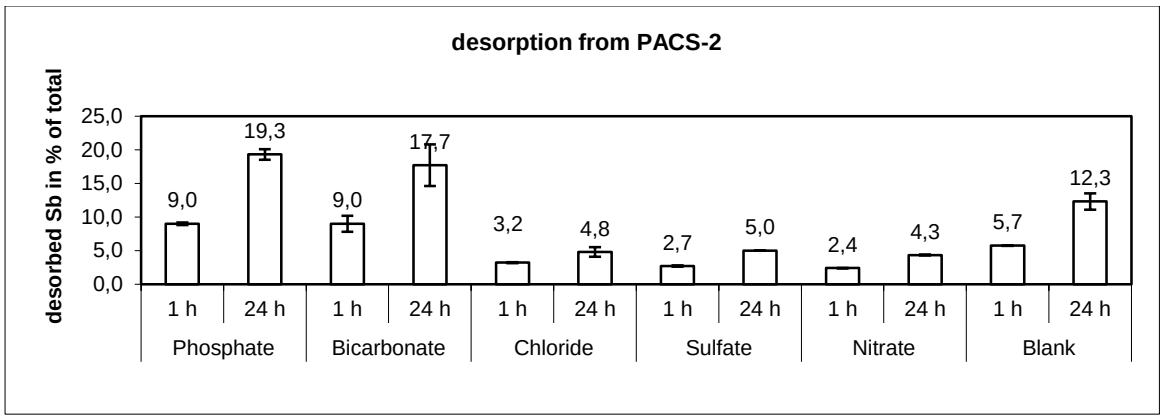

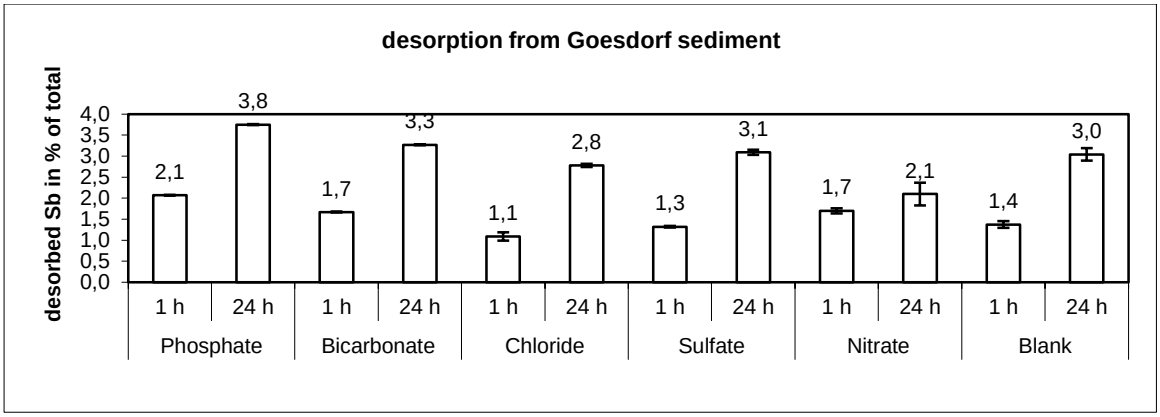

Fig. VI.1 Desorption of Sb from PACS-2 and Goesdorf sediment

In this latter case, the sediment contains a large proportion of Sb that is not easily mobilized (cf. the above mentioned BCR extraction). Chloride, sulfate and nitrate appear to stabilise the adsorbed Sb(V) on PACS-2 sediment, while this effect is only observed with chloride and nitrate in the case of Goesdorf sediment. This apparent stabilising effect corroborates the observations made by Blay (Blay, 1999) in the desorption from soils.

The fractions desorbed by phosphate (3.75%) and bicarbonate (3.21%) from Goesdorf sediment slightly exceed the easily exchangeable, first fraction of the BCR sequential extraction (3.06%), while desorption by the blank solution (3.04%) coincides with that fraction.

Desorption from sediments is slower than that from hydrous metal oxides, with only about half of the amount desorbed at equilibrium being desorbed after 1 h (see also fig. VI.2). There is little difference in desorption rate between the sediments and the clay phases (fig. VI.3).

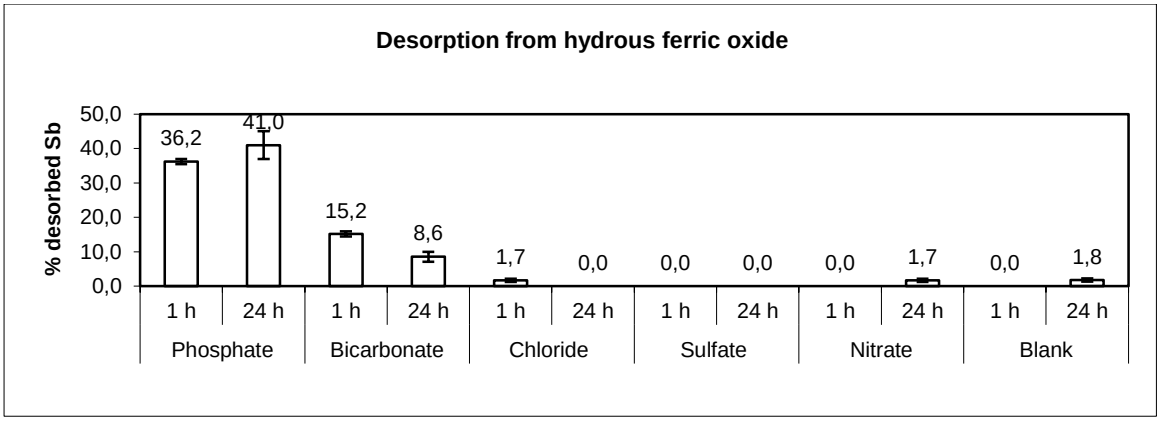

Fig. VI.2 Desorption from hydrous ferric oxide

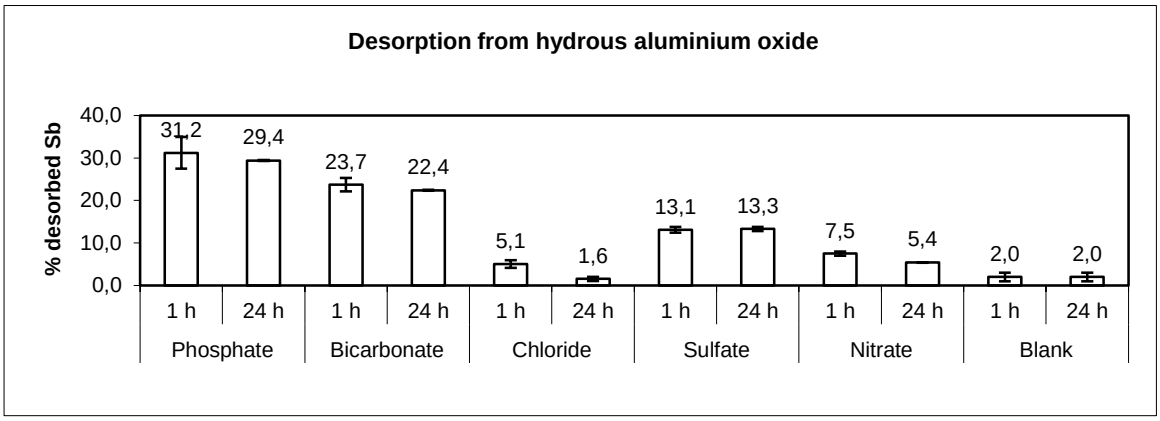

Fig. VI.3 Desorption from hydrous aluminium oxide

VI.4.2 Desorption from hydrous oxides

In each adsorption experiment, the quantity of hydrous oxide used was chosen to be equivalent to 5×10^{-4} mol of the metal. The quantity of adsorbed Sb(V) amounted to 4×10^{-9} mol. This corresponds to an adsorption density of 8×10^{-6} mol Sb / mol metal or 9.74×10^{-4} g Sb / mol metal. The adsorption experiments with aluminium hydroxide are an exception in that the initially adsorbed amount of Sb(V) has to be calculated for each individual experiment since the adsorption was not quantitative.

In fig. VI. 2, we report the percentages of desorption, after 1 h or 24 h respectively, for each of the chosen electrolytes. Desorptions below the detection

limit (corresponding to 0.0045%) are reported as 0% in the graphs. The results of the experiments with hydrous manganese oxide were positive only for phosphate, thus no graph is presented but the findings are discussed in the text below.

As regards the binding of Sb(V) to hydrous ferric oxide, formation constants are known for $\equiv FeSbO(OH)_4$ and $\equiv FeOHSbO(OH)_4^-$ (Dzombak and Morel, 1990). Microscopically, the situation appears to be much more complex: Scheinost and co-workers (Scheinost et al., 2006) were able to show that antimony sorbed to ferric iron in soils by the formation of both edge-sharing and bidentate corner-sharing $Sb(O,OH)_6$ and $Fe(O,OH)_6$ octahedra. The sorption of phosphate and carbonate to the hydrous ferric oxide or goethite surface is well documented, both with regard to surface complexation constants and to surface speciation (Russell et al., 1975; Sigg and Stumm, 1980; Van Geen et al., 1994; Li and Stanforth, 2000; Appelo et al., 2002; Atkinson et al., 1972) Phosphate and carbonate are known to bind strongly and specifically. With regard to sulfate, there appears to be some specific sorption (monodentate) on goethite at pH<6 (Wijnja and Schulthess, 2000b) whereas the anion exists in outer-sphere complexes at higher pH. Chloride sorption is variously regarded as specific (Parfitt et al., 1977) or non-specific (Sigg and Stumm, 1980). There may be monodentate binding of nitrate (Parfitt and Russel, 1977) even though nitrate generally forms weak outer-sphere complexes. Sulfate, chloride and nitrate are clearly weaker ligands with respect to the ferric oxide surface.

Phosphate and carbonate adsorb specifically to aluminium oxide surfaces (Wijnja and Schulthess, 2000a). Sulfate exists predominantly as outer-sphere complexes, although a small fraction is sorbed inner-spherically below pH 6 (Wijnja and Schulthess, 2000). Chloride is weakly adsorbed through electrostatic interactions (Schulthess and McCarthy, 1990). Tanada and co-workers (Tanada et al., 2003) show that the selectivity of anion adsorption onto aluminium oxide hydroxide increases in sequence $Cl^- < NO_3^- < CO_3^{2-} < SO_4^{2-} < PO_4^{3-}$. In our experiments, the mobilising effect of these anions on adsorbed Sb(V) parallels this trend, with the positions of carbonate and sulfate swapped.

The major difference between the hydrous ferric oxide surface and the manganese(IV)oxide surface is that, owing to the low pH_{pzc} (about 2.25 for δ-MnO_2 (Murray, 1973)) of the latter, this phase has negative surface charges over the entire range of environmentally relevant pH values. Its capacity to adsorb anions should therefore be minimal (Balistrieri and Murray, 1982). Chloride and sulfate for instance do not adsorb at all on δ-MnO_2 for 2<pH<9. Phosphate adsorbs relatively strongly to δ-MnO_2 (Yao and Millero, 1996), but the authors were unable to fit the adsorption envelopes with various inner-sphere surface species within the triple layer model. Studies on crystalline β-MnO_2 (pyrolusite) confirm that phosphate forms outer-sphere complexes (Mustafa et al., 2006). Takamatsu et al. found that no appreciable adsorption of arsenate by hydrous Mn(IV) oxide takes place, unless a divalent cation (e.g. Mn^{2+}) is present, shifting the surface charge to more positive values (Takamatsu et al., 1985). Similar observations were made with phosphate (Kawashima et al., 1986). In our own

experiments, we found that adsorption of Sb(V) (8 µmol Sb/mol MnO_2) was quantitative and rapid. This may be due to residual Mn^{2+} present in the hydrous oxide phase prepared from $Mn(ClO_4)_2$. No data seem to exist on the adsorption of carbonate by manganese oxide. The observations in the desorption experiments presented here are in line with existing data.

Specifically, among all the ligands tested in this work, phosphate is found to strongly displace Sb(V) adsorbed to hydrous metal oxides. Bicarbonate desorbs significantly more Sb than the blank solution from hydrous ferric and aluminium oxide, while there is no significant difference in the case of Mn(IV) oxide. In the case of Mn(IV) oxide, phosphate is the only species that desorbs Sb to a measurable extent. After 1 h, 17.7±4.0 % of the adsorbed antimony were desorbed, after 24 h, 16.6±0.3%. Thus, the desorbed Sb(V) percentage from Mn(IV)oxide by phosphate is only about half the desorbed percentage from HFO and aluminium hydroxide. None of the other electrolyte solutions desorbed Sb to a measurable extent from the manganese oxide surface. Sb(V) thus binds much more strongly to Mn(IV)oxide than to any of the other considered surfaces. Bicarbonate is more effective in desorbing Sb(V) from aluminium hydroxide than from hydrous ferric oxide. Sulfate, which has no effect on the desorption form HFO or Mn(IV) oxide, desorbs Sb from the aluminium oxide phase, although less strongly so than either phosphate or bicarbonate. In contrast to the aluminium hydroxide surface, chloride, sulfate and nitrate have little or no effect on Sb adsorbed on HFO or Mn(IV) oxide.

The desorption by phosphate and bicarbonate is much more rapid (the bulk of desorption is reached after 1 h) than in the case of sediments and clays. The results shown in Fig. VI.2 indicated that some resorption/reprecipitation must take place when Sb(V) is desorbed by bicarbonate from hydrous ferric oxide and by chloride and nitrate from aluminium hydroxide.

A mechanism involving displacement of Sb(V), adsorbed to hydrous metal oxide surfaces as $[Sb(OH)_6]^-$, by surface complexation or possible surface precipitation at higher concentrations, is likely to operate in the desorption by phosphate and carbonate.

VI.4.3 Desorption from clay minerals

Phosphate is again the most effective desorbing species (cf. figs. VI.4 and VI.5). Phosphate adsorbs on clays by ligand exchange with Al-OH edge sites (Parfitt, 1978). We can therefore conclude that adsorption of Sb(V) takes place, at least in parts, on the same sites.

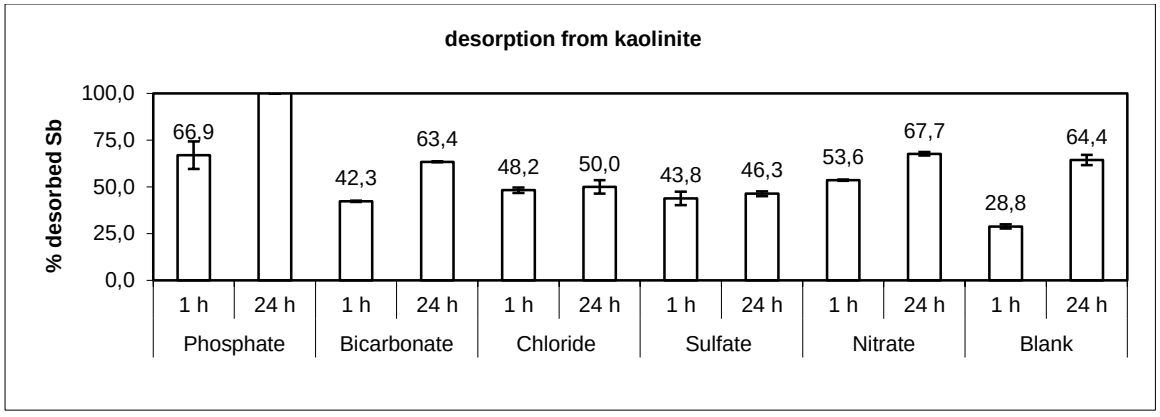

Fig. VI.4 Desorption from kaolinite

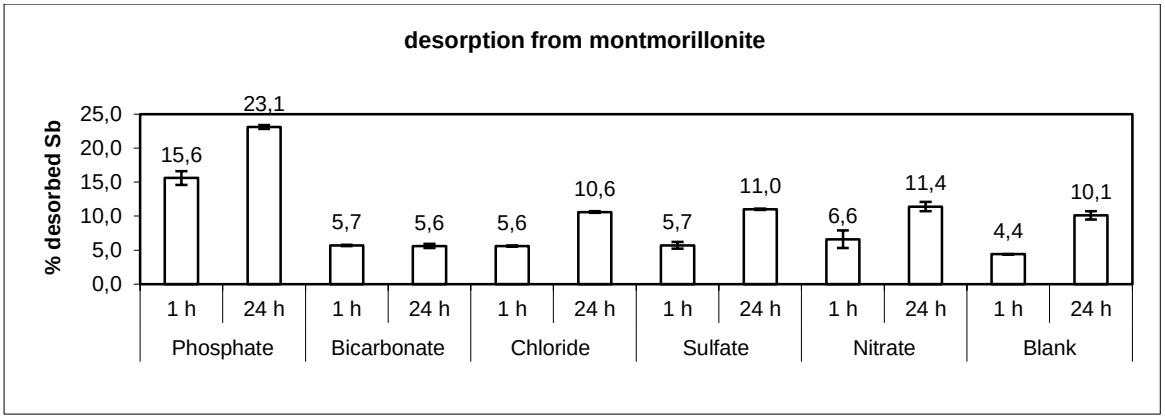

Fig. VI.5 Desorption from montmorillonite

Phosphate can be desorbed from kaolinite by bicarbonate, but the exchange does not take place on a mole for mole basis (Nagarajah et al., 1968). Again, even though bicarbonate adsorption may take place, in parts, at the same sites as phosphate adsorption, surface charge effects are important (Kafkafi et al., 1988). With regard to its desorbing capacity on adsorbed Sb(V), in contrast to the behaviour at hydrous oxide surfaces, bicarbonate is no more effective than the blank (buffer) solution. In the case of montmorillonite, it is actually found to desorb more weakly than the blank solution. It is the only material used in this study where carbonate is less effective than the blank. Comparison of the desorbed amounts after 1 h shows that all considered anions accelerate the desorption of Sb(V), while the amount desorbed at equilibrium is (i) higher than the blank (phosphate), (ii) not very different from the blank (nitrate), or (iii) lower than the blank (chloride and sulfate). Note that kaolinite is the only pure material used in this study from which large amounts of Sb(V) (> 60%) are desorbed by the blank solution, an effect that is observed with the sediments but

not with the hydrous metal oxides. Kaolinite thus exhibits the smallest adsorption density of all the materials considered in this study, and the weakest binding of Sb.

The rate of desorption from clays is intermediate between that observed with sediments (slow) and that observed with hydrous metal oxides (fast).

The common anions chloride, nitrate and sulfate do not, in general, promote the mobilization of antimony and in some cases (PACS-2 sediment) even inhibit it. These results also show that in oxic, circumneutral waters, no more antimony will be mobilized than can be extracted by the first stage of the BCR protocol. This protocol can therefore be expected to give a realistic estimate of the mobile fraction of antimony in sediment.

VI.4.4 Adsorption envelopes

The sorption capacities decrease with increasing pH (figs. VI.6-9), as would be expected for the adsorption of an anionic species.

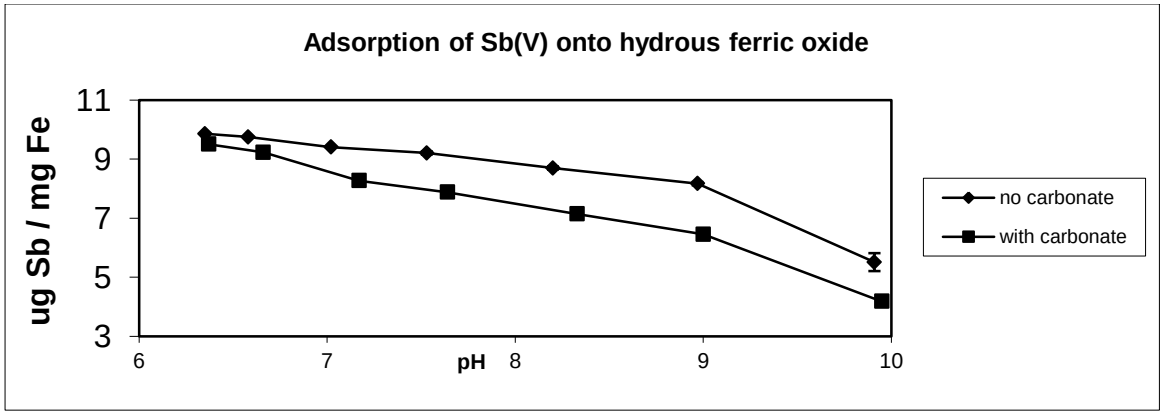

Fig. VI.6 Adsorption envelope of Sb(V) on hydrous ferric oxide

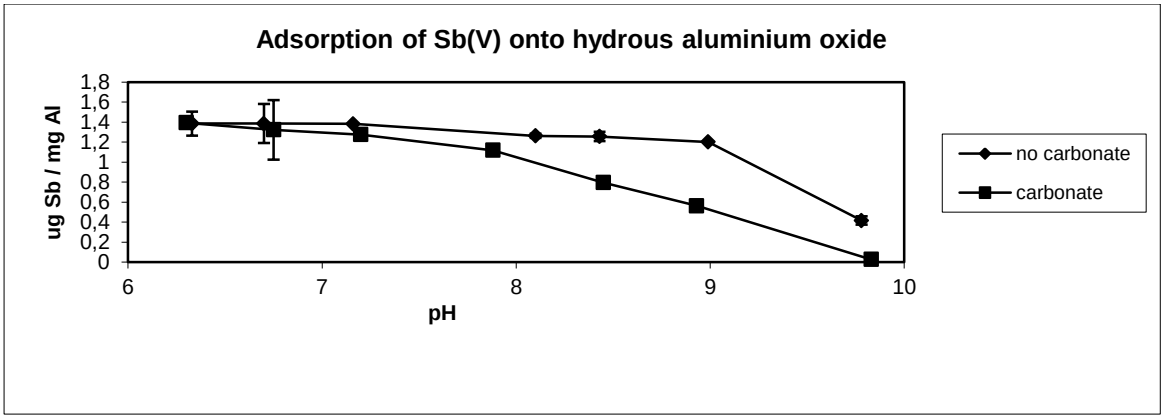

Fig. VI.7 Adsorption envelope of Sb(V) on hydrous aluminium oxide

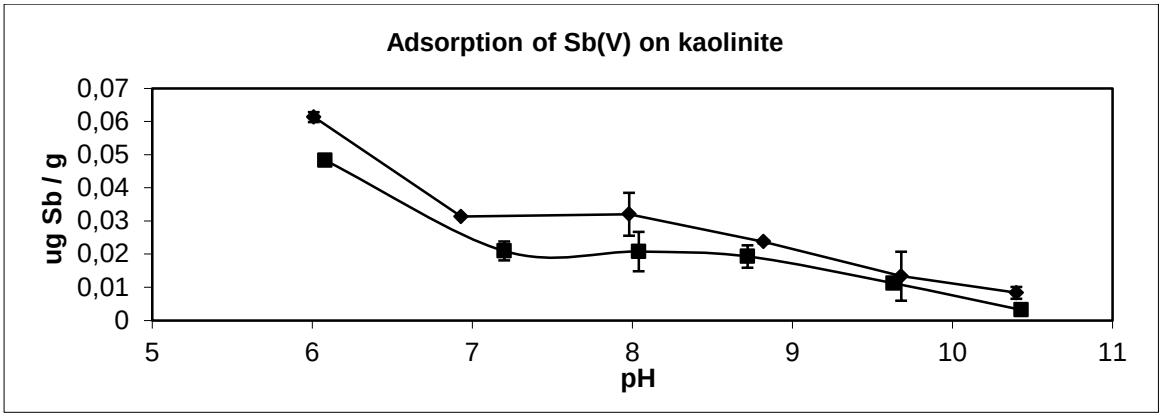

Fig. VI.8 Adsorption envelope of Sb(V) on kaolinite

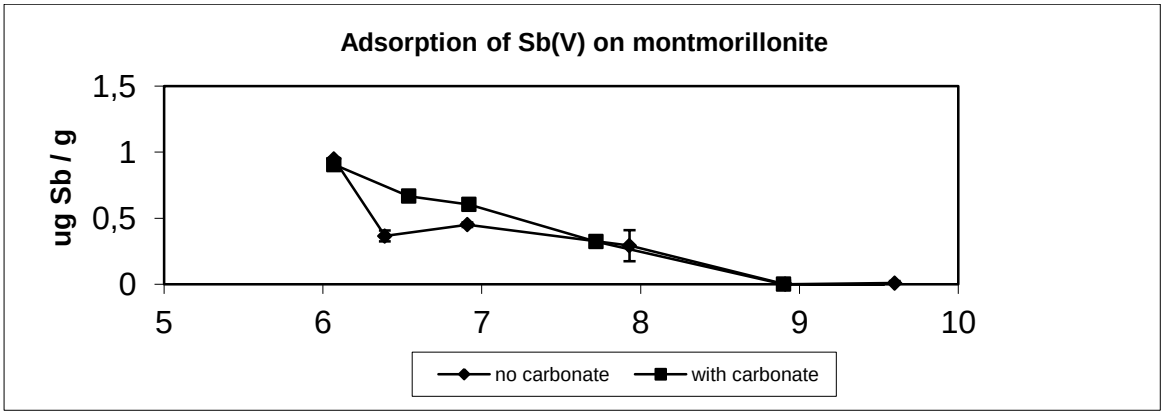

Fig. VI.9 Adsorption envelope of Sb(V) on montmorillonite

For all the considered sorbents except montmorillonite, the capacity is further decreased in the presence of carbonate. Note that the adsorption capacity at the lowest pH considered (pH ca. 6) is about an order of magnitude

larger for hydrous ferric oxide (ca. 500 mg Sb/mol Fe) than for aluminium hydroxide (40 mg Sb/mol Al) (cf. figs VI.6 and 7).

The difference between the two envelopes in the cases of hydrous ferric oxide and aluminium hydroxide is most marked at a pH of about 9, while it occurs at pH 8 for kaolinite (fig. VI.8). The pH beyond which the adsorption begins to fall off more markedly is roughly in line with the pH_{pzc} of the considered phase. In the case of hydrous ferric oxide (fig. VI.6), the adsorption edge is lowered, but not shifted in the presence of carbonate. This suggests that bicarbonate competes with Sb(V) for adsorption sites on the hydrous ferric oxide surface, and that the reduced adsorption of Sb(V) is not solely due to a variation in surface charge brought about by adsorbed carbonate. By contrast, in case of hydrous aluminium oxide, the profile (Fig. VI.7) is both lowered and shifted to smaller pH, indicating that charge effects, in addition to anion competition, may be important.

In the case of kaolinite (fig. VI.8), no shift is again observed, only a lowering of the envelope due to competitive adsorption.

Edzwald and co-workers (Etzwald et al., 1976) report that for montmorillonite, phosphate adsorption increases with increasing pH, but this is not true of antimonate (Fig. VI.9). The adsorption envelope on montmorillonite is altogether atypical, in the sense that carbonate does not have much effect on the adsorption of Sb(V) at low (pH 6) and at high pH (pH > 8), whereas it promotes rather than hinders the adsorption at intermediate pH values. These findings are in line with the observed behaviour of bicarbonate in the desorption experiments

with montmorillonite, where bicarbonate showed a smaller mobilising ability than the blank solution (fig. VI.5)

VI.4.5 Desorption as a function of phosphate and carbonate concentration

Fig. VI.10 : The extent of desorption by phosphate decreases with decreasing concentration and approaches that of the blank solution at the smallest phosphate concentration used (10^{-4} M = 9.5 ppm). Waters carrying such elevated phosphate concentrations are not commonly encountered and would be regarded as extremely polluted. Thus under normal circumstances, desorption of antimony from sediment by phosphate is not likely to occur, even if the sediment itself is severely contaminated by antimony, as is the case of the Goesdorf sample.

The use of phosphate has been suggested in order to tackle acide mine drainage caused by weathering of pyrite (Huang and Evangelou, 1994). While this might be a logical recommendation for helping to immobilize potentially toxic cationic trace metals such as Pb, it would likely have the opposite effect on Sb.

In contrast, in the presence of environmentally realistic total carbonate concentrations (0.005 mol/L), the extent of desorption of Sb(V) is slightly increased (6.6±1.4% of total Sb at 5×10^{-3} M carbonate vs. 4.6±0.3% by the blank solution on PACS-2 sediment, and 1.83±0.01% at 5×10^{-3} M carbonate vs 1.34±0.36% by the blank solution on Goesdorf sediment, Fig. VI.10).

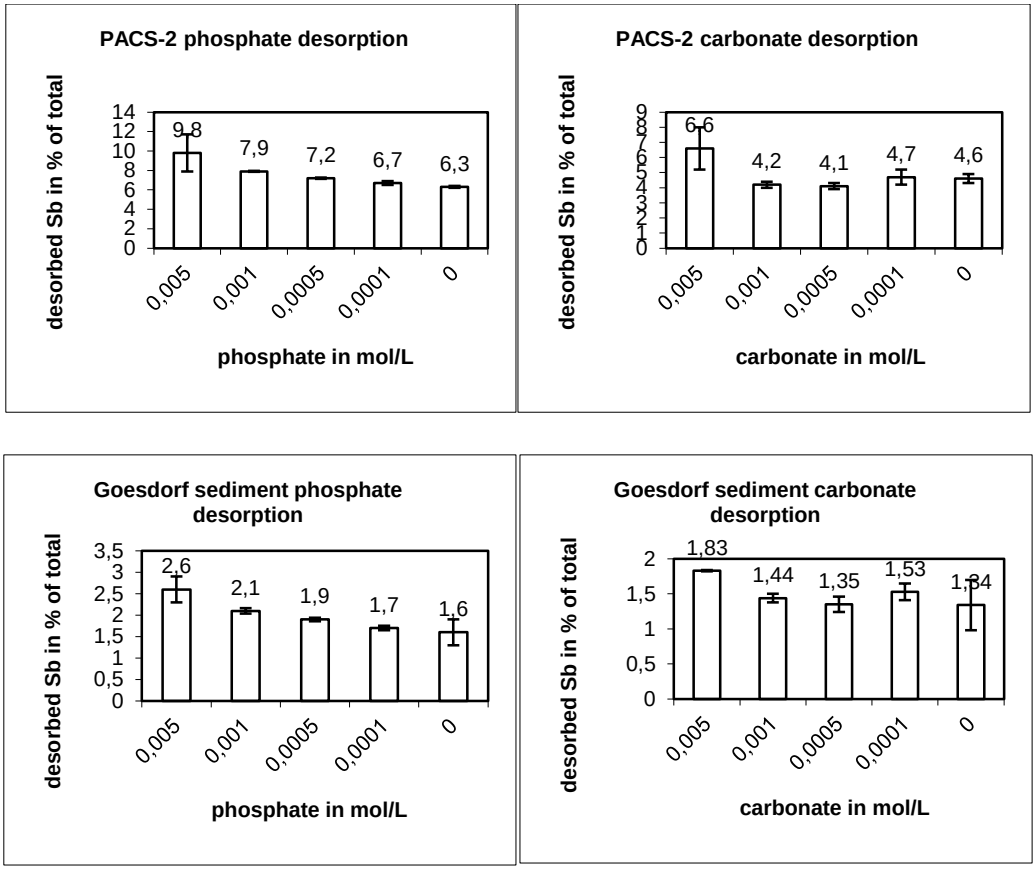

Fig. VI.10 Desorption of Sb(V) by phosphate and carbonate from PACS-2 and Goesdorf sediment.

Thus, carbonate at concentrations typical of natural waters with high alkalinity favours the desorption of sediment-bound antimony, however the effect is very slight. Remediation of acid mine drainage using carbonate minerals, therefore, may in fact slightly promote the mobilization of antimony downstream. The common anions chloride, sulfate and nitrate are not expected to contribute to the mobilization of Sb(V) from sediment within the concentration range they normally occupy.

The common occurrence of elevated Sb concentrations (up to hundreds of parts per million) in iron oxide ores (Goldschmidt, 1937) as well as recent lacustrine Fe and Mn oxide formations (Boyle and Jonasson, 1984) are clear

evidence of the importance of adsorption processes for the natural geochemical cycle of Sb. Phosphate is expected to compete with these sorption phenomena only when it is present in highly anomalous concentrations.

VI.5. Acknowledgements

Dr Constantin Hoch of the Max Planck Institut für Festkörperforschung, Stuttgart, is gratefully acknowledged for recording X-ray diffractograms and Prof. Garrison Sposito for his helpful comments on an earlier version of the paper.

VI.6. Supporting information

Numerical tables containing the information presented in the diagrams are available in Appendix A.IV.

VI.7. References for chapter VI

Adriano, D.C., Iskandar A.K. and Murarka I.P. (eds.) (1994) Contamination of Groundwaters (Advances in Environmental Science). Press Inc. Boca Raton.

Anawar, H.M., Akai J. and Sakugawa H. (2004) Mobilization of arsenic from subsurface sediments by effect of bicarbonate ions in groundwater. *Chemosphere* **54,** 753-762

Appelo, C.A.J., van der Weiden M.J.J., Tournassat C. and Charlet L. (2002) Surface complexation of ferrous iron and carbonate on ferrihydrite and the mobilization of arsenic*. Environ. Sci. Technol.* **36,** 3096-3103.

Atkinson R.J., Posner A.M. and Quirk J.P. (1972) Kinetics of Isotopic exchange of phosphate at the α-FeOOH-Aqueous Solution Interface. *J. Inorg. Nucl. Chem.* **34,** 2201-2211.

Balistrieri L.S. and Murray J.W. (1982) The surface chemistry of δ-MnO_2 in major ion seawater. *Geochim. Cosmochim. Acta* **46,** 1041-1052

Blay K. (1999) Sorption wässriger Antimon-Spezies an bodenbildende Festphasen und Remobilisierung durch natürliche Komplexbildner, PhD Thesis, Technische Universität München, Germany.

Boyle R.W. and Jonasson I.R. (1984) The geochemistry of antimony and its use as an indicator in geochemical prospecting. *J. Geochem. Explor.* **20,** 223-302

Cloy J.M., Farmer J.G., Graham M.C., MacKenzie A.B and Cook G.T.(2005) A comparison of antimony and lead profiles over the past 2500 years in Flanders Moss ombrotrophic Peat bog, Scotland. *J. Envir. Monit.* **7**, 1137-1147

Council of the European Communities (1976) Council Directive 76/464/EEC of 4 May 1976 on pollution caused by certain dangerous substances discharged into the aquatic environment of the Community. *Official Journal* **L 129**, 18/05/1976, pp. 23-29.

Diemar G.A., Filella M., Leverett P. and Williams P.A. (2008) Dispersion of antimony from oxidising ore deposits. 13th International Symposium on Solubility Phenomena and Related Equilibrium Processes (13th ISSP), Dublin, Ireland, 27-31 July 2008.

Duff M.C. and Amrhein C. (1996) Uranium(VI) adsorption on goethite and soil in carbonate solution. *Soil Sci. Soc. Am. J.* **60**, 1393-1400

Dzombak D.A. and Morel F.M.M. (1990) Surface Complexation Modeling. Hydrous Ferric Oxide; Wiley, New York.

Edzwald J.K., Toensing D.C. and Chi-Yew Leung M. (1976) Phosphate adsorption reactions with clay minerals*. Environ. Sci. Technol.* **10**, 485-490.

Emsley J. (2001) Nature's Building Blocks. An A-Z Guide to the Elements. Oxford University Press, Oxford

Filella M., Belzile N. and Chen, Y.-W. (2002) Antimony in the environment : a review focused on natural waters. I. Occurrence. *Earth-Science Reviews* **57**, 125-176

Filella M., Chanudet V., Philippo S. and Quentel F. (2009) Particle size and mineralogical composition of inorganic colloids in waters draining the adit of an abandoned mine, Goesdorf, Luxembourg. *Appl. Geochem.* **24**, 52-61

Furuta N., Iijima A., Kambe A., Sakai K. and Sato K. (2005) Concentrations, enrichment and predominant sources of Sb and other trace elements in size classified airborne particulate matter collected in Tokyo from 1995 to 2004. *J. Envir. Monit*. **7**, 1155-1161

Goldschmidt, V.M. (1937) The principles of distribution of chemical elements in minerals and rocks. The seventh Hugo Müller Lecture, delivered before the Chemical Society on March 17th, 1937. *J. Chem. Soc*. 655-673.

Gomez D.R, Giné M.F., Bellato A.C.S. and Smichowski P. (2005) Antimony: a traffic-related element in the atmosphere of Buenos Aires, Argentina. J. *Environ. Monit.* **7**, 1162-1168

Huang X. and Evangelou V.P.(1994) Suppression of Pyrite Oxidation Rate by Phosphate Addition. In Environmental Geochemistry of Sulfide Oxidation. ACS Symposium Series 550, C.N. Alpers, D.W. Blowes, Eds.; American Chemical Society: Washington DC 1994; chapter 34.

Johnson C.A., Moench H., Wersin P., Kugler P. and Wenger C.(2005) Solubility of antimony and other elements in samples taken from shooting ranges. *J. Environ. Qual.* **34**, 248-254

Kafkafi U., Bar-Yosef B., Rosenberg R. and Sposito G. (1988) Phosphorus adsorption by kaolinite and montmorillonite : II. Organic Anion Competition. *Soil Sci. Soc. Am. J.* **52**, 1585-1589.

Kawashima M., Tainaka Y., Hori T., Koyama M. and Takamatsu T. (1986) Phosphate adsorption onto hydrous manganese(IV) oxide in the presence of divalent cations. *Water Res.* **20**, 471-475.

Keon N.E., Swartz C.H., Brabander D.J., Harvey C. and Hemond H.F. (2001) Validation of an arsenic sequential extraction method for evaluating mobility in sediments. *Environ. Sci. Technol.* **35**, 2778-2784

Kim M.J., Nriagu J. and Haack S. (2000) Carbonate ions and arsenic dissolution by groundwater. *Environ. Sci. Technol*. **24**, 3094-3100

Kim M.J., Korshin G.V., Frenkel A.L. and Velichenko A.B. (2006) Electrochemical and EXAFS studies of effects of carbonate on the oxidation of arsenite. *Environ. Sci. Technol*. **40**, 228-234

Krachler M., Zheng J., Koerner R., Zdanowicz C., Fisher D. and Shotyk W. (2005) Increasing atmospheric antimony contamination in the northern hemisphere : snow and ice evidence from Devon Island, Arctic Canada. J. *Environ. Monit*. **7**, 1169-1176

Krachler M., Zheng J., Fisher D. and Shotyk W. (2008) Atmospheric Sb in the Arctic during the past 16,000 years: Responses to climate change and human impacts*. Global Biogeochem. Cycles*. **22**, GB1015

Li L. and Stanforth R.(2000) Distinguishing Adsorption and Surface Precipitation of Phosphate on Goethite (α-FeOOH). *J. Colloid. Interfac. Sci*. **230**, 12-21.

Lindner G., Kaminski S., Greiner I., Wunderer M., Behrschmidt J., Schroeder G. and Kress S. (1993) *Verh. Int. Verein. Limnol*. **25**, 238-241

Manning B.A. and Goldberg S. (1996) Modeling Arsenate Competitive Adsorption on Kaolinite, Montmorillonite and Illite. *Clay and Clay Minerals* **55**, 609-623

Murray J. (1973) The Surface Chemistry of Hydrous Manganese Dioxide, *J. Colloid Interface Sci.* **46**, 357-371

Mustafa S., Zaman M.I. and Khan S.(2006) pH Effect on phosphate sorption by crystalline MnO_2. *J. Colloid Interface Sci*. **301**, 370-375.

Nagarajah S., Posner A.M. and Quirk J.P. (1968) Desorption of phosphate from kaolinite by citrate and bicarbonate. *Soil Sci. Soc. Am. J.* **32**, 507-510.

Nakamaru Y., Tagami K. and Uccida S. (2006) Antimony mobility in japanese agricultural soils and factors affecting antimony sorption behavior. *Environ. Poll.* **141**, 321-326

Parfitt R.L. (1978) Anion adsorption by soils and soil materials. *Adv. Agron.* **30**, 1-50 and references cited therein.

Parfitt R.L., Farmer V.C. and Russell J.D. (1977) Adsorption on Hydrous Oxides. I. Oxalate and Benzoate on Goethite. *J. Soil Sci*. **28**, 24-39.

Parfitt R.L. and Russell J.D. (1977) Adsorption on Hydrous Oxides. IV. Mechanism of Adsorption of various Anions on Goethite. *J. Soil Sci.* **28**, 297-305

Quentel F. and Filella M. (2002) Determination of inorganic antimony species in seawater by differential pulse anodic stripping voltammetry : stability of the trivalent state*. Anal. Chim. Acta* **452**, 237-244

Rietra R.P.J.J., Hiemstra T. and Riemsdijk W.H.(2000) Electrolyte anion affinity and its effects on oxyanion adsorption on goethite. *J. Colloid and Interface Science* **229**, 199-206

Russell J.D., Paterson E., Fraser A.R. and Farmer V.C. (1975) Adsorption of carbon dioxide on goethite (α-FeOOH) surfaces and its implications for anion adsorption*. J. Chem. Soc. Faraday Trans*. **71**, 1623-1630

Scheinost A.C., Rossberg A., Vantelon D., Xifra I., Kretzschmar R., Leuz A.-K., Funke H. and Johnson C.A. (2006) Quantitative antimony speciation in

shooting range soils by EXAFS spectroscopy. *Geochim. et Cosmochim. Acta.* **70**, 3299-3312

Schulthess C.P. and McCarthy J.F. (1990) Competitive adsorption of aqueous carbonic and acetic acids on an aluminum oxide. *Soil Sci. Soc. Am. J.* **54**, 688–694

Shotyk W., Krachler M. and Chen B. (2004) Antimony in recent, ombrotrophic peat from Switzerland and Scotland: Comparison with natural background values (5,320 and 8,020 14C yr BP) and implications for the global atmospheric Sb cycle. *Global Biogeochemical Cycles* **18**, BG1016.

Shotyk W., Chen B. and Krachler M. (2005) Lithogenic, oceanic and anthropogenic sources of atmospheric Sb to a maritime blanket bog, Myarnar, Faroe Islands. *J. Environ. Monit*. **7**, 1148-1154

Shotyk W., Krachler M., Aeschbach-Hertig W., Hillier S. and Zheng J.(2010) Trace elements in recent groundwater of an artesian flow system and comparison with snow: enrichments, depletions, and chemical evolution of the water. *J. Environ. Monit*. **12**, 208-217

Sigel A., Sigel H. and Sigel R. (2005) Metal Ions in Biological Systems, Volume 44: Biogeochemistry, Availability, and Transport of Metals in the Environment. Dekker, New York.

Sigg L. and Stumm W. (1980) The interaction of anions and weak acids with the hydrous goethite (α-FeOOH) surface. *Colloids and Surfaces*. **2**, 101-117

Sposito, G. 2008. The Chemistry of Soils. Oxford University Press, Oxford.

Takamatsu T., Kawashima M. and Koyama M. (1985) The role of Mn^{2+}-rich hydrous manganese oxide in the accumulation of arsenic in lake sediments. *Water Res*. **19**, 1029-1032.

Tanada S., Kabayama M., Kawasaki N., Sakiyama T., Nakamura T., Araki M. and Tamura T. (2003) Removal of phosphate by aluminium oxide hydroxide, *J. Colloid Interface Sci.* **257**:135-140.

Tejedor-Tejedor I. and Anderson M. (1986) 'In Situ' attenuated total reflection fourier transform infrared studies of the goethite (α-FeOOH) –aqueous solution interface. *Langmuir* **2**, 203-210

Tighe M., Lockwood P. and Wilson S.(2005) Adsorption of antimony(V) by floodplain soils, amorphous iron(III) hydroxide and humic acid. *J. Environ. Monit.* **7**, 1177-1185

United States Environmental Protection Agency (1979) Water Related Fate of the 129 Priority Pollutants, vol. 1. USEPA, Washington, DC, USA, EP-440/4-79-029A.

Ure A.M. and Davidson C.M. (2002) Chemical Speciation in soils and related materials by selective chemical extraction. In Chemical Speciation in the Environment, Ure, A.M.; Davidson, C.M., Eds., Blackwell Science, Oxford.

Van Geen A., Robertson A.P. and Leckie J.O. (1994) Complexation of carbonate species at the goethite surface : implications for adsorption of metal ions in natural waters. *Geochim. Cosmochim. Acta* **58**, 2073-2086

Weckwerth G. (2001) Verification of traffic emitted aerosol components in the ambient air of Cologne (Germany). *Atmospheric environment* **35**, 5525-5536

Weckwerth G. (2010) Origin of fine dust in urban environmental zones – Evidence from element patterns reveived by dichotomous collection and INAA*. Applied radiation and isotopes* **68**, 1878-1883

Wijnja H. and Schulthess C.P (2000a) Interaction of carbonate and organic anions with sulfate and selenate adsorption on an aluminum oxide. *Soil Sci. Soc. Am. J.* **64**, 898-908

Wijnja, H. and Schulthess C.P. (2000b) Vibrational Spectroscopy Study of Selenate and Sulfate Adsorption Mechanism on Fe and Al (Hydr)oxide Surfaces. *J. Colloid Interface Sci*. **229**, 286-297

Wijnja, H. and Schulthess C.P. (2002) Effect of carbonate on the adsorption of selenate and sulfate on goethite. *Soil Sci. Soc. Am. J*. **66**, 1190-1197

Yao W. and Millero F.J. (1996) Adsorption of Phosphate on Manganese Dioxide in Seawater. *Environ. Sci. Technol.* **30**, 536-541.

Zachara J.M., Girvin D.C., Schmidt R.L. and Resch C.T. (1987) Chromate adsorption on amorphous iron oxyhydroxides in the presence of major groundwater ions. *Environ. Sci. Technol.* **21**, 589-594

Appendix AI

Literature Synopsis ‘Antimony in Plants’ and Plant Inventory at the Goesdorf Site

Antimony in plants
Literature synopsis

Species	Type	Concentration/ mg Sb kg^{-1}	Part	Digestion	Technique	Reference
Achillea ageratum (1)[i]	N[ii]	1.68	Root	$HNO_3+H_2O_2$	HG-AAS	Baroni et al. (2000)
		6.09	Basal lf			
Achillea ageratum (2)	C	6.83	Root			
		8.09	Shoot			
		8.75	Basal lf			
		9.27	Cauline lf			
		27.08	Infloresc.			
Achillea ageratum (3)	C	337.92	Root			
		121.35	Basal lf			
Achillea ageratum (4)	C	193.40	Root			
		227.95	Shoot			
		74.27	Basal lf			
		164.31	Cauline lf			
		306.19	Infloresc.			
Achillea ageratum (5)	C	206.35	Root			
		215.75	Shoot			
		1367.29	Basal lf			
		358.61	Cauline lf			
		1105.26	Infloresc.			
Achillea ageratum (6)	C	129.61	Root			
		96.38	Shoot			
		329.51	Basal lf			
		128.15	Cauline lf			
		217.36	Infloresc.			
Plantago lanceolata (1)	C	10.37	Root			

Species	Type	Concentration/ mg Sb kg^{-1}	Part	Digestion	Technique	Reference
		28.45	Basal lf	$HNO_3+H_2O_2$	HG-AAS	Baroni et al. (2000)
Plantago lanceolata (2)	C	185.31	Root			
		53.64	Basal lf			
Plantago lanceolata (3)	C	93.47	Root			
		33.58	Basal lf			
Plantago lanceolata (4)	C	1150.31	Root			
		569.34	Basal lf			
Plantago lanceolata (5)	C	741.37	Root			
		274.63	Basal lf			
Silene vulgaris	C	16.09	Root			
		35.47	Shoot			
		51.77	Basal lf			
Silene vulgaris	C	13.75	Root			
		17.61	Shoot			
		19.45	Basal lf			
Silene vulgaris	C	249.52	Root			
		1163.81	Shoot			
		853.75	Basal lf			
Silene vulgaris	C	209.81	Root			
		473.55	Shoot			
		349.62	Basal lf			
Cytisus striatus (spring)	N	1.0	Total ?	n/a	NAA	Murciego et al. (2006)
Cytisus striatus (spring)	C	1.0				
Cistus ladanifer (1) (spring)	N	0.0				
Cistus ladanifer (1) (autumn)	N	0.1				
Cistus ladanifer (1) (spring)	C	3.9				
Cistus ladanifer (1) (autumn)	C	8.1				
Cistus ladanifer (2) (spring)	N	0.5				

Species	Type	Concentration/ mg Sb kg^{-1}	Part	Digestion	Technique	Reference
Cistus ladanifer (2) (autumn)	N	0.2	Total ?	n/a	NAA	Murciego et al. (2006)
Cistus ladanifer (2) (spring)	C	20.2				
Cistus ladanifer (2) (autumn)	C	36.8				
Cistus ladanifer (3) (spring)	C	74.3				
Cistus ladanifer (3) (autumn)	C	59.3				
Dittrichia viscosa (spring)	N	22.4				
Dittrichia viscosa (spring)	C	1136.0				
Daucus carota (1)	C	<0.02-0.03	Edible parts	$HNO_3+H_2O_2$	HG-AAS	Hammel et al. (2000)
Daucus carota (2)	C	0.17-0.80	Leafs			
Beta vulgaris (1)	C	<0.02-0.09	Edible parts			
Beta vulgaris (2)	C	<0.02				
Allium cepa	C	<0.02-0.03				
Solanum tuberosum	C	<0.02				
Cichorium endiva	C	0.14-2.20				
Valerianella locusta	C	0.31-1.00				
Brassica oleracea	C	0.08-0.28				
Spinacia oleracea	C	0.15-1.13				
Petrosilenum crispum (1) (annual)	C	0.05-0.42				
Petrosilenum crispum (2) (biannual)	C	0.13-1.73				
Zea mays	C	0.06-0.35				
« Herbage »	C	<0.02-0.08				
Lypersicon esculentum	C	<0.02	Fruit & Grain			
Triticum aestivum	C	<0.02	Grain	$HNO_3+H_2O_2$	HG-AAS	Hammel et al. (2006)

Species	Type	Concentration/ mg Sb kg^{-1}	Part	Digestion	Technique	Reference
Hordeum vulgare	C	<0.02	Grain	$HNO_3+H_2O_2$	HG-AAS	Hammel et al. (2006)
Secale cereale	C	<0.02				
Avena sativa	C	<0.02-0.06				
Sambucus[iii] [Virgin elder] (1)	N	5.2	Leaf	$HNO_3+HF+HClO_4+H_2SO_4$	HG-AAS	Krachler et al. (1999)
Sambucus [Virgin elder] (2-6)	C	153-589				
Populus[ii] [Virgin poplar] (1,2)	N	3.9-4.3	Leaf			
Populus [Virgin poplar] (3-6)	C	19.6-150	Leaf			
Picea[ii] [Spruce] (1)	N	64	Shoot			
Picea [Sruce] (2)	C	51				
Fagus[ii] [Beech] (1)	N	39	Leaf			
Agropyron repens (1-6)	C	56-336	Leaf	HNO_3	AAS	Ainsworth et al. (1989)
Agropyron repens (7-12)	C	8-24				
Dactylis glomerata (1-6)	C	48-152				
Dactylis glomerata (7-12)	C	8-30				
Dactylis glomerata (13-17)	N	0.1-0.32				
Festuca rubra (1-6)	C	64-232				
Festuca rubra (7-12)	C	15-28				
Hydnum cupressiforme	C	27.05	Total ?	$HNO_3+H_2O_2$	HG-AAS	Miravet et al. (2005)
Dryopteris filix-max (1)	C	17.08				
Dryopteris filix-max (2)	C	28.19				
Stellaria halostea	C	7.87				
Chaenorhinum asarina	C	26.23				

[i] Numbers refer to individual samples or mean values of samples
[ii] N,C = plant grown non-contaminated or contaminated soil, respectively
[iii] The authors' species taxonomy is incomplete

Inventory of Plants at the Goesdorf Mining Site (Colling, 2006):

Achillea millefolium	Trifolium campestre
Agrostis capillaris	Trifolium repens
Bromus hordeaceus	Vicia cracca
Cerastium semidecandrum	Ajuga reptans
Crepis capillaris	Cardamine flexuosa
Cytisus scoparius	Cardamine pratensis
Dactylis glomerata	Carex demissa
Elymus repens	Chrysosplenium oppositifolium
Festuca grex	Cirsium palustre
Hieracium pilosella	Dryopteris carthusiana
Hypericum perforatum	Dryopteris filix-mas
Hypochoeris radicata	Epilobium montanum
Lolium perenne	Epilobium parviflorum
Malva moschata	Galeopsis tetrahit
Matricaria maritima inodora	Galium palustre
Poa annua	Geranium robertianum
Poa pratensis	Geum urbanum
Poa trivialis	Hypericum
Rumex acetosa	Lamium galeobdolon
Rumex acetosella	Milium effusum
Rumex crispus	Poa trivialis
Senecio jacobaea	Ranunculus repens
Taraxacum	Senecio ovatus
Trifolium arvense	Urtica dioica

References for Appendix AI

Ainsworth N. and Cooke J.A. (1990) Distribution of Antimony in Contaminated Grassland: 1-Vegetation and Soils. *Environ. Pollut.* **65**, 65-77

Baroni F., Boscagli A., Protano G. and Riccobono F. (2000) Antimony in *Achillea ageratum, Plantago lanceolata* and *Silene vulgaris* growing in an old Sb-mining area*. Environ. Pollut.* **109**, 347-352

Colling C. (2006) Personal Communication

Hammel W., Debus R. and Steubing L. (2000) Mobility of antimony in soil and its availability to plants. *Chemosphere* **41**, 1791-1798

Krachler M. and Emons H. (2000) Extraction of antimony and arsenic from fresh and freeze-dried plant samples as determined by HG-AAS. *Fresenius J. Anal. Chem.* **368**, 702-707

Miravet R., Bonilla E., Lopez-Sanchez J.F. and Rubio R. (2005) Antimony speciation in terrestrial plants. Comparative studies on extraction methods. *J. Environ. Monit.* **7**, 1207-1213

Murciego Murciego A., Garcia Sanchez A., Rodriguez Gonzalez M.A., Pinilla Gil E., Toro Gordillo C., Cabezas Fernandez J. and Buyolo Triguero T. (2007) Antimony distribution and mobility in topsoils and plants (*Cytisus striatus, Cistus ladanifer* and *Dittrichia viscosa*) from polluted Sb-mining areas in Extremadura (Spain). *Environ. Pollut.* **145**, 15-21

Appendix AII

Sequential Extraction Analyses of Sediments

from the Goesdorf Mining Site

Sediments taken from the drainage tunnel of the abandoned antimony mine in Goesdorf, Luxembourg, and from the receiving creeks and rivers were collected and analysed according to the BCR scheme (chapter I.8.3.4). See Fig. I.3 for a map with the sampling points, and Table I.8 for details on the BCR scheme.

The sediment was sampled by hand, using a PP beaker, air dried and sieved. The fraction below 0.5 mm was retained for analysis. The creek draining the mine and the receiving creek called 'Schnäp' are fast-flowing with a stony bed, with very little sediment. This is the reason why no finer fraction was chosen.

The analytical data in the tables below are expressed as ppm of dry sediment (the error is always smaller than 5%). The elements Sb, Zn, Cd, Pb, Ni and Co were determined voltammetrically and Cu, Fe, Mn and Al were determined by optical ICP. In some samples, correlations are observed between

- Sb in the reducible fraction (fraction 2) and Mn+Fe in fraction 2
- Sb in the reducible fraction and total Al
- total Sb and total Al
- total Sb and total Pb

In the correlation graphs (Figs AII.1-4), the data labels 'US' and 'DS' refer to samples taken upstream and downstream of a confluence, respectively.

Sample origin : **MINE ADIT**

Element	**Fraction 1**	**Fraction 2**	**Fraction 3**	**Total**
Sb	2.9	20.4	2.7	26.0
Zn	141.1	111.1	2.6	254.8
Cd	0.3	0.2	0	0.5
Pb	0.6	16.9	0.06	17.6
Cu	5.6	2.1	1.9	9.6
Fe	14.0	1753.9	17.9	1785.8
Mn	374.2	1730.7	15.2	2120.1
Al	66.0	177.7	31.1	274.8
Ni	7.7	21.1	0.7	29.5
Co	1.3	11.7	0	13.0

Sample mass/g	Residual fraction mass/g	Percentage analysed
0.8873	0.6719	24.27

Table AII.1 Sequential extraction data for sediment from the mine adit

Sample origin : **UNNAMED CREEK** (directly receives the mine drainage)

Element	**Fraction 1**	**Fraction 2**	**Fraction 3**	**Total**
Sb	1.8	2.4	1.6	5.8
Zn	95.9	109.7	9.3	214.9
Cd	0.1	0.09	0.008	0.2
Pb	1.1	5.4	0.1	6.6
Cu	0.8	6.0	2.7	9.5
Fe	26.2	767.9	25.1	819.2
Mn	442.4	241.9	16.1	700.4
Al	412.4	552.8	144.7	1109.9
Ni	11.3	4.3	2.0	17.6
Co	1.6	0.5	5.4	7.5

Sample mass/g	Residual fraction mass/g	Percentage analysed
0.8692	0.7432	14.50

Table AII.2 Sequential extraction data for sediment from the creek receiving the mine drainage

Sample origin : **SCHLIERBACH UPSTREAM**

Element	**Fraction 1**	**Fraction 2**	**Fraction 3**	**Total**
Sb	0.4	1.0	0.5	1.9
Zn	106.2	10.6	18.4	135.2
Cd	0.3	0.1	0	0.4
Pb	0.7	5.4	1.7	7.8
Cu	1.7	0.6	3.1	5.4
Fe	13.6	1507.8	27.3	1548.7
Mn	401.4	711.7	45.9	1159.0
Al	189.3	345.3	532.7	1067.3
Ni	9.4	10.1	4.8	24.3
Co	0.2	5.3	0.6	6.1

Sample mass/g	Residual fraction mass/g	Percentage analysed
1.0512	0.9075	13.67

Table AII.3 Sequential extraction data for sediment from the 'Schlierbach', upstream from the confluence with the 'Schnäp'

Sample origin : **SCHLIERBACH DOWNSTREAM**

Element	**Fraction 1**	**Fraction 2**	**Fraction 3**	**Total**
Sb	0.1	0.7	3.2	4.0
Zn	9.0	10.8	9.2	29.0
Cd	0.07	0.2	0	0.3
Pb	0.2	10.3	0.2	10.7
Cu	1.2	0.5	1.6	3.3
Fe	5.5	1254.2	1.5	1262.2
Mn	211.9	664.9	22.9	899.7
Al	104.6	296.7	79.7	481.0
Ni	8.5	7.8	2.4	18.7
Co	0.4	5.4	0	5.8

Sample mass/g	Residual fraction mass/g	Percentage analysed
1.0415	0.8943	14.13

Table AII.4 Sequential extraction data for sediment from the 'Schlierbach', downstream from the confluence with the 'Schnäp'

Sample origin : **SCHLIERBACH-SURE**

Element	**Fraction 1**	**Fraction 2**	**Fraction 3**	**Total**
Sb	0.2	0.3	0.2	0.7
Zn	32.3	5.9	3.6	41.8
Cd	0.2	0.1	0.02	0.3
Pb	0.4	3.7	0.2	4.3
Cu	1.7	0.5	3.3	5.5
Fe	9.4	1703.8	24.4	1737.6
Mn	735.7	551.7	13.6	1301.0
Al	198.6	414.7	243.3	856.6
Ni	12.8	4.6	3.9	213.0
Co	2.1	3.6	0.9	6.6

Sample mass/g	Residual fraction mass/g	Percentage analysed
0.9090	0.6993	23.07

Table AII.5 Sequential extraction data for sediment from the 'Schlierbach', close to the confluence with the 'Sûre'

Sample origin : **SCHNÄP UPSTREAM**

Element	**Fraction 1**	**Fraction 2**	**Fraction 3**	**Total**
Sb	0.2	0.8	0.1	1.1
Zn	61.7	14.6	10.1	86.4
Cd	0.1	0.06	0.003	0.2
Pb	0.4	5.2	0.3	5.9
Cu	2.6	0.6	8.9	12.1
Fe	8.5	1626.5	7.4	1642.4
Mn	443.8	1010.1	84.5	1538.4
Al	310.4	693.4	1035.0	2038.8
Ni	0.8	4.0	4.9	9.7
Co	0.7	4.0	0	4.7

Sample mass/g	Residual fraction mass/g	Percentage analysed
0.9937	0.8131	18.27

Table AII.6 Sequential extraction data for sediment from the 'Schnäp', upstream from the confluence with the unnamed creek

Sample origin : **SCHNÄP DOWNSTREAM 1st sample**

Element	Fraction 1	Fraction 2	Fraction 3	Total
Sb	1.3	3.0	0.9	5.2
Zn	155.0	36.0	2.4	193.4
Cd	0.2	0	0	0.2
Pb	1.3	9.9	1.3	12.5
Cu	10.5	1.1	4.3	15.9
Fe	44.0	2295.9	80.3	2420.2
Mn	673.8	607.1	5.9	1286.8
Al	826.2	968.6	340.7	2135.5
Ni	9.5	6.2	0	15.7
Co	3.7	4.5	0	8.2

Sample mass/g	Residual fraction mass/g	Percentage analysed
0.3283	0.1716	47.73

Table AII.7 Sequential extraction data for sediment from the 'Schnäp' downstream from the confluence with the unnamed creek, 1st sample

Sample origin : **SCHNÄP DOWNSTREAM 2nd sample**

Element	Fraction 1	Fraction 2	Fraction 3	Total
Sb	0.2	0.5	0.2	0.9
Zn	68.1	30.2	2.3	100.6
Cd	0.1	0.07	0.01	0.2
Pb	0.2	3.8	0.1	4.1
Cu	1.8	1.1	4.6	7.5
Fe	3.9	1351.5	12.5	1367.9
Mn	457.9	1123.0	13.3	1594.2
Al	156.9	399.0	155.3	711.2
Ni	4.3	3.8	1.1	9.2
Co	1.0	6.4	0	7.4

Sample mass/g	Residual fraction mass/g	Percentage analysed
1.0613	0.8609	57.38

Table AII.8 Sequential extraction data for sediment from the 'Schnäp' downstream from the confluence with the unnamed creek, 2nd sample

Sample origin : **WILTZ AT WINSELER (UNCONTAMINATED CONTROL)**

Element	**Fraction 1**	**Fraction 2**	**Fraction 3**	**Total**
Sb	0.2	0.2	0.2	0.6
Zn	171.5	87.3	1.9	260.7
Cd	0.5	0.07	0.2	0.8
Pb	1.8	6.7	1.0	9.5
Cu	2.2	6.5	1.5	10.2
Fe	21.3	1100.7	13.2	1135.2
Mn	310.4	157.1	2.8	470.3
Al	217.0	232.1	62.2	511.3
Ni	27.3	2.6	0.9	30.8
Co	1.3	7.8	0	9.1

Sample mass/g	Residual fraction mass/g	Percentage analysed
0.9358	0.8812	5.83

Table AII.9 Sequential extraction data for sediment from the river 'Wiltz' at Winseler, essentially uncontaminated (control sample)

Sample origin : **WILTZ AT WILTZ (CONTAMINATED CONTROL)**

Element	**Fraction 1**	**Fraction 2**	**Fraction 3**	**Total**
Sb	0.6	0.7	0.3	1.6
Zn	148.5	31.0	12.8	192.3
Cd	1.0	0.2	0.03	1.2
Pb	1.9	8.6	0.2	10.7
Cu	6.1	1.0	13.5	20.6
Fe	84.8	1155.6	17.7	1258.1
Mn	444.5	77.9	10.4	532.8
Al	442.6	409.8	176.6	1029.0
Ni	19.9	2.6	2.9	254.0
Co	1.9	0.8	0	2.7

Sample mass/g	Residual fraction mass/g	Percentage analysed
1.0438	0.7383	29.27

Table AII.10 Sequential extraction data for sediment from the river 'Wiltz' at Wiltz, moderate industrial contamination

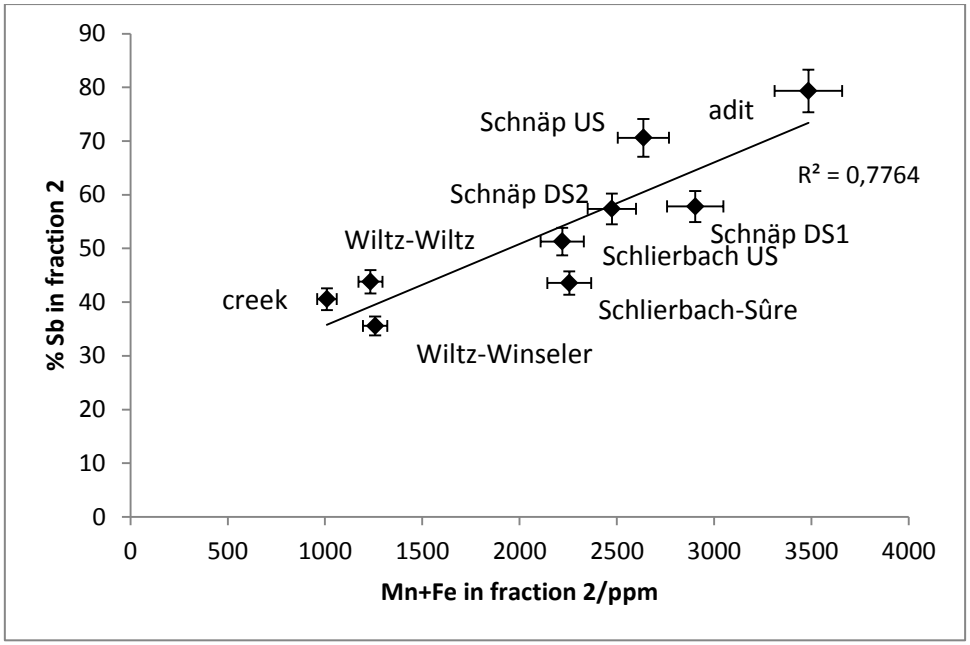

Fig.AII.1 Correlation between %Sb in fraction 2 vs sum of Fe+Mn in fraction 2

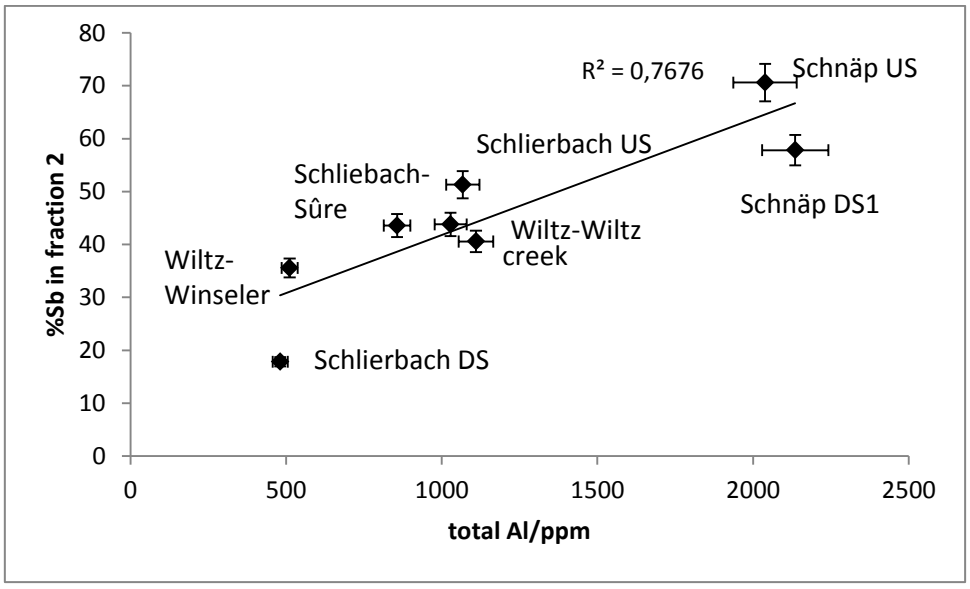

Fig.AII.2 Correlation between %Sb in fraction 2 vs total Al

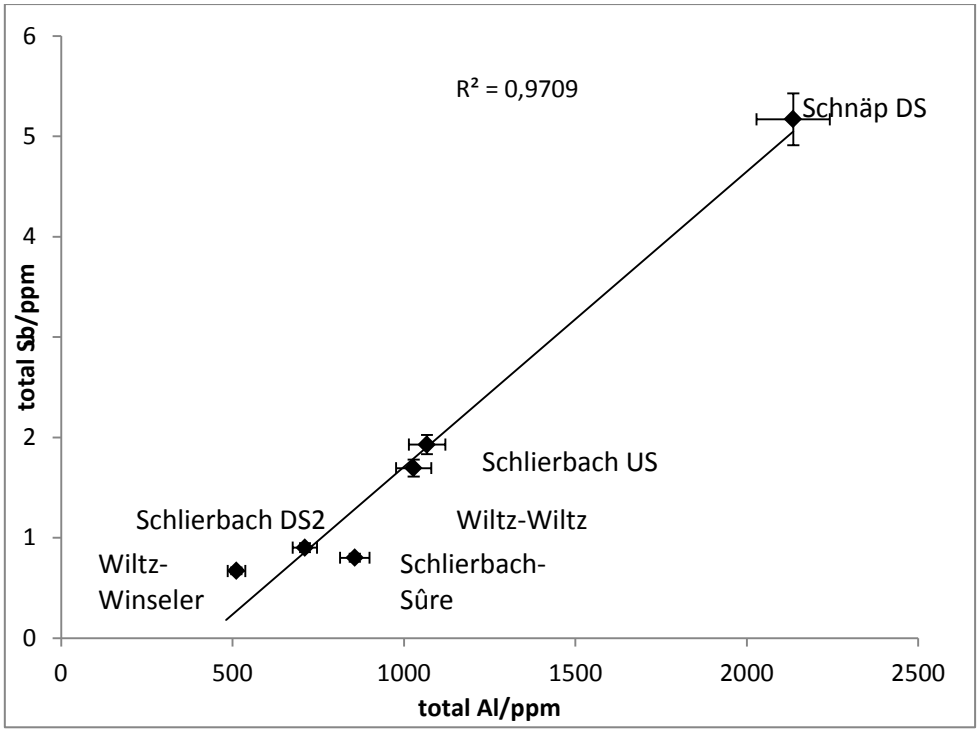

Fig.AII.3 Correlation between total Sb and total Al

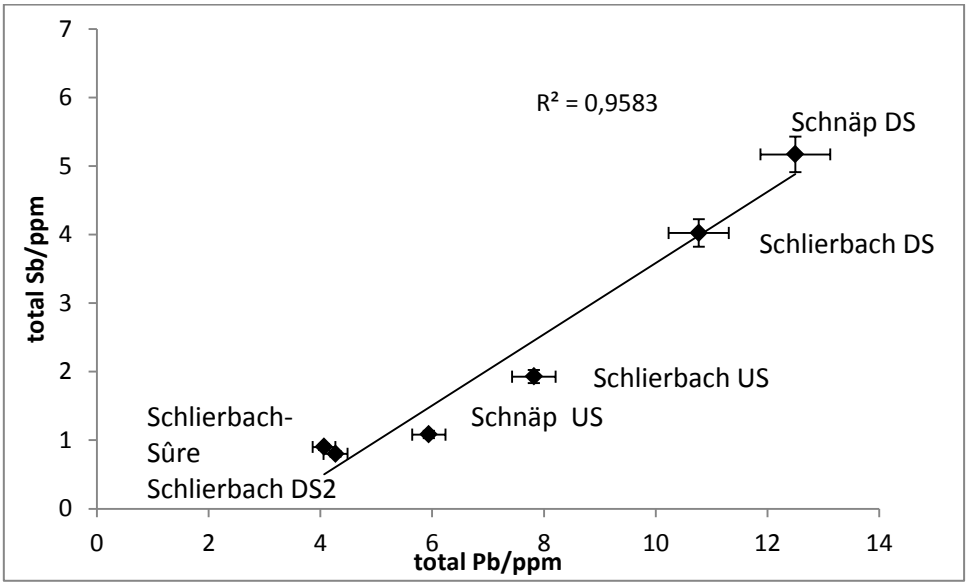

Fig.AII.4 Correlation between total Sb and total Pb

Appendix AIII

Macroscopic Physical Properties of the Minerals

Used in this Work

(These data are taken from the online database www.webminerals.com)

AIII.1 Stibnite

Cleavage: {010} Perfect

Color: Lead gray, Bluish lead gray, Steel gray, Black.

Density: 4.63

Diaphaneity: Opaque

Fracture: Conchoidal - Fractures developed in brittle materials characterized by smoothly curving surfaces, (e.g. quartz).

Habit: Granular - Generally occurs as anhedral to subhedral crystals in matrix.

Habit: Prismatic - Crystals Shaped like Slender Prisms (e.g. tourmaline).

Habit: Striated - Parallel lines on crystal surface or cleavage face.

Hardness: 2 – Gypsum

Luminescence: Non-fluorescent.

Luster: Metallic

Streak: blackish gray

AIII.2 Senarmontite

Cleavage: {111} Imperfect, {111} Imperfect, {111} Imperfect

Color: White, Colorless, Gray.

Density: 5.2 - 5.3, Average = 5.25

Diaphaneity: Transparent to translucent

Fracture: Uneven - Flat surfaces (not cleavage) fractured in an uneven pattern.

Habit: Encrustations - Forms crust-like aggregates on matrix.

Habit: Euhedral Crystals - Occurs as well-formed crystals showing good external form.

Habit: Massive - Granular - Common texture observed in granite and other igneous rock.

Hardness: 2 – Gypsum

Luminescence: Non-fluorescent.

Luster: Adamantine

Streak: white

AIII.3 Valentinite

Cleavage: {110} Perfect, {010} Distinct

Color: Brownish reddish, Colorless, Gray white, Grayish, Yellowish.

Density: 5.6 - 5.8, Average = 5.69

Diaphaneity: Transparent

Fracture: Uneven - Flat surfaces (not cleavage) fractured in an uneven pattern.

Habit: Divergent - Crystals radiate from a center without producing stellar forms.

Habit: Euhedral Crystals - Occurs as well-formed crystals showing good external form.

Habit: Striated - Parallel lines on crystal surface or cleavage face.

Hardness: 2.5-3 - Finger Nail-Calcite

Luminescence: Non-fluorescent.

Luster: Adamantine

Streak: white

AIII.4 Stibiconite

Cleavage: None

Color: Brown, Gray, Lemon white, Light yellow, Orange brown.

Density: 4.1 - 5.8, Average = 4.94

Diaphaneity: Transparent to translucent

Fracture: Earthy - Dull, clay-like fractures with no visible crystalline affinities, (e.g. howlite).

Habit: Earthy - Dull, clay-like texture with no visible crystalline affinities, (e.g. howlite).

Habit: Encrustations - Forms crust-like aggregates on matrix.

Hardness: 4-5 - Fluorite-Apatite

Luminescence: Non-fluorescent.

Luster: Vitreous - Dull

Streak: light yellow

Appendix AIV

Determination of Elemental Sulfur on Mineral Surfaces, and Application to Weathering of thirteen Sulfides in Acidic Solutions

Abstract. A new method for the determination of elemental sulfur on weathered sulfide mineral surfaces is presented. Sulfur is extracted using cyclohexane and determined by direct UV photometry. The method represents two significant improvements over existing methods in that it has a much lower limit of detection (approximately three orders of magnitude) and it circumvents the use of toxic solvents. Thirteen sulfide minerals, namely arsenopyrite (FeAsS), bornite (Cu_5FeS_4), chalcocite (Cu_2S), chalcopyrite ($CuFeS_2$), cinnabar (HgS), enargite (Cu_3AsS_4), galena (PbS), orpiment (As_2S_3), pyrite (FeS_2), pyrrhotite ($Fe_{1-x}S$) stibnite (Sb_2S_3), zinc blende (sphalerite, α-(Zn,Fe)S), and fahlore were subjected to weathering in the laboratory under acid mine drainage (pH 1, oxic) conditions. Elemental sulfur released to the aqueous phase was determined using an existing voltammetric technique. Total dissolved sulfur and metals released were determined using ICP-OES. All of the minerals studied dissolve incongruently, with elemental sulfur on the dissolving mineral surface accounting for a substantial proportion of the total sulfur released upon weathering. In addition, the amount of elemental sulfur released to the aqueous phase is always in excess of its solubility in water, with supersaturation up to eight times in the case of pyrite. Clearly, elemental sulfur, both in the aqueous phase and on the surface of reacting metal sulfdes, must be carefully considered in any experimental studies of weathering in acid mine drainage conditions.

AIV.1 Introduction

Metal sulfide weathering, and the acid mine drainage which it often creates, is a contemporary environmental problem affecting surface waters and groundwaters worldwide (Edwards et al., 2000; Domènech et al., 2002; Moncur et al., 2005; Moncur et al., 2009; Asta et al., 2010; Alpers and Blowes, 1994; Lottermoser, 2007). For a comprehensive review of acid mine drainage, see (Nordstrom, 2000). Whether the sulfide minerals are hosted in massive sulfide ore deposits, coal, or black shales, an important step towards understanding the relevant chemical transformations is the speciation of the released sulfur. With four possible formal oxidation states, sulfate is the dominant aqueous species in oxic solutions, sulfide in anoxic solutions, but elemental sulfur is also commonly found in sedimentary environments. Numerous studies have shown that elemental sulfur formed at the surface of mineral grains is one of the products of oxidative weathering of sulfide minerals. Elemental sulfur has been detected using X-ray photoelectron spectroscopy (Sasaki et al., 1995; Mycroft et al., 1990), Raman spectroscopy (Sasaki et al., 1995; Mycroft et al., 1990; Turcotte and Benner, 1993) and near-infrared Raman imaging microscopy (McGuire et al., 2001) and HPLC after solvent extraction of the mineral (McGuire et al., 2000).

McGuire et al. (2000) proposed a powerful analytical tool for the determination of elemental sulfur on mineral surfaces, involving extraction of the mineral surface by a solvent which dissolves sulfur well (tetrachloroethene) and subsequent quantification of sulfur in the dissolved state by HPLC. Nevertheless,

the proposed method suffers from a few disadvantages: the detection limit, given by the authors as 5 mg S(0)/l, is relatively high, so that comparatively large masses of sample must be processed. The method requires costly instrumentation (HPLC) but more importantly, uses highly toxic and environmentally problematic solvents, namely carbon disulfide and tetrachloroethene. The LD_{50} values of tetrachloroethene for mice are between 2,400 and 13,000 mg/kg (US National Library of Medicine, 2010) and the compound has been found to induce cancer in laboratory animals, and can reasonably be expected to do so in humans (US National Library of Medicine, 2010; US Environmental Protection Agency, 2010). The central nervous system is a major target for tetrachloroethene toxicity, with a threshold for acute inhalation toxicity in the range of 100-200 ppmv (US Environmental Protection Agency, 2010).

Here, we present an alternative extraction solvent, namely cyclohexane. The LD_{50} of cyclohexane for mice is 29,820 mg/kg (US National Library of Medicine, 2010), it has not been found to be carcinogenic and has a low acute toxicity (US Environmental Protection Agency, 2010). Moreover, elemental sulfur dissolved in cyclohexane may be directly determined by its strong absorption in the ultraviolet. Beer's law is obeyed between 1 and 4 mg l^{-1}, with a detection limit well below 1 mg l^{-1}. Samples with higher concentrations than 4 mg l^{-1} may be analysed after dilution, or by two alternative photometric methods.

Elemental sulfur contained in the aqueous phase was determined by McGuire et al. (2000) by filtration of a large sample volume and extraction of the

filter paper by tetrachloroethene. Truly dissolved sulfur in the aqueous phase is therefore ignored. We propose the use of square-wave voltammetry, which requires a much smaller sample volume (maximum 6 ml vs. 40 ml) and is much more sensitive (detection limit below 1 µg l^{-1}). Using this approach, we find that acid solutions in contact with weathering sulfides very quickly become supersaturated with respect to elemental sulfur.

The new experimental techniques were applied to the experimental weathering of thirteen sulfide minerals in 0.1 M perchloric acid with access of atmospheric oxygen at room temperature. In addition to the measurements of elemental sulfur, the released amounts of metals as well as total aqueous sulfur were determined using ICP-OES. In each case it was shown that oxidative dissolution of the sulfides was always highly incongruent, leading to a metal-depleted (and consequently sulfur-enriched) phase, with a very substantial proportion of total released sulfur being present as an elemental sulfur coatings on the surface.

AIV.2 Experimental

AIV.2.1 Mineral samples

Hand specimens of arsenopyrite (FeAsS), bornite (Cu_5FeS_4), chalcocite (Cu_2S), chalcopyrite ($CuFeS_2$), cinnabar (HgS), enargite (Cu_3AsS_4), fahlore, galena (PbS), orpiment (As_2S_3), pyrite (FeS_2), pyrrhotite ($Fe_{1-x}S$), stibnite (Sb_2S_3), zinc blende (sphalerite, α-(Zn,Fe)S), and were bought from Dr F. Krantz,

Rheinisches Mineralien-Kontor, Bonn, Germany. The fahlore sample had a composition intermediate between that of tennantite ($(Cu,Fe)_{12}As_4S_{13}$) and tetraedrite ($(Cu,Fe)_{12}Sb_4S_{13}$) with 48.06% Cu, 9.44% Fe, 5.45% As, 10.37% Sb and 26.66% S, as determined by ICP-OES after fusion with sodium peroxide.

AIV.2.2 Sample pretreatment

Mineral samples were crushed in a percussion mortar, ground to a fine powder in an agate mortar and sieved. The fraction between 0.122 mm and 0.062 mm was retained for the experiments. In order to remove finer particles physically adhering to the ground mineral, the pretreatment adopted by McGuire et al. (2000) was then applied, with modifications : the samples (about 100 mg each, accurately weighed) were sonicated for 30 min. at 100 W in 75% (v/v) aqueous ethanol, resuspended in molar hydrochloric acid and mixed on a tumbler overnight. The acid was removed by centrifugation. They were rinsed again with 96% (v/v) ethanol, dried *in vacuo*, and washed twice with UV-grade cyclohexane for several hours. The second fraction of cyclohexane was shown to be free of sulfur by the UV spectroscopic method described below. The cyclohexane was removed by centrifugation and the samples dried and stored until use *in vacuo.* An assessment of the pretreatment procedure was undertaken by obtaining SEM micrographs of gold-coated samples before and after the pretreatment. In all cases, the pretreatment very effectively removed adhering fine particles, as can be clearly seen in the case of orpiment, As_2S_3 (compare Figs. AIV.1 and 2). Galena and arsenopyrite were free of fine particles after grinding; they were nevertheless subject to the same pre-treatment for consistency.

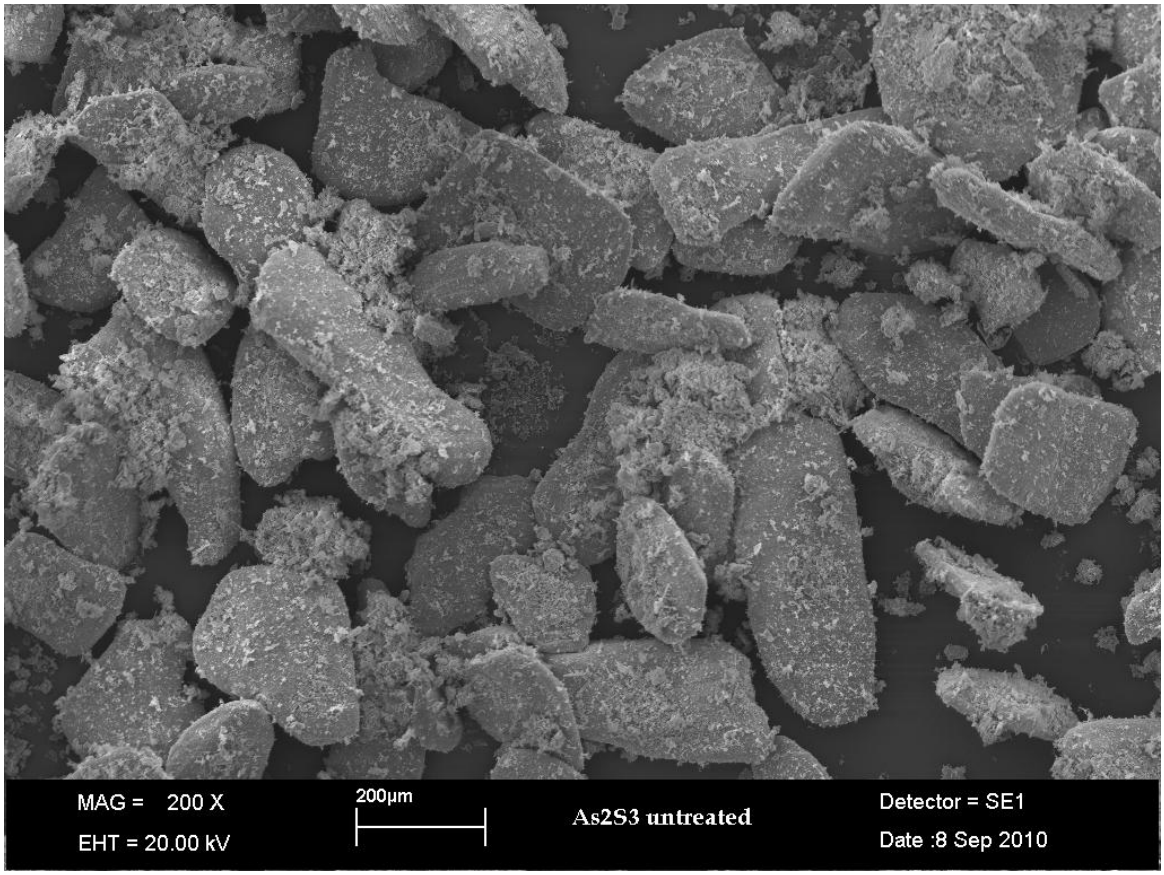

Fig. AIV. 1 SEM micrograph of gold-coated orpiment (As_2S_3) before pretreatment

AIV.2.3 Photometric determination of elemental sulfur

As an alternative to the HPLC method of McGuire et al. (2000), the photometric method for the determination of sulfur in hydrocarbons described by Bartlett and Skoog (1954) may be used. Elemental sulfur in a hydrocarbon is reacted with cyanide ion in a mixed water-acetone solvent to yield thiocyanate. Ferric ion is added, which produces the familiar cherry-red ferric thiocyanate complex, whose absorption in the visible is measured.

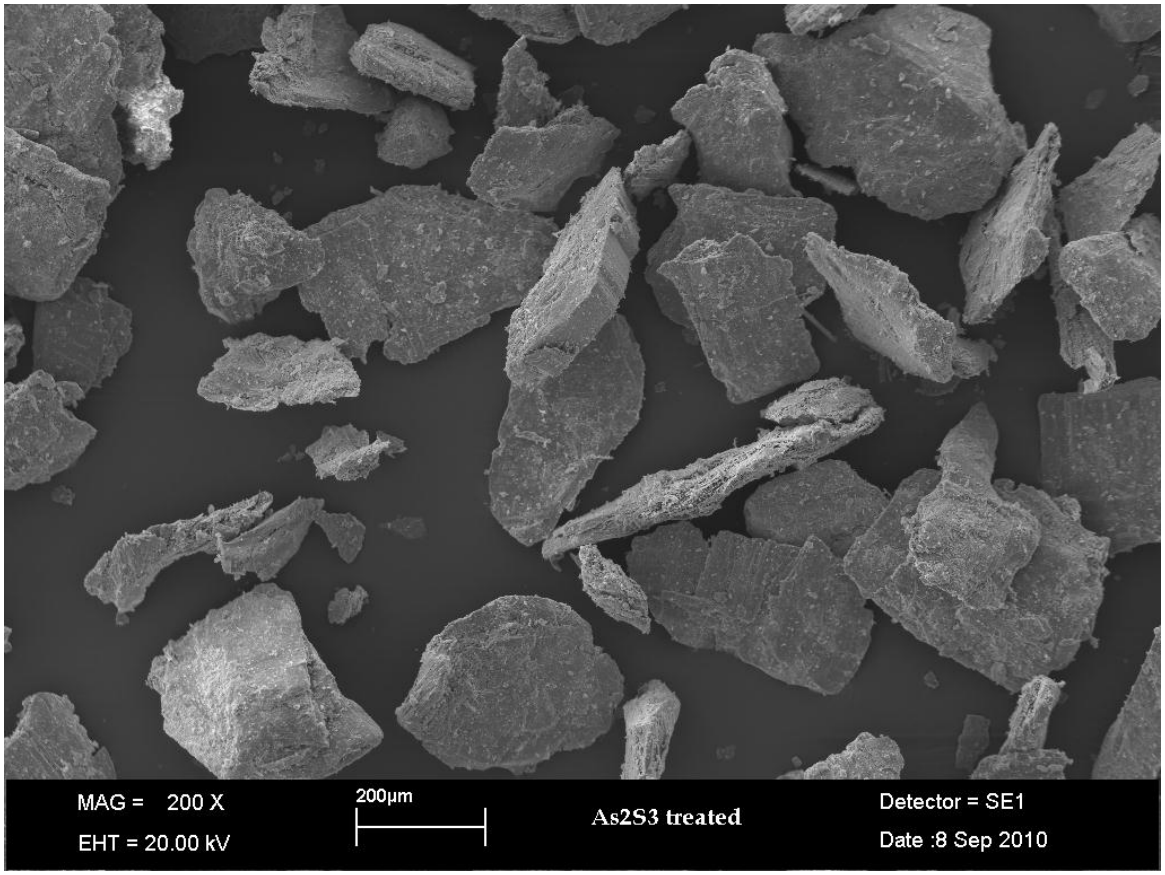

Fig. AIV.2 SEM micrograph of gold-coated orpiment (As_2S_3) after pretreatment

Cyclohexane or tetrachloroethene may be used for the extraction of sulfur from the mineral surface, and the photometric method can be implemented as described, with cyclohexane or tetrachloroethene substituted for the petroleum ether used in the original procedure. The limit of quantification of this photometric method is the same as that of the HPLC method of McGuire (5 mg l^{-1}).

However, a much more sensitive and precise quantification of elemental sulfur can be achieved by direct measurement of the UV absorption of sulfur in cyclohexane. Sulfur strongly absorbs at 206.3 nm in cyclohexane (Fig.AIV.3). Absorption at this wavelength is extremely sensitive to impurities in the solvent, so it is essential that spectroscopic-grade cyclohexane be used. UV-grade

cyclohexane (>99.9%) from Carl Roth, Germany, was found to be suitable. Since the absorption maximum is very close to the cut-off wavelength of cyclohexane ($A_{1\ cm}$=1 at 200 nm), every possible precaution must be taken to minimise instrument drift.

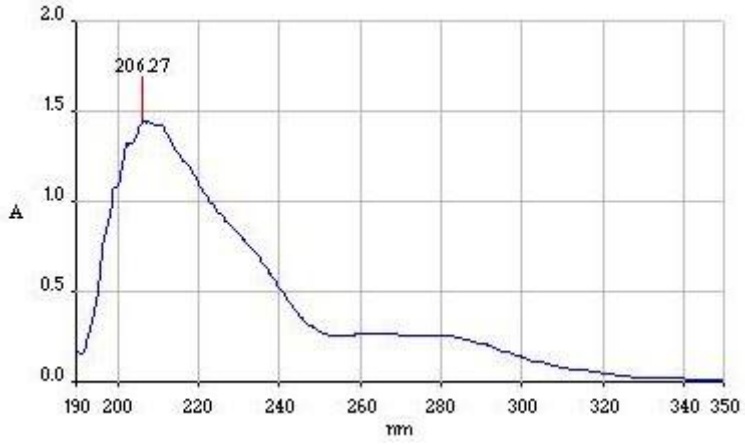

Fig. AIV.3 UV Absorption spectrum of elemental sulfur in cyclohexane

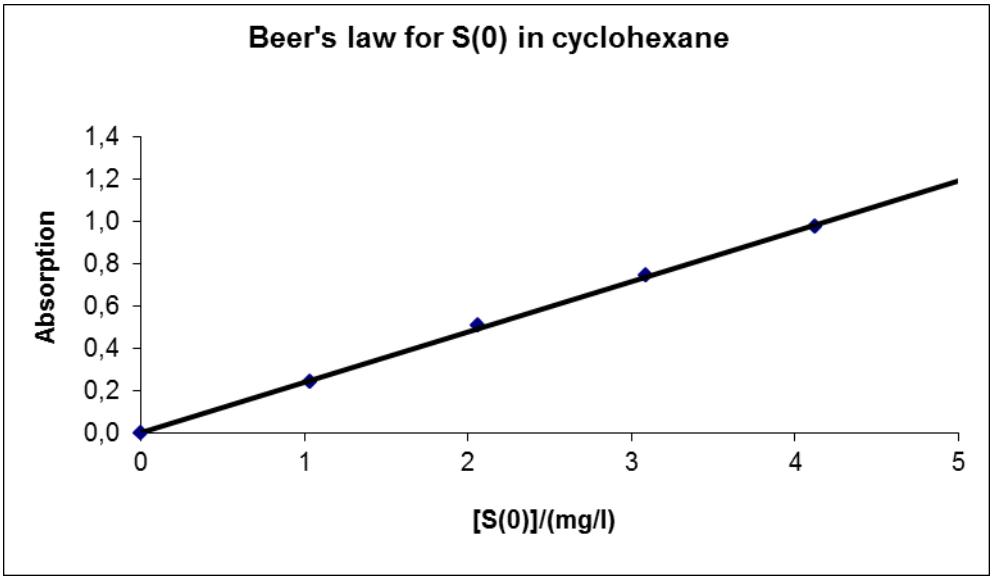

Fig. AIV.4 Beer's law plot for the absorption of elemental sulfur in cyclohexane at 206.3 nm. The error in each absorption measurement is better than 5 x 10^{-4} absorption units

Beer's law was obeyed between 0 and 5 mg l^{-1} with an extinction coefficient of 0.238±0.004 l mg^{-1} cm^{-1}, a correlation coefficient >0.9996 (Fig.

AIV.4) and an estimated limit of detection of 5 µg l^{-1}. As an alternative, the absorption of sulfur in chloroform was examined. On the one hand, the absorption maximum (264.3 nm) is farther away from the cut-off wavelength (240 nm), on the other, the sensitivity (extinction coefficient 0.026±0.002 l mg^{-1} cm^{-1}) is reduced by roughly an order of magnitude compared to the cyclohexane method. A spectrophotometric determination in tetrachloroethene is impossible as the absorption of the solvent hides the absorption of sulfur.

In the following experiments, all determinations of elemental sulfur extracted from surfaces were made using the cyclohexane method. Samples with concentrations higher than 4 mg l^{-1} were diluted with cyclohexane to bring the absorption into the calibrated range. A Perkin-Elmer Lambda 20 UV-VIS spectrophotometer and quartz cells were used for all UV measurements.

AIV.2.4 Square wave voltammetric determination of dissolved or colloidal S(0) in the aqueous phase

The present procedure is adapted from (Wang et al., 1998) and differs from the original one in that larger sample volumes are taken and a chelating agent (EDTA) is added to mask metal ions present in high concentrations that would interfere. The working electrode was a hanging mercury drop; a platinum auxiliary electrode was used in the present work rather than a glassy carbon electrode. The principle of the determination is as follows : During the deposition step, sulfur diffuses to the electrode surface and reacts with mercury to form mercury(II)-sulfide. In the determination step, mercury sulfide on the electrode surface is reduced back to metallic mercury and sulfide ion.

A mixed solvent was prepared by adding to 100 ml ethanol 96% (v/v) : 20 ml of molar sodium nitrate solution, 2 ml of tetrahydrofurane, and 200 µl of molar nitric acid. A sulfur standard solution (320 mg/L) was prepared by dissolving 32.0 mg elemental sulfur in 10 ml of tetrahydrofurane and diluting to 100 ml with 96%(v/v) ethanol. A working solution of 320 µg l^{-1} was prepared by 1000 fold dilution of the stock solution in the same solvent (96% ethanol containing 10% (v/v) tetrahydrofurane). This working solution was used for standard additions, typically 50 µl per run. Both stock and working solutions were stable for at least a week. The square wave voltammetric method was implemented on a Metrohm VA797 Computrace with a standard electrode assembly, comprising a mercury drop electrode, a platinum auxiliary electrode and a Ag/AgCl/3 M KCl reference electrode. Immediately before the measurement, 6 ml of aqueous sample solution were added to 10 ml of the mixed solvent and 0.1 ml of 0.1 M EDTA solution in the polarographic cell. In the case of acidic samples, the solution was neutralised by addition of the stoichiometric quantity of molar potassium hydroxide solution (in all cases <0.5 ml). The following instrumental parameters were used for the determination : deoxygenation of the sample by purging with ultrapure nitrogen for 3 min., deposition time 60 s at a potential of -0.100 V, followed by 20 s equilibration time, then the potential was scanned in the cathodic direction from –0.100 V to –0.800 V with a pulse amplitude of 25 mV and a potential step amplitude of 2 mV at a frequency of 50 Hz. A hanging mercury drop of size 4 was used. Under these conditions, elemental sulfur yields a very well defined peak at –0.378 V with a

limit of detection of about 2 ng l^{-1}. In chapter I.9, we described the principle of differential-pulse polarography. In the present determination, a so-called square-wave pulse is applied, which also yields a derivative-like voltammogram. The principle of square-wave polarography is illustrated in Fig. AIV.5. A square-wave alternating potential with amplitude ΔE_A is superimposed on the linearly increasing direct potential. Two current values are measured at each oscillation: i_+ at the positive pulse end (measuring point 1) and i_- at the negative pulse end (measuring point 2). The difference between the two current values, i_+-i_-, is proportional to the derivative of the current-potential curve. This implies that the difference i_+-i_- goes through a maximum at the inflection points of the current-potential curve, i.e. at those potentials which correspond to the deposition or the 'stripping' of an electroactive species at the working electrode surface. The voltammogram thus exhibits bell-shaped maxima. In modern instruments, the application of the square-wave can be synchronised with the drop time, so that measurements are recorded at a constant electrode surface area. A variant of square-wave voltammetry, known as SQV according to Osteryoung is applied. The characteristic of this variant is that the whole measuring procedure takes place at a single mercury drop with very rapid potential sweeps. The duration of the potential step is identical with the length of the square-wave pulse, as shown in Fig.AIV.6.

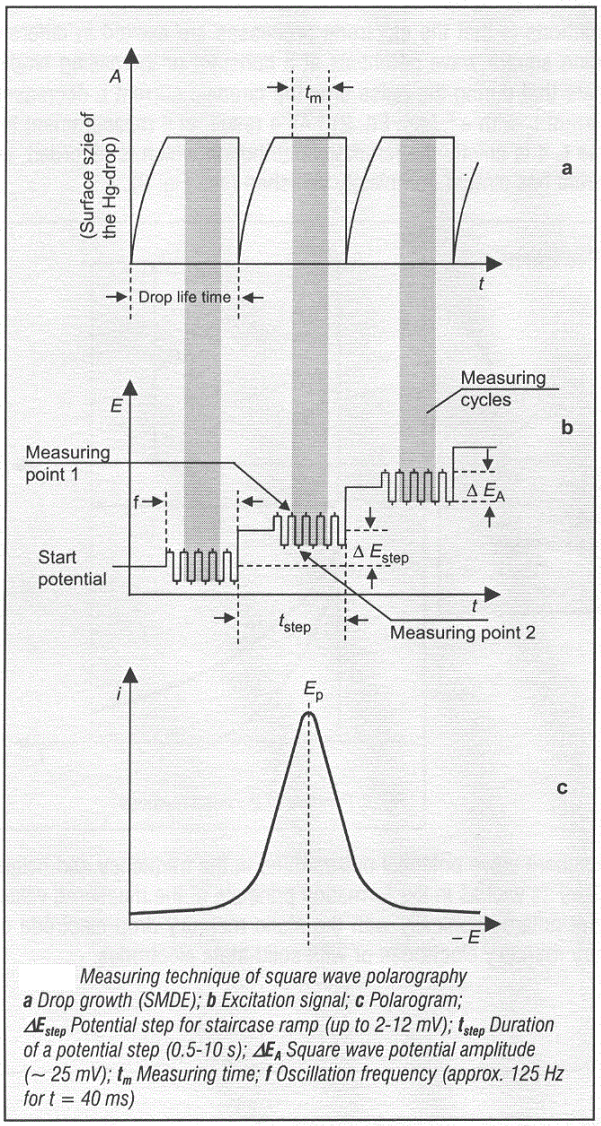

Measuring technique of square wave polarography
a *Drop growth (SMDE);* ***b*** *Excitation signal;* ***c*** *Polarogram;* ΔE_{step} *Potential step for staircase ramp (up to 2-12 mV);* t_{step} *Duration of a potential step (0.5-10 s);* ΔE_A *Square wave potential amplitude (~ 25 mV);* t_m *Measuring time;* ***f*** *Oscillation frequency (approx. 125 Hz for t = 40 ms)*

Fig.AIV.5 Measurement principle of square-wave voltammetry (from Henze, s.d.)

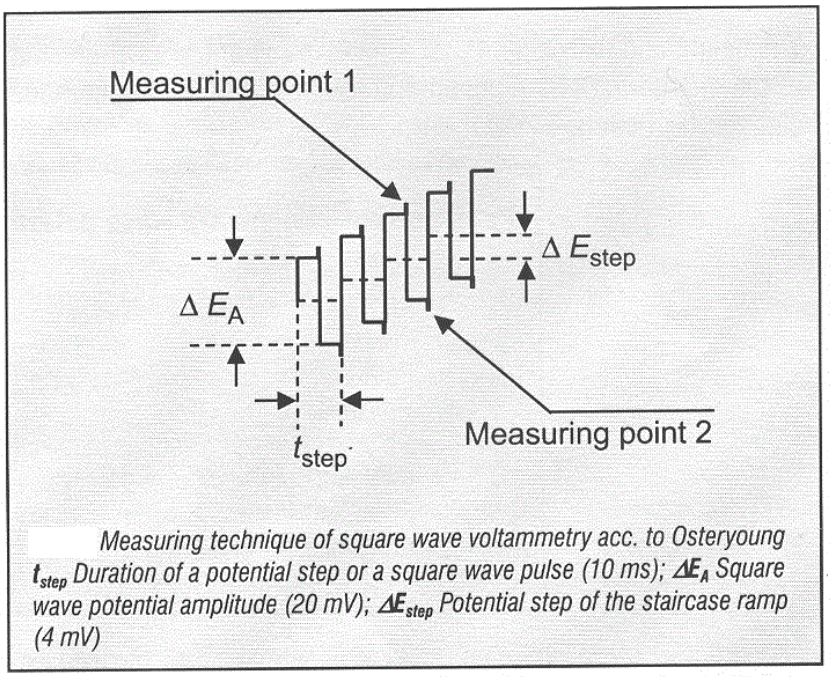

Fig.AIV.6 Square-wave voltammetry acc. to Osteryoung (from Henze, s.d.)

As a check on the method, the solubility of sulfur in water was measured. To this effect, a few mg of finely powdered sulfur were added to 15 ml of ultrapure water and the mixture placed on a tumbler for a week at room temperature. The solution was centrifuged and the supernatant withdrawn using a syringe fitted with a 0.45 µm hydrophilic CME filter (Millipore). The measured concentration of S(0) (aq.) amounted to 6.62 ± 0.05 µg l^{-1}, which is in excellent agreement with the published value (Wang and Tessier, 2009), given as 6.732 ± 0.096 µg l^{-1} for rhombic α-S_8.

Through the use of EDTA, interfering voltammetric signals of metals are shifted away from the sulfur peak. For example, up to 10 mg l^{-1} of Fe^{3+} and probably more can be tolerated. Very high concentrations of metals (>100 mg l^{-1} Fe^{3+}) cannot be tolerated and sulfur cannot be determined in their presence by this method.

AIV.2.5 Weathering experiments

The mineral samples (about 100 mg of each), after the pretreatment described above, were suspended in 40 ml of 0.1 M $HClO_4$ prepared from suprapure perchloric acid (Merck) in conical flasks and mixed on magnetic stirrers for 4 days with free access of atmospheric oxygen at room temperature (20 ± 2°C). The suspensions were filtered into volumetric flasks (50 ml). The solutions were completed to volume with ultrapure water. The mineral residues on the filters were dried *in vacuo.* Dissolved elemental and colloidal sulfur were measured in the solutions by the voltammetric method described above. Metal concentrations and total dissolved sulfur species were determined using ICP-OES (Spectroflame Modula, Spectro Analytical Instruments, Kleve, Germany), calibrated with a Merck multielement standard. To extract the elemental sulfur formed on the mineral surfaces, the dried filter papers with the mineral residues were introduced in PTFE centrifuge tubes, to which exactly 10 ml of UV-grade cyclohexane were added. The tubes were sealed with PTFE screw caps and mixed on a tumbler for a day. The use of PTFE tubes fitted with PTFE caps is essential, since disposable PP tubes release traces of substances that absorb in the UV region of interest. Glass tubes were found to be equally inadequate, because of contaminations introduced by plastic or rubber caps. After a day of mixing, the solutions were directly decanted into the quartz photometric cell or pipetted into a volumetric flask for dilution prior to the absorption measurement.

It was verified in separate experiments that neither 0.1 M perchloric acid, nor ferric iron at 10 mg l^{-1} in the presence of oxygen in 0.1 M perchloric acid, nor

atmospheric oxygen alone were able to oxidize dissolved and colloidal aqueous sulfur. To this effect, solutions containing about 32 μg l^{-1} S(0) (1 μmol l^{-1}) in 0.1 M perchloric acid were prepared. One of the solutions was spiked with 10 mg l^{-1} iron(III). The solutions were stirred under contact with air for 4 days and the original concentration of S(0) was quantitatively recovered within experimental error in all solutions, using the voltammetric method described above.

AIV.3 Results and discussion

Full analytical details with error margins are available in section AIV.5.

Ten minerals that behave similarly in the weathering experiments are grouped together in Fig.A.III.5. The top graph shows the amounts of sulfur recovered from the mineral surface (lower part of the columns), and the amounts of total sulfur released into the aqueous phase (top part of the columns), in millimoles of sulfur per mole of mineral, respectively. It is clear that a considerable sulfur layer is formed on the weathered surface in every single instance and that none of these minerals dissolve congruently. The proportion of sulfur formed on the surface relative to the total amount of sulfur released varies from 32% (cinnabar) to 74% (chalcopyrite).

The middle graph (Fig. AIV.7) shows the amounts of zerovalent sulfur released into the aqueous phase, in micromoles of sulfur per mol of mineral. These amounts are generally small with respect to the total amounts of sulfur formed (minimum value: 0.26% for chalcopyrite), but they can become considerable in

some cases (maximum value: 2.48% for orpiment). The concentrations thus achieved are always in excess of the solubility of sulfur in water: saturation occurs at 0.21 μmol l^{-1}, and all the weathering solutions are found to be supersaturated with respect to sulfur, up to a maximum of eight times in the case of pyrite. The findings presented here illustrate the need for quantifying elemental sulfur in kinetic studies of sulfide weathering, where the concentration of sulfur in solution, sometimes even taken as the reaction progress variable, is typically monitored by techniques that detect only sulfoxy-species such as sulfate, polythionates and thiosulfate, usually measured using ion-chromatography.

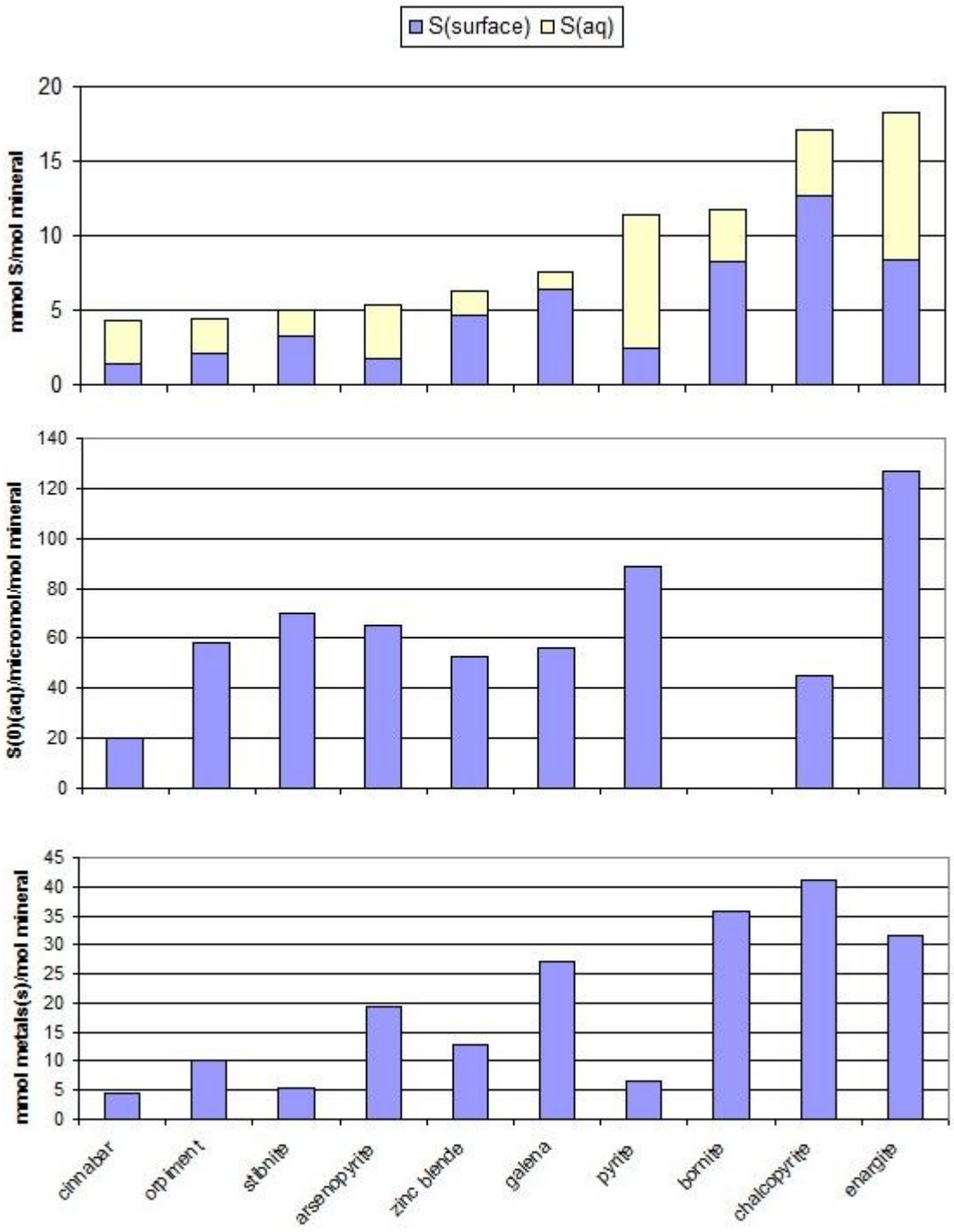

Fig.AIV.7 Amounts of sulfur and metals released by sulfide minerals under acidic, oxic conditions

The bottom graph shows the amounts of metal(s) released to the aqueous phases. In this group of minerals, these amounts are always larger than stoichiometrically predicted on the basis of the total amounts of sulfur liberated,

including sulfur in the surface layer. In the case of cinnabar, the dissolution is nearly stoichiometric : 97.5% of the stoichiometrically expected amount of sulfur can be detected. In the case of orpiment, however, only 15% of the stoichiometric amount can be found. Values for the other minerals lie in between these extremes. On the basis of the amounts of metal released to the aqueous phase, the minerals can be classified in the following sequence of decreasing resistance (or increasing susceptibility) to weathering, with the values in brackets representing the amounts of metals released into solution (mmol metal(s)/mol mineral), *normalized with respect to the number of ions per formula unit*:

stibnite (1.1) < orpiment (2.0) < cinnabar (2.2) < pyrite (3.3) <
bornite (3.6) <enargite (3.9) < zinc blende (6.4) < arsenopyrite (6.5) <
chalcopyrite (12.8) < galena (13.5).

This sequence agrees in part with that given by Moncur et al. (2009) who investigated the relative resistance to alteration of sulfides in oxidized mine tailings.

For at least six out of these minerals, the trend in weathering susceptibility correlates with the lattice energies of the solids (Fig.AIV.8). The amounts of released metal(s) and lattice energies in this graph are normalized with respect to the number of ions per formula unit. Lattice energies are literature values (pyrite, chalcopyrite, zinc blende, galena (Dang et al., 2002) or calculated using Kapustinskii's equation (Dasent, 1982) and the simple salt approximation (Yoder and Rowand, 2006).

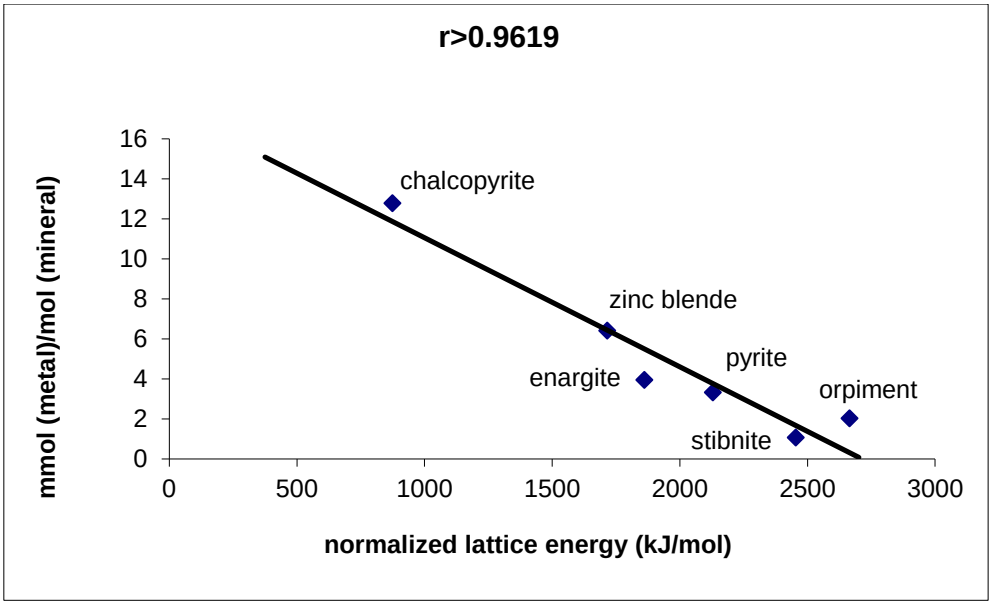

Fig.AIV.8 Normalized amounts of metals released on weathering vs. lattice energies of metal sulfides

The remaining three minerals, i.e. chalcocite, fahlore and pyrrhotite, show a different behaviour in that the amounts of released metals are larger by roughly an order of magnitude than for the minerals shown in Fig.AIV.7. Therefore, for these three minerals, their dissolution behaviour are presented in the same way as those shown in Fig. AIV.7, but using a different concentration scale (Fig.AIV.9). Again, dissolution is incongruent with elemental sulfur on the mineral surface formed in very significant proportions: 21% of all the released S

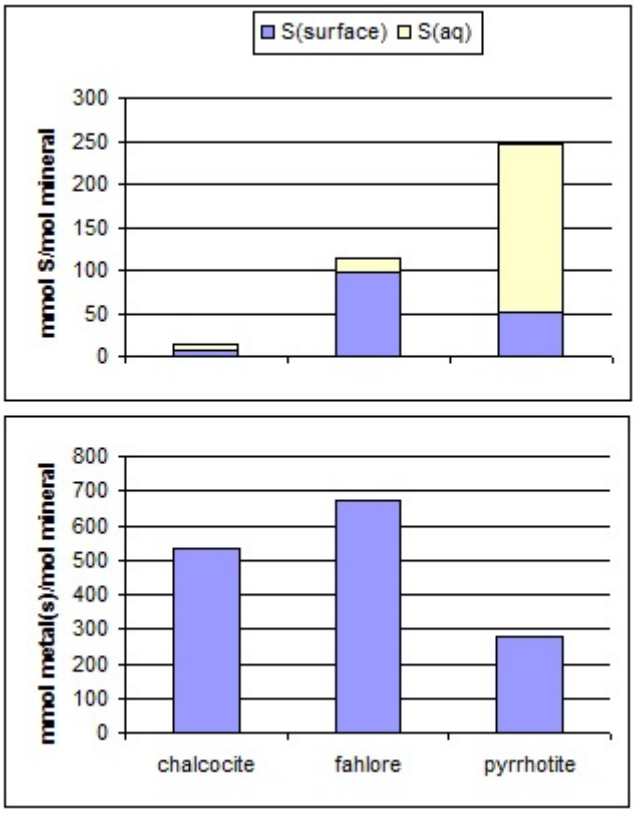

Fig.AIV.9 Amounts of sulfur and metals released under acidic, oxic conditions by three sulfide minerals whose reactivities are highly non-stoichiometric

is found as S(0) at the surface in the case of pyrrhotite, 52% in the case of chalcocite, and 86% in the case of fahlore. The heightened solubility of these three minerals may be due to a much higher degree of non-stoichiometry in these phases. Pyrrhotite, for instance, also appears in Moncur's list as the mineral with the least resistance towards alteration. Due to the very high metal loads in these weathering solutions, dissolved S(0) could not be determined. Based on the amounts of metals released, the total amount of sulfur recovered from the surface and released to solution (measured using ICP-OES) accounts for only 5.2% of the stoichiometric amount in the case of chalcocite and for 88.7% in the case pyrrhotite.

Considering the amount of metals released from the thirteen common sulfide minerals studied here, it appears that the total amount of sulfur liberated during weathering in acidic solutions is always lower than that expected based on the stoichiometry, and that significant amounts of sulfur remain as elemental sulfur at the surface of the mineral. Zerovalent sulfur in solution is, in all the examined cases, well in excess of the solubility of sulfur in aqueous solution. This is consistent with the view that sulfide ions at the surface of the mineral are oxidized with formation of polysulfide chains, which remain largely bound to the surface and which are to some extent decomposed under acid conditions to hydrogen sulfide and elemental sulfur (Schippers and Sand, 1999; Steudel, 1996). Another route to elemental sulfur is the breakdown of thiosulfate in acid solution (Rimstidt and Vaughan, 2003).

Since the independent experiments described above show elemental sulfur in solution to be stable with respect to oxidation by iron(III) and/or oxygen, sulphoxy-species in solution must arise through oxidation reactions at the mineral surface, e.g. via the multi-step oxidation mechanism postulated for pyrite (Rimstidt and Vaughan, 2003). Thiosulfate may however also be formed by oxidation of hydrogen polysulfides in solution by oxygen in the presence of iron(III) (Schippers and Sand, 1999). Elemental sulfur in solution or at a surface can only be further oxidized by bacterial action, e.g. by Thiobacillus or Halothiobacillus (Munz et al., 2009).

AIV.4 References

Alpers C.N. and Blowes D.W. (Eds.) (1994) *Environmental Geochemistry of Sulfide Oxidation*, ACS Symposium Series 550; American Chemical Society, Washington.

Asta M.P., Ayora C., Roman-Ross G., Cama J., Acero P., Gault A.G., Charnok J.M. and Bardelli, F. (2010) Natural attenuation of arsenic in the Tinto Santa Rosa acid stream (Iberian Pyritic Belt, SW Spain): The role of iron precipitates. *Chem. Geol.* **271**, 1-12

Bartlett J.K. and Skoog D.A. (1954) Colorimetric Determination of Elemental Sulfur in Hydrocarbons. *Anal. Chem.* **26**, 1008-1011

Dang Z., Liu C. and Haigh, M.J. (2002) Mobility of heavy metals associated with the natural weathering of coal mine spoils. *Environ. Pol.* **118**, 419-426

Dasent W.E. (1982) Inorganic Energetics, Cambrigde University Press, Cambridge, U.K.

Domènech C., de Pablo J. and Ayora C. (2002) Oxidative dissolution of pyritic sludge from the Aznallcóllar mine (SW Spain). *Chem. Geol.* **190**, 339-353

Edwards K.J., Bond P.L., Druschel G.K., McGuire M.M., Hamers R.J. and Banfield, J.F. (2000) Geochemical and biological aspects of sulfide mineral dissolution: lessons from Iron Mountain, California. *Chem. Geol.* **169**, 383-397

Henze G. (s.d.) Introduction to polarography and voltammetry. Metrohm Ltd. Herisau, Switzerland.

Lottermoser B. (2007) Mine Wastes: Characterization, Treatment and Environmental Impacts, Springer, Berlin

McGuire M.M. and Hamers R.J. (2000) Extraction and Quantitative Analysis of Elemental Sulfur from Sulfide Mineral Surfaces by High-Performance Liquid Chromatography. *Environ. Sci. Technol.* ***34,*** 4651-4655

McGuire M.M., Jallad, K.N., Ben-Amotz D. and Hamers, R. (2001) Chemical mapping of elemental sulfur on pyrite and arsenopyrite surfaces using near-infrared Raman imaging miscroscopy. *Appl. Surf. Sci.* **178**, 105-115

Moncur M.C, Jambor J.L., Ptacek C.J. and Blowes D.W. (2009) Mine drainage from the weathering of sulfide minerals and magnetite. *Appl. Geochem.* **24**, 2362-2373

Moncur M.C., Ptacek C.J., Blowes D.W. and Jambor J.L. (2005) Release, transport and attenuation of metals from an old minings impoundment. *Appl. Geochem.* **20**, 639-659

Munz G., Gori R., Mori G. and Lubello C. (2009) Monitoring biological sulfide oxidation processes using combined respirometric and titrimetric techniques. *Chemosphere* **76**, 644-650

Mycroft J.R., Bancroft G.M., McIntyre N.S., Lorimer J.W. and Hill I.R. (1990) Detection of sulfur and polysulfides on electrochemically oxidised pyrite surfaces by X-ray photoelectron spectroscopy and Raman spectroscopy. *J. Electroanal. Chem.* **292,** 139-152

Nordstrom D.K. (2000) Advances in the Hydrogeochemistry and Microbiology of Acid Mine Waters. *Int. Geol. Rev.* **42**, 499-515

Rimstidt J.D. and Vaughan D.J. (2003) Pyrite Oxidation : A state-of-the-art assessment of the reaction mechanism. *Geochim. Cosmochim. Acta* **67**, 873-880

Sasaki K., Tsunekawa M., Ohtsuka T. and Konno H. (1995) Confirmation of a sulfur-rich layer on pyrite after oxidative dissolution by Fe(III) ions around pH 2, *Geochim. Cosmochim. Acta* **59**, 3155-3158

Schippers, A., Sand, W. Bacterial Leaching of Metal Sulfides Proceeds by Two Indirect Mechanisms via Thiosulfate or via Polysulfides and Sulfur. *Appl. Environ. Microbiol.* **1999**, *65(1)*, 319-321

Steudel R. (1996) Mechanism for the Formation of Elemental Sulfur from Aqueous Sulfide in the Chemical and Microbiological Desulfurization Processes. *Ind. Eng. Chem. Res.* **35**, 1417-1423

Turcotte S.B. and Benner R.E. (1993) Surface analysis of electrochemically oxidized metal sulfides using Raman spectroscopy. *J. Electroanal. Chem.* **347**, 195-205

U.S. Environmental Protection Agency (2010) Chemical Summaries for Cyclohexane and Perchloroethylene. Prepared by the Office of Pollution Prevention and Toxics. Accessed online at www.epa.gov/chemfact on 11th March 2010.

U.S. National Library of Medicine (2010) TOXNET-Toxicology Data Network (toxnet.nlm.nih.gov) accessed on 11th March 2010.

Wang F., Tessier, A. and Buffle J. (1998) Voltammetric Determination of Elemental Sulfur in Pore Waters. *Limnol. Oceanogr.* **43**, 1353-1361

Wang F. and Tessier A. (2009) Zero-Valent Sulfur and Metal Speciation in Sediment Porewaters fo Freshwater Lakes, *Environ. Sci. Technol.* **43**, 7252-7257

Yoder C.H. and Rowand J.P. (2006) Application of the simple salt lattice energy approximation to the solubility of minerals. *Am. Mineral.* **91**, 747-752

AIV.5 Supporting Information

Mineral	Formula	S(surface)	S(tot, aq)	S(0, aq)	Metals
Arsenopyrite	FeAsS	1.77±0.59	3.58±0.05	0.065±0.003	Fe 9.729±0.001 As 9.709±0.001
Bornite	Cu_5FeS_4	8.31±0.16	3.45±0.13	n/a	Cu 27.9±0.3 Fe 7.83±0.11
Chalcocite	Cu_2S	7.12±0.15	6.65±0.05	n/a	Cu 533.0±0.5
Chalcopyrite	$CuFeS_2$	12.65±2.15	4.44±0.06	0.0449±0.001	Cu 24.49±0.42 Fe 26.6±3.7
Cinnabar	HgS	1.37±0.03	2.90±0.05	0.0020±0.001	Hg 4.38±0.05
Enargite	Cu_3AsS_4	8.34±0.48	9.92±0.36	0.127±0.006	Cu 25.45±0.16 As 6.09±0.01
Fahlore		98.27±0.01	16.57±0.01	n/a	Fe 209.93±0.01 Cu 351.50±0.01 As 33.38±1.33 Sb 75.78±0.80
Galena	PbS	6.35±0.01	1.22±0.04	0.056±0.005	Pb 34.3±0.7
Orpiment	As_2S_3	2.12±0.01	2.27±0.09	0.058±0.001	As 10.1±0.1
Pyrite	FeS_2	2.45±0.01	8.90±0.01	0.089±0.005	Fe 6.64±0.02
Pyrrhotite	$Fe_{1-x}S$	50.78±0.01	196.7±0.5	n/a	Fe 279.0±0.5
Stibnite	Sb_2S_3	3.29±0.73	1.70±0.40	0.070±0.001	Sb 5.31±0.05
Zinc blende	ZnS	4.68±0.04	1.61±0.01	0.053±0.001	Zn 12.81±0.14

Table AIV.1 Analytical results
(all figures represent mmol of leached element per mol of mineral)

Arsenopyrite	FeAsS	33%
Bornite	Cu_5FeS_4	71%
Chalcocite	Cu_2S	52%
Chalcopyrite	$CuFeS_2$	74%
Cinnabar	HgS	32%
Enargite	Cu_3AsS_4	46%
Fahlore		86%
Galena	PbS	84%
Orpiment	As_2S_3	48%
Pyrite	FeS_2	22%
Pyrrhotite	$Fe_{1-x}S$	21%
Stibnite	Sb_2S_3	66%
Zinc blende	ZnS	74%

Table AIV.2 Sulfur formed at the surface as percent of total recovered sulfur

Arsenopyrite	FeAsS	1.21%
Chalcopyrite	$CuFeS_2$	0.26%
Cinnabar	HgS	0.46%
Enargite	Cu_3AsS_4	0.70%
Galena	PbS	0.73%
Orpiment	As_2S_3	2.48%
Pyrite	FeS_2	0.79%
Stibnite	Sb_2S_3	1.40%
Zinc blende	ZnS	0.84%

Table AIV.3 Zerovalent sulfur in solution as percent of total recovered sulfur

Arsenopyrite	FeAsS	55.1%
Bornite	Cu_5FeS_4	37.3% w.r.t. Cu 26.5% w.r.t. Fe
Chalcocite	Cu_2S	5.2%
Chalcopyrite	$CuFeS_2$	33.5 w.r.t Cu and Fe
Cinnabar	HgS	97.5%
Enargite	Cu_3AsS_4	53.8% w.r.t. Cu 74.9% w.r.t. As
Fahlore		11.1% w.r.t. Fe 29.7% w.r.t Cu 30.2% w.r.t. As 15.5% w.r.t. Sb
Galena	PbS	28.0%
Orpiment	As_2S_3	15.4%
Pyrite	FeS_2	85.5%
Pyrrhotite	$Fe_{1-x}S$	88.7%
Stibnite	Sb_2S_3	62.7%
Zinc blende	ZnS	49.1%

Table AIV.4 Total recovered sulfur as percent of the stoichiometric amount

Appendix AV

Rates of Ligand-Promoted Dissolution of Stibnite

Ligand	**pH=4**	**pH=6**	**pH=8**
Blank	5.52±0.10	5.20±0.08	4.62±0.04
Acetate	4.944±0.004	4.80±0.06	4.02±0.05
Catechol	5.23±0.04	5.56±0.11	5.56±0.01
Citrate	6.83±0.14	6.43±0.05	5.18±0.01
Cysteine	4.21±0.01	4.14±0.04	5.12±0.10
DFOB	3.41±0.08	3.82±0.02	3.426±0.004
DFOB+citrate	5.26±0.02	4.616±0.008	3.50±0.03
EDTA	7.93±0.02	6.81±0.03	5.25±0.01
Glucose	4.75±0.06	4.89±0.08	4.222±0.004
Glycine	4.96±0.04	5.18±0.08	4.40±0.12
LLE	1.78±0.02	2.303±0.001	3.10±0.02
Oxalate	6.14±0.02	6.021±0.004	4.79±0.04
Salicylate	4.95±0.03	4.88±0.03	4.32±0.03

Table AV.1 Initial rates (1st five minutes) in 10^{-5} mol m^{-2} min^{-1}

Ligand	**pH=4**	**pH=6**	**pH=8**
Blank	1.24±0.06	1.17±0.08	0.74±0.05
Acetate	0.88±0.08	1.23±0.08	0.96±0.08
Catechol	0.99±0.05	0.86±0.06	2.37±0.10
Citrate	0.76±0.05	1.17±0.09	1.49±0.08
Cysteine	1.00±0.04	1.20±0.10	0.78±0.08
DFOB	1.18±0.09	1.04±0.08	0.63±0.02
DFOB+citrate	1.98±0.12	1.49±0.09	0.63±0.05
EDTA	2.65±0.14	1.60±0.07	2.01±0.09
Glucose	1.48±0.09	1.47±0.12	1.00±0.06
Glycine	0.83±0.07	1.43±0.08	1.10±0.03
LLE	1.31±0.05	1.20±0.06	0.91±0.03
Oxalate	1.34±0.09	1.12±0.07	0.90±0.06
Salicylate	1.54±0.09	1.39±0.07	0.95±0.07

Table AV.2 Steady state dissolution rates in 10^{-6} mol m^{-2} min^{-1}

Appendix AVI

Supplemental information for chapter VI

	1 h PO_4^{3-}	24 h PO_4^{3-}	1 h HCO_3^-	24 h HCO_3^-	1 h Cl^-	24 h Cl^-	1 h SO_4^{2-}	24 h SO_4^{2-}	1 h NO_3^-	24 h NO_3^-	1 h Blank	24 h blank
% Sb	9.0± 0.2	19.3± 0.8	9.0± 1.2	17.7± 3.1	3.21± 0.06	4.8± 0.7	2.7± 0.1	5.01± 0.01	2.40± 0.01	4.34± 0.06	5.74± 0.02	12.3 ±1.2

Table AVI.1: Percentage of Sb(V) desorption from the CRM PACS-2 sediment

	1 h PO_4^{3-}	24 h PO_4^{3-}	1 h HCO_3^-	24 h HCO_3^-	1 h Cl^-	24 h Cl^-	1 h SO_4^{2-}	24 h SO_4^{2-}	1 h NO_3^-	24 h NO_3^-	1 h Blank	24 h blank
% Sb	2.07± 0.01	3.75± 0.01	1.67± 0.01	3.27± 0.01	1.09± 0.01	2.78± 0.04	1.32± 0.02	3.09± 0.06	1.70± 0.06	2.10± 0.27	1.37± 0.08	3.04± 0.15

Table AVI.2 : Percentage of Sb(V) desorption from the Goesdord sediment sample

	1 h PO_4^{3-}	24 h PO_4^{3-}	1 h HCO_3^-	24 h HCO_3^-	1 h Cl^-	24 h Cl^-	1 h SO_4^{2-}	24 h SO_4^{2-}	1 h NO_3^-	24 h NO_3^-	1 h Blank	24 h blank
% of desorb. Sb	36.20± 0.76 %	41.00± 4.01 %	15.16± 0.76 %	8.55± 1.44 %	1.7± 0.5%	<LOD	<LOD	<LOD	<LOD	1.7± 0.5%	<LOD	1.8± 0.5%

Table AVI.3: Percentage of Sb(V) desorption from hydrous ferric oxide. The calculated limit of detection (LOD) corresponds to 0.0045%.

	1 h PO_4^{3-}	24 h PO_4^{3-}	1 h HCO_3^-	24 h HCO_3^-	1 h Cl^-	24 h Cl^-	1 h SO_4^{2-}	24 h SO_4^{2-}	1 h NO_3^-	24 h NO_3^-	1 h Blank	24 h blank
% of desorb. Sb	31.25± 3.67	29.39± 0.14	23.75± 1.63	22.39± 0.14	5.05± 0.88	1.55± 0.5%	13.08± 0.68	13.34± 0.50	7.49± 0.48	5.36± 0.03	2±1%	2±1%

Table AVI.4 : Percentage of Sb(V) desorption from aluminium hydroxide

	1 h PO_4^{3-}	24 h PO_4^{3-}
% of desorbed Sb	17.73±4.01	16.59±0.28

Table VI.5 : Percentage of Sb(V) desorption from manganese(IV) oxide

	1 h PO_4^{3-}	24 h PO_4^{3-}	1 h HCO_3^-	24 h HCO_3^-	1 h Cl^-	24 h Cl^-	1 h SO_4^{2-}	24 h SO_4^{2-}	1 h NO_3^-	24 h NO_3^-	1 h blank	24 h blank
% of desorb Sb	66.95 ± 7.38	100.76 ± 1.04	42.32 ± 0.31	63.45 ± 0.28	48.17 ± 1.39	49.96 ± 3.56	43.83 ± 3.59	46.34 ± 1.31	53.59 ± 0.33	67.69 ± 0.98	28.81 ± 1.10	64.44 ± 2.77

Table AVI.6 : Percentage of Sb(V) desorption from kaolinite

	1 h PO_4^{3-}	24 h PO_4^{3-}	1 h HCO_3^-	24 h HCO_3^-	1 h Cl^-	24 h Cl^-	1 h SO_4^{2-}	24 h SO_4^{2-}	1 h NO_3^-	24 h NO_3^-	1 h Blank	24 h blank
% of desorb. Sb	15.55 ± 1.02	23.06 ± 0.29	5.66± 0.05	5.59± 0.29	5.62 ± 0.15	±10.56 0.12	5.75 ± 0.51	±10.98 0.14	6.60 ± 1.32	11.44 ± 0.68	4.38± 0.03	10.07 ± 0.62

Table AVI.7: Percentage of Sb(V) desorption from montmorillonite

Phosphate conc./moll^{-1}	0	0.0001	0.0005	0.001	0.005
% of desorbed Sb	6.3±0.1	6.7±0.2	7.2±0.08	7.9±0.05	9.8±1.9

Table AVI.8: Percentage of Sb(V) desorption from PACS-2 by different phosphate concentrations

Carbonate conc./moll^{-1}	0	0.0001	0.0005	0.001	0.005
% of desorbed Sb	4.6±0.3	4.7±0.5	4.1±0.2	4.2±0.2	6.6±1.4

Table AVI.9: Percentage of Sb(V) desorption from PACS-2 by different carbonate concentrations

Phosphate conc./moll^{-1}	0	0.0001	0.0005	0.001	0.005
% of desorbed Sb	1.6±0.3	1.7±0.05	1.9±0.04	2.1±0.06	2.6±0.3

Table AVI.10: Percentage of Sb(V) desorption from Goesdorf sediment by different phosphate concentrations

Carbonate conc./moll^{-1}	0	0.0001	0.0005	0.001	0.005
% of desorbed Sb	1.34±0.36	1.53±0.12	1.35±0.11	1.44±0.06	1.83±0.01

Table AVI.11: Percentage of Sb(V) desorption from Goesdorf sediment by different carbonate concentrations

EIDESSTATTLICHE VERSICHERUNG

Erklärung gem. § 8 (3) b) und c) der Promotionsordnung der Naturwissenschaftlich-Mathematischen Gesamtfakultät der Ruprecht-Karls-Universität Heidelberg

Ich erkläre hiermit, daß ich die vorgelegte Dissertation selbst verfasst und mich keiner anderen als der von mir ausdrücklich bezeichneten Quellen und Hilfen bedient habe.

Ausserdem erkläre ich hiermit, daß ich an keiner anderen Stelle ein Prüfungsverfahren beantragt bzw. die Dissertation nicht in dieser oder anderer Form bereits anderweitig als Prüfungsarbeit verwendet oder einer anderen Fakultät als Dissertation vorgelegt habe.

Marc Biver

Addendum

Some pieces of information in section I.6.1 (‚Discovery of antimony and etymology of the name‘) are taken from the online encyclopedia Wikipedia (http://en.wikipedia.org/wiki/Main_Page). Given the ephemeral character of many internet resources, only the original references, which were checked against the text of the encyclopedia, are cited in the text of the thesis.